SURFACE CHARACTERISATION OF MODIFIED PAN BASED CARBON FIBRES

Susan Osbeck

A thesis submitted in partial fulfilment of the requirements of The Robert Gordon University for the degree of Doctor of Philosophy.

This research programme was carried out in collaboration with Cytec Engineered Materials Ltd.

May 2011

Abstract

This thesis examines the surfaces of polyacrylonitrile (PAN) based high strength (HT) carbon fibres modified by electrochemical and ultra-violet ozone (UV/O$_3$) treatment methods. The surface and bulk study was conducted by x-ray photoelectron spectroscopy, scanning electron microscopy, transmission electron microscopy and Raman spectroscopy. In addition, immersion calorimetry in polar and non-polar liquids, as well as dilute resins, is used to investigate fibre surface energies while temperature programmed desorption (TPD) is used to investigate adsorption of linear alcohols (C1 to C4) on the fibres. One of the main aims of the work is to understand the reaction mechanisms that take place between the surface oxygen functionalities on treated carbon fibres and the resin molecules that are used in forming composites.

UV/O$_3$ treatments were shown to produce significant levels of oxygen on the fibre surface. Anodic treatments did not alter the surface morphology, while UV/O$_3$ treatments were seen to increase surface areas six fold. Immersion calorimetry measurements showed similar trends to carbon black materials but, due to the small surface areas of the fibre (typically 1 m^2/g), the rush-in effect and heat of ampoule breakage was found to overshadow the signal from the fibre. TPD measurements showed that alcohol adsorption was considerably enhanced by the presence of surface oxygen. In addition a relationship between the acidity scale of the alcohols in the gas phase and the extent of their dissociative adsorption at room temperature was established. Overall this work has shown UV/O$_3$ to be a successful surface treatment method, superior to electrochemical treatments and TPD to be a promising method for investigating bonding.

Success is the ability to go from one failure
to another with no loss of enthusiasm.

Sir Winston Churchill

Acknowledgements

I first have to thank my supervisors; Professor Robert Bradley, Dr. Chaozong Liu and Professor Hicham Idriss for their support and guidance during my studies. I particularly wish to express my appreciation to Hicham and Chaozong for taking me on so late in my PhD and helping me get it all finished. I also wish to thank my industrial supervisors from Cytec Engineered Materials; Dr. Isabelle Ammar-Khodja, Dr Alex Baidak (both formally of Cytec) and Dr Steven Ward. Their help has been very useful and I am grateful for the funding that gave me this opportunity to undertake a PhD.

I also wish to thank the following people for their help during my studies:

Dr Aurik Andreu for teaching me how to use all the equipment and helping me keep it running.

Dr Steven Mitchell, Allan MacPherson, Andy Ross, Alan Owen, and Alan McLean for helping keep the lab open and working.

John Dickson and Bill Walker for their help in ordering all the strange things I needed.

Steven and Martin for making all the equipment and sample holders I asked for.

Dr Angela Kruth, from Aberdeen University and Dr Elizabeth Dawson from the University of Huddersfield for helping me so much with BET measurements.

The EPSRC equipment loan pool for the use of the Laser Raman microscope and Richard Brownsword for fixing it when it broke.

Petrena Morrison for her support and encouragement.

Martin Simpson and Rosie Mearns for their support and help organising my viva.

A great number of other people that have helped along the way.

And always Christopher, who puts up with so much.

Symbols and Acronyms

a_i	Number of electrons of a particular binding energy
A	Acid treated fibres
AES	Auger electron spectroscopy
AFM	Atomic force microscopy
A_i	Area under a desorption peak in a desorption spectrum for species, i
a_m	Mean cross-sectional area of a molecule
A_s	Adsorbent surface area
A_x	Cross-sectional area of the fibre
β	Heating rate of TPD system
b	Width of test composite used in 3/ 4 point bend test
B	Base treated fibres
BE	Binding energy
BET	Brunauer-Emmett-Teller
CA	Contact angle
CCD	Charge coupled device
CF_i	Correction factor for the desorption spectrum of a mass fragment, i, in TPD
CFRP	Carbon fibre reinforced plastic
CHA	Concentric hemispherical analyser
CVD	Chemical vapour deposition
$\delta\alpha$	Angle of entrance of electrons to a hemispherical analyser
ΔG^a	Free energy of adhesion
$\Delta_{imm}G$	Change in surface energy due to immersion in liquid
$\Delta_{imm}H$	Enthalpy of immersion
Δp	Change in pressure
d	Depth of immersion of fibre in liquid
d_{002}	Diffraction plane of the 002 crystal layer
D	Disorder peak in Raman
DCM	Dichloromethane
DDS	Curing agent
DMSO	Dimethyl sulfoxide
ε	Strain
E_y	Young's modulus
E	True energy of a peak in XPS analysis
E_a	Activation energy of adsorption in TPD
$E(B)$	Width in eV of the base of a peak in XPS analysis

E_b	Binding Energy
E_d	Activation energy of desorption in TPD
EDX	Energy dispersive x-ray microanalysis
EELS	Electron energy-loss spectroscopy
E_k	Kinetic Energy
F	Force
FAT	Fixed analyser transmission
F_m	Mass fragment yield of desorbing particle in TPD
F_o	Force acting on the fibre as it just touches the surface of a liquid
FRR	Fixed retard ratio
FTIR	Fourier transform infrared spectroscopy
FWHM	Full width half maximum
$FWHM_D$	Full width half maximum of D peak in Raman
$FWHM_G$	Full width half maximum of G peak in Raman
γ_{LV}	Surface free energy of the liquid/vapour interface
γ_{LV}^d	Dispersive component of the surface free energy of the liquid/vapour interface
γ_{LV}^p	Polar component of the surface free energy of the liquid/vapour interface
γ_S	Surface energy of a solid in vacuum
γ_S^d	Dispersive component of the surface free energy of a solid in vacuum
γ_S^p	Polar component of the surface free energy of a solid in vacuum
γ_{SL}	Surface free energy of the solid/liquid interface
γ_{SV}	Surface free energy of the solid/vapour interface
g	Acceleration due to gravity
G	Graphite peak in Raman
GC	Gas chromatography
G/L	Gaussian/ Lorenzian mix
G_m	Correction factor in TPD for electron multiplier gain
h	Planck's constant
H	Enthalpy
HM	High modulus
HOPG	Highly orientated pyrolytic graphite
HT	High (tensile) strength
I_D	Intensity of D band in Raman spectra of carbon materials
IFSS	Interfacial shear strength

I_G	Intensity of G band in Raman spectra of carbon materials
IGC	Inverse gas chromatography
I_λ	Intensity of the emitted light at wavelength λ
IM	Intermediate modulus
IUPAC	International Union of Pure and Applied Chemistry
I_x	Ionisation efficiency of desorbing particle in TPD
j	Total angular momentum
κ_{185}^{air}	The absorption coefficient of UV light in air at 185 nm
κ_{254}^{ozone}	The absorption coefficient of UV light in ozone at 254 nm
k	Boltzmann's constant
KE	Kinetic Energy
KM	Polyaromatic ether sulfone based thermoplastic
λ	Wavelength of light
l	Angular momentum
L	Path length of light
L_1	Length of the composite at the initial load
L_2	Length of the composite at the final load
L_1	Length of the defect free part of the layer in a graphitic system
L_2	The real length of the layer in a graphitic system
L_a	The coherent length of a structural unit in a graphitic system
L_c	The coherent height of a structural unit in a graphitic system
LM	Low modulus
lpm	Litres per minute
MW	Molecular weight
MWNT	Multi-walled carbon nanotubes
MY	Type of epoxy resin
m/z	Mass to charge ratio of an ion
v	Pre-exponential factor of desorption in TPD
v_D	Frequency of D peak in Raman
v_G	Frequency of G peak in Raman
n	Principle quantum number
N	The number of layers in the stack in a graphitic system
N_T	The total number of adsorption sites on the adsorbent
N	Number of adsorbed molecules
n_{air}	Molecular concentration of air
N_a	Avogadro's number
N/C	Nitrogen to carbon ratio

n_e	Number of electrons in a molecule
$\dot{n}_\lambda$	Flux of photons of wavelength λ
n_m	Monolayer capacity, amount of adsorbate required to completely cover the surface of 1g of solid with one layer of molecules
n_{ozone}^{eq}	Molecular concentration of ozone at equilibrium
N_S	The number of surface sites occupied by the adsorbate
O/C	Oxygen to carbon ratio
φ	Work function
p	Pressure
P_1	Initial load on composite
P_2	Final load on composite
PAN	Polyacrylonitrile
P_b	Breaking load of test composite used in 3/ 4 point bend test
PES	Polyaromatic ether sulphone
p_f	Perimeter of fibre in Wilhelmy Plate method
p_o	Saturation vapour pressure of the adsorptive
PY	Type of epoxy resin
q_1-q_L	Net heat of adsorption
Q_{diss}	Gas-phase dissociation energy
q_i	Sensitivity factor for XPS to account for interaction cross sections and instrumental factors
ρ	Density of liquid
ρ_f	Fibre density
r	Interatomic spacing
R	The universal gas constant
R_0	Radius of the median equipotential surface in the CHA
R_1	Radius of the inner hemisphere in the CHA
R_2	Radius of the outer hemisphere in the CHA
σ	Tensile strength
σ_S	Interlaminar shear strength
σ_u	Ultimate tensile strength
s	Spin quantum number
S	Pumping speed of TPD system
SEM	Scanning electron microscope
S/N	Signal to noise ratio
STEM	Scanning transmission electron microscope
STM	Scanning tunnelling microscope

STP	Standard temperature and pressure conditions
θ	Surface coverage of the adsorbate on the adsorbent
θ_a	Contact angle of advancing fibre in Wilhelmy Plate method
θ_m	Measured angle formed between the liquid drop/ vapour interface and the solid surface in contact angle experiments
τ	Characteristic pumping speed of TPD system
t	Thickness of test composite used in 3/ 4 point bend test
T	Temperature
T_m	Correction factor in TPD for quadrupole transmission
TEM	Transmission electron microscopy
T_p	Temperature of the peak of maximum desorption in TPD
TPD	Temperature programmed desorption
υ	Frequency of x-rays
U	Internal energy
UHM	Ultra-high modulus
UST	Untreated carbon fibres
UV/O_3	Ultraviolet ozone treatment
V	Volume
V_1	Voltage of inner hemisphere in the CHA
V_2	Voltage of the outer hemisphere of the CHA
V_f	Volume fraction, volume of carbon fibres used in a composite
V_{mol}	Molar volume
V_m	The monolayer capacity as a volume
VOC	Volatile organic compound
W_1	Width of entrance slit in the CHA
W_2	Width of exit slit in the CHA
XPS	X-ray photoelectron spectroscopy
XRD	X-ray diffraction
Y	The relative yield of a desorbed species in TPD

Contents

1 Introduction

1.1 Introduction

In the manufacturing industry, there is often a large demand for materials which possess a high degree of strength but which are also lightweight. Carbon fibres can provide this as they have a strength to weight ratio 15 times higher than steel and have the added advantages that at normal temperatures they behave elastically until failure, and are chemically inert [1,2]. Unfortunately, they are also very brittle (i.e. allow propagation of cracks). This means that in order to make use of the high strength, it is necessary to introduce the fibres into a matrix of different mechanically tough material [2].

A prime example is carbon fibre reinforced plastic (CFRP) which is very light and stiff and therefore much used in aerospace construction. The mechanical properties of such a composite depend not only on the properties of the fibres and the matrix, but also on how well the fibres attach to the matrix and thus how well stress transfers between the two [3]. It is known that two factors affect this process: chemical bonding and physical interactions, typified by mechanical 'keying together' of the matrix and the fibre surface [4,5]. The mechanical process is well understood and is dominated by fibre surface roughness effects. However few, if any, detailed models exist which directly relate the overall interfacial chemical interactions (i.e. covalent, ionic and van der Waals) to the composite properties. Neither have detailed attempts been made to identify key specific interfacial interactions for specific fibre-matrix pairs i.e. to design fibre surface chemistry to interact with specific matrix compounds. Table 1.1 lists some of the characterisation techniques available to investigate the fibre-matrix interface. This chapter gives background information on carbon fibres, surface treatments, composites, and previous work relevant to this thesis.

Table 1.1 Characterisation Techniques (after [6]**)**

Technique	Acronym	Informs
X-ray Photoelectron Spectroscopy	XPS	Surface chemistry (including bonding)
Scanning Electron Microscopy	SEM	Surface topography
Immersion Calorimetry		Surface energy
Atomic Force Microscopy	AFM	Topography, chemical and mechanical properties
Contact Angle	CA	Surface free energy, hydrophilic/ hydrophobic nature, acid-base interactions
Transmission Electron Microscopy	TEM	Atomic structure
Electron Energy-Loss Spectroscopy	EELS	Surface chemistry and structure
X-ray Diffraction	XRD	Atomic structure and crystalline orientation
Raman Spectroscopy		Surface chemistry and structure
Fourier Transform Infrared Spectroscopy	FTIR	Chemical species
Auger Electron Spectroscopy	AES	Elemental composition
Scanning Tunnelling Microscopy	STM	Topography
Brunauer-Emmett-Teller adsorption	BET	Surface areas and porosity
Boehm Titrations		Surface chemistry

1.2   Carbon Fibres

1.2.1   Carbon

Carbon, with its atomic number of 6, has a ground-state electron configuration of $1s^2$, $2s^2$, $2p^2$ which allows it to bond with many other elements as well as itself in a variety of arrangements [1]. The properties of a carbon material depend on the bonding type. Well known configurations of carbon include diamond and graphite. The high level of allotropy exhibited in carbon can be explained by hybridisation theory. Three types of hybridised orbitals exist, generated by promotion of an electron from a 2s orbital to a 2p orbital before hybridisation. The bond types are sp^3, sp^2 and sp, describing single (σ), double (π, σ)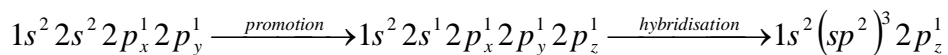 and triple (π_y, π_z, σ), bonds, respectively. In diamond, the hybridization follows Equation 1.1 [1]. The four sp^3 bonds form a non-planar crystal network and the structure is known to be extremely strong and isotropic. Graphite, on the other hand, follows Equation 1.2, producing three sp^2 bonds and one pure 2p orbital. Each carbon in the ring is bonded to three other carbons by the overlap of sp^2 bonds and the remaining p orbital forms a shared π bond. The carbon forms planar layers of hexagonal rings, the layers being held together by weak van der Waal forces that can slip over each other giving graphite its well known lubricating properties [1]. The dissociated π electron also gives graphite high electrical conductivity. Graphite has the highest level of anisotropy known in nature [1].

Equation 1.1

$$1s^2 2s^2 2p_x^1 2p_y^1 \xrightarrow{\quad promotion \quad} 1s^2 2s^1 2p_x^1 2p_y^1 2p_z^1 \xrightarrow{\quad hybridisation \quad} 1s^2 \left(sp^3\right)^4$$

Equation 1.2

$$1s^2 2s^2 2p_x^1 2p_y^1 \xrightarrow{\quad promotion \quad} 1s^2 2s^1 2p_x^1 2p_y^1 2p_z^1 \xrightarrow{\quad hybridisation \quad} 1s^2 \left(sp^2\right)^3 2p_z^1$$
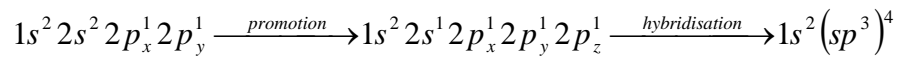
Graphite has a hexagonal unit cell containing 4 atoms with the dimensions $c = 671$ pm and $a = 246$ pm. In Figure 1.1, the unit cell atoms are labelled A, A', B, and B'. The *A* atoms have neighbouring atoms directly above and below them on

3

adjacent layers while the *B* atoms only have neighbouring atoms in the next layer above or below them, 671pm away [7].
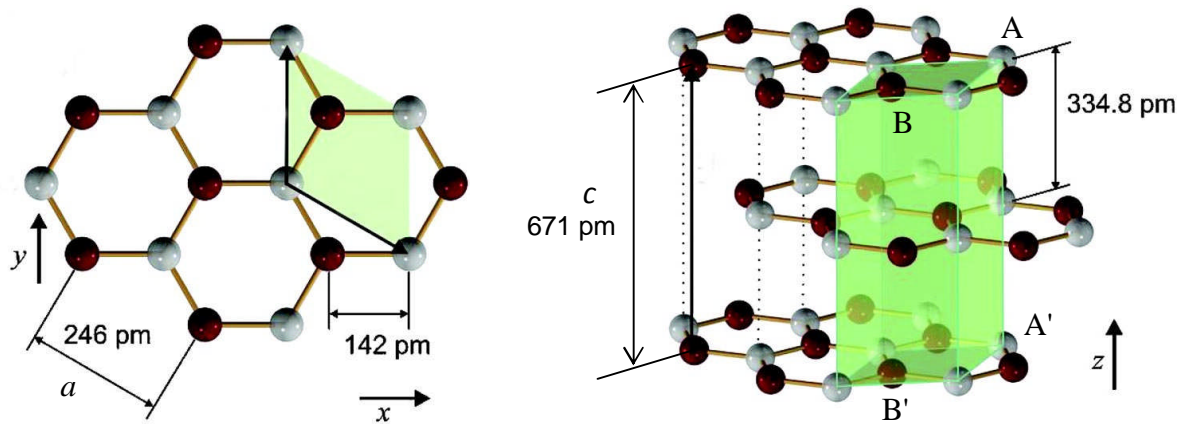
Figure 1.1 Structure of graphite [8]**.**

Carbon black and carbon fibres are considered turbostratic forms of graphite. Turbostratic forms of graphite are made from stacks of graphite layers which are roughly parallel and equidistance, with interlayer spacing no less than 344 pm but which are orientated randomly to the normal layer [1]. Some carbon materials can be graphitized from this state by heating.

Carbon fibres consist of long winding ribbons of sp^2 hybridized six-membered carbon rings, held together by defects (i.e. some sp^3 hybridized bridging bonds) in the chain [9,10]. These defective layers are generally known as graphene [2]. The filaments of carbon are arranged in a regular but non-graphitized state [1].

1.2.2 Precursors and Fibre Production

There are three main precursors of carbon fibres for manufacture; pitch, cellulose, or Polyacrylonitrile (PAN). PAN-based fibres are currently the most popular due to the relative ease of manufacture [1,11].

The three main steps to produce a PAN fibre from a precursor are: spinning the PAN, stabilisation of the PAN into a condensed heterocyclic ring structure and carbonisation via high temperature heat treatment [11]. Figure 1.2 shows a

schematic of the process [12]. The PAN is first spun and stretched into a fibre. This helps to align the polymer molecules along the axis. The polymer is then stabilised by heating in an oxidizing atmosphere. The PAN is heated to 200-300 ^{o}C for 1-2 hours while being kept under tension to maintain alignment along the fibre axis and to prevent shrinkage. The ladder polymers are then carbonized by heating to high temperatures of between 1000 to 1500 ^{o}C for ~ 5 minutes. This removes hydrogen and nitrogen from the fibres leaving relatively aligned graphitic ribbons. Further heat treatment of the fibres at this stage up to temperatures of approximately 3000 ^{o}C causes the ribbons to further align, i.e. the fibre graphitizes [12]. Fibres can be aligned to produce a required Young's modus by careful choice of the graphitization heat [12,13].
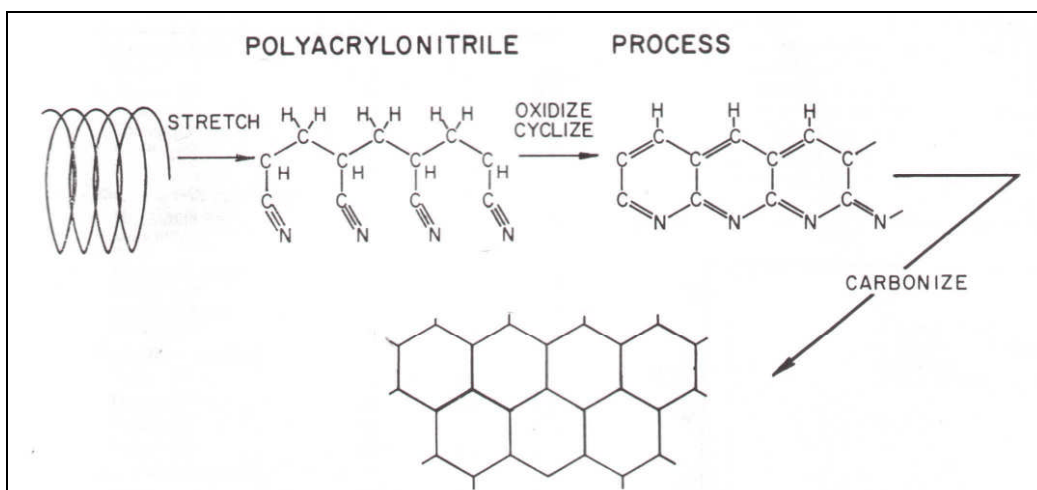
Figure 1.2 Polyacrylonitrile fibre production process [12]**.**

There are several methods available to spin polymer fibres, however wet spinning is the standard for PAN fibres [5]. In this method, a highly concentrated solution of polymer in, for example, a dimethylacetamide solvent is extruded into a coagulation bath via a multi-holed spinneret. The coagulation bath forces the polymer to precipitate in thin strands by extracting the solvent as the polymer is forced out of the small spinneret holes. The fibres are then washed before further processing [5]. The spinning process affects the fibre shape, size, morphology and texture. For example, the extraction rate can cause concentration gradients to occur in the coagulation bath resulting in non-circular fibre cross-section. Flaw

5

development is also influenced by the extraction rate [14]. Figure 1.3 shows an example wet spinning system.
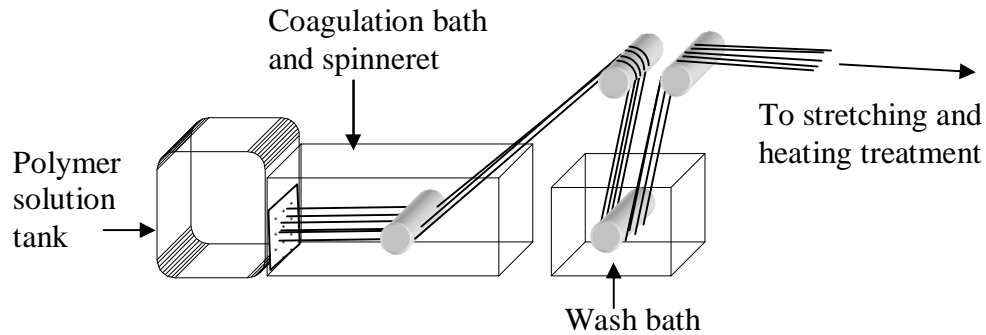
Figure 1.3 Wet-spinning and washing set up for PAN fibres (after [14])**.**

1.2.3 Fibre Characterisation: Structure and Strength

Carbon fibres have been classified by the International Union of Pure and Applied Chemistry (IUPAC) into five types [15]. These are listed in Table 1.2. Previously fibres were classified into two main groups; Type I and Type II; high modulus and high strength respectively although this classification has become redundant as the range of fibres has increased to meet demand for specific characteristics [16].

Table 1.2 Fibre Classification [15,17]

Classification	Acronym	Young's Modulus (GPa)	Tensile strength
Ultra-high modulus	UHM	> 600	
High modulus	HM	> 300	Strength to stiffness ratio < 1 %
Intermediate modulus	IM	~275 to 350	Strength to stiffness ratio > 1 %
Low modulus	LM	As low as 100	Low strength
High strength	HT	150 to 300	Strength to stiffness ratio ~1.5 to 2 %

A carbon fibre may be thought of as a composite system, built up of anisotropic units [12]. Therefore the strength of the fibre will be dependent on the axial and radial textures and gradients as well as intra-bonding and surface flaws [12,13]. The structures of various commercially available carbon fibres and precursors have been investigated in the literature using several techniques including transmission electron microscopy [12,18-20], x-ray diffraction [21-23] and scanning electron microscopy [24]. Several models for the macro-structure of fibres have been proposed based on the images acquired [16]. The current favoured description of HT PAN-based carbon fibre texture is summarised in the model proposed by Bennett *et al.*, in 1976, shown in Figure 1.4 [16,25]. There exists a difference in cross-sectional structure between the core of the fibre and the outer layers, i.e. a skin. The graphene layers in the skin are generally aligned and parallel to the surface of the fibre whereas the core shows a turbostratic texture [1,5,25]. The heterogeneity can be due to the heat of the graphitization treatment, heat gradients through the fibre during carbonization, and differences in the stretching force felt by the skin compared to the core [5].
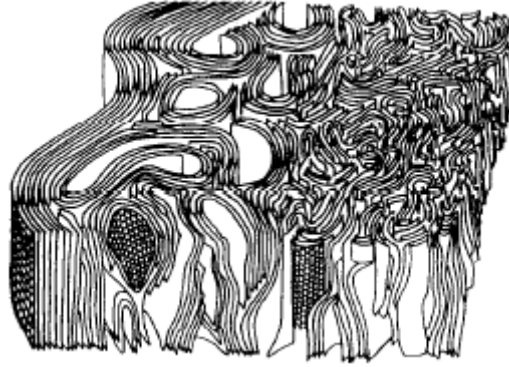
Figure 1.4 Structural model for HT PAN-based carbon fibres showing a skin-core heterogeneity (from reference [5]).

The micro-structure of all graphitic carbons can be described by the following parameters which are shown graphically in Figure 1.5 [1]:

1. The length of the defect free part of the layer (L_1)

2. The real length of the layer (L_2)

3. The number of layers in the stack (N)

4. The coherent length (L_a)

5. The coherent height (L_c)

L_a and L_c define the coherent domain. These parameters can be retrieved from TEM images or x-ray diffraction. Also of interest is the mean interlayer spacing of the (002) basal planes (d_{002}) which is also accessible from TEM or x-ray diffraction. The d_{002} interlayer spacing is used as a means to compare the relative degree of graphitization in a material although it has never been successfully related to it directly [1].

 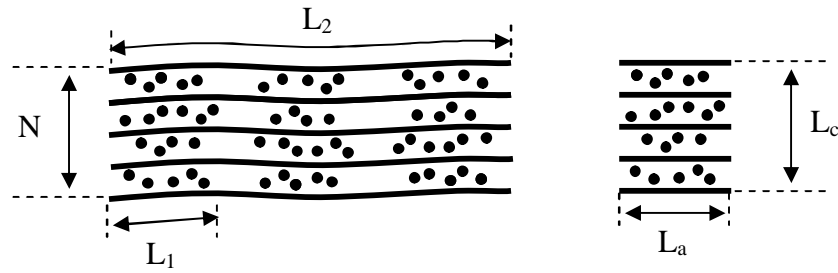
L2
N
L1
Lc
La

Figure 1.5 Paracrystalline structure of graphitic carbons showing the length of defect free layer (L_1), the real length of the layer (L_2), the number of layers in the stack (N), the coherent length (L_a) and the coherent height (L_c) (after [1]**).**

The high specific strength of carbon fibres is due to the layers of graphene ribbons tending to lie parallel to, but not always flat along, the fibre axis [5]. The graphene layers have the highest elastic modulus known in nature due to the covalent bonds being the shortest known to exist in a plane [1]. The high strength, toughness, and low density of carbon fibres compared to traditional engineering materials make them very attractive for manufacturing. In addition, they also benefit from being very inert to most chemicals and low oxidising atmospheres, have high thermal and electrical conductivity, and do not change with reasonably high temperatures [5]. Unfortunately disadvantages include low compressive strength, low impact strength, low elongation ratio to fibre axis, and high manufacturing costs [5]. Fibres are generally used in composites as will be discussed in Section 1.4 although activated carbon fibres (fibres with large surface areas and pores) are increasingly being used for filtration, and catalyst support among other applications [13].

The fibre's tensile strength is equivalent to the stress at which it breaks and is dependent on the frequency and severity of flaws within the fibres. The observed strength of the fibres is therefore seen to be the strength of the weakest, most flawed part of the fibre [14]. The tensile modulus, known as Young's modulus or the stiffness, is the ratio of the stress to strain applied to the fibre and is dependent on molecular order of the fibre [2]. Macroscopic flaws result from impurities incorporated into the fibre, surface damage or large voids created during the manufacturing process. Microscopic flaws are more difficult to

quantify but have been attributed to misalignment of the stacks of graphene (or crystallites) which interlink to create voids [14]. Highly ordered fibres show more sensitivity to crystallite misalignment so fibres with high moduli are more likely to have flaws and low tensile strength. Thus it is difficult to optimise the tensile strength and modulus of fibres at the same time [14].

1.2.4 Safety

A study into the effects of carbon fibre dust on rats has been undertaken by Zhang *et al.,* [26]. Rats were dosed with either carbon fibre dust or a control substance. Control substances included saline, TiO_2 (a biologically inert dust) and quartz (a known toxic dust). The weight of the rats' lungs was compared as well as the presence and morphology of macrophages. The carbon fibre dust showed similar effects to TiO_2 and the authors concluded that the experiments showed little evidence of toxicity in lungs due to carbon fibre dust [26]. Fibres and dust still act as an irritant if inhaled or contacted with the skin but this is a minor problem for an otherwise useful material.

1.3 Carbon Black

Carbon black is another common type of carbon that is used in composite systems to alter the mechanical properties of materials, such as in car tyres [1]. The term carbon black is a generic name which covers many colloidal spherical carbons and their aggregates when the aggregates are less than 1000 nm [1,17]. Carbon blacks are formed by thermal decomposition or incomplete combustion of carbon and hydrogen based compounds [17]. Carbon black has a concentric texture, the structure of which is determined by the growth temperature. The structure can be categorised into one of four groups: isometric turbostratic, columnar turbostratic, large distorted layered or large straight layered. The latter two groups are fairly self explanatory. In isometric turbostratic carbon blacks the coherent domain is symmetric, i.e. $L_a \approx L_c$ while for columnar turbostratic $L_a <L_c$ [1]. Figure 1.6 shows an example of each structure.
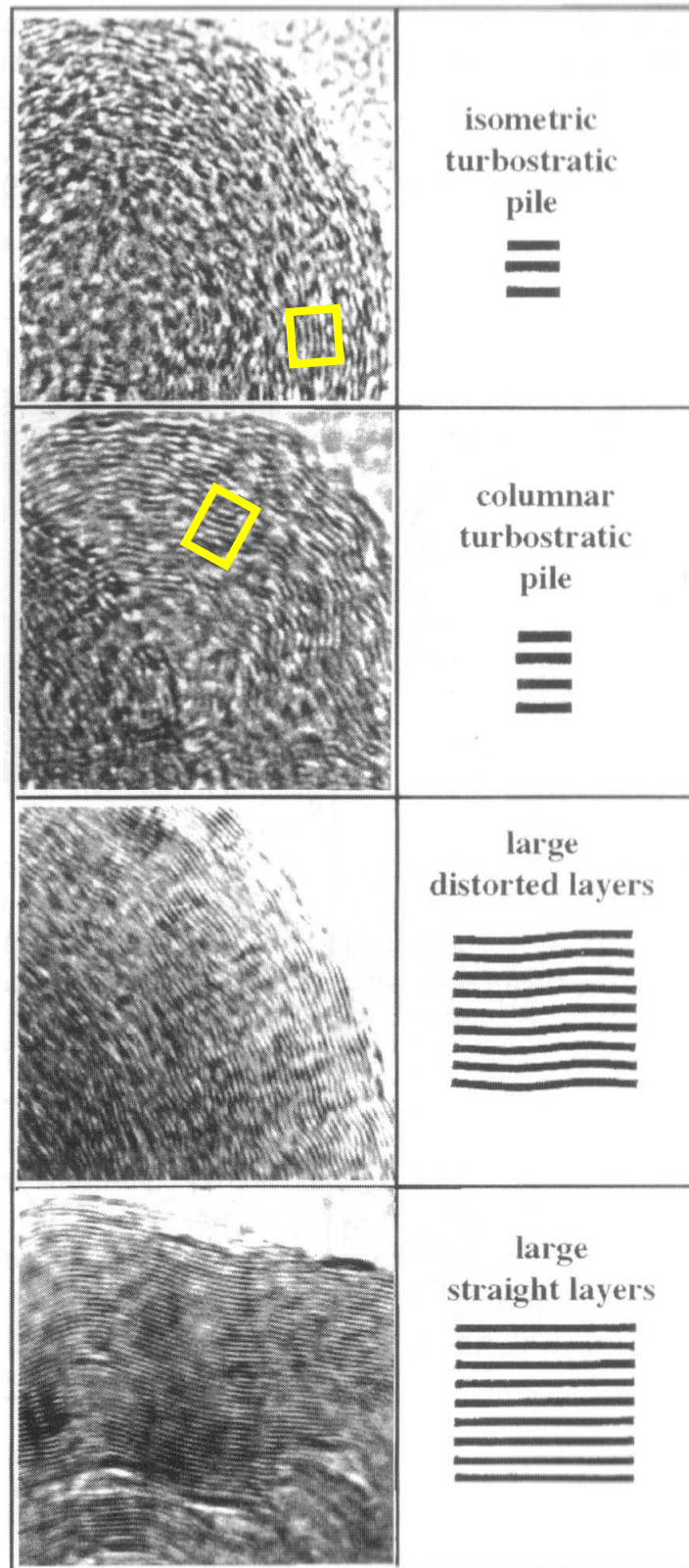
Figure 1.6 Types of carbon black structure [1]**. The coherent domain in the isometric turbostratic pile and the columnar turbostratic are highlighted. Isometric turbostratic piles have symmetric coherent domains while columnar piles have elongated coherent domains.**

1.4 Composites

1.4.1 Introduction

A composite is a material consisting of more than one phase, formed by the artificial blending of two or more different materials [5]. It should encompass significant properties of the constituent materials such that the final composite will display significant improvements in characteristics compared to the individual components [27]. Carbon fibres can be created in either long, continuous tows (i.e. in long lengths) or as short discontinuous fibres to form a variety of classes of composite, as Figure 1.7 shows [5,27]. Fibres are used to reinforce metals, carbons, cements and ceramics as well as polymers [5,13]. This section discusses carbon fibre reinforced plastics (CFRP) as used in the aerospace industry.
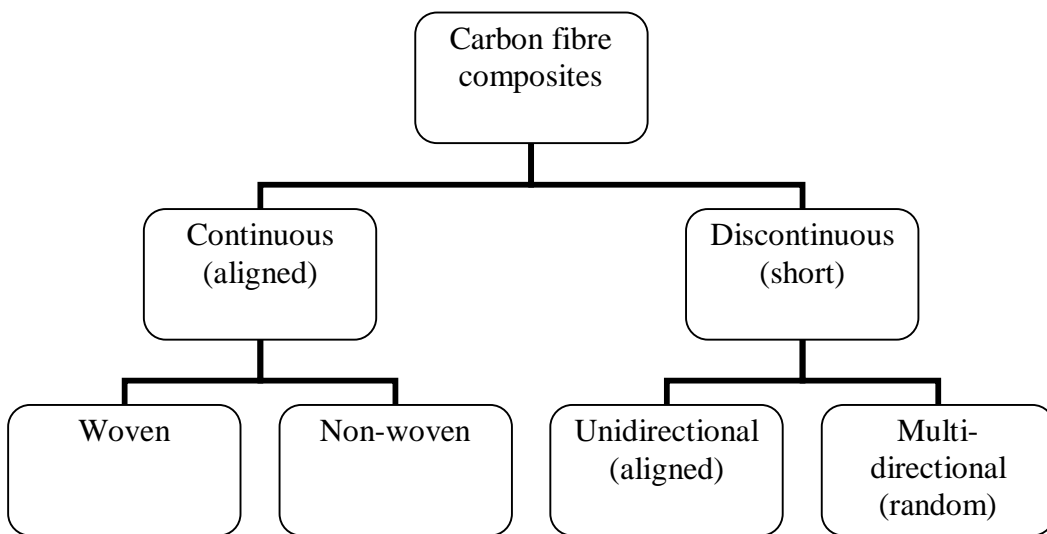
Figure 1.7 Classification of carbon composites types (after [27]**).**

1.4.2 Resins Matrices

The most common matrices used for CFRP are thermosetting polymers, particularly epoxy resins [5,28,29]. Fibres set in thermosetting plastics are known as thermoset composites. The popularity of epoxy resins for CFRP used in the aerospace industry is due to their low cost, low processing temperatures, good adhesion, good mechanical properties, low shrinkage during curing, lack of volatile solvents and low creep [5,30]. Epoxies can also cross link with many

different amines, anhydrides and acids as well as many other polymers [29]. Figure 1.8 shows the epoxide functional group. An epoxy resin normally contains two or more epoxide groups [5].
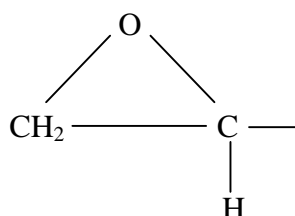
Figure 1.8 Epoxy functional group in the epoxy resin.

In order to harden a thermosetting epoxy resin, it is normal to apply heat and pressure to complete polymerisation and create cross-linking between epoxy and hydroxyl groups [5]. To aid this, a cross linking agent and/ or a catalyst is added to the resin. Figure 1.9 shows an example cross linking event between epoxy molecules and a cross linking agent (ethylene diamine). The epoxide group undergoes ring scission upon a nucleophilic addition of the amine groups [5].
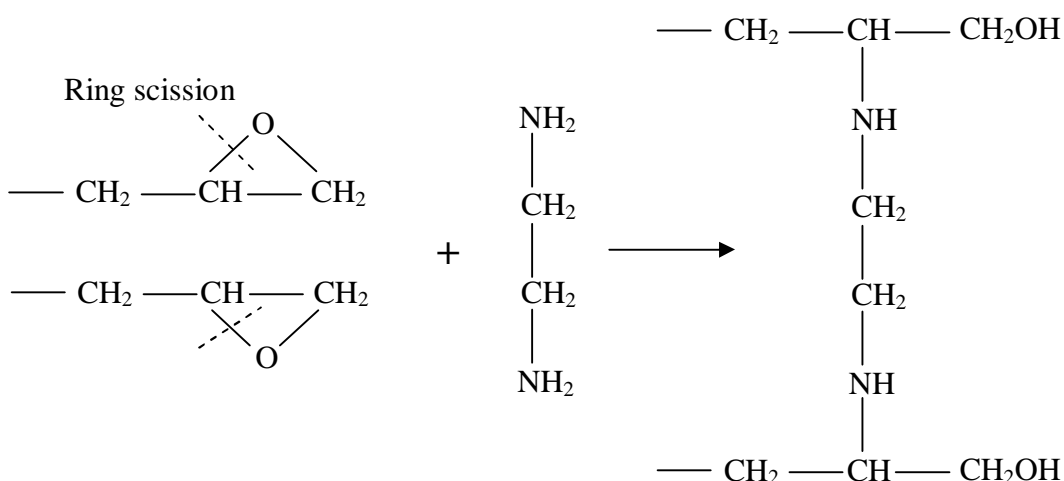
Figure 1.9 Cross linking event in epoxy resins [5]**.**

Thermoplastic composites, i.e. composites made with fibres set into thermoplastic resins, are becoming more common as they have two main advantages over thermoset composites which are: lower manufacturing costs and

better performance [5]. Thermoplastic composites perform better, in that they are less easily damaged than thermosets (increased toughness), are more ductile, and can withstand high temperatures. Thermoplastics cost less to produce because they [5]:

1. do not need to be cured

2. have unlimited shelf-life

3. can be reprocessed (i.e. repaired or recycled)

4. have less health issues associated with the processing chemicals, and

5. have low moisture content.

Disadvantages include limitations in processing methods, high processing temperatures being required, and high viscosity at room temperature [5]. Thermoplastic polymers have also been shown to adhere less well to carbon fibres than thermosetting polymers, although neither adheres well to untreated fibres as will be discussed in Section 1.6 [29]. The difference in adhesion is evident from SEM images of failed composites which show a layer of polymer on the fibres for thermoset matrices but not for thermoplastic matrices, and from mechanical testing of composites [31].

The exact nature of the resin matrix used in commercial production is proprietary knowledge. Different epoxies can be blended as well as different curing agents and catalysts used depending on the end use for the composite [32,33].

1.4.3 Manufacture of Composites

Using fibres in polymer matrices results in increased impact strength and facture toughness for the composite [28]. Composites are manufactured by different methods depending on the fibre type. Short fibres can be used with liquid resin to form a slurry before being moulded into the desired shape and hardened. They can also be formed into a mat or yarn before being impregnated with resin. Or yarns can be formed using short carbon fibres and short thermoplast fibres which

melt upon application of heat and pressure to form the composite [5,27]. Since fibres are electrically conducting, short fibres can be aligned in a composite by applying an external electric field. Continuous fibres are normally made into unidirectional tapes or woven fabrics before being impregnated with resin. In the case of the skins used for aircrafts, the impregnated tapes or fabrics are bag moulded, where a high pressure gas or a vacuum is applied to the impregnated tapes/ fibres via a bag while they are held in a die [5,27].

1.4.4 Strength of Composites

When a load is placed on a composite, the energy can be dissipated by two routes; the plastic matrix can absorb the force by deformation or the carbon fibres can separate from the matrix [2]. Thus, the strength of the composite depends on several factors [2]:

1.   The fibre strength and elasticity
2.   The matrix strength and elasticity
3.   The fibre-matrix interface and therefore the interfacial bonding and
4.   The volume of fibres used in the composite (known as the volume fraction V_f).

If a fibre is bonded weakly to the matrix, the resulting composite will have relatively low strength and stiffness as the applied stress can be absorbed through debonding. Strong interfacial bonding results in composites that will be strong and stiff but also brittle as there will be no mechanism to dissipate the applied force.

The strength of the composite can be tested using a 3-point or 4-point bend test; i.e. the composite test piece is placed on two stationary points and a third applies a force in the centre of the test piece to force it to bend. A set of regular shaped test pieces can be prepared from the composite. Equation 1.3 shows the calculation for determining interlaminar shear strength (σ_S, in Pascal) where P_b is the breaking load in Newtons, b is the width and t the thickness of the test pieces [2]. This assumes the failure occurs parallel to the fibre axis.

Equation 1.3

$$\sigma_S = \frac{0.75P_b}{bt}$$

The tensile strength, strain and modulus can be tested by applying a load parallel to the fibres. Varying the load and measuring the resulting change in length of the test specimen allows calculation of Young's modulus (E_y) as described by Equation 1.4, where σ is the tensile strength, ε is the strain, L_1 is the length of the composite at the initial load, P_1, and L_2 is the length of composite at the final load, P_2 [2].

Equation 1.4

$$E_y = \frac{\sigma}{\varepsilon} = \frac{P_2 - P_1}{bt} \times \frac{L}{L_2 - L_1}$$

Applying a load (P) to the test piece until failure allows calculation of the ultimate tensile strength (σ_u) using Equation 1.5 [2].

Equation 1.5

$$\sigma_u = \frac{P}{bt}$$

1.4.5 The Fibre- Matrix Interface

As mentioned above, the interfacial bonding between the fibre and the matrix is important for the end composite strength. Chapter 1.5 discusses some of the theories behind the bonding and adhesion that occurs between the fibre and the matrix. It is first important to define the interface where these interactions are taking place. Figure 1.10 shows a schematic of the fibre-matrix interface. Region A is a layer of functional groups on the surface of the fibre, B is the size, and C is a region of the matrix different in structure to the bulk of the matrix in region D

[34]. Size is normally a thin organic compound applied to fibres to aid handling and is discussed further in Section 1.6.5.
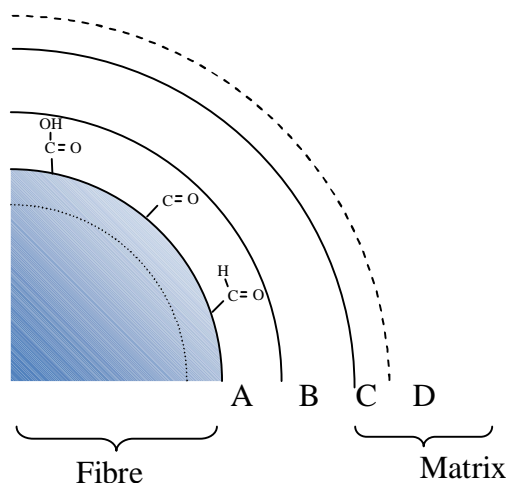
Figure 1.10 Fibre-matrix interface (after [34]**). See text for definitions of regions.**

1.5 Adhesion Theories

1.5.1 Introduction

There have been several theories proposed to explain and predict adhesion. Traditionally the main four were mechanical, adsorption, diffusion and electrostatic theory [36]. In mechanical theory, the physical roughness of the surface causes interlocking. In adsorption, the matrix molecules adsorb onto the surface. Diffusion theory considers the interface to be eliminated by the adhesive molecules diffusing into the substrate while electrostatic theory considers the two materials to be held together by electrostatic forces [36]. More recently, other theories have been put forward. Table 1.3 summarises the current theories and the scale on which they act. Adsorption theory is considered the most applicable to real systems but generally a mix of mechanisms may be responsible for the adhesion [35,36].

Table 1.3 Theories of adhesion (after [36]**)**

Scale of interaction	Adhesion theory
Macroscopic	Electrostatic
Microscopic	Mechanical interlocking
Molecular	Diffusion
	Wettability
	Adsorption
	Weak boundary layer
	Acid- base
Atomic	Chemical bonding

The adhesion between carbon fibres and resin matrices is known to improve with surface treatments on the fibres as will be discussed in Section 1.6, but the exact reason for improvement is still under debate and is very much still being investigated [29]. For example, recently Zaldivar *et al.,* examined the adhesion between plasma treated PAN-based carbon fibres and an epoxy-thermoplastic resin [37]. XPS, AFM and SEM measurements showed the mechanical interlocking contribution to be significantly less than the chemical effects [37]. This section will outline the two adhesion mechanisms relevant to this work; namely wetting, and adsorption.

1.5.2 Wetting

In order to obtain the highest probability of bonding, the contact between the liquid resin and the fibre surface should be maximized, i.e. the surface should be easily wetted and voids avoided [38]. Increasing the surface energy of the fibre increases the wettability and therefore much work has been done into measuring the surface energy of fibres.

Traditionally, surface energies are measured using contact angle methods where a drop of liquid of known surface tension (energy) forms an interface with a solid

[39]. The resulting angle between the liquid surface and the solid surface can be used to calculate the surface free energy of the solid using the well known Young's equation shown in Equation 1.6.

Equation 1.6

$$\gamma_{SV} = \gamma_{SL} + \gamma_{LV}\cos\theta_m$$

Where γ_{SV} is the surface free energy of the solid/vapour interface, γ_{SL} is the surface free energy of the solid/liquid interface, γ_{LV} is the surface free energy of the liquid/vapour interface and θ_m is the measured angle formed between the liquid drop/ vapour interface and the solid surface.

The change in free energy per unit area when two bodies of differing material, i.e. a solid and liquid, are brought together reversibly is known as the free energy of adhesion (ΔG^a). It can be calculated using the Young-Dupré equation shown in Equation 1.7 [40].

Equation 1.7

$$\Delta G_{SL}^a = -\gamma_{LV}\left(1 + \cos\theta_m\right)$$

Contact angle analysis is not straight forward for fibres due to their curved surface and size [41]. The most appropriate method for contact angle analysis on fibres is the Wilhelmy Plate method [42]. The fibre is suspended from a microbalance and the force acting on the fibre as it just touches the surface of the liquid (F_o) is measured. The contact angle of the advancing fibre (θ_a) can be calculated using Equation 1.8, where p_f is the perimeter of the fibre. As the fibre submerges deeper into the liquid, a buoyancy force counteracts the surface tension. The buoyancy force is accounted for in Equation 1.9, where ρ is the density of the liquid, g is the acceleration due to gravity, A_x is the cross-sectional area of the fibre and d is the depth of immersion. Plotting a graph of F against d, and extrapolating back to zero depth gives the contact angle for the surface. The fibre can also be pulled out of the liquid and a receding contact angle measured in a similar fashion [42].

Equation 1.8

$$F_o = p_f \gamma_{LV} \cos\theta_a$$

Equation 1.9

$$F = p_f \gamma_{LV} \cos\theta_a - \rho\, g\, A_x\, d$$

Even the Wilhelmy plate method is not ideal for fibres as it requires highly sensitive balances and the fibre perimeter is normally assumed to be circular which is not always the case. Measurements of several fibres would be required to get an average and the measured angle can often vary due to the chemical heterogeneity on the fibre surface. In the literature, other methods have been proposed to look at fibre surface energy and are discussed in Section 1.7.4.

1.5.3 Adsorption

Adsorption is defined as the enrichment of a surface (the substrate) with one or more components (the adsorptive). Molecules of gas or liquid adsorbed on the surface are referred to as the adsorbates. [43-45]. **Ad**sorption should not be confused with **ab**sorption, where molecules enter the bulk of the solid. Equation 1.10 defines the fractional coverage (θ) for the adsorbate, where N_S is the number of surface sites occupied by the adsorbate and N_T is the total number of adsorption sites on the adsorbent. When $\theta = 1$, the level of adsorption is referred to as a monolayer [46].

Equation 1.10

$$\theta = \frac{N_S}{N_T}$$

If a molecule adsorbs on a surface without fragmentation it is known as associative (or molecular) adsorption. When fragmentation occurs the adsorption is referred to as dissociative [46]. Adsorption is a spontaneous process that

occurs due to unbalanced attractive forces that exist in the surface molecules of a solid. The gas or liquid molecules which adsorb on the surface help to rebalance the forces [44]. The adsorbate has less freedom when adsorbed to the surface than when in the adsorptive phase, resulting in a decrease in entropy and a decrease in the free energy of the system. Thus adsorption is usually exothermic [44,47]. Adsorption can be broadly classified into two types; chemisorption or physisorption, depending on the magnitude and origin of the attractive forces.

Physisorption involves weak intermolecular forces (such as van der Waals forces) acting between the adsorptive and the adsorbent [44-46,48]. Van der Waal forces are caused by a combination of forces arising from molecules with permanent dipoles (Keeson forces), dipoles induced by molecules with permanent dipoles via polarisation (Debye forces), and forces from dipoles induced instantaneously by the motion of the molecule's electrons (London forces) [49]. There is not a significant change in the electron orbital patterns and any redistribution of electron density within the adsorbate and the adsorbent occurs separately [45,46]. The process of physisorption is analogous to the condensation of a liquid and the heat of adsorption for a physisorption process is of the same order as the heat of condensation (< 35 kJ/mol) [44,46]. Figure 1.11 shows the potential energy diagram for a physisorbed inert atom or molecule on a surface [48]. A useful example of physisorption is that of nitrogen or krypton at 77 K adsorbed onto a carbon surface which can be used to determine the surface area of the sample, as will be discussed in Section 1.7.3.
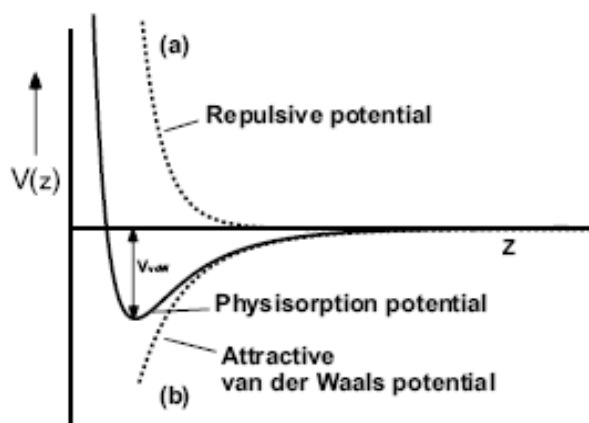
Figure 1.11 One dimensional potential energy diagram for the physisorption of a neutral atom or molecule on a surface. The contributing repulsive and attractive potentials are shown by dashed lines [48]**.**

Chemisorption on the other hand involves the overlap of one or more electron orbitals between the adsorbate and the adsorbent [48] i.e. a monolayer of a specific chemical compound is formed on the surface of the adsorbent [46]. The heat of adsorption is generally greater than 35 kJ/mol. Figure 1.12 shows the potential energy diagram for a diatomic molecule which chemisorbs dissociatively to a solid surface [48]. In the diagram, E_b is the binding energy of the dissociated atoms chemisorbed to the surface, E_d is the activation energy of desorption, E_a is the activation energy of adsorption, Q_{diss} is the gas-phase dissociation energy. As the molecule approaches the surface, it experiences van der Waal attraction forces leading to a precursor state where the molecule is physisorbed. As the distance, z, decreases to z', the molecule's electron orbitals overlaps with that of the surface's orbitals leading to a redistribution of electron density in both materials which causes the cleavage of the molecule. The two atoms can then chemisorb to the surface if they have enough energy to overcome the activation energy (E_a). Since E_a is much smaller than Q_{diss}, dissociation is much more likely to occur at the surface than in the gas phase [48]. Note that a molecule can be trapped in a molecular adsorption form as it needs to cross an activation barrier before being dissociated. Electron-electron repulsions are the reason for the increase in the potential again when the molecule or atom are too close to the surface. The balance between attraction and repulsion result in the formation of the equilibrium distance.
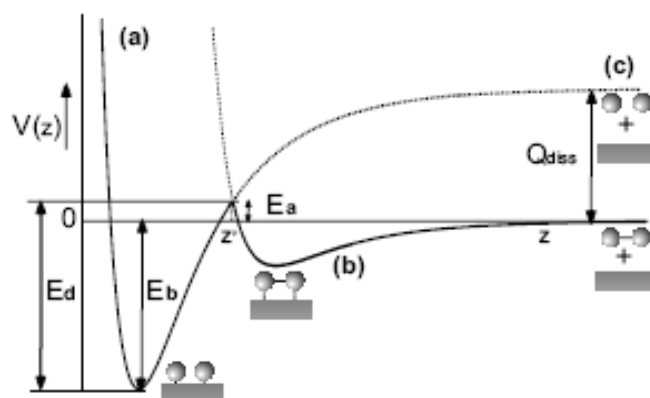
Figure 1.12 One dimensional potential energy diagram for the dissociative chemisorption of a neutral diatomic molecule on a surface (solid line in curve a) [48]**. Curve a is a combination of the potential energy for the physisorption of an undissociated molecule (curve b) and the potential energy for two dissociated atoms chemisorbed to the surface (curve c).**

Chemisorption can be used to investigate the chemical bonding of species of interest on carbon surfaces. Like all surfaces, reactions do not occur across the entire carbon surface but instead occur at discrete sites where the valency is not satisfied, known as active sites [47]. In the case of carbon, these sites include edges of basal planes, twin boundaries, and imperfections such as vacancies, dislocations and impurity sites (e.g. oxygen functionalities). The active sites are significantly more reactive than the atoms in the basal planes; ~1000 times more for edge atoms [47]. Investigating the level of chemisorption occurring on a surface indicates the level of active sites available which will be of use for full understanding of the bonding processes that occur in composites.

1.6 Fibre Treatments

1.6.1 Introduction

The surface of unmodified carbon is generally unreactive with mainly weak dispersion interactions taking place [50]. Indeed, as-produced carbon fibres do not bond well with epoxy resins and other plastic matrices [29]. The interfacial bonding between the fibre and the matrix has been found to depend on chemical bonding, van der Waal interactions and mechanical keying [5]. Thus the chemistry of the surface of the carbon fibre and the surface texture are important

aspects [51]. The well ordered skin normally seen in PAN-based fibres is detrimental to the surface chemistry as the presence of large, relatively low polar graphene basal planes means the surface does not have many layer edge sites to allow oxygen functionalities to attach to [2,12]. There are several features related to the fibre that can be altered to improve bonding, namely increasing the surface energy of the fibre, increasing the specific functional groups on the surface, and increasing the surface roughness.

A wide range of surface treatments designed to improve the adhesion between the fibre and the matrices have been described in the literature including:

- Chemical wet treatments [52-55], e.g. treating with nitric acid, potassium permanganate, chromic acid, or sodium hypo-chlorite etc.
- Chemical dry treatments [56-60], e.g. oxidation by oxygen or ozone, radio-frequency plasma treatment etc.
- Electrochemical methods [61-67], e.g. anodic oxidation in various electrolytes such as nitric acid, ammonium salts, etc.
- Coating methods [68-73], e.g. pyrolytic graphite, silicon carbide whiskers, nickel coating, etc.

Each treatment has its own advantages and disadvantages although currently electrochemical oxidation is preferred in industry [62]. Manufacturers of carbon fibres are naturally cautious about revealing details about the composition of their products and of any surface treatments that are performed. This section discusses some of the treatments examined in the literature.

1.6.2 Electrochemical

In practice, electrochemical oxidation, also known as anodic oxidation, is used by industry to alter carbon fibres [62] as it is provides a quick, uniform treatment that can be used in mass production [34]. Figure 1.13 shows an example set up which allows for the continuous treatment of a fibre [5]. The fibres are passed

through an aqueous electrolytic solution which contains a cathode, while a current is applied to the fibres. The fibres act as an anode [67].
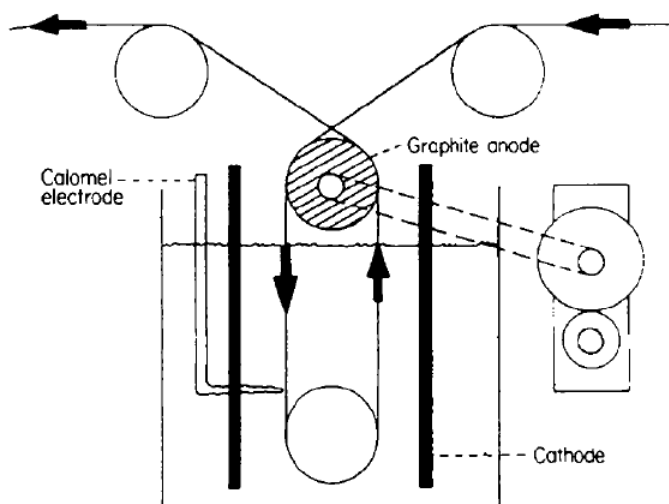
Figure 1.13 Electrochemical bath allowing continuous treatment of fibres [5].

Many different electrolytes have been examined in the literature [34]. For example, Bismarck *et al.*, investigated the effect of alkaline electrolytes on previously untreated and unsized PAN-based fibres [64]. They treated the fibres using a 1:1 mixture of 0.1 M potassium hydroxide (KOH) with either 0.5 M potassium carbonate (K_2CO_3) or 0.5 M potassium nitrate (KNO_3). The treated fibres were then analysed using XPS, contact angle (using the modified Wilhelmy technique), SEM, single-fibre tensile tests, zeta (ζ)-potential measurements, electrical conductivity measurements, and interfacial shear strength (IFSS) [34]. ζ-potential measurements use an electrokinetic analyser to assess the potential differences between the bulk electrolyte and the layer of electrolyte that forms at the fibre surface (the double layer). XPS measurements showed the untreated fibres to have ~ 4% oxygen on the surface which was increased to ~ 15 % with 10 minutes of KOH/ K_2CO_3 treatment and ~ 24 % with KOH/ KNO_3 treatment. Peaks within the XPS carbon 1s spectrum were attributed to alkoxide groups (–C-OH) and C-O-C, carbonyl groups (C=O) and O-C-O, and carboxylic groups (O=C-OH) in addition to C-C and C-H bonds. Most of the oxygen on the surface was found to be OH functionalities. The SEM

images showed the treatments smoothed the fibre surface slightly. The contact angle measurements with water showed an initial increase in wettability of the fibre with treatment time but further treatment did not cause further increases. The ζ-potential measurements confirmed this trend. The IFSS and single fibre tensile strength were not affected by the treatments [34]. This study is a particularly good example of the range of techniques that are required to fully analyse carbon fibres.

Yue *et al.*, also used KNO$_3$ as an electrolyte on PAN-based fibres [74]. Their investigations included XPS, FTIR and adsorption studies. The XPS revealed similar levels of oxygen, ~24% to those found in reference [64]. The carbon ratios (O/C), were between 0.23 - 0.27 while the nitrogen to carbon ratio (N/C) did not vary from 0.04. Similar functional groups were found from the XPS peak fits. Carboxyl groups were found to increase with increasing treatment time which was confirmed with FTIR measurements [74].

While Bismarck and co-workers did not find an improvement in IFSS with treatment [34], other work in the literature has shown a correlation. For example, Gulyás *et al.*, used a wide range of electrolytes to alter PAN-based fibres and then produced composites using an epoxy resin [62]. The 21 resulting samples were characterised by FTIR and the strength of the fibres was characterised by an undisclosed method. The IFSS was investigated by fragmentation, where a load is applied to the composite and the number of fragments in the fibre and their length is determined by a microscope. SEM images were also acquired of the fracture surface. Electrolytes included sodium hydroxide (NaOH), ammonium bicarbonate (NH$_4$HCO$_3$), ammonium carbonate ((NH$_4$)$_2$CO$_3$), sulphuric acid (H$_2$SO$_4$) and nitric acid (HNO$_3$) in concentrations between 3 to 20 wt. % and the applied voltage was varied between 0.5 and 5 V. The fibre strength was unaffected by any of the electrochemical treatments. The authors discussed the difficulties involved in using FTIR to study the chemical composition of carbon fibres; i.e. the high adsorption of infrared by the fibres, and the low levels of functional groups on the surface (i.e. low signal to noise ratio). With this in mind, a correlation between IFSS and certain bands present in the FTIR was found, for

example the IFSS was found to increase with increasing carboxyl groups but decrease with increasing sodium hydroxide. SEM images supported a change in adhesion with treatment with long pulled out fragments of fibres showing at the fracture surface for weakly bound fibres compared to short fragments for strongly bound fibres [62]. It was concluded that the IFSS depends on the entire surface chemistry of the fibre and not just one functional group. The functional groups introduced to the fibre surface depended on the type of electrolyte while the amount of groups depended on the concentration of electrolyte and the voltage applied [62].

Other electrolytes tried in the literature include phosphoric acid (H_3PO_4) [75], dichromates, and permanganates [34]. Ammonium bicarbonate (NH_4HCO_3) is considered one of the most useful electrolytes as it does not leave a residue so simplifies the washing and rinsing process. This can be particularly important in order to improve fibre-matrix adhesion. Százdi *et al*., showed that sodium hydroxide (NaOH) adsorbs to the surface of carbon fibres when used as an electrolyte and this reduces the IFSS [76]. Removal of the adsorbed NaOH produces improved composites [76].

The studies discussed above examine treatments applied in the laboratory setting. Treatments applied by manufacturers have also been examined. Wang *et al*., investigated PAN-based fibres that had been treated industrially (IM7 Hercules fibres) [61]. The fibres were also de-treated by heating in a vacuum before being re-treated using nitric acid as an electrolyte. The fibres were analysed using XPS, and voltammetry. The industrial treatment resulted in an O/C ratio of 0.36 while de-treatment reduced the O/C ratio to 0.02. The fibres were found to be altered by the de-treatment such that they produced different surface chemistry to fibres treated directly [61].

Drawbacks for electrochemical treatments, as with any wet treatment, include needing to wash and dry the fibre, thus increased processing time [59]. In addition, the chemicals used for treatment require careful disposal and can pose a health hazard. It is desirable for any oxidising treatment to be safe, simple, cost efficient, and environmentally friendly.

1.6.3 Ozone and UV/O$_3$

Ozone oxidation has been examined by several studies as it is known to be able to remove impurities from surfaces and introduce different oxygen functional groups. Ozone has the added advantage that any residual gas can be converted back into oxygen thus leaving no by-product [77]. One study by Park and Kim used ozone concentrations of 10-40 mg/l to alter PAN-based fibres [77]. Using XPS, they found the ozone introduced acidic functionalities to the surface of the carbon fibre, (e.g. carboxyl and carbonyl groups) but the C-C peak decreased with increasing concentration. They suggested the ozone was capable of breaking the C-C bonds. No figure was given for the surface oxygen %. Contact angle testing showed the fibre surface energy increased with treatment. Mechanical testing, including the 3-point bend test, showed the ozone treatment improved the adhesion between the fibre and an epoxy matrix [77].

Jin *et al*. treated pitch-based fibres with ozone gas at different temperatures (from room temperature up to 160 ^{o}C) after applying a vacuum to the fibres [60]. The resulting pressure of ozone was 0.4 Pa, while the flow rate was 0.12 m^3/h. Carbon fibre-carbon composites were manufactured. Mechanical tests showed an increase in compressive and flexural strength with the heat of treatment up to 160 ^{o}C, when the ozone decomposition was too rapid to oxidise the carbon fibres and the strength decreased [60]. SEM images of the fracture morphology confirmed this. XPS measurements showed the six minute ozone treatment at 120 ^{o}C doubled the surface oxygen present (~ 9% increased to ~ 23 %). Similar functional groups were found on the surface as in the previous studies discussed. AFM was used to examine the fibre surface. The surface roughness was shown to increase with ozone treatment. Raman measurements also showed the surface became less graphitic with treatment, reinforcing Park and Kim's suggestions that the C-C bonds are broken by the ozone [60].

Treatments on carbon surfaces using ultraviolet generated ozone (UV/O$_3$) have been examined in the literature. This method has previously been used to alter wool fibres to improve wettability [78] and on polymer surfaces [79]. A study by Sham and Kim used UV/O$_3$ to alter the surface functionalities of multi-walled

carbon nanotubes (MWNT) [80]. A Jelight UV/Ozone cleaning system was used and nanotubes were treated for times from 2 minutes to 1 hour. Epoxy resin composites were prepared with the treated nanotubes. TEM images did not show any visible change in the structure of the MWNTs. XPS showed the UV/O_3 treatment introduced increasing carboxylic groups to the surface with increasing treatment time. The treated nanotubes showed improved dispersion in the composites as the thermodynamic characteristics of the tubes changed from hydrophobic to hydrophilic [80].

UV/O_3 treatment has been applied to carbon fibres, although there is very little in the literature. Rich *et al.* treated PAN-based and pitch-based fibres using a specially built UV/O_3 generator that pumped in extra ozone [81]. Treatment times as low as 5 seconds were shown to improve the O/C ratio as measured by XPS. An O/C of 0.27 was seen after 10 minutes of treatment. STM images showed some slight surface roughening was caused by the treatment. Unlike electrochemical treatments, the tensile strength of the individual fibre increased by ~ 11 % with treatment. Rich *et al.* suggested this was due to removal of an outer layer of defects on the fibre [81]. The IFSS of a fibre-epoxy resin composite was also shown to increase substantially with UV/O_3 treatment; ~ 15 MPa for a commercially treated fibre up to ~ 30 MPa for UV/O_3 treated fibre [81]. The study did not examine functional groups generated by the treatment.

Although the studies discussed here have shown UV/O_3 to be a very promising new treatment method with several advantages over electrochemical treatments, very little research has been has been published on it. The work in this thesis further examines the effects of UV/O_3 treatment on fibres, including functional group analysis.

1.6.4 Other Methods

Chemical wet methods suffer from similar disadvantages to the electrochemical treatments and they are also time consuming, requiring treatments lasting from 15 minutes to hundreds of hours [34]. The fibres are generally boiled in the chemical solution, for example Kaushik treated PAN-based fibres in a potassium

permanganate (KMnO$_4$) solution at 85 ^{o}C for up to 30 minutes. XPS measurements showed the treatment increased the level of surface oxygen, with 10 minutes producing ~11% O [55]. In previous studies by other authors, it has been suggested that this treatment prevents the fibres from having skin-core heterogeneity. This is due to diffusion of MnO$_4$ ions into the fibre which form MnO$_4$-C=N conjugation groups. These groups have a plasticising effect on the fibre resulting in better molecular orientation [82]. While removing problems associated with the skin-core difference (i.e. possible improvement in fibre-matrix adhesion), the fibre itself suffers from a decrease in mechanical strength as a result of extended treatment times [82]. Boiling nitric acid and sulphuric acid have frequently been used in the past to treat fibres [34]. Nitric acid is still frequently used to create activated carbon fibres [52,53,83].

Coatings for carbon fibres have been used to protect the fibres when they are used in carbon-carbon composites that experience high temperatures in oxidizing environments, e.g. shuttle shields or braking systems [72]. The coatings include boron nitride, titanium carbide, and silicon carbide. The coating is normally applied by chemical vapour deposition (CVD) or reactive-CVD (RCVD). Similar adhesion problems to those seen in fibre-resin matrices exist for the coatings and generally the same analysis techniques, e.g. XPS, or SEM, can be used [72]. Metal coatings, such as nickel, have also been used to improve metal matrix and plastic matrix composites [71].

Plasma deposition offers several advantages over electrochemical treatments; the main two being that the treatments are more environmentally friendly, and the fibres do not degrade [57]. The effect of the treatment on the fibre surface can be controlled by varying the power of the radiofrequency used to generate the plasma, the treatment time, the reactor pressure and the gas used [24]. Gases such as nitrogen, argon, oxygen or air can be used in low pressure vessels [24,31,34,56,57,84], or low pressure liquids can be introduced such as ammonia [85]. For example, Smiley and Delgass examined PAN-based fibres etched in oxygen plasmas using AFM, SEM and XPS [24]. A power of ~ 25 W was used for 2 to 60 minutes. O/C ratios were seen to increase immediately from ~0.16 to ~ 0.32 with 2 minutes of plasma treatment but further increases were slower; the

60 minute treatment producing an O/C ratio of 0.38. The carbonyl and carboxyl groups showed gradual increases with treatment time while alkoxide groups showed a gradual decrease [24]. Pitting on the fibre surface was evident on the SEM images after 15 minutes of treatment and AFM images showed short treatments of 2 minutes roughened the surface while treatments of 15 minutes smoothed the surface again [24]. Ho *et al.* has used atmospheric plasma fluorination (APF) to treat fibres since atmospheric conditions are much more suitable for industrial scale treatments [86]. APF was shown by XPS to introduce fluorine to the fibre surface which led to improved wettability by poly(vinylidene fluoride) (PVDF) as measured by the Wilhelmy contact angle technique. The surface area of the fibres, measured by the BET (N_2) technique, increased from 0.22 to 0.44 m^2/g with plasma treatment [86].

Other, more unusual treatment methods have also been examined in the literature. A study by Li *et al.* used a Co^{60} source to irradiate fibres held in a glass container full of chloroepoxy propane by different radiation doses [87]. Using XPS, contact angle analysis and mechanical tests, they found that the radiation could increase the oxygen containing functional groups on the surface of the fibre and increase the wettability of the fibres by water as well as increasing the surface roughness leading to improved mechanical interlocking. The gamma rays create radicals in the chloroepoxy propane which attack the fibre surface and attach functional groups to it [87]. Li *et al.* reported that radiation treatment would mean fibres could be treated directly after leaving the production line in a quick time (since dose rate did not affect the results) and the process would not leave any pollutants, thus being environmentally friendly [87]. This is not entirely the case as the Cobalt source would require shielding for safety, and would eventually reach the end of its useful life and need to be disposed of safely. An alternative would be to use some form of linear accelerator or kV x-ray unit to achieve the high doses electrically which would negate the disposal problem but not the shielding and would still be costly.

1.6.5 Sizing

Normally a thin coating is applied to the carbon fibres immediately after production to make them easier to handle and to protect them before use .This is known as a size and is generally made from an organic polymeric material. Two such common sizes are epoxy resin and poly(vinyl alcohol) (PVA) [34] although the choice of coating depends on the polymer matrix that the fibres will be used in [5]. When epoxy resin is used, little to no curing agent is added meaning the size layer is expected to be more brittle than the rest of the resin matrix [29]. The thickness of the size layer has been found to range from 0.03 to 1 μm [5,34].

The effect of different sizes on composite strengths has been investigated in the literature. Dilsiz and Wightman investigated polyetherimide and poly(thioarylene phosphine oxide) sizings on PAN-based fibres [4]. Dynamic contact angle analysis showed the size decreased the fibre surface energy and XPS showed it also decreased the functional groups present at the surface. Both of these factors would lead to reduced adhesion between fibre and matrix however AFM showed the size increased the roughness of the fibres which could improve adhesion [4].

Size can be a hindrance for experimentation as it masks the surface chemistry of the fibre. Size removal is, however, a complex process and it is therefore preferable to receive the fibres unsized [28].

1.7 Fibre Characterisation

1.7.1 Introduction

Fibres present several problems for characterisation due to their size, colour, surface area, handling difficulties and low concentrations of surface functional groups [29]. In addition, electron beans and ion beams can damage the surface depending on the intensity [28]. A range of characterisation techniques have been used in the literature. In 1986 a working party of the International Union of Pure and Applied Chemistry presented a review of the techniques used to characterise

fibres; these included SEM, TEM, EELS, XPS, Raman Microscopy, FTIR, and AES [11]. Some research has focussed on characterising only the fibres (e.g. [3,4,88]), while other research has looked at characterising the interface between the fibres and the matrix (e.g. [89,90]).

This Section discusses some of the different techniques used to investigate the surface chemistry, surface texture, adsorption properties, surface energy, and mechanical properties of carbon fibres as presented in the literature. Detailed descriptions of the techniques used in this work are given in Chapter 2.

1.7.2 Functional Groups

As is probably clear from the preceding section on fibre treatments, x-ray photoelectron spectroscopy (XPS) is one of the most commonly used techniques for characterising the surface chemistry of fibres [29]. Several examples of the use of XPS to identify and quantify surface elements were presented in Section 1.6. XPS can also be used to examine the fibre-matrix interface. For example, Weitzsacker *et al.,* used XPS to model the interaction between the fibre and matrix [89]. A monolayer of a compound, chosen to model those used in composites, was added to the fibre. The fibre was then heat treated as it would be in production of the composite before the model compound was dissolved using a solvent, leaving behind the altered fibre. The authors found the surface composition of the fibres was altered depending on the model compound used [89]. This method has limitations as the reaction between the modelling compound and the fibre does not fully mirror the whole matrix material and competing interactions are not taken into account.

Due to the low concentrations of surface groups on carbon fibres, the XPS carbon signal can be overshadowed by the graphitic backbone [29]. Another disadvantage of XPS is the subjectivity of the peak fitting and functional groups assignment process [35]. Fourier Transform Infrared spectroscopy (FTIR) is also used to analyse the functional groups present on the fibre surface. Several examples of FTIR use to characterise surface treatments are mentioned in

Section 1.6. Figure 1.14 shows the FTIR results from Yue *et al.*'s work where the fibres were treated electrochemically in a KNO_3 solution using different levels of charge [74]. The treated fibres were prepared for FTIR by grinding to a powder and were mixed in with KBr to form pellets for analysis. This means the analysis was of the bulk composition and not just the surface layers. Two broad peaks are visible in these results; one at approximately 1727 cm^{-1} and another that shifts gradually from ~1628 to ~1606 cm^{-1} as the charge applied increases. The peak at ~ 1727 cm^{-1} was assigned to C=O stretching vibrations in ketones and/or carboxyl groups. The other peak was assigned to aromatic (C=C) stretching vibrations or the bending vibrations of physisorbed water. The C=O peak increases in intensity with the increasing charge applied to the fibres which shows the quantity of the functional group increases with treatment. No explanation was suggested for the shift in the second peak but it could be as a result of less C=C bonds being present after the treatment [74]. The pellet method used by Yue *et al.* is not surface sensitive as the fibres are ground to a powder but it is often the way fibres are prepared for FTIR analysis. The high adsorption of infrared by the fibres, and the low levels of functional groups on the surface (i.e. low signal to noise ratio) also add to limitations in the use of FTIR.
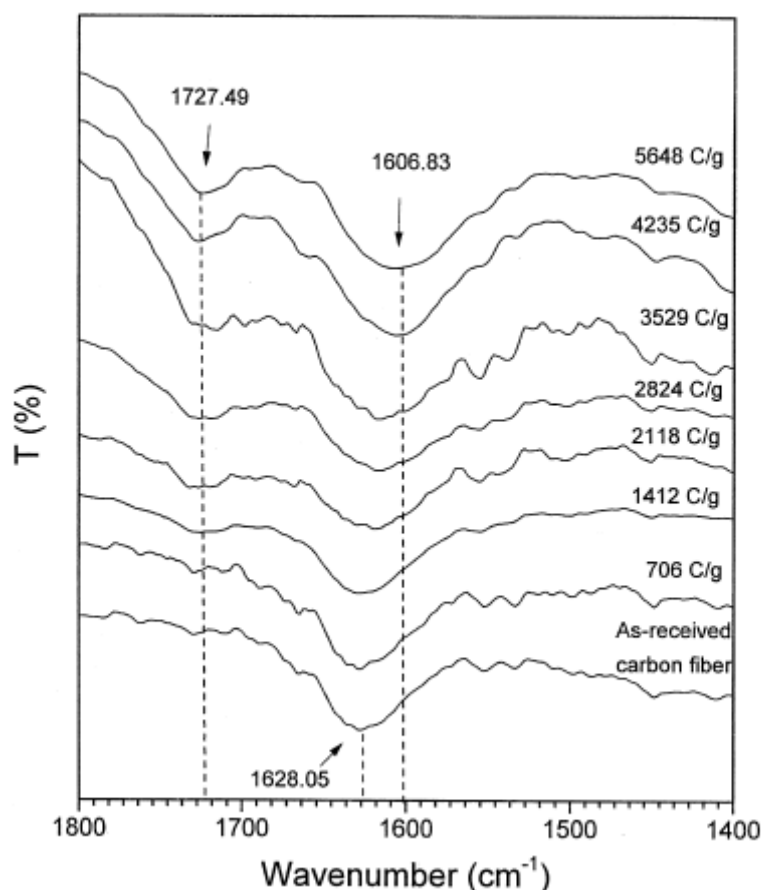
Figure 1.14 FTIR spectra for fibres treated electrochemically in a KNO₃ solution using different levels of charge [74]**.**

Temperature programmed desorption (TPD) has been used on fibres to determine the total oxygen present as well as the functional groups present. If carbon is heated in a vacuum or in a flow of nonreactive gas, chemisorbed oxygen reacts with surface carbon giving carbon monoxide (CO) and carbon dioxide (CO_2), other sources of CO_x are decomposition of O containing functional groups . The quantity of evolved gas can be monitored by a mass spectrometer [28,91]. TPD has the advantage that quantitative values of compounds can be measured and the surface chemistry for the whole of the fibres might be assessed [92]. Unfortunately group assignment is again, not straight forward. Surface functional groups can interact before decomposition, and secondary interactions can also occur skewing the results [91]. In some instances, TPD group assignment can be as difficult as XPS group assignment. Figure 1.15 shows CO_2 and CO spectra gathered by Zielke *et al.* for a fibre treated by an unknown industrial method

before washing (a) and after washing (b) [93]. While it may be difficult to assign groups to these peaks, it is clear the act of washing does affect the spectra.
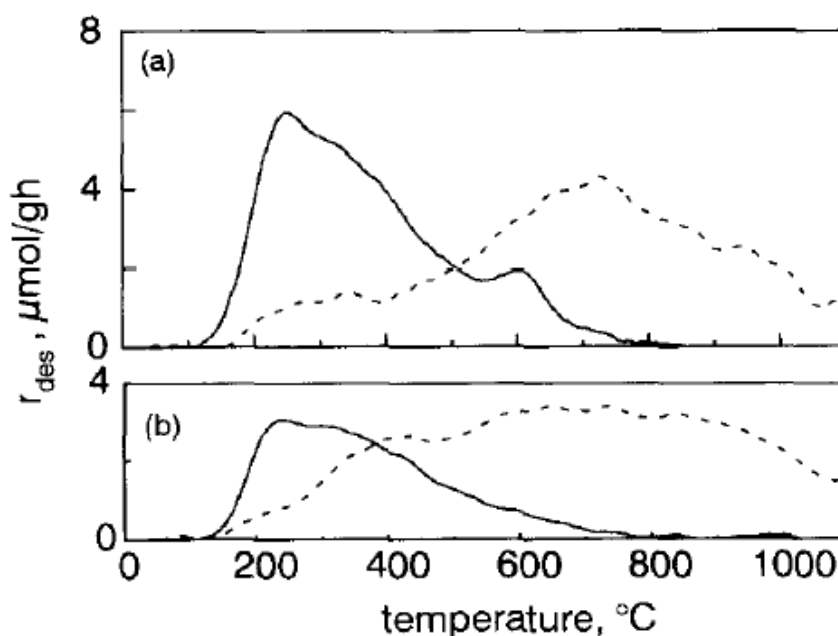

Figure 1.15 TPD spectra for carbon dioxide (solid lines) and carbon monoxide (dashed lines) of a) treated fibres and b) treated and washed fibres [93]**.**

Boehm titrations, so named after Hans Boehm who first proposed the method, use a base of known concentration to neutralise the acid sites on the fibres [91]. The resulting solution is then filtered and the remaining base is neutralised with an acid by titration. This allows the number of acid sites on the fibre to be calculated. Different bases can be used to examine different acidic groups and acids may be used in a similar manner to determine the basic sites [91]. A number of authors have used this method to characterise activated carbons [94-97] and activated carbon fibres [83,98]. Wang *et al.* examined pitch based activated carbon fibres using Boehm titration, FTIR and XPS [98]. Fibre samples of 0.25 g were submerged in 25 cm^3 of 0.05 N NaOH, 0.1 N Na_2CO_3, or 0.1 N $NaHCO_3$ and sealed in a vessel which was shaken at room temperature for 48 hours. It was assumed that NaOH neutralized carboxylic, phenolic and lactonic groups; Na_2CO_3 carboxylic and lactonic; and $NaHCO_3$ only carboxylic groups. Thus the concentration of each group could be calculated. Hydrochloric acid was

used on the fibre to determine the number of surface basic sites on the fibre. A good correlation between the total oxygen as measured by XPS and Boehm titrations was found. FTIR measurements agreed with the type of groups identified by the Boehm titrations [98]. The activated fibres had < 5% oxygen on the surface and the surface area was greater than 1000 m^2/g. The titration yielded ~ 1 meq(H^+)/g of oxygen groups on the surface [98]. From these numbers, it seems unlikely the Boehm method would be practical for carbon fibres with areas ~ 1 m^2/g as titrations would involve very dilute acids/ bases.

Pittman *et al*. used NaOH uptake to try to calculate surface areas on carbon fibres [99]. They found the sodium hydroxide penetrated into the fibre, swelling some of the internal surfaces and overestimating the surface area compared to BET measurements with CO_2 [99]. This suggests Boehm titrations may see more oxygen functionalities than other methods if the oxygen is contained within pores.

It is generally accepted that to fully characterise the surface chemistry of carbon, several complimentary techniques are required. Although functional group analysis by XPS is not definitive, it is by far the most convenient and reliable of the methods outlined in this section. XPS is used in this work to quantify total percentages of oxygen on fibre surfaces and to identify functional groups present.

1.7.3 Morphology, Structure and Surface Area

Several studies described in Section 1.6 used SEM to examine the effect of treatment on fibre texture or the mechanism of composite failure. For example, Bismarck *et al*. treated PAN-based fibres anodically and examined the effect on the surface roughness using SEM [65]. Figure 1.16 shows an example from Bismarck *et al.*'s work. The fibre displays large flakes breaking away from the surface, demonstrating that electrochemical treatments are able to cause substantial roughening to the fibre surface so it is important to examine the surface morphology [65]. Energy dispersive X-ray microanalysis (EDX) was also used to determine the elements present on the fibre surface, and the spectra for

fibres treated by different times are shown in Figure 1.16b). The EDX shows an increase in oxygen but also several other contaminants (e.g. K and Na) with increasing treatment time. SEM images were not used to investigate the adhesion between the fibres and composites, instead wetting measurements using water were performed to determine surface energies. The contact angle decreased, i.e. the wettability increased, with increasing treatment time for a KNO_3/KOH solution [65]. Examining the damaged fibre in Figure 1.16, one might not be inclined to take the wettability as a good predictor of adhesion to a resin. In this case, the treatment has caused large flakes to appear on the surface which may only be loosely bound and would reduce the strength of the composite. In the absence of mechanical testing, SEM can give an indication of how the surface treatment may affect the composite strength.
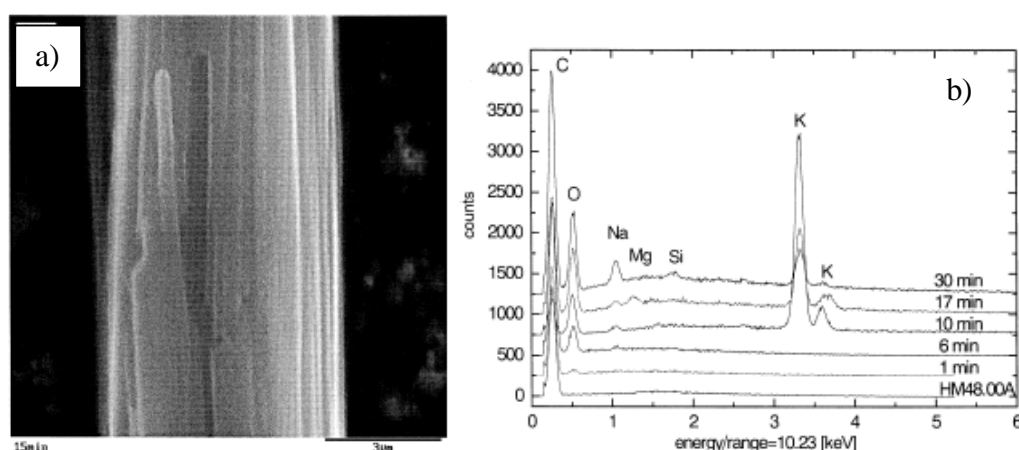

Figure 1.16 a) SEM image of PAN-based carbon fibre treated for 15 minutes using KNO_3/KOH electrochemical solution and b) EDX spectra for fibres treated using a range of times [65]**.**

Jin *et al*. used SEM to evaluate the adhesion between pitch based carbon fibres and a carbon matrix in addition to contact angle analysis [60]. Fibres were set into a composite, the composite was fractured and the fracture surface imaged. Figure 1.17 shows two of the images [60]. The untreated fibres had ~10 % surface oxygen while the treated fibres had ~23 %. Contact angle analysis with water showed the surface energy of the treated fibres increased with increasing surface oxygen, similar to the work of Bismarck *et al* in reference [65]. The SEM images show the untreated fibre pulls out cleaner than the treated fibre during

fracture, suggesting a lower adhesion between fibre and matrix [60]. It was also reported that ruptures were visible in the matrix and interface for the treated fibre but only the interface for the untreated fibre [60].

The surface morphology can also be imaged using scanning tunnelling microscopy (STM) or atomic force microscopy (AFM) [28]. Lee and Drzal showed that proprietary electrochemical treatments roughen surfaces to ~ 1.5 times the untreated surface roughness [100]. Liu and Lu used AFM to measure surface roughening on PAN-based fibres subjected to nitrogen plasma treatments [101]. They found the surface roughness doubled with 7 minutes of treatment [101]. Gao *et al*, used AFM to measure the surface roughness of carbon fibres and fracture surfaces of composites [102]. The surface roughness of the fibres was found to correlate with adhesion level [102]. The work by Jin *et al*, [60] described in Section 1.6.3 used AFM and SEM to show ozone treatment caused surface roughening at the microscopic level as well as the macroscopic level. Figure 1.17 shows the AFM images for an untreated high modulus pitch based fibre and a fibre treated to 6 minutes of ozone at 120°C by Jin's group [60]. Pitting very obviously occurs with the treatment. This figure also shows the SEM images of the fibre after pullout from the composite as described earlier.
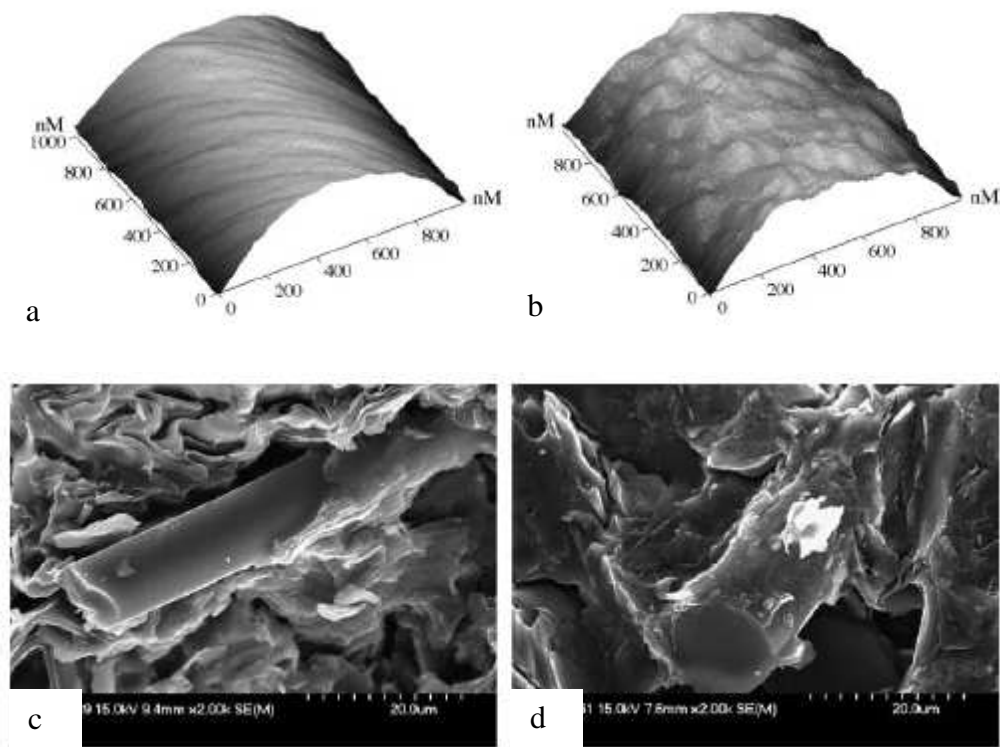
Figure 1.17 AFM images of a) unmodified and b) 6 minutes, 120°C ozone treated HM pitch based fibre and SEM images (c and d) of the same fibres respectively in composites [60]**.**

Surface areas reported in the literature for non-activated PAN-based fibres measured using nitrogen adsorption, range from 0.2 to 2 m^2/g [86,93,103-106].

TEM images have been used to show lattice imperfections in carbon fibres [20], the structure of fibres [12], the structure of fibre precursors [19], the effect of surface treatment on the fibres [107] and the adhesion of fibres to a composite [90]. Figure 1.18 shows an example TEM lattice fringe image of a PAN-based carbon fibre sliced longitudinally; a defect in the fibre is highlighted [109]. TEM images are not a common investigation for fibres as the fibres are difficult to prepare for imaging. Normally fibres are set into a resin and ultramicrotomed [108] but adhesion between the fibres and resin is subject to similar problems as experienced between fibres and composite resins. For example, Figure 1.19 shows a TEM image of a PAN-based activated carbon fibre set into a resin and sliced through the cross-section [110]. Although the fibre shows areas of debonding from the matrix, this image is useful to show that this fibre has two structurally different regions; a core and a skin.
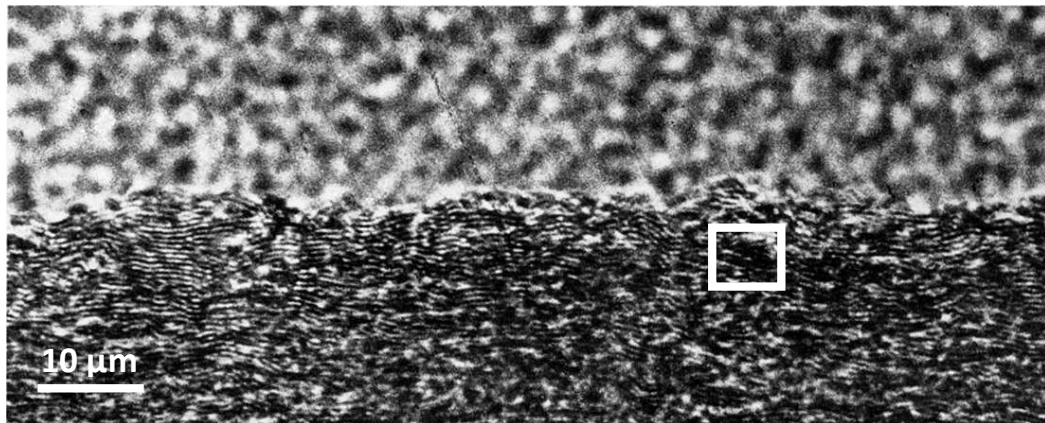
Figure 1.18 Lattice fringe TEM image of longitudinal section of a PAN-based type II carbon fibre showing lattice defects (highlighted by box) [109]**.**
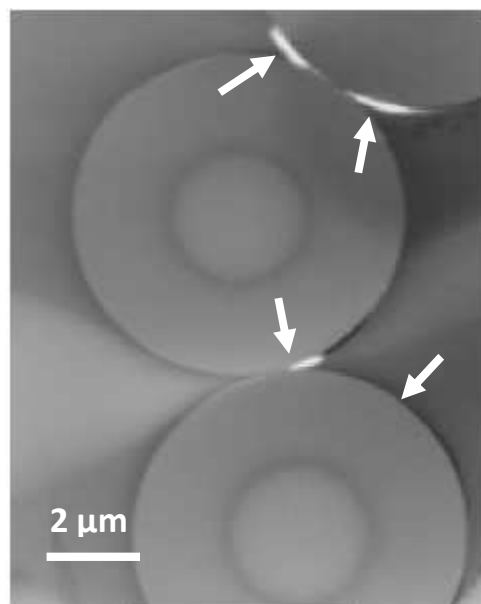
Figure 1.19 Cross-sectional TEM image of PAN-based fibre embedded in resin. Arrows highlight areas of debonding from the resin matrix. The fibre displays a skin-core heterogeneity [110]**.**

Ideally TEM can be used to examine the top most surface layers of a treated fibre to investigate whether the treatment alters the surface structure. It is however, difficult to prepare the samples in such a way so as not to damage the fibre. Figure 1.20 shows two different pitch-based fibres, set into a silicon-carbide matrix; a) is a disordered fibre and b) is a more graphitic fibre [111]. The

interface between the fibre in image a) and the matrix is quite rough compared to the interface in image b) suggesting greater adhesion. The top most interface between the fibre in image b) and the SiC matrix shows signs of debonding which was attributed to the ion-milling process and was taken as evidence of lower adhesion between fibre and matrix. The level of adhesion was confirmed using bend tests and SEM fracture images on composites [111]. In this case, although the sample was damaged by the preparation process, the TEM images still contributed to the understanding of the adhesion process.
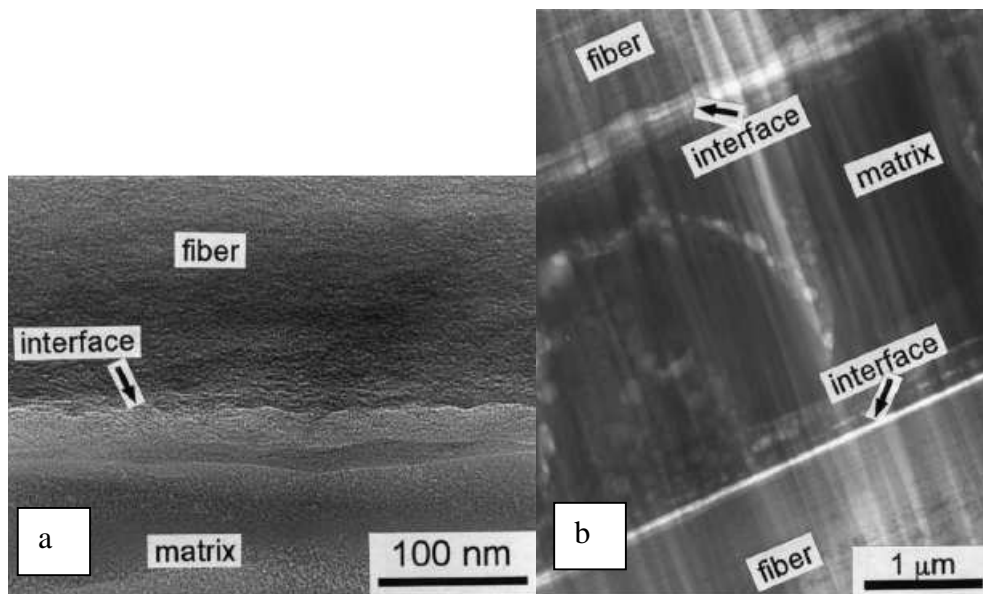
Figure 1.20 TEM images of a) a disordered fibre and b) a highly graphitic pitch based carbon fibre set into a silicon-carbide composite [111]**.**

Raman can be used to measure the structural characteristics of carbon surfaces. There are two main peaks of interest that appear for non-perfect carbon materials; the disorder (D) peak and the graphite (G) peak. A ratio of the intensities of D and G (or the ratio of the intensity of D to the sum of the intensity of D and G) allows a relative assessment of the level of graphitization on the surface [112-114]. Figure 1.21 shows the Raman spectra for the ozone treated fibres from Jin *et al.*'s work [60] shown above in Figure 1.17. Two extra peaks, which were not identified in the paper, are present meaning some peak fitting was required. In this example, the Raman showed the treated fibres to be less ordered than the untreated fibres which matched the AFM images [60].

Montes-Morán and Young examined the effect of plasma treatment on the fibre surface structure using Raman and compared the results to x-ray diffraction (XRD) d_{002} spacings [115]. They found a relationship between the width of the G band and the interlayer spacing. Figure 1.22 shows a plot of the G band width against XRD measured d_{002} spacing using data taken from this reference. The plot makes the relationship clear; as the interlayer spacing increases, i.e. the surface becomes more disordered; the width of the G peak also increases. The plasma treatment was found to disrupt the surface layers of the fibres [115]. The D to D+G intensity ratios reported in the literature for fibres vary considerably, for example, in references [63,115,116] the ratios vary from 0.2 to 0.80 .
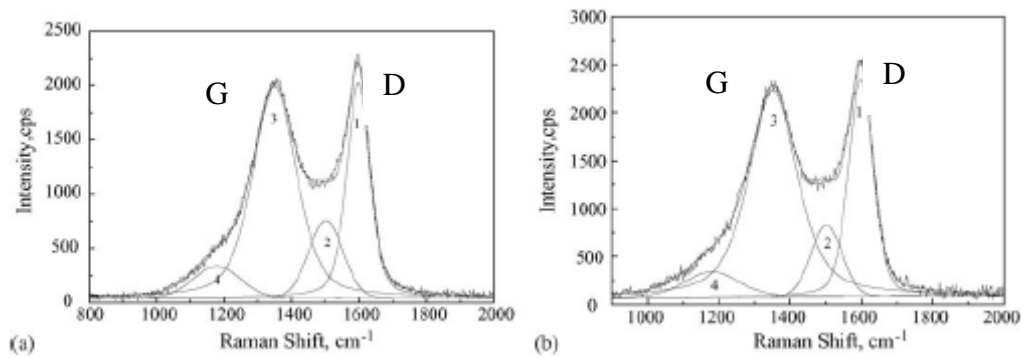

Figure 1.21 Raman spectra of a) unmodified and b) 6 minutes, 120°C ozone treated HM pitch based fibre [60]**.**
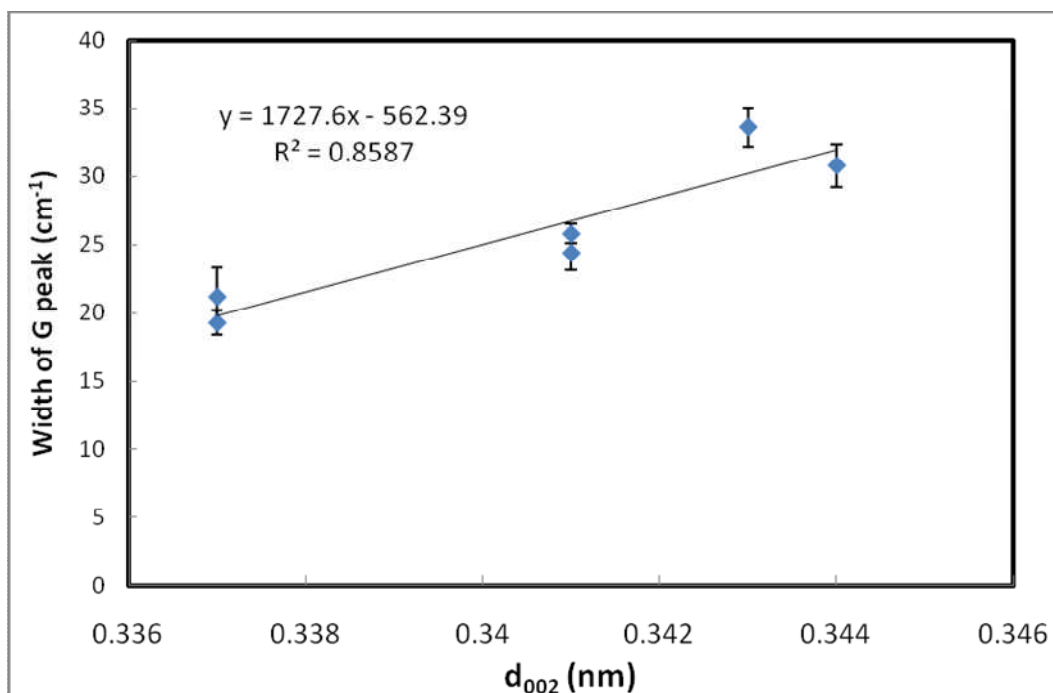
Figure 1.22 Width of Raman G peak as a function of the interlayer spacing d_{002} extracted from data in reference [115]**.**

It is important to examine the effect of any fibre treatment on the surface roughness of the fibre in order to fully understand any increase in bonding between fibre and matrix. AFM is difficult to perform on fibres due to their size so was not performed. SEM, nitrogen surface areas and laser Raman were used to investigate the effect of surface treatment on the surface morphology. Although difficult to perform, TEM images were acquired to examine the level of crystallinity in the fibres following treatment.

1.7.4 Surface Energy

Several different methods have been used in the literature to estimate the surface energy of carbon fibres and other carbon materials including contact angle analysis (CA) [4,85,93,117-120], inverse gas chromatography (IGC) [38,39,56,121-123], and calorimetry [50,94,96,124-128]. As discussed in Section 1.5.2, contact angle measurements are difficult to perform on fibres. Several authors used the modified Wilhelmy plate method, as described in Section 1.5.2, to measure surface energies of carbon fibres, and the polar and dispersion contributions to the surface energy [93,117-120]. A two liquid method has also

been investigated for contact angle analysis [4,85]. This uses two immiscible liquids; one polar, such as formamide, and one non-polar, usually a linear alkane to form two interfaces. The force of the fibre as it is immersed in the two liquids can be related to the dispersive and non-dispersive components of the fibre surface energy in a similar manner to the Wilhelmy method [4,85]. Song *et al.* proposed a generalized model for measuring the contact angle of a drop of liquid on a fibre (the drop-on method) in order to overcome the reproducibility issues found with the Wilhelmy plate method [41]. A drop of liquid is placed on the fibre and the shape it forms is mathematically analysed [41]. The method requires a good imaging system, and the ability to form drops of liquid small enough that gravity can be neglected (i.e. < 50 μm in diameter).

Using the Wilhelmy plate contact angle method, Bradley *et al.* found the surface energy of untreated high modulus PAN-based carbon fibres increased from ~54 mJ/m^2 to ~ 65 mJ/m^2 when anodically treated with ammonium bicarbonate as the electrolyte [117]. The dispersion contribution remained constant at ~50 mJ/m^2 but the polar contribution increased from ~ 4 to ~14 mJ/m^2, this coincided with the increase in oxygen and nitrogen on the fibre surface as measured by XPS [117].

Inverse gas chromatography measures the retention time of solute molecules in an inert carrier gas as they are passed over a column packed with the solid surface of interest [123]. The standard free energy and enthalpy of adsorption can be calculated from the retention volume. By using probes of differing polarity and those which only interact via dispersion, the polar and dispersion components of the surface energy can be calculated [123]. Montes-Morán *et al.* [56] and Vickers *et al.* [38] both found the dispersive component of the surface energy for untreated PAN-based fibres to be ~100 mJ/m^2. Vickers *et al.* quoted the surface oxygen level to be ~ 4% from XPS measurements [38]. Montes-Morán *et al.* applied plasma treatments to the fibres and found the dispersion increased with the treatment [56] while Vickers *et al.* applied an industrial electrochemical treatment and found the dispersion contribution decreased [38]. Both groups suggested the addition of functional groups to the surface caused the difference [38.56]. Vickers *et al.* also used contact angle analysis on the fibres

and found the dispersion contribution from this method to be ~ 37 mJ/m^2 [38]. The difference was attributed to the IGC technique being more specific to high energy sites while the contact angle technique acts at the macroscopic level, measuring all the energy sites on the fibre [38].

Lindsay *et al.* furthered this method by using resin analogues, such as acetone or ethyl acetate, as probe liquids [121]. All resin analogue probes showed greater polar contributions to the work of adhesion with increasing surface oxygen level. They concluded that hydrogen bonding and acid-base interactions between the fibre and the resin components are likely to be the dominating source for adhesion [121].

Several authors have used immersion calorimetry to investigate the surface energy/ polarity of carbon surfaces as it negates the problems associated with the surface geometry in contact angle measurements [125]. Immersion of a degassed sample into a liquid will normally result in a release of heat, known as the enthalpy of immersion. The change in enthalpy of immersion can be plotted against the oxygen level on the carbon surface. For example, previous work by Bradley *et al.* used immersion calorimetry to characterise ozone modified carbon blacks [124]. A polar probe liquid (water) was used on carbon blacks with various levels of oxygen on the surface. It was found that the heats of immersion had an approximately linear relationship with the surface oxygen levels on the carbon blacks and that the enthalpy of immersion for an oxygen free surface (i.e. dispersion only interactions) would be 35 mJ/m^2 [124]. Other workers have found similar results [50,128]. The dispersion contribution to surface energy for carbon blacks is lower than the dispersion values found for carbon fibres using CA and IGC. It has already been suggested that IGC methods are more sensitive to high-energy sites; similarly contact angle analysis suffers from variations due to chemical heterogeneities on the fibre surface. Immersion calorimetry provides an average value over the whole surface which could lead to an improved method for surface energy analysis for fibres.

Immersion calorimetry has also been used in conjunction with the Boehm titration method. Lopez-Ramon *et al.* measured the quantity of NaOH required to

neutralise the surface groups on carbon blacks and successfully related it to the enthalpy of immersion of the carbon black in NaOH [96]. The level of surface groups were confirmed by TPD measurements. This means calorimetry can not only provide surface energy data but could also allow functional group identification and quantification [96].

In addition to carbon black, immersion calorimetry has also been used on activated carbon cloths which are a product of activated carbon fibres. The cloths have high surface areas of ~200 -800 m^2/g [126]. Although immersion calorimetry offers a reasonably quick and straight forward method of measuring surface energies and surface chemistry, it has not been performed on non-porous carbon fibres. Immersion calorimetry on carbon fibres is investigated in this work in an attempt to measure surface energies.

1.7.5 Mechanical Strength

The strength of the bond between the fibre and the matrix has been investigated by SEM images, where fractured surfaces are examined for fibre pull out characteristics as shown in Section 1.7.3 [60]. Fibres that pull out clean are considered to have bonded weakly to the matrix while those that have a layer of resin still on them are considered to be bonded strongly although the origin of the fracture can not be determined from the images [34]. Light microscopy has also been used to image the fragmentation of a fibre. A single fibre is held in a plastic resin and a force is applied until all the fragments are approximately the same length, known as the critical length. The average length of the fragments is inversely proportional to the fibre-matrix adhesion strength [31]. Bascom and Yon used this method to show the differences between thermoset and thermoplastic adhesions to fibres [31]. Figure 1.23 shows a fragmentation test for an untreated pitch based carbon fibre and a 90 second treated UV/O_3 fibre from the work by Rich *et al* [81]. The UV/O_3 treated fibre shows more fragments suggesting improved adhesion to the matrix [81].
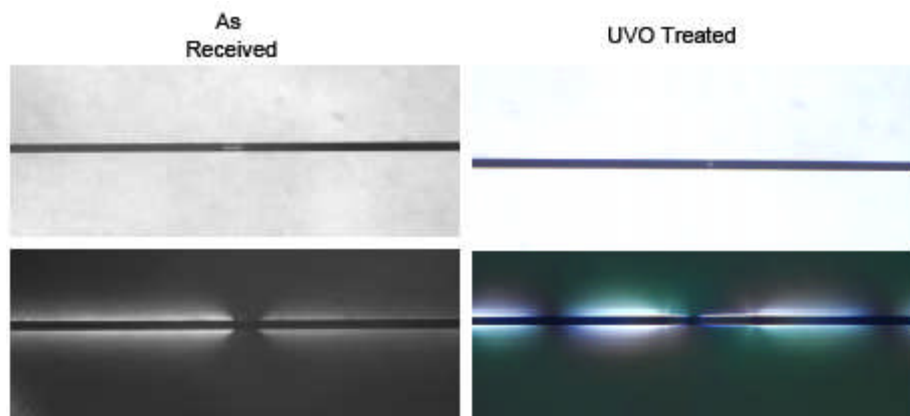
Figure 1.23 Microscopy images (above) and associated birefringe patterns showing stress around fracture points (below) for untreated and UV/O$_3$ treated fibres [81]**.**

Drzal has used TEM to image the mode of failure between both untreated and industrially treated PAN-based carbon fibres and an epoxy [90]. Images showed that not only did the untreated fibre separate from the matrix but some surface layers of the fibre failed as well, separating from the fibre itself. Treated fibres showed failure of adhesion occurred in the matrix, rather than at the interface [90]. Figure 1.24 shows the TEM images for the untreated and treated fibres in the resin after a 6% strain was applied.
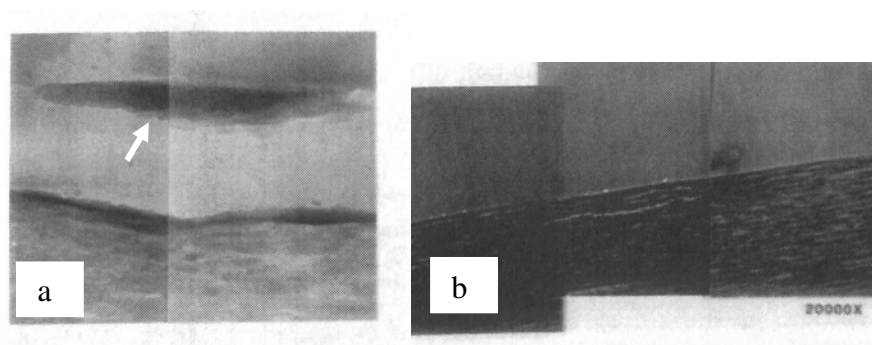
Figure 1.24 TEM images of a) untreated and b) treated PAN-based fibres in an epoxy resin after a strain has been applied [90]**.**

Several authors have used laser Raman to investigate the strain in carbon materials [115,129-131]. Montes-Morán and Young collected Raman spectra from epoxy embedded carbon fibres as the composite was deformed and the strain measured [131]. The Raman wavenumber for the G' band (a band associated with the G band) was shown to decrease with increasing tension applied to the composite [131].

1.8   Objectives of Thesis

This work examines the effect of ultraviolet generated ozone treatment methods on the surface properties of carbon fibres and compares it to commercial anodic treatments. Surface chemistry is examined using XPS as well as surface texture using SEM. TEM and laser Raman spectroscopy are used to investigate the effect of the treatment on the structure of the fibres. A thermodynamic based approach is used to model the interactions between carbon fibres of varying surface reactivity and a small range of epoxy resins and molecules of varying polarity using immersion calorimetry. The adsorption kinetics of alcohols of varying polarity on carbon fibre surfaces are investigated using TPD. The overall aims of this project were to investigate the effects of UV/O_3 treatment as a practical industrial method and to develop a new approach to identify first-principle methods for controlling interfacial bonding and stress transfer using fibre surface state and matrix reactivity, hence predicting and optimising composite properties.

The materials, equipment and methods used in this study are detailed in Chapter 2 along with background theory on the methods. Chapters 3 to 5 present the results along with discussion. Chapter 6 summarises the results and gives suggestions for future work.

1.9   References

[1] Bourrat X. Structure in carbons and carbon artefacts. In: Marsh H, Rodríguez-Reinoso F, editors. *Sciences of carbon materials.* Alicante: Universidad de Alicante; 2000: 1-97.

[2] Bradley RH. Mechanical properties of carbon materials. In: Marsh H, Rodríguez-Reinoso F, editors. *Sciences of carbon materials.* Alicante: Universidad de Alicante; 2000: 485-509.

[3] Denison P, Jones FR, Watts JF. The use of XPS and labelling techniques to study the surface chemistry of carbon fibres. *Journal of Physics D: Applied Physics.* 1987; 20:306-310.

[4] Dilsiz N, Wightman JP. Surface analysis of unsized and sized carbon fibers. *Carbon.* 1999; 37:1105-1114.

[5] Chung DDL. *Carbon fiber composites.* 1st Edition ed. Newton, USA: Butterworth-Heinemann; 1994.

[6] Brundle CR, Evans CA, Wilson S. *Encyclopaedia of materials characterization, surfaces, interfaces, thin films.* Oxford: Elsevier; 1992.

[7] Chung DDL. Review graphite. *Journal of Materials Science.* 2002; 37:1475-1489.

[8] Hembacher S, Giessibl FJ, Mannhart J, Quate CF. Revealing the hidden atom in graphite by low-temperature atomic force microscopy. *Proceedings of the National Academy of Sciences of the United States of America.* 2003; 100(22):12539-12542.

[9] Jenkins GM, Kawamura K. *Polymeric carbons: carbon fibre, glass and char.* Cambridge, UK: Cambridge University Press; 1976.

[10] Shindo A. Polyacrylonitrile (PAN)-based carbon fibers. In: Kelly A, Zweben C, editors. *Comprehensive composite materials.* Oxford: Pergamon; 2000: 1-33.

[11] Morita K, Murata Y, Ishitani A, Murayama K, Ono T, Nakajima A. Characterization of commercially available PAN (Polyacrylonitrile)-based carbon fibers. *Pure and Applied Chemistry.* 1986; 58(3):455-468.

[12] Diefendorf RJ, Tokarsky E. High performance carbon fibers. *Polymer Engineering and Science.* 1975; 15(3):150-159.

[13] Yoon S, Korai Y, Mochida I. Carbon fibres and active fibres. In: Marsh H, Rodríguez-Reinoso F, editors. *Sciences of carbon materials.* Alicante: Universidad de Alicante; 2000: 287-326.

[14] Edie DD, McHugh JJ, Newell JA. Spinning of carbon fibre precursors. In: Marsh H, Rodríguez-Reinoso F, editors. *Sciences of carbon materials.* Alicante: Universidad de Alicante; 2000: 327-351.

[15] Donnet JB, Bahl OP, Bansal RC, Wang TK. Carbon fibers. In: Robert A. Meyers, editor. *Encyclopaedia of physical science and technology.* New York: Academic Press; 2001: 431-455.

[16] Bascom WD and Drzal LT. [NASA contractor report 4084]. *The surface properties of carbon fibers and their adhesion to organic polymers.* Washington, D.C.: National Aeronautics and Space Administration; 1987.

[17] Fitzer E, Köchling K-, Boehm HP, Marsh H. Recommended terminology for the description of carbon as a solid. *Pure and Applied Chemistry.* 1995; 67(3):473-506.

[18] Bennett SC, Johnson DJ. Electron-microscope studies of structural heterogeneity in pan-based carbon fibres. *Carbon.* 1979; 17(1):25-39.

[19] Bai Y, Wang C, Lun N, Wang Y, Yu M, Zhu B. HRTEM microstructures of PAN precursor fibers. *Carbon.* 2006; 44(9):1773-1778.

[20] Dobb MG, Guo H, Johnson DJ. Image analysis of lattice imperfections in carbon fibres. *Carbon.* 1995; 33(8):1115-1120.

[21] Endo M, Kim C, Karaki T, Kasai T, Matthews MJ, Brown SDM, et al. Structural characterization of milled mesophase pitch-based carbon fibers. *Carbon.* 1998; 36(11):1633-1641.

[22] Dobiásová L, Starý V, Glogar P, Valvoda V. Analysis of carbon fibers and carbon composites by asymmetric X-ray diffraction technique. *Carbon.* 1999; 37(3):421-425.

[23] Zickler GA, Smarsly B, Gierlinger N, Peterlik H, Paris O. A reconsideration of the relationship between the crystallite size La of carbons determined by X-ray diffraction and Raman spectroscopy. *Carbon.* 2006; 44(15):3239-3246.

[24] Smiley RJ, Delgass WN. AFM, SEM and XPS characterization of PAN-based carbon fibres etched in oxygen plasmas. *Journal of Materials Science.* 1993; 28:3601-3611.

[25] Bennett SC, Johnson DJ, Murray R. Structural characterisation of a high-modulus carbon fibre by high-resolution electron microscopy and electron diffraction. *Carbon.* 1976; 14(2):117-122.

[26] Zhang Z, Wang X, Lin L, Xing S, Wu Y, Li Y, et al. The effects of carbon fibre and carbon fibre composite dusts on bronchoalveolar lavage component of rats. *Journal of Occupational Health.* 2001; 43:75-79.

[27] Callister WDJ. *Materials science and engineering: an introduction.* 5th Edition ed. New York, USA: John Wiley and Sons Inc.; 2000.

[28] Sherwood PMA. Surface analysis of carbon and carbon fibers for composites. *Journal of Electron Spectroscopy and Related Phenomena.* 1996; 81:319-342.

[29] Jones C. The chemistry of carbon fibre surfaces and its effect on interfacial phenomena in fibre/epoxy composites. *Composites Science and Technology.* 1991; 42(1-3):275-298.

[30] Abel M, Rattana A, Watts JF. Interaction of epoxy analogue molecules with organosilane-treated aluminium: a study by XPS and ToF-SIMS. *Langmuir.* 2000; 16(16):6510-6518.

[31] Bascom WD, Yon K-. The adhesion of carbon fibers to thermoset and thermoplastic polymers. *Journal of Adhesion.* 1991; 34:79-98.

[32] Blanco M, Lopez M, Fernandez R, Martin L, Riccardi C, Mondragon I. Thermoplastic-modified epoxy resins cured with different functionalities amine mixtures. Kinetics and miscibility study. *Journal of Thermal Analysis and Calorimetry.* 2009; 97(3):969-978.

[33] Awaja F, Gilbert M, Kelly G, Fox B, Pigram PJ. Adhesion of polymers. *Progress in Polymer Science.* 2009; 34(9):948-968.

[34] Hughes JDH. The carbon fibre/epoxy interface—a review. *Composites Science and Technology.* 1991; 41(1):13-45.

[35] Briggs D, Seah MP. *Practical surface analysis, Volume 1- Auger and x-ray photoelectron spectroscopy.* 2nd Edition ed. Chichester, UK: John Wiley and Sons Ltd.; 1983.

[36] Ebnesajjad S, Ebnesajjad CF. *Surface treatment of materials for adhesion bonding.* New York, USA: William Andrew Inc.; 2006.

[37] Zaldivar RJ, Nokes J, Steckel GL, Kim HI, Morgan BA. The effect of atmospheric plasma treatment on the chemistry, morphology and resultant bonding behaviour of a Pan-based carbon fiber-reinforced epoxy composite. *Journal of Composite Materials.* 2010; 44(2):137-156.

[38] Vickers PE, Watts JF, Perruchot C, Chehimi MM. The surface chemistry and acid–base properties of a PAN-based carbon fibre. *Carbon.* 2000; 38(5):675-689.

[39] Thielmann F and Burnett D. Determination of carbon fibre-polymer interactions by inverse gas chromatography. Determination of carbon fibre-polymer interactions by inverse gas chromatography. *Carbon; 11th-16th July 2004;* 2004.

[40] Good RJ. Contact angle, wetting, and adhesion: a critical review. *Journal of Adhesion Science and Technology.* 1992; 6:1269-1302.

[41] Song B, Bismarck A, Tahhan R, Springer J. A generalized drop length-height methods for determination of contact angle in drop-on-fibre systems. *Journal of Colloid and Interface Science.* 1998; 197:68-77.

[42] Rance DG. Thermodynamic approach to adhesion problems. In: Brewis DM, Briggs D, editors. *Industrial adhesion problems.* 1st Edition ed. Oxford: Orbital Press; 1985: 48-86.

[43] Sing KSW. Reporting physisorption data for gas/solid systems with special reference to the determination of surface area and porosity (Recommendations 1984). *Pure and Applied Chemistry.* 1985; 57(4):603-619.

[44] Yates DJC. Physical and chemical adsorption: measurement of solid surface areas. In: Brundle CR, Evans CA, Wilson S, editors. *Encyclopaedia of materials*

characterization - surfaces, interfaces, thin films. Oxford: Elsevier; 1992: 736-744.

[45] Everett DH. *Definitions, terminology, and symbols in colloid and surface chemistry—I. Appendix to the manual of symbols and terminology for physicochemical quantities and units.* London, UK: Butterworths; 1973.

[46] Attard G, Barnes C. *Surfaces.* Oxford, UK: Oxford University Press; 1998.

[47] Hoffman WP. Chemi-sorption processes on carbons. In: Marsh H, Rodríguez-Reinoso F, editors. *Sciences of carbon materials.* Alicante: Universidad de Alicante; 2000: 437-483.

[48] Zacharia R. *Desorption of gases from graphitic and porous carbon surfaces.* [Unpublished PhD thesis]. Berlin: Freien Universität Berlin; 2004.

[49] Owens DK, Wendt RC. Estimation of the surface free energy of polymers. *Journal of Applied Polymer Science.* 1969; 13(8):1741-1747.

[50] Andreu A, Stoeckli HF, Bradley RH. Specific and non-specific interactions on non-porous carbon black surfaces. *Carbon.* 2007; 45:1854-1864.

[51] Wang S, Chen Z-, Ma W-, Ma Q-. Influence of heat treatment on physical-chemical properties of PAN-based carbon fiber. *Ceramics International.* 2006; 32:291-295.

[52] Kim B-, Ryu S-, Kim B-, Park S-. Adsorption behaviour of propylamine on activated carbon fiber surfaces as induced by oxygen functional complexes. *Journal of Colloid and Interface Science.* 2006; 302:695-697.

[53] Park S-, Shin J-, Shim J-, Ryu S-. Effect of acidic treatment on metal adsorptions of pitch-based activated carbon fibers. *Journal of Colloid and Interface Science.* 2004; 275:342-344.

[54] Xu B, Wang X, Lu Y. Surface modification of polyacrylonitrile-based carbon fiber and its interaction with imide. *Applied Surface Science.* 2006; 253:2695-2701.

[55] Kaushik VK. Surface characterization of KMnO4 treated carbon fiber precursors using X-ray photoelectron spectroscopy. *Polymer Testing.* 2000; 19:17-25.

[56] Montes-Morán MA, Martinez-Alonso A, Tascon JMD, Paiva MC, Bernardo CA. Effects of plasma oxidation on the surface and interfacial properties of carbon fibres/ polycarbonate composites. *Carbon.* 2001; 39:1057-1068.

[57] Montes-Morán MA, Martinez-Alonso A, Tascon JMD, Young RJ. Effects of plasma oxidation on the surface and interfacial properties of ultra-high modulus carbon fibres. *Composites: Part A.* 2001; 32:361-371.

[58] Lee J-, Kang T-. Changes in Physico-chemical and morphological properties of carbon fiber by surface treatment. *Carbon.* 1997; 35(2):209-216.

[59] Fukunaga A, Ueda S, Nagumo M. Air-oxidation and anodization of pitch-based carbon fibers. *Carbon.* 1999; 37:1081-1085.

[60] Jin Z, Zhang Z, Meng L. Effects of ozone method treating carbon fibers on mechanical properties of carbon/carbon composites. *Materials Chemistry and Physics.* 2006; 97:167-172.

[61] Wang Y, Viswanathan H, Audi AA, Sherwood PMA. X-ray photoelectron spectroscopic studies of carbon fiber surfaces. 22. Comparison between surface treatment of untreated and previously surface treated fibers. *Chemistry of Materials.* 2000; 12:1100-1107.

[62] Gulyas J, Foldes E, Lazar A, Pukanszky B. Electrochemical oxidation of carbon fibres: surface chemistry and adhesion. *Composites: Part A.* 2001; 32:353-360.

[63] Fukunaga A, Ueda S. Anodic surface oxidation for pitch-based carbon fibers and the interfacial bond strengths in epoxy matrices. *Composites Science and Technology.* 2000; 60:249-254.

[64] Bismarck A, Kumru ME, Song B, Springer J, Moos E, Karger-Kocsis J. Study on surface and mechanical fiber characteristics and their effect on the adhesion properties to a polycarbonate matrix tuned by anodic carbon fiber oxidation. *Composites: Part A.* 1999; 30:1351-1366.

[65] Bismarck A, Kumru ME, Springer J, Simitzis J. Surface properties of PAN-based carbon fibers tuned by anodic oxidation in different alkaline electrolyte systems. *Applied Surface Science.* 1999; 143:45-55.

[66] Alexander MR, Jones FR. Effect of electrolytic oxidation upon the surface chemistry of type A carbon fibres- Part II, analysis of derivatised surface functionalities by XPS ,and TOF SIMS. *Carbon.* 1995; 33(5):569-580.

[67] Alexander MR, Jones FR. Effect of electrolytic oxidation on the surface chemistry of type a carbon fibres—Part I, X-ray photoelectron spectroscopy. *Carbon.* 1994; 32(5):785-794.

[68] Tzeng S. Catalytic graphitization of electroless Ni–P coated PAN-based carbon fibers. *Carbon.* 2006; 44(10):1986-1993.

[69] Tzeng S, Lin Y. The role of electroless Ni–P coating in the catalytic graphitization of PAN-based carbon fibers. *Carbon.* 2008; 46(3):555-558.

[70] Tang Y, Deng Y, Zhang K, Liu L, Wu Y, Hu W. Improvement of interface between Al and short carbon fibers by a-Al_2O_3 coatings deposited by sol-gel technology. *Ceramics International.* 2008; 34(7):1787-1790.

[71] Park S-, Jang Y-. X-ray diffraction and X-ray photoelectron spectroscopy studies of Ni-P deposited onto carbon fiber surfaces: impact properties of a carbon-fibe-reinforced matrix. *Journal of Colloid and Interface Science.* 2003; 263:170-176.

[72] Piquero T, Vincent H, Vincent C, Bouix J. Influence of carbide coatings on the oxidation behaviour of carbon fibers. *Carbon.* 1995; 33(4):455-467.

[73] Lee Y-. Formation of silicon carbide on carbon fibers by carbothermal reduction of silica. *Diamond and Related Materials.* 2004; 13:383-388.

[74] Yue ZR, Jiang W, Gardner SD, Pittman CU. Surface characterization of electrochemically oxidized carbon fibers. *Carbon.* 1999; 37:1785-1796.

[75] Park S-, Kim M-. Effect of acidic anode treatment on carbon fibers for increasing fiber-matrix adhesion and its relationship to interlaminar shear strength of composites. *Journal of Materials Science.* 2000; 35:1901-1905.

[76] Százdi L, Gulyás J, Pukánszky B. Electrochemical oxidation of carbon fibres: adsorption of the electrolyte and its effect on interfacial adhesion. *Composites: Part A.* 2002; 33:1361-1365.

[77] Park S-, Kim B-. Roles of acidic functional groups of carbon fiber surfaces in enhancing interfacial adhesion behaviour. *Materials Science and Engineering A.* 2005; 408:269-273.

[78] Bradley RH, Mathieson I. Chemical Interactions of Ultraviolet Light with Wool Fiber Surfaces. *Journal of Colloid and Interface Science.* 1997; 194(2):338-343.

[79] Lubarsky GV, Davidson MR, Bradley RH. Characterisation of polystyrene microspheres surface-modified using a novel UV-ozone/fluidised-bed reactor. *Applied Surface Science.* 2004; 227(1-4):268-274.

[80] Sham M-, Kim J-. Surface functionalities of multi-wall carbon nanotubes after UV/ozone and TETA treatments. *Carbon.* 2006; 44:768-777.

[81] Rich MJ, Askeland P, Liang X and Drzal L. Photo-oxidative treatment of carbonaceous fibers to promote adhesion in polymer matrix composites. *Carbon 2004; 11-16th July 2004;* 2004.

[82] Mathur RB, Mittal J, Bahl OP, Sandle NK. Characteristics of $KMnO_4$-modified PAN fibres—its influence on the resulting carbon fibres' properties. *Carbon.* 1994; 32(1):71-77.

[83] Park S-, Jang Y-, Shim J-, Ryu S-. Studies on pore structures and surface functional groups of pitch-based activiated carbon fibers. *Journal of Colloid and Interface Science.* 2003; 260:259-264.

[84] Fukunaga A, Komami T, Ueda S, Nagumo M. Plasma treatment of pitch-based ultra high modulus carbon fibers. *Carbon.* 1999; 37(7):1087-1091.

[85] Commerçon P, Wightman JP. Surface characterization of plasma treated carbon fibers and adhesion to a thermoplastic polymer. *The Journal of Adhesion.* 1992; 38(1):55.

[86] Ho KKC, Lamoriniere S, Kalinka G, Schulz E, Bismarck A. Interfacial behaviour between atmospheric-plasma-fluorinated carbon fibers and poly(vinylidene fluoride). *Journal of Colloid and Interface Science.* 2007; 313(2):476-484.

[87] Li J, Huang Y, Xu Z, Wang Z. High-energy radiation technique treat on the surface of carbon fiber. *Materials Chemistry and Physics.* 2005; 94:315-321.

[88] Gardner SD, Singamsetty CSK, Booth GL. Surface characterization of carbon fibers using angle-resolved XPS and ISS. *Carbon.* 1995; 33(5):587-595.

[89] Weitzsacker CL, Xie M, Drzal LT. Using XPS to investigate fiber/matrix chemical interactions in carbon-fiber-reinforced composites. *Surface and Interface Analysis.* 1997; 25:53-63.

[90] Drzal LT. Adhesion of carbon fibers to epoxy matrices. In: Patrick RL, editor. *Treatise on adhesion and adhesives.* New York, USA: Marcel Dekker; 1989: 187-211.

[91] Boehm HP. Surface oxides on carbon and their analysis: a critical assessment. *Carbon.* 2002; 40(2):145-149.

[92] Zhou J, Sui Z, Zhu J, Li P, Chen D, Dai Y, et al. Characterization of surface oxygen complexes on carbon nanofibers by TPD, XPS and FT-IR. *Carbon.* 2007; 45(4):785-796.

[93] Zielke U, Huttinger KJ, Hoffman WP. Surface-oxidized carbon fibers: I. Surface structure and chemistry. *Carbon.* 1996; 34(8):983-998.

[94] Stoeckli F, Moreno-Castilla C, Carrasco-Marín F, López-Ramón MV. Distribution of surface oxygen complexes on activated carbons from immersion calorimetry, titration and temperature-programmed desorption techniques. *Carbon.* 2001; 39(14):2235-2237.

[95] Szymanski GS, Biniak S, Rychlicki G. Carbon surface polarity from immersion calorimetry. *Fuel Processing Technology.* 2002; 79(3):217-223.

[96] Lopez-Ramon MV, Stoeckli F, Moreno-Castilla C, Carrasco-Marin F. On the characterization of acidic and basic surface sites on carbons by various techniques. *Carbon.* 1999; 37(8):1215-1221.

[97] Bagreev A, Bandosz TJ. H_2S adsorption/oxidation on unmodified activated carbons: importance of prehumidification. *Carbon.* 2001; 39(15):2303-2311.

[98] Wang Z-, Yamashita N, Wang Z-, Hoshinoo K, Kanoh H. Air oxidation effects on microporosity, surface property, and CH_4 adsorptivity of pitch-based activated carbon fibers. *Journal of Colloid and Interface Science.* 2004; 276(1):143-150.

[99] Pittman CU, Jiang W, Yue ZR, Gardner S, Wang L, Toghiani H, et al. Surface properties of electrochemically oxidized carbon fibers. *Carbon.* 1999; 37:1797-1807.

[100] Lee J, Drzal LT. Surface characterization and adhesion of carbon fibers to epoxy and polycarbonate. *International Journal of Adhesion and Adhesives.* 2005; 25(5):389-394.

[101] Liu YC, Lu DN. Surface energy and wettability of plasma-treated polyacrylonitrile fibers. *Plasma Chemistry and Plasma Processing.* 2006; 26(2):119-126.

[102] Gao S, Mäder E, Zhandarov SF. Carbon fibers and composites with epoxy resins: Topography, fractography and interphases. *Carbon.* 2004; 42(3):515-529.

[103] Goldstein B, Aronhime MT, Avny Y, Marom G. The bonding of carbon fibres to epoxy resins as affected by the manufacturing and surface treatment processes. *International Journal of Adhesion and Adhesives.* 1987; 7(3):135-139.

[104] Pittman CU, Jiang W, Yue ZR, Leon y Leon CA. Surface area and pore size distribution of microporous carbon fibers prepared by electrochemical oxidation. *Carbon.* 1999; 37:85-96.

[105] Pittman CU, He G-, Wu B, Gardner SD. Chemical modification of carbon fiber surfaces by nitric acid oxidation followed by reaction with tetraethylenepentamine. *Carbon.* 1997; 35(3):317-331.

[106] Rand B, Robinson R. Surface characteristics of carbon fibres from PAN. *Carbon.* 1977; 15(4):257-263.

[107] Bogoeva-Gaceva G, Mäder E, Haüssler L, Dekanski A. Characterization of the surface and interphase of plasma-treated HM carbon fibres. *Composites Part A: Applied Science and Manufacturing.* 1997; 28(5):445-452.

[108] Macur JE, Marti J, Lui S. Microscopy. In: Sibilia JP, editor. *A Guide to Materials Characterisation and Chemical Analysis.* 2nd Edition ed. New York, USA: VCH Publishers, Inc.; 1996: 167-198.

[109] Johnson DJ, Frank C. Recent Advances in Studies of Carbon Fibre Structure [and Discussion]. *Philosophical Transactions of the Royal Society of*

London.Series A, Mathematical and Physical Sciences. 1980; 294(1411):443-449.

[110] Lozano-Castelló D, Maciá-Agulló JA, Cazorla-Amorós D, Linares-Solano A, Müller M, Burghammer M, et al. Isotropic and anisotropic microporosity development upon chemical activation of carbon fibers, revealed by microbeam small-angle X-ray scattering. *Carbon.* 2006; 44(7):1121-1129.

[111] Zheng G, Sano H, Suzuki K, Kobayashi K, Uchiyama Y, Cheng H. A TEM study of microstructure of carbon fiber/polycarbosilane-derived SiC composites. *Carbon.* 1999; 37(12):2057-2062.

[112] Pimenta MA, Dresselhaus G, Dresselhaus MS, Cançado LG, Jorio A, Saito R. Studying disorder in graphite-based systems by Raman spectroscopy. *Physical Chemistry Chemical Physics.* 2007; 9:1276-1290.

[113] Reich S, Thomsen C. Raman spectroscopy of graphite. *Philosophical Transactions of the Royal Society of London. Series A: Mathematical, Physical and Engineering Sciences.* 2004; 362(1824):2271-2288.

[114] Angoni K. A study of highly ordered carbons by use of macroscopic and microscopic Raman spectroscopy. *Journal of Materials Science.* 1998; 33(14):3693-3698.

[115] Montes-Morán MA, Young RJ. Raman spectroscopy study of HM carbon fibres: effect of plasma treatment on the interfacial properties of single fibre/ epoxy composites. *Carbon.* 2002; 40:845-855.

[116] Melanitis N, Tetlow PL, Galiotis C. Characterization of PAN-based carbon fibres with laser Raman spectroscopy. *Journal of Materials Science.* 1996; 31:851-860.

[117] Bradley RH, Ling X, Sutherland I. An investigation of carbon fibre surface chemistry and reactivity based on XPS and surface free energy. *Carbon.* 1993; 31(7):1115-1120.

[118] Zielke U, Hüttinger KJ, Hoffman WP. Surface-oxidized carbon fibers: II. Chemical modification. *Carbon.* 1996; 34(8):999-1005.

[119] Zielke U, Hüttinger KJ, Hoffman WP. Surface-oxidized carbon fibers: III. Characterization of carbon fiber surfaces by the work of adhesion/ pH diagram. *Carbon.* 1996; 34(8):1007-1013.

[120] Zielke U, Hüttinger KJ, Hoffman WP. Surface-oxidized carbon fibers: IV. Interaction with high-temperature thermoplastics. *Carbon.* 1996; 34(8):1015-1026.

[121] Lindsay B, Abel M, Watts JF. A study of electrochemically treated PAN based carbon fibres by IGC and XPS. *Carbon.* 2007; 45(12):2433-2444.

[122] Allington RD, Attwood D, Hamerton I, Hay JN, Howlin BJ. A model of the surface of oxidatively treated carbon fibre based on calculations of adsorption interactions with small molecules. *Composites Part A: Applied Science and Manufacturing.* 1998; 29(9-10):1283-1290.

[123] Ylä-Mäihäniemi PP, Heng JYY, Thielmann F, Williams DR. Inverse Gas Chromatographic Method for Measuring the Dispersive Surface Energy Distribution for Particulates. *Langmuir.* 2008; 24(17):9551-9557.

[124] Bradley RH, Daley R, Le Goff F. Polar and dispersion interactions at carbon surfaces: further development of the XPS-based model. *Carbon.* 2002; 40(8):1173-1179.

[125] Gonzalez-Martin ML, Janczuk B, Labajos-Broncano L, Bruque JM. Determination of the carbon black surface free energy components from the heat of immersion measurements. *Langmuir.* 1997; 13:5991-5994.

[126] Rodríguez GA, Giraldo L, Moreno JC. Calorimetric study of the immersion enthalpies of activated carbon cloths in different solvents and aqueous solutions. *Journal of Thermal Analysis and Calorimetry.* 2009; 96(2):547-552.

[127] Rodríguez-Reinoso F, Molina-Sabio M, González MT. Effect of oxygen surface groups on the immersion enthalpy of activated carbons in liquids of different polarity. *Langmuir.* 1997; 13(8):2354-2358.

[128] Sheng E, Sutherland I, Bradley RH, Freakley PK. Heat of immersion calorimetry studies of carbon blacks. *Materials Chemistry and Physics.* 1997; 50(1):25-30.

[129] Huang Y, Young RJ. Effect of fibre microstructure upon the modulus of PAN- and pitch-based carbon fibres. *Carbon.* 1995; 33(2):97-107.

[130] Paipetis A, Galiotis C. Effect of fibre sizing on the stress transfer efficiency in carbon/epoxy model composites. *Composites Part A: Applied Science and Manufacturing.* 1996; 27(9):755-767.

[131] Montes-Morán MA, Young RJ. Raman spectroscopy study of high-modulus carbon fibres: effect of plasma-treatment on the interfacial properties of single-fibre epoxy composites. Part II: Characterisation of the fibre-matrix interface. *Carbon.* 2002; 40:857-875.

2 Materials and Methods

2.1 Introduction

The interfacial bonding between the fibre and the matrix largely depends on the chemistry of the surface of the carbon fibre but also on the surface texture [1]. It is therefore important to have a detailed knowledge about several aspects of the surface. Various methods exist to characterise surfaces, however the investigation method should be chosen by considering the type of material to be analysed and the end use of that material [2]. This Chapter outlines the theory behind the techniques used in this project and sets out the experimental details used.

2.2 Carbon Materials

2.2.1 Untreated Fibres

The carbon fibres used in this study are T80-400, high strength, intermediate modulus, PAN based carbon fibres (Cytec Engineered Materials Ltd., Wilton, UK). Three batches of untreated, unsized, fibres (UST) were studied. Table 2.1 lists some of the properties quoted by the manufacturer for standard treated fibres.

Table 2.1 Characteristics of T80-400 fibres

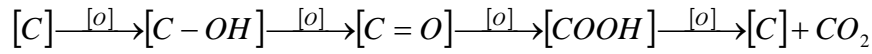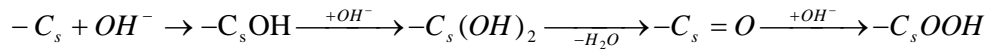| Characteristic	Value
Tensile Strength	5.52 GPa (800 ksi)
Tensile Modulus	276 GPa (40 Msi)
Fibre diameter	5.1 μm
Surface Area	0.85 m^2/g

2.2.2 Carbon Black

Carbon black was used as a model surface for some calorimetric experiments due to the small surface areas available on fibres. The carbon black was N330 (Cabot Co., Boston, USA). It is non-porous. The manufacturers quote a surface area of 77 m^2/g and other BET studies using nitrogen have returned surface areas of 80 ($\pm$ 8) m^2/g [3].

2.3 Electrochemical Treatments

2.3.1 Theory

Electrochemical treatments, also known as shear or anodic treatments, are currently the most used treatment method in industry [4], although details of the process are rarely released due to the commercial sensitivity of the information [5,6]. Generally, a current is applied to the fibres while they are passed through an electrolytic solution. The fibre acts as an anode, while carbon electrodes also inserted into the electrolytic bath act as cathodes [7]. During the process, the cathode undergoes reduction (gains electrons) while the anode undergoes oxidation (loses electrons), thereby modifying the fibre surface [7]. The rate at which this occurs is related to the current density by Faraday's law of electrolysis which states that the mass of reactants converted at the electrode is proportional to the charge applied [8,9].

A range of electrolytes can be used including acid and bases. Ammonium bicarbonate is one of the most useful bases as it does not leave a residue so simplifies the final cleaning process [10]. It is generally accepted that progressive oxidation of a carbon surface can be summarised as in Equation 2.1 [11,12]. In the case of a base treatment, surface atoms on the fibre will react with hydroxyl ions. Equation 2.2 shows a likely process for the base-fibre interaction. The OH ion reacts with surface carbons (C_s) to form -C_sOH groups. Continuing oxidation by a second OH ion would make -$C_s(OH)_2$ that will lose one molecule of water and make -C_s=O. A subsequent attack of a third OH ion will make a carboxylic acid that may de-protonate to give a more stable carboxylate.

Equation 2.1

$$[C] \xrightarrow{[O]} [C-OH] \xrightarrow{[O]} [C=O] \xrightarrow{[O]} [COOH] \xrightarrow{[O]} [C] + CO_2$$

Equation 2.2

$$-C_s + OH^- \rightarrow -C_sOH \xrightarrow{+OH^-} -C_s(OH)_2 \xrightarrow{-H_2O} -C_s = O \xrightarrow{+OH^-} -C_sOOH$$

In acid treatments, the surface is modified by protons. The acid involves H^+ ions in an aqueous environment (H_3O^+). Equation 2.3 shows a likely process for the acid-fibre interaction. H_3O^+ can react with a surface carbon, transferring an electron to one H^+ to make one C-H bond, and producing HC_sOH_2. This may give an alkoxide group that can be further oxidised to carbonyl. Carbonyl can be oxidised in acid conditions giving rise to the carboxylic acid.

Equation 2.3

$$-C_s + H_3O^+ \rightarrow -HC_sOH_2 \xrightarrow{-H^+} -HC_sOH \xrightarrow{-H^+} -HC_s = O \xrightarrow{+H_2O \ and \ -H_2} -C_sOOH$$
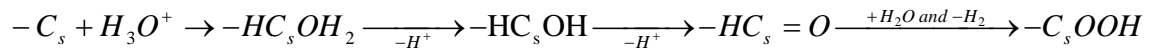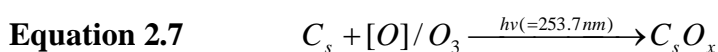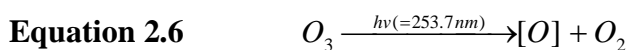
2.3.2 Equipment and Experimental Set-up

Unsized PAN based carbon fibres, described in Section 2.2.1, were treated by Cytec Engineered Materials Ltd. (Wilton, UK) using an industrial anodic process. The fibres were used as anodes and were modified using two electrolytic baths consecutively; an oxygen bath and an ammonium bath. In the oxygen bath, an aqueous solution of an acid or base was used. The second bath, the ammonium bath, contained an aqueous solution of an ammonium compound with a pH of at least 8. The ammonium bath produces nitrogen containing compounds some of which may react with the surface of the fibre making $-NH_x$ [13].

The charge applied to the fibres (i.e. the coulombs per gram) affects the oxygen and nitrogen concentration generated on the surface. The charge applied to the base treated fibres was varied from 0.2x up to 6x, where x is the standard charge. The acid modified fibres were treated at 3x. Five batches of each treatment were produced. Acid (A) and base (B) treatments are identified by the charge level followed by the letter A or B respectively, e.g. 3A.
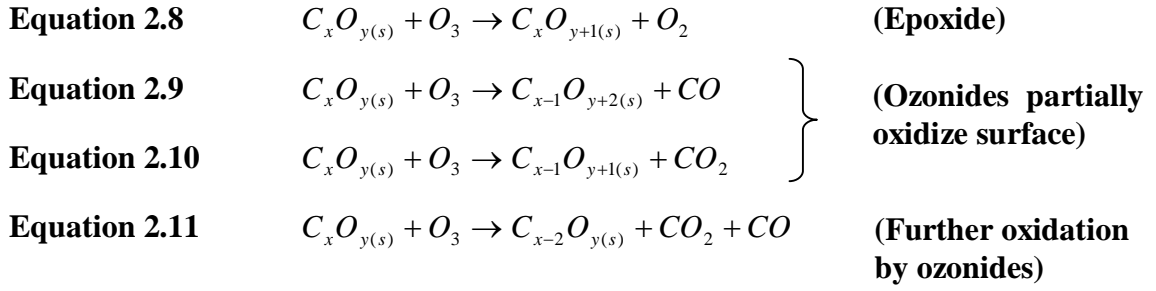
2.4 UV Ozone Treatments

2.4.1 Theory

As described earlier in Chapter 1.6.3, ultraviolet light and ozone can be used to alter the chemistry and near surface composition and structure of a material. In ultraviolet/ozone (UVO_3) treatments, the reactions in the ambient air and on the surface of a carbon sample can be simplified as follows [14]:

Equation 2.4 $\qquad O_2 \xrightarrow{hv(\lambda=184.9nm)} 2[O]$

Equation 2.5 $\qquad [O] + O_2 \rightarrow O_3$

Equation 2.6 $\qquad O_3 \xrightarrow{hv(=253.7nm)} [O] + O_2$

Equation 2.7 $\qquad C_s + [O]/O_3 \xrightarrow{hv(=253.7nm)} C_sO_x$
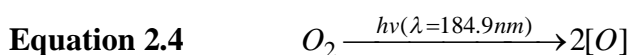
where $[O]$ stands for atomic oxygen, s stands for surface and near surface, and x is the number of oxygen atoms in the functional group.

Edge planes on the surface of the carbon fibres react with the ozone and atomic oxygen allowing the formation of functional groups [15]. Three mechanisms of interaction between carbon and ozone have been postulated [16]; (i) the ozone interacts with C=C bonds to form epoxide (Equation 2.8), (ii) the ozone interacts with C=C bonds to form ozonides which go on to partially oxidise the surface (Equation 2.9 and Equation 2.10), (iii) the ozone converts olefinic bonds to ozonides, again oxidizing the surface but to a higher level, i.e. 2 moles of gas are produced for every 1 mole of ozone (Equation 2.11).

| Equation 2.8 | $C_xO_{y(s)} + O_3 \rightarrow C_xO_{y+1(s)} + O_2$ | **(Epoxide)** |

| Equation 2.9 | $C_xO_{y(s)} + O_3 \rightarrow C_{x-1}O_{y+2(s)} + CO$ | **(Ozonides partially oxidize surface)** |
| Equation 2.10 | $C_xO_{y(s)} + O_3 \rightarrow C_{x-1}O_{y+1(s)} + CO_2$ | |

| Equation 2.11 | $C_xO_{y(s)} + O_3 \rightarrow C_{x-2}O_{y(s)} + CO_2 + CO$ | **(Further oxidation by ozonides)** |

While UV light in the range of 185 to 255 nm does not have enough energy to break carbon-carbon bonds in the ring structure (binding energy per atom =7.4 eV [17]), it is possible for chemical scission to occur at incomplete rings and end groups and radicals generated by the UV light can break the C-C bonds by electrophilic addition thus making more sites for oxidation to occur at.

2.4.2 Equipment and Experimental Set-up

Fibres were treated in a Jelight UVO cleaner/oxidizer; Model 42-220 (Jelight Company Inc., California, USA), shown in Figure 2.1. The cleaner/oxidizer uses a low pressure mercury vapour grid lamp to produce the UV. It has high transmittance, emitting 184.9 nm and 253.7 nm wavelengths and a quoted output of 28 mW/cm^2 at 254 nm, 6 mm distance. Fibres were mounted on an XPS stub and irradiated for a range of times (1-120 minutes) after allowing the lamp to warm up for at least 15 minutes. Fibres were held at a distance of 3 cm from the lamp where temperatures in the cleaner can reach 90 ^{o}C, as measured by a K-type thermocouple [18]. Due to the design of the XPS stub only a circle of ~6 mm diameter of fibres were exposed to the light. Long tows of fibres (~1.5 g) for TPD measurements were also treated for 4 hours with the fibres being regularly turned to achieve all over treatment.

Figure 2.1 Ultraviolet ozone cleaner.

The concentration of ozone produced by the UV/O$_3$ cleaner is quoted as 500-1000 ppm by the manufacturer. However, this assumes a blower is attached to the unit, removing the ozone before destruction by the 254 nm light which is not the case in our set up. A model to estimate the amount of ozone produced by a low pressure mercury lamp has been proposed by Voronov, [19]. The model covers situations without air flow such as the one here. The molecular concentration of ozone can be calculated by solving Equation 2.12.

Equation 2.12

$$2\left(1 - e^{-\kappa_{185}^{air}L}\right)\dot{n}_{185} = \left(1 - e^{-\kappa_{254}^{ozone}L\frac{n_{ozone}^{eq}}{n_{air}}}\right)\dot{n}_{254}$$

Where κ_{185}^{air} is the absorption coefficient in air at 185 nm, κ_{254}^{ozone} is the absorption coefficient in ozone at 254 nm, L is the path length of the light, $\dot{n}_{\lambda}$ is the flux of photons of wavelength λ (nm), n_{ozone}^{eq} is the molecular concentration of ozone at equilibrium, and n_{air} is the molecular concentration of air in the chamber. Rearranging Equation 2.12 and substituting $\dot{n}_{\lambda} = \lambda I_{\lambda}/hc$ where I_{λ} is the intensity of the emitted light at wavelength λ and h is Planck's constant gives Equation 2.13.

Equation 2.13

$$\frac{n_{ozone}^{eq}}{n_{air}} = \frac{\ln\left(1 - 2\left(1 - e^{-\kappa_{185}^{air}L}\right)\frac{I_{185}}{I_{254}}\frac{\lambda_{185}}{\lambda_{254}}\right)}{-\kappa_{254}^{ozone}L}$$

The following values were used, $\kappa_{185}^{air} = 0.1$ cm^{-1} [20], $\kappa_{254}^{ozone} = 309$ cm^{-1} [21], $L = 3$ cm, $I_{185} = 5.6$ mW/cm^2, and $I_{254} = 28$ mW/cm^2. At standard temperature and pressure (STP), this would give a molecular concentration of 2.27×10^{15} molecules/cm^3 or 140 ppm. However, the cleaning unit can reach temperatures of 90 ^{o}C. The unit is not sealed so according to the ideal gas law, only the number of molecules in the treatment chamber will change. At 90 ^{o}C, the molecular concentration of air will be 0.81 times the concentration at STP so the molecular concentration of ozone will be 1.84×10^{15} molecules/cm^3 or 110 ppm. The absorption coefficients also vary with temperature but they do not alter the calculation significantly.

Addition of ozone gas from an ozone generator (Ozonia Triogen Ltd, East Kilbride, UK, model TOGC2) was also flowed into the UV/O$_3$ generator during UV irradiation. The generator consists of a ceramic dielectric tube with a stainless steel electrode in the centre. Oxygen was flowed into the tube and a voltage applied to the electrode. The potential difference between the electrode and the ceramic tube increases until it eventually reaches the breakdown voltage of the oxygen which goes on to form ozone in a manner similar to Equation 2.4 and Equation 2.5 [22]. The manufacturers quote a maximum of 8 g/hr (0.133 g/min) of ozone generated using an input flow of 5 litres/min of oxygen ($\approx 1.7 \times 10^{21}$ ozone molecules/min or 18000 ppm).

2.5   Resin Molecules

2.5.1   Background

Epoxy resins are one of the most popular polymer matrices used in the aerospace industry due to their low cost, low processing temperatures, good adhesion, good mechanical properties, low shrinkage during curing, lack of volatile solvents and low creep [23,24].   As with surface treatments, the exact nature of the resin matrix used in commercial production is proprietary knowledge. Different epoxies can be blended as well as different curing agents and catalysts used [25,26].

2.5.2   Materials

Four components of a typical industrial resin were examined in this study; two epoxies (PY and MY), one thermoplastic (KM), and a curing agent (DDS) (Cytec Engineered Materials Ltd., Wilton, UK). The thermoplastic is a polyaromatic ether sulfone (PES) based polymer with the general structure as shown in Figure 2.2.
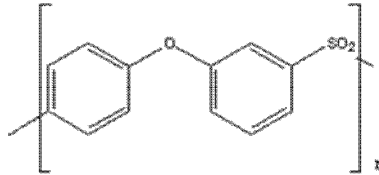

Figure 2.2 PES thermoplastic generic structure.

The   mean   molecular   cross-sectional   area, a_m,   of   each   molecule   was approximated using Equation 2.14 [27]. Resins were used in dilute forms for calorimetry see Section 2.11.4.

Equation 2.14

$$a_m = \sqrt{3}\left(\frac{V_{mol}}{2N_a}\right)^{2/3}$$

Where V_{mol} is the molar volume, and N_a is Avogadro's number.

2.6 X-ray Photoelectron Spectroscopy

2.6.1 Theory

X-ray photoelectron Spectroscopy (XPS) utilises the photoelectric effect and the unique binding energy (BE) of core electrons in an element to provide information about the surface chemical composition of a sample [29]. It is currently considered the most successful technique for examining the surface chemistry of carbon fibres [5]. The x-ray photoelectron spectrometer consists of three main parts; the x-ray source, the energy analyser and an electron detector [29]. Figure 2.3 shows a schematic of a Kratos spectrometer (Kratos Analytical Ltd., UK). A sample is placed on a small stub and degassed before being transferred into the analysis chamber. The analysis chamber is maintained at a vacuum of ~10^{-7} Pa to ensure emitted electrons are not scattered before reaching the detector and to ensure the sample surface does not become contaminated with gas molecules. The sample is then irradiated with monochromatic x-rays [29,30].
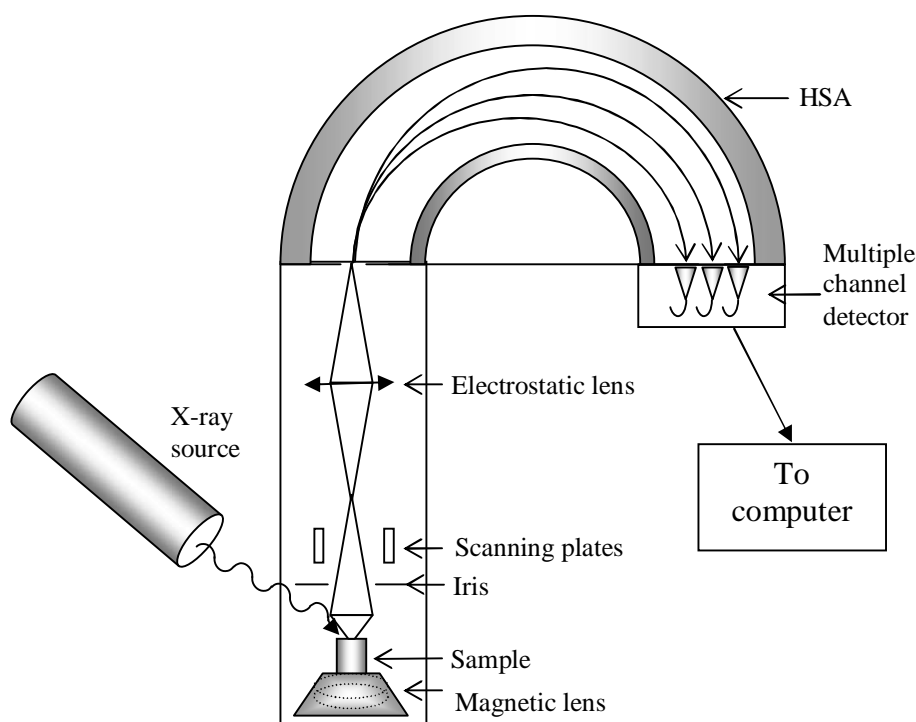

Figure 2.3 X-ray photoelectron spectrometer schematic, fitted with an x-ray source, a concentric hemispherical analyser, and a multiple channel detector (after [28]**).**

The x-rays are generated by accelerating electrons towards a high voltage target which releases x-rays when the electrons strike it. The electrons are often generated thermionically from a tungsten filament. The target is chosen to produce x-rays that have energy high enough to eject core electrons from a large range of elements but a narrow characteristic x-ray emission line to prevent broadening of the measured spectra. Very few materials meet these requirements and only two are currently used, namely the Magnesium K_α line (energy 1253.6 eV, width 0.7 eV) and the Aluminium K_α line (energy 1486.6 eV, width 0.85 eV). In some spectrometers, such as the one used in this study, a monochromator is fitted to further narrow the line width of the x-rays and to reduce the bremsstrahlung background [29,30].

The emitted x-rays are directed at the surface of the sample and electrons are ejected from the inner core shells of the atoms. This is known as the photoelectric effect. The kinetic energy of the ejected electron (E_k) is measured and the binding energy of the electron (E_b), which is unique to that element, is calculated using Equation 2.15 [29,30].

Equation 2.15

$$E_b = h\upsilon - E_k - \varphi$$

where h is Planck's constant, υ is the frequency of the x-rays, and φ is the work function which depends on the sample and the spectrometer.

In XPS, it is customary to use spectroscopist's notation to identity which electrons in the elemental atom are being examined. The ejected electron is labelled nl_j, where n is the principle quantum number, l is angular momentum and j is the total angular momentum, (i.e. $j = l + s$, where s is the spin quantum number). The principle quantum number can take integer values of 1, 2, 3 etc., s can take values of $\pm \frac{1}{2}$, and l can take integer values of 0, 1, 2, 3 etc. although l is more normally assigned a letter; s, p, d, and f for each integer listed respectively [30]. For example, in the case of carbon, the most important

transition is from the 1s shell. Figure 2.4 shows the photoelectric transition for a 1s electron.

Following removal of a core electron, another electron from an outer shell fills the vacancy releasing a quanta of energy which is removed from the atom. This relaxation occurs through either characteristic x-ray emission or Auger electron emission. Neither is used for analysis in XPS but the latter is the basis of Auger electron spectroscopy [31].
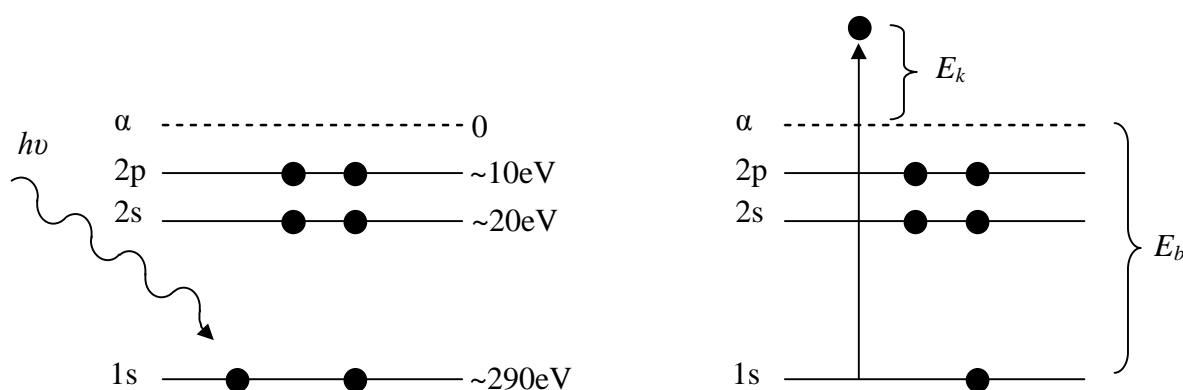

Figure 2.4 Photoelectric emission from the 1s shell in a carbon atom (after [32]**). α represents the vacuum level.**

The ejected electrons are focused via a series of electrostatic lenses towards the energy analyser which removes any electrons that do not have the kinetic energy of interest before they reach the electron detector. The energy analyser is normally a concentric hemispherical analyser (CHA) [29]. Figure 2.5 shows a schematic of a CHA. The CHA consists of two concentric hemispheres with the inner hemisphere radius being R_1 and the outer radius being R_2. The inner and outer hemispheres are held at different potentials; $-V_1$ and $-V_2$ respectively with $V_2 > V_1$. Electrons enter the analyser through the first slit (1) and are deflected by the potential difference. Electrons with too high, or too low, of energy will not be focussed correctly for the exit slit (2) and will not reach the detector but a small range will. The absolute resolution of the analyser in terms of the base width of a chosen peak (*E(B)*) is given by Equation 2.16 [29].

Equation 2.16
$$\frac{\Delta E(B)}{E} = \frac{W_1 + W_2}{2R_0} + \delta\alpha^2$$

Where E is the correct energy of the peak, W_1 and W_2 are the widths of the entrance and exit slits respectively, R_0 is the radius of the median equipotential surface, and $\delta\alpha$ is the angle of entrance of electrons with respect to a path tangential to R_0. The resolution can therefore be increased by increasing the radius of the median surface, i.e. increasing the size of the spectrometer. It is normally more convenient to retard the energy of the electrons, i.e. decrease the pass energy [31].
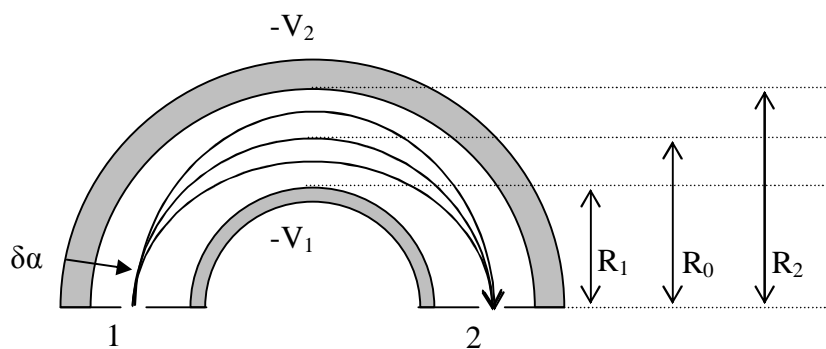

Figure 2.5 Concentric Hemispherical Analyser (after [31]**).**

The voltages of the hemispheres are altered to allow electrons of different energy through to the detectors. The CHA can be operated in one of two modes; fixed analyser transmission (FAT) or fixed retard ratio (FRR). In FAT mode, all electrons are retarded to a set pass energy [29,30,31]. This means the resolution is the same for all binding energies being analysed. The voltages of the hemispheres will be altered linearly by a constant value. In FRR mode, the electrons are retarded to a set fraction of their initial kinetic energies resulting in the absolute resolution varying with the binding energy under analysis. The voltages of the hemispheres will be altered linearly by a value that varies with incoming kinetic energy. It is normal to use FRR in Auger spectroscopy but FAT mode is more useful for quantification in XPS [31].

The spectrometer can be operated using a variety of pass energies and can perform survey scans or narrow scans. A survey scans across all the kinetic

energies relatively quickly using a high pass energy. This means the analyser allows a large transmission (many counts) but has low resolution. In narrow scans, a small pass energy is chosen and the dwell time is increased to improve the resolution. Narrow scans are normally used to obtain detailed chemical shift information. The scans, which are in the form of kinetic energy distributions, are conventionally converted to binding energies using Equation 2.15 to give a spectrum of the type shown in Figure 2.6.
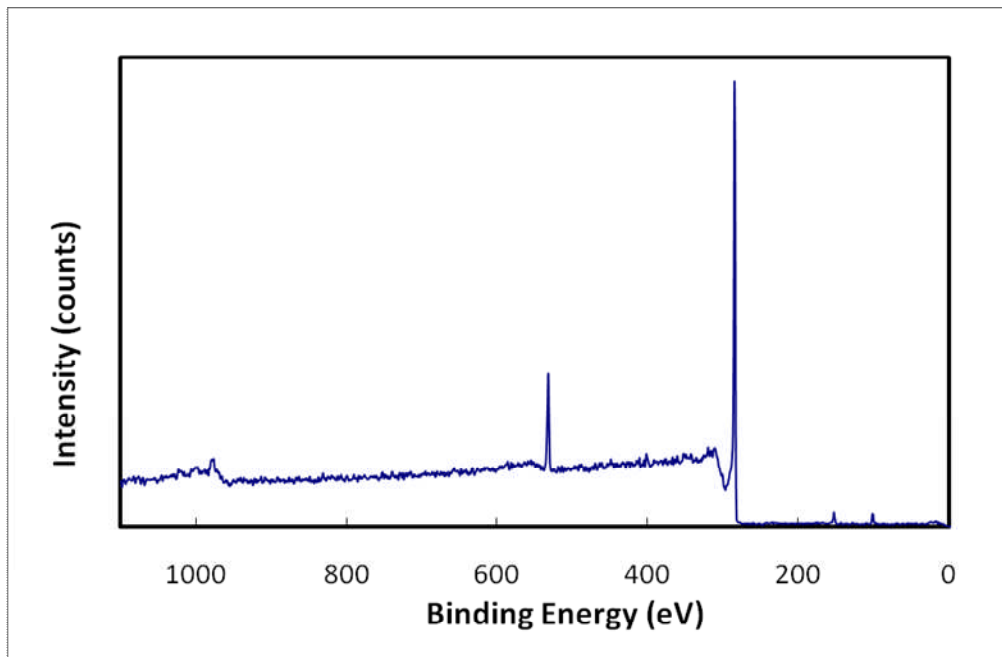

Figure 2.6 Example FAT survey scan.

By counting the number of electrons of a particular binding energy, a_i, (i.e. calculating the area underneath a peak following a background subtraction) and multiplying by a sensitivity factor, q_i, to account for interaction cross sections and instrumental factors, the relative quantity of the element within the surface can be calculated as in Equation 2.17 [30]. Sensitivity factors can be determined theoretically or experimentally.

Equation 2.17

$$At.(\%)_i = \frac{a_i/q_i}{\sum_j \dfrac{a_j}{q_j}} \times 100$$

2.6.2 Chemical Shifts

From the inception of XPS, it was clear that emitted electrons from elements within an analysed sample showed different energies depending on the surrounding environment of the emitting atom or molecule [33]. These "chemical shifts" can have several origins, e.g. a difference in oxidation state or a difference in bonding [29]. Indeed, the more bonds between an electronegative element and the element under investigation; the more positive the chemical shift will be [30]. For example, the C-C bond has a binding energy of 284.6 eV while the carbonyl group (C=O) has a higher binding energy of 289.1 eV due to the double bond [34].

Due to the linewidth of the x-ray source and the small chemical shifts involved, it is not always possible to resolve individual peaks attributed to different atom environments [30]. To derive surface chemistry information, curves are mathematically fitted to the narrow scans to determine how much of the carbon peak is due to certain types of bonding. This is an iterative process performed by a software package. As such, the results depend on the background subtraction method, the fitting algorithms and the fitting parameters chosen by the operator.

Many chemical shifts have been reported in the literature. Table 2.2 lists a review of some of the shifts reported for the carbon peak in carbon fibres.

Table 2.2 Review of literature values for chemical shifts (in eV) from the carbon to carbon bond peak (284.6 eV) [35-47]

C-C or C-H	C-OH or C-OR or C=N	C=O & O-C-O	COOH or COOR	CO_3^-, $\pi \rightarrow \pi^*$ shake up	Plasmon
Maximum and minimum shift	1.0-1.7	2.7-3.8	3.5-4.8	5.75-6.2	6.1-6.9
Corresponding regions (284.6)	285.6-286.3	287.3-288.4	288.1-289.4	290.35-290.8	290.7-291.5
Average shift	1.5	3.0	4.2	6.0	6.6

2.6.3 Equipment and Experimental Set-up

XPS experiments were performed on a Kratos Axis HSi spectrometer at a residual vacuum of 10^{-7} Pa, using a monochromatic Al Kα source (energy 1486.6 eV). Figure 2.7 shows the XPS used. The vacuum for the analysis chamber was maintained by an ion diffusion pump. The vacuum in the introductory chamber was maintained by a turbomolecular pump (Pfeiffer, Asslar, Germany, Type TPU 060) backed up by a 8 vane rotary pump (Edwards, West Sussex, UK, model number RV8).

Figure 2.7 Kratos Axis x-ray photoelectron spectrometer and (inset) constant height stub.

Fibres were mounted on a "constant height" stub such that the analysed surface was completely composed of fibres (shown as inset in Figure 2.7). Narrow scans (pass energy = 20eV) for C1s, O1s, N1s and Si2p were performed three times and averaged at three positions on each sample. The average surface composition was determined from the area beneath the elemental peaks following a Shirley background subtraction and using relevant empirical atomic sensitivity factors; C1s (0.25), O1s (0.66), N1s (0.42), Si2p (0.23) and Na1s (2.3) (Kratos Analytical Ltd., Manchester, UK). The sensitivity factors are a combination of photoelectric cross section, transmission function and inelastic mean free path factors referenced to F1s = 1.00. Curve fitting was performed using XPSPEAK 4.1 (Dr Kwok, Chinese University of Hong Kong). The Gaussian/ Lorentzian (G/L) mix

was fixed to 0.2 for the graphite peak and 0.5 for all the others. Peak shifts were fixed in relation to the graphite peak.

Treated fibres were placed in the XPS vacuum directly after treatment, except where the effect of ageing was examined. In this case, two sets of UST fibres were treated for 40 minutes by UV/O$_3$ at the same time. One set was examined immediately after treatment and the other left for 1 month at room temperature and at atmospheric pressure before XPS analysis.

2.7   Scanning Electron Microscopy

2.7.1   Theory

In addition to surface chemistry; surface morphology of carbon fibres can also play a part in the bonding process. It is therefore of interest to know how treatments affect the surface of the fibres physically.

The scanning electron microscope (SEM) provides highly magnified topographical images of the samples. A beam of electrons is scanned across a sample resulting in several interactions taking place that lead to the emission of electrons or photons from the surface. The exiting electrons can be measured and the signal used to form an image of the surface [48,49]. The SEM consists of three main stages; the electron source, the beam steering and the detector. As with the XPS, the SEM must be kept at a high vacuum to allow the electrons to reach the detector without further interaction, however the vacuum only needs to be ~1 Pa. Electrons can be generated by heating a tungsten filament to ~2700 K until thermionic emission occurs. The resulting electrons are accelerated towards an anode with an aperture in it. The electrons pass through the aperture into the beam steering/ focussing section. Electrostatic lenses (condensers) narrow the electron beam to ~ 5nm in diameter. Electromagnetic scanning coils raster the electron beam across the sample surface [48,49]. Figure 2.8 shows a schematic of the whole SEM system while Figure 2.9 shows a schematic of the electrostatic lens system and an example lens. The lens consists of an electromagnetic coil encased in iron which generates a magnetic field at a gap in the casing (known as

a polepiece gap). The magnetic field deflects the incoming electrons, focussing those of the same energy to a single point [48].
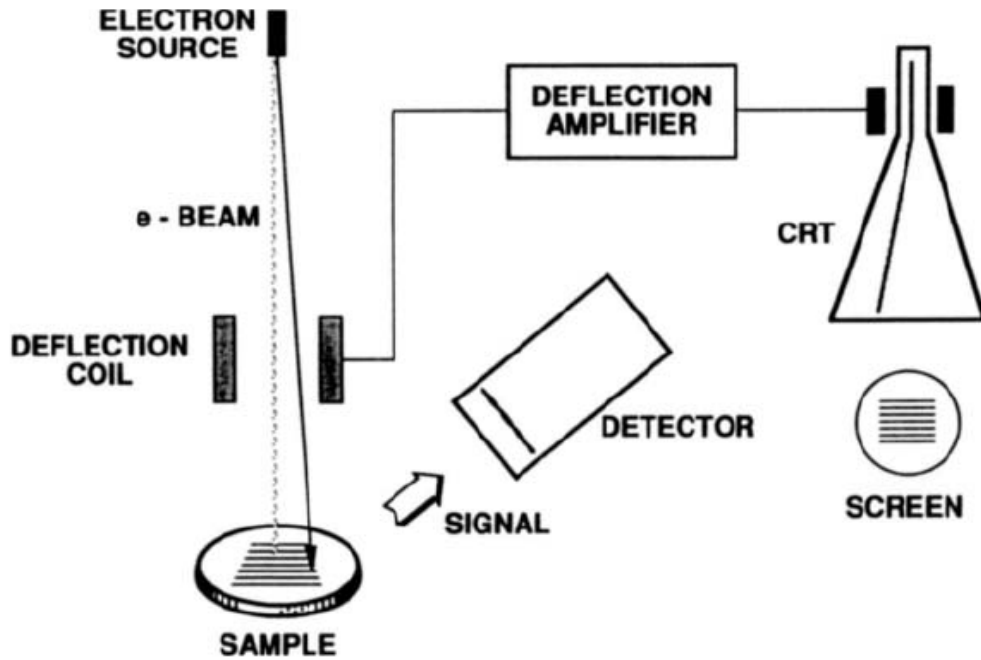

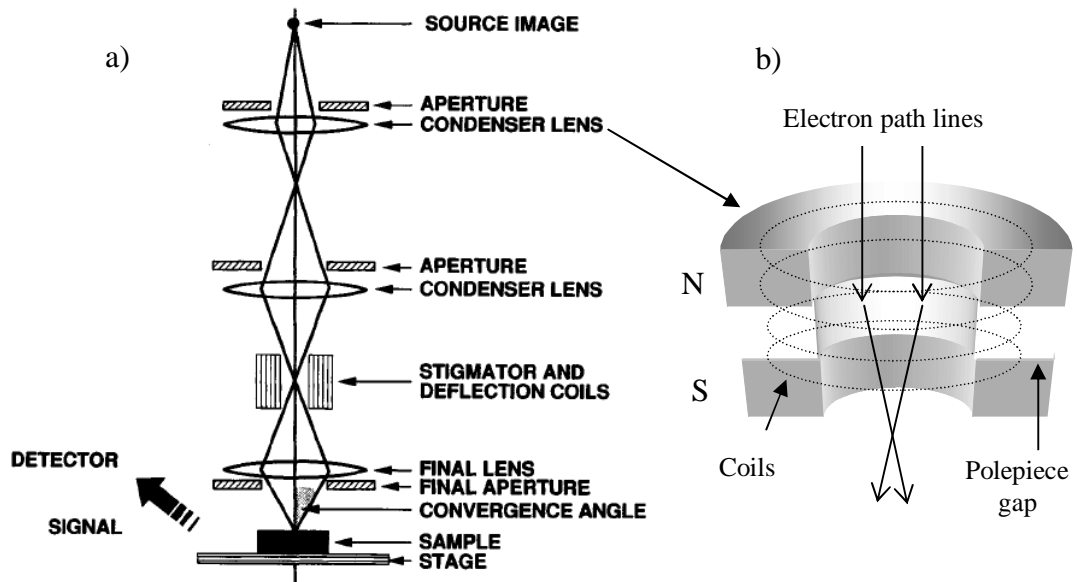**Figure 2.8 Schematic of a scanning electron microscope** [49]**.**

Figure 2.9 a) Schematic of SEM electrostatic lens system [49] **b) simplified lens coil (after** [48]**).**

Electrons can interact with the sample in a combination of ways [48,49]:

1) The electrons pass through the sample unscattered (particularly in the case of thin samples) or

2) The electrons are scattered elastically in all directions including back towards the source by the atomic nucleus (particularly materials with high atomic number) or

3) The electrons are scattered inelastically by the atomic electrons (particularly materials with low atomic number).

Inelastic collisions can produce secondary electrons if enough energy is transferred to eject an atomic electron. By convention emitted electrons with energies < 50 eV are called secondaries [49]. Most of the secondary electrons detected are produced within the first few nm of the surface as deeper secondaries are subject to further collisions preventing their escape. Elastically scattered electrons are referred to as primary electrons. Backscattered electrons have energies >50 eV, comparable to primary electron energies. Backscattering is more likely to occur with increasing atomic number so a natural contrast occurs with different elements [49].

Inelastically scattered electrons produce a number of effects in addition to secondary electrons, some of which are not used for imaging but can be used to gain other information (e.g. chemical information). These effects include Auger electron emission, x-ray emission and phonon production (vibrations in the molecular lattice). Images can be formed using the signal from secondary electrons or backscattered electrons or from the sum of both signals [48,49].

The detectors used will be either photomultiplier tubes or, more recently, semiconductor detectors. The intensity of the signal of detected electrons is then scanned across a monitor forming a magnified image of the sample surface. The magnification can be calculated using Equation 2.18 [48].

Equation 2.18

$$Magnification = \frac{screen\,resolution}{beam\,diameter}$$

Approximately 90% of the interactions between the electrons and the sample generate heat [48]. Thus it is important for the sample to be able to conduct the heat away to avoid damage. If the sample is non-conducting, there is also the problem of charge accumulation which can distort the image. Samples which are non-conducting can be sputter coated with gold, or other conducting material, so that the topography is unchanged via the coating process but the conduction properties will be changed [49].

The choice of accelerating voltage varies with the need to protect the sample. A high voltage reduces the chromic aberration present in the image, thus producing the best resolution, but it can damage the sample. Voltages are normally in the kV range [48].

The overall resolution varies with several factors [48]:
   a) Beam diameter: a larger spot size produces more signal but more noise at high magnifications.
   b) Accelerating voltage: a high voltage reduces chromic aberration.
   c) Scan speeds: a long scan speed increases the signal but does not amplify the noise, improving the signal to noise ratio (S/N).
   d) Working distance: a small distance between the sample and the final lens produces as higher resolution as there is less beam divergence.

Generally, the resolution can be considered to be approximately equal to the spot size [48].

Carbon fibres and carbon blacks are conducting so do not need to be sputter coated. They are also tolerant to high energy electrons and heat meaning SEM is a practical tool to image the surface.

2.7.2 Equipment and Experimental Set-up

SEM images were acquired for all treated and untreated fibres using a Leo S430 electron microscope (Zeiss, Nano Technology Systems Division, Cambridge, UK). The vacuum was provided by a 12 vane rotary pump (Edwards, West

Sussex, UK, model number RV12). The microscope uses a semiconductor detector for backscatter collection and an Everhart-Thornley detector coupled to a photomultiplier tube for secondary electron detection. The Leo S430 can provide a maximum resolution of approximately 50 nm.

Fibres and carbon black samples were attached to a stainless steel stub using a carbon tab. It was not necessary to sputter coat the samples. Fibres were degassed to approximately 10^{-3} Pa. A spacer bar was used to reduce the working distance to ~ 10 mm or less. Images were acquired at various magnifications for fibres and for the carbon black.

2.8 Transmission Electron Microscopy

2.8.1 Theory

While SEM can provide surface morphology of samples, transmission electron microscopy (TEM) can provide atomic scale images, and diffraction patterns of the microstructure of very thin samples.

The TEM has three main components, similar to the SEM; the electron source, beam steering and the detectors. Electrons can be generated using a tungsten filament, LaB_6 crystal or a field emission gun. In TEM, the electrons are accelerated towards an anode up to higher energies (typically 100-400keV) before interaction with the sample and very thin samples are used to allow the beam to pass through the sample [50]. The equipment is maintained at vacuum to prevent scattering of electrons before entering and after exiting the sample. The electron beam can pass through the sample unaltered or can be diffracted. The resulting diffraction pattern can be imaged on a fluorescent screen beneath the sample or recorded on a CCD, allowing the crystal spacing to be measured [50,51]. Bright field and dark field images can be recorded using just the transmitted beam and diffracted beam signals respectively. The beams can also be used together to form a high resolution image of the sample with resolution down to ~0.2 nm [50,51]. Some TEM are capable of scanning the electron beam across a sample and are referred to as scanning transmission electron

microscopes (STEM). Figure 2.10 shows a typical axial TEM image of a carbon fibre. This will be discussed in detail in Chapter 3.

Because thin samples are required for this technique, the sample preparation is an important factor which can limit the range of materials investigated. Samples are typically required to be less than 0.2 µm thick. This can be performed via dispersion in a solvent for powders or ultramicrotomy for larger specimens [51].
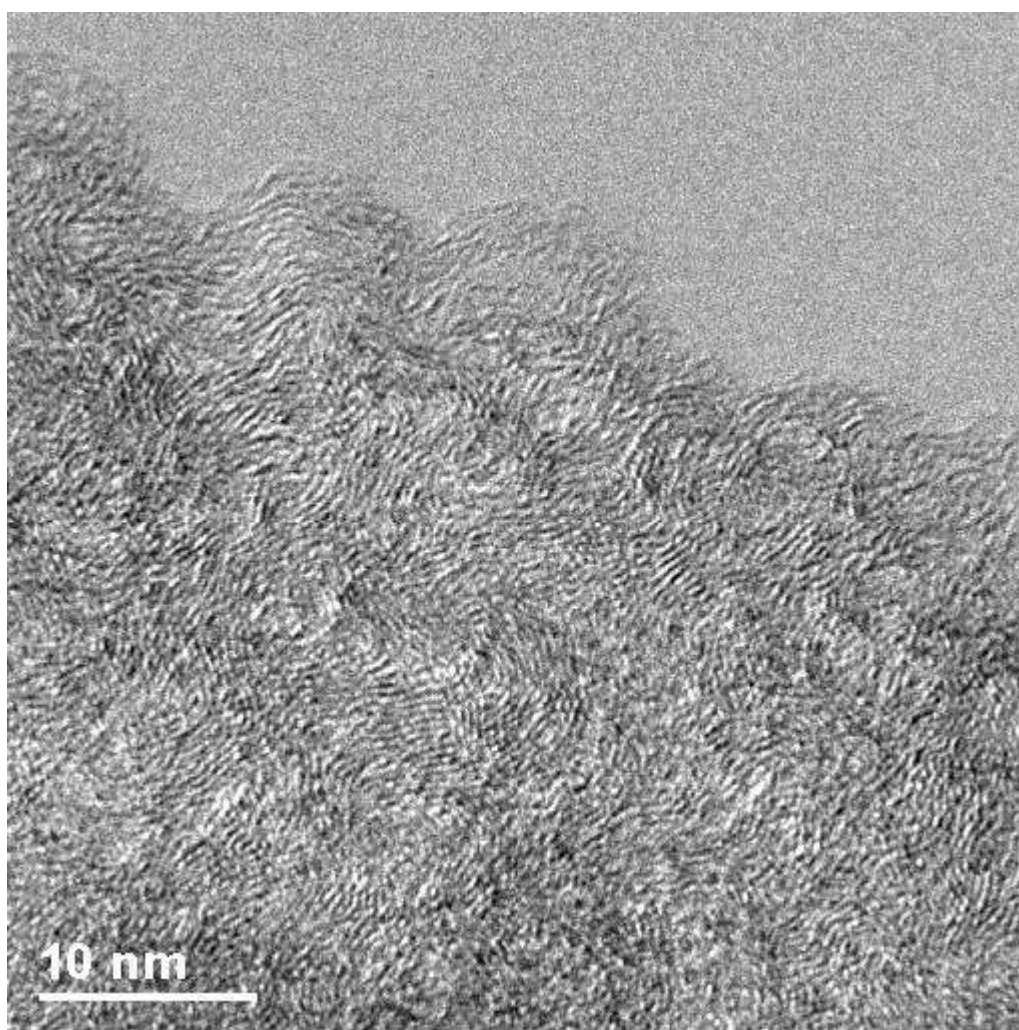

Figure 2.10 Typical TEM image of a carbon fibre.

2.8.2 Equipment and Experimental Set-up

All TEM images were recorded on a JEOL JEM-2011 high resolution (HR) TEM (JEOL Ltd., Tokyo, Japan). The electrons were produced by a LaB_6 crystal and accelerated up to 200 kV. The TEM is capable of producing a beam diameter as

small as 0.5 nm, with 0.19 nm resolution. Magnification up to 1,500,000x was possible. Images were recorded on a Gatan 794 CCD camera (Gatan Inc., Pleasanton, California, USA).

Carbon black samples were gently ground in a pestle and mortar and dispersed in acetone. The dispersion was then dropped onto a copper mesh grid and the acetone was allowed to evaporate leaving behind the carbon black. Fibres were also prepared by this method and by ultramicrotomy. Fibres were set in an Epon resin and ultramicrotomed using a diamond cutter to ~100 nm width. The slices were then placed on the copper grids.

2.9   Raman Spectroscopy

2.9.1   Theory

Laser Raman has several uses in surface characterisation. It can be used to fingerprint unknown samples which can then be compared against spectra databases to aid identification. It can also be used to identify when changes occur in the order of crystals as a function of temperature [52]. In the field of graphitic materials, Raman has long been known as a method to characterise the degree of graphitization in a sample [53,54].

Raman spectroscopy measures molecular vibrations induced by irradiating a sample with monochromatic light. Modern Raman spectroscopes use lasers as the light source. When the laser light enters the sample, a combination of three processes can occur [52]:

1) The light passes through the sample without interaction or
2) The light is scattered elastically by molecules in the sample, leaving the sample with the same frequency as it entered (Rayleigh scattering) or
3) The light is scattered inelastically by molecules in the sample (Raman scattering).

In Raman scattering, the laser can either excite vibrational modes in the molecules; reducing the energy returned in the light, or it can annihilate existing thermally activated vibrational modes and gain energy. These two processes are known as Stokes and Anti-Stokes scattering respectively [52]. Anti-Stokes scattering is rarely used in analysis as it is strongly temperature dependent. The difference between the wavelength of the incident light and the scattered light is known as the Raman shift and is normally measured in cm^{-1} [52].

By comparison to the elastic Rayleigh scattering, Raman scattering is very weak and appears in a spectrograph as weak lines either side of the Rayleigh line (Figure 2.11).
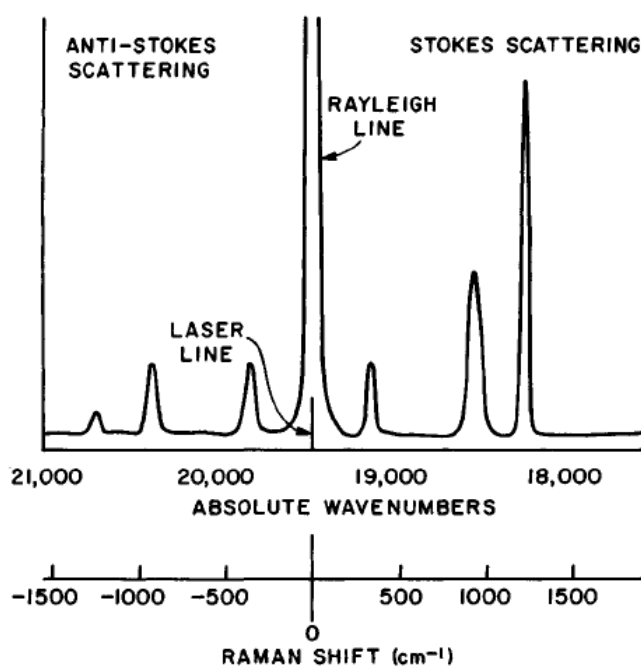

Figure 2.11 Example spectrum showing all scattering processes of light in the Raman technique [52]**.**

Coupling a laser Raman system to an optical microscope allows very small samples to be examined to a resolution of a few micrometers. This is particularly useful for carbon fibres. Figure 2.12 shows the optics system for a Raman microscope. The laser light is directed towards the sample through the microscope objective via a series of mirrors and a beam splitter. Backscattered light from the sample is then collected via the microscope lens and directed

85

towards the spectrometer [56]. Several designs of spectrometer are available but all perform the same function; that is to reject unwanted light and direct light of different wavelengths to separate detectors. Most modern Raman microscopes use a CCD as the detector [55]. Figure 2.13 shows the spectrometer used in Renishaw Raman microscopes (Renishaw plc, Gloucestershire, UK). The diffraction grating rotates in small steps that focus each wavelength on a different detection element of the CCD allowing a large range of wavelengths to be measured.
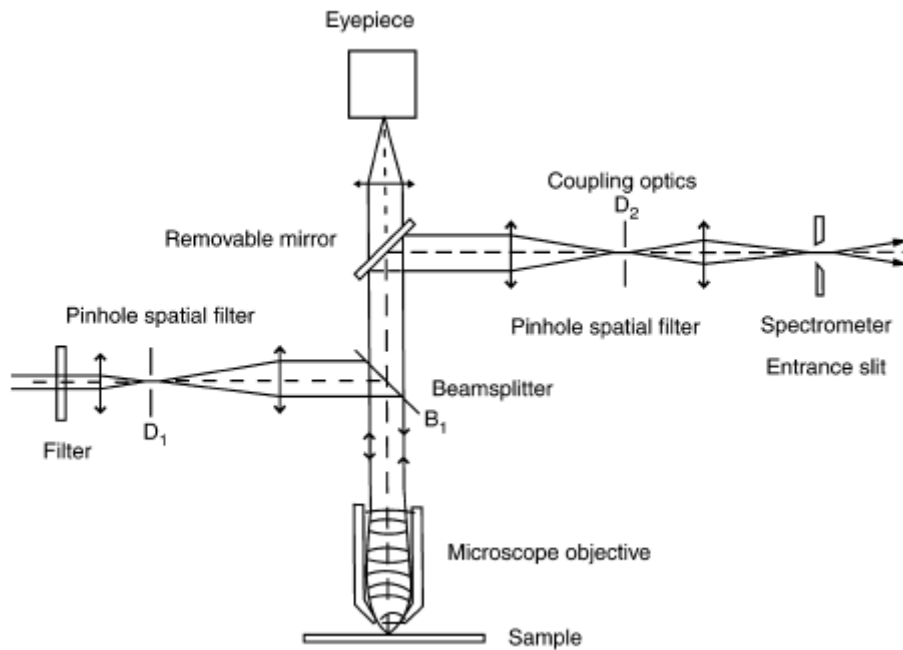

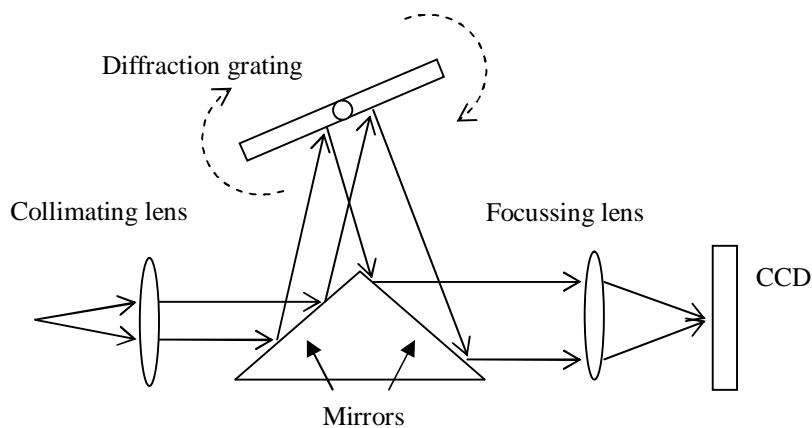**Figure 2.12 Raman microscope optics** [56]**.**

Figure 2.13 Ray path diagram for SynchroScan spectrometer (after [57]**).**

The analysis region is a volume, the depth of which depends on the sample and the laser wavelength. For carbon materials and a laser with a visible wavelength, this depth has been estimated to be in the region of ~10-50 nm [58-60].

There are several optical phonon modes possible for graphite. Table 2.3 lists the symmetry species possible and the associated mode of activation. Raman spectra for carbon materials generally have two main bands of interest; one at ~ 1330 cm^{-1} and one at ~1585 cm^{-1}. These bands have traditionally been referred to as the D (disorder) band and the G (graphite) band respectively [58]. The E_{2g2} mode corresponds to the G peak. Less is known about the E_{2g1} mode which is predicted to occur at ~ 210 cm^{-1} [61]. Although seen experimentally for over 30 years, it is only in the last 10 years that a reason for the defect band has been formulated that encompasses all of the experimental observations [62].

Thomson and Reich proposed that the vibrations in the disorder band are due to double resonance events occurring in the material [63]. That is to say, *two resonances* occur from one incoming photon. The incoming light generates an electron hole pair in the material. The electron is then scattered to a different energy band (first resonance) before being elastically scattered back (second resonance) by a defect in the lattice to recombine with the hole releasing a photon [54,62,63]. The energy band that the electron is scattered to depends on the energy of the incoming light thus the Raman shift of the D peak will vary with the laser type, as seen experimentally.

Table 2.3 Optical vibration modes for graphite [61]
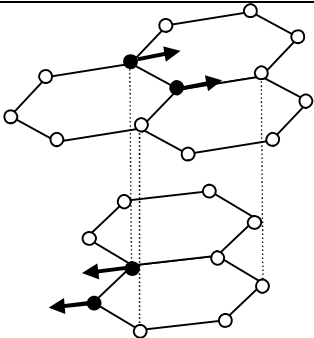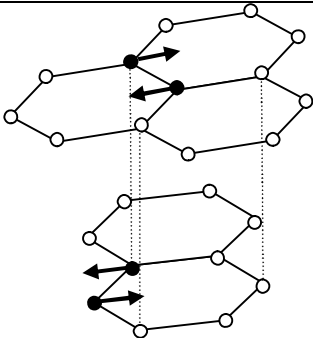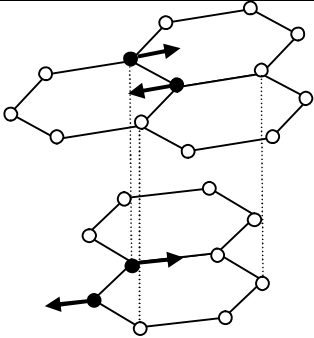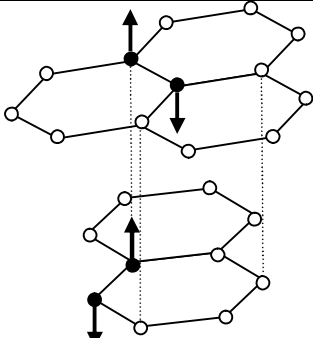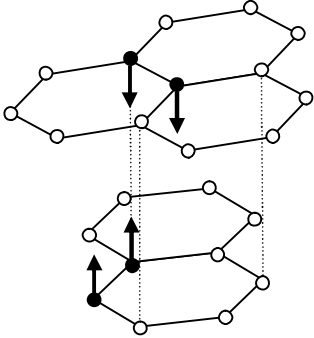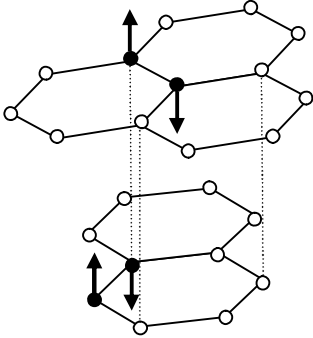
Symmetry species	E_{2g1}	E_{2g2}
Raman Active		

Symmetry species	E_{1u}	A_{2u}
Infrared Active		

Symmetry species	B_{1g1}	B_{1g2}
Silent		

Table 2.4 summarises the main peaks visible in the Raman spectra for carbon fibres and gives a basic explanation of molecular vibrations they are attributed to. Several other peaks are reported in the literature but not all are evident in certain carbon materials.

Table 2.4 Raman peaks in carbon materials (after [60]) [58,60,64-67]

	D	G	D'	G'
Location (cm^{-1})	1330-1360	1575-1600	~1620	2660-2730
Due to:	Edge planes and breakdown of the lattice symmetry	Doubly degenerate vibrational mode of graphite cell (E$_{2g}$)	Edge planes and breakdown of the lattice symmetry, related to D band	Overtone of the D peak

In pure graphite, only the G band will be evident in the first-order spectrum. Figure 2.14 shows an example spectrum of highly orientated pyrolytic graphite (HOPG). The ratio of the intensity of the D band to the intensity of the G band (I_D/I_G) was first introduced as a measure of the graphitization in 1970 by Tuinstra and Koenig reporting the investigation of graphite by Raman for the first time (cited in [68]). In their paper, they reported a relationship between the reciprocal of the crystallite size ($1/L_a$) and the ratio of D/G bands intensities. However, more recent research [68] has shown this to be a tenuous link, with the equation producing errors as large as 100%, and it is more suitable as a starting point for the crystallite size than a direct measurement.
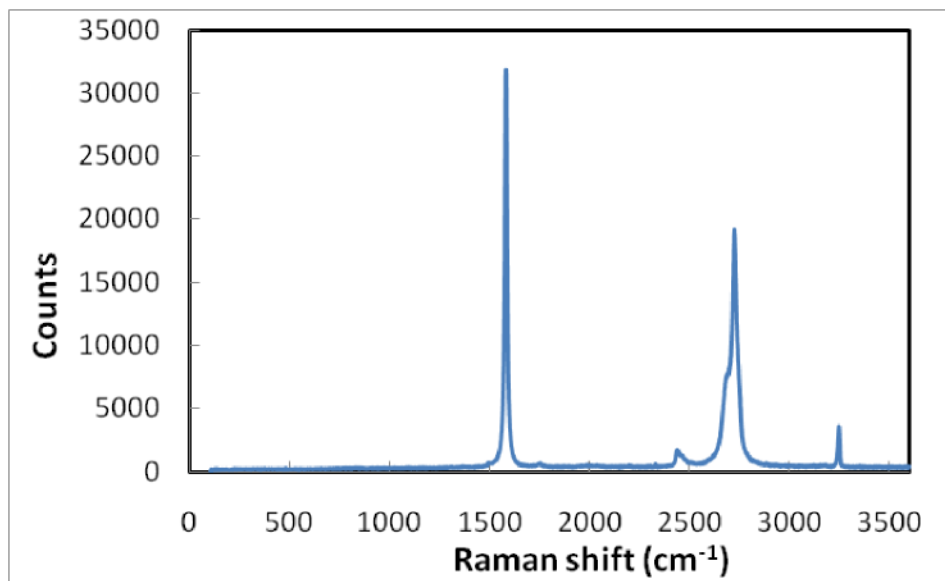

Figure 2.14 Raman spectrum of a pure graphite sample showing the G-band at ~1580 as a very sharp peak and secondary vibrational modes which are generally overtones of the primary region.

The ratio I_D/I_G, or $I_D/(I_D+I_G)$ as is considered more suitable for highly disordered carbons, is still used as a measure of the graphitic order of a carbon material. The higher the ratio, the more disordered a sample is considered to be. In addition to the ratio, the width of the G peak has been linked to the graphitization. An increase in the width of the G peak indicates a reduction in the graphitic nature of the surface and in the case of fibres, a reduction in the Young's modulus [60, 58, 68].

2.9.2 Equipment and Experimental Set-up

Changes in the graphitization of the surface layers were investigated by laser Raman using a Renishaw InVia Raman microscope spectrometer (Renishaw plc, Gloucestershire, UK). Raman spectra were collected using the 514 nm (green) line of a Helium Neon laser through a x50 objective. Fibres were mounted on an XPS stub and six positions were examined for each set of treated fibres. Ten cumulative scans were acquired for each position. Peaks were fitted to the data using the WIRES software provided with the microscope, allowing unrestrained G/L mixing. Raman spectra were also collected for carbon black, and carbon nanotubes for comparison.

2.10 BET Surface Area

2.10.1 Theory

Increasing the surface area on a carbon fibre can increase the area of fibre-matrix interface. It is therefore of interest to investigate the effect of surface treatment on the surface area. Surface areas are normally estimated by gas adsorption techniques; the most popular being the Brunauer-Emmett-Teller (BET) theoretical model [10]. The BET method has come under extensive criticism in the literature but it continues to be the most widely used model for non-porous solids [69].

If a gas of known pressure is introduced to a clean sample in a closed system, the pressure will decrease as adsorption occurs on the sample surface until equilibrium is reached. If an inert gas is used then only physisorption will take place. The pressure decrease can be measured and the amount of gas adsorbed determined or the increase in sample weight can be measured; known as the volumetric or gravimetric method respectively [70]. An adsorption isotherm can be created by plotting the volume of gas adsorbed (V) at a set temperature against either the pressure (p), or the pressure relative to the saturation vapour pressure of the adsorptive (p/p_o) [70]. In general, isotherms can be fitted into one of six groups from the BDDT classification system [69,70,90]. Figure 2.15 shows the types possible. Type I isotherms are produced by microporous samples whereas Type II isotherms are characteristic of monolayer and multilayer adsorption on non-porous or macroporous samples. Type IV is characteristic of mesoporous samples and Type VI represents stepped multilayer adsorption on a non-porous sample. Types III and V are uncommon but are associated with weak adsorbent-adsorbate interactions [71].
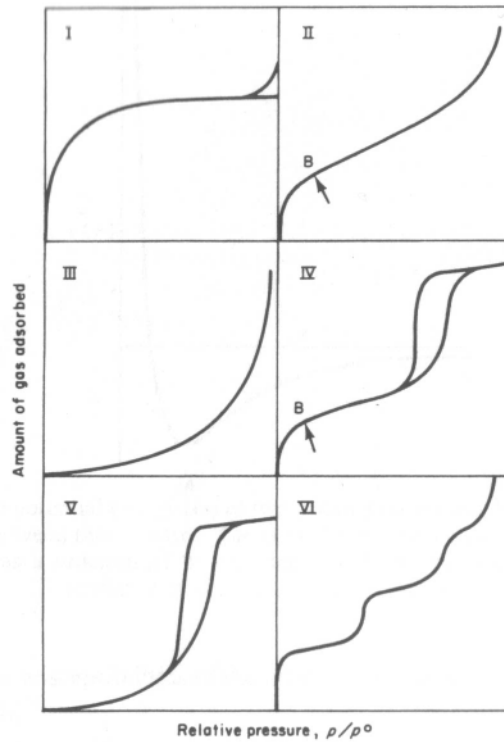
Figure 2.15 The six different types of isotherms used for classification [70]**.**

From the adsorption isotherm it is possible to estimate the monolayer capacity (n_m) of the sample; that is, the amount of adsorbate required to completely cover the surface of 1g of solid with one layer of molecules. If an inert gas of known physical dimensions is used as a probe, then the specific surface area (A_s) of the sample can be calculated using Equation 2.19 [70]. The specific surface area is the surface area of 1g of the sample.

Equation 2.19

$$A_s = n_m a_m N_a$$

where a_m is the average area occupied by a molecule of the adsorbate in a monolayer and N_a is Avogadro's number.

The BET method is based on the Langmuir kinetic model which assumes the surface is an array of adsorption sites and that a dynamic equilibrium exists

where the rate of adsorption is equal to the rate of evaporation [90]. Equation 2.20 shows the BET equation for a volumetric system written in a form convenient for plotting.

Equation 2.20

$$\frac{p}{V(p_o - p)} = \frac{1}{V_m c} + \frac{c-1}{V_m c}\frac{p}{p_o}$$

where p is the pressure, p_o is the saturation pressure, V is the volume of gas adsorbed, V_m is the monolayer capacity as a volume and c is normally taken to be equal to Equation 2.21, where $(q_1 - q_L)$ is the net heat of adsorption, R is the universal gas constant (J/mol) and T is the temperature [70].

Equation 2.21

$$c = e^{(q_1 - q_L)/RT}$$

Thus by plotting $p/V(p_o - p)$ against p/p_o a straight line should be produced with a slope $= \frac{c-1}{V_m c}$ and an intercept $= \frac{1}{V_m c}$. The c term can be eliminated from the equation so that the monolayer capacity can be calculated using Equation 2.22 and the specific surface area using Equation 2.19 [70].

Equation 2.22

$$V_m = \frac{1}{slope + intercept}$$

In practice the plot is usually only linear in a small range and typically BET plots are performed for relative pressures between ~0.05 and ~0.35 [70].

There are only a small number of adsorptives suitable for surface area studies as the molecules need to meet the following conditions [70]:

a) The adsorptive must be chemically inert towards the chosen solid,

b) The saturation vapour pressure must be large enough to allow sufficient accuracy in relative pressure measurement ($\sim0.001 < p/p_o < \sim0.5$) at the chosen temperature,

c) Temperatures less than the boiling point of the adsorptive should be achievable in a lab setting (e.g. 77K for N_2), and

d) The adsorptive will ideally have a spherical shape to minimise the effect of orientation on the measurement of a_m.

Generally, nitrogen is the recommended and standard gas used in surface area calculations [71]. Due to large correction factors required to account for unadsorbed gas in the dead-space of the experimental equipment, nitrogen is, in practice, only useful for specific surface areas greater than ~ 1 m^2/g [70]. As carbon fibres are known to show little uptake of N_2, other adsorptives may be more suitable for determining the surface area. For example carbon dioxide at 273 K or Krypton at 77 K [70,72]. Krypton is particularly useful for small surface areas because it has a low saturation pressure (~ 270 Pa) and therefore a small dead-space correction [70].

2.10.2 Equipment and Experimental Set-up

Specific surface areas were measured for untreated fibres (UST), the most treated electrochemical fibres (6B), and UV/O$_3$ treated fibres using the BET method and krypton at 77K. Nitrogen isotherms were also acquired for the UST and 6B fibres. The UV/O$_3$ fibres were treated for 4 hours as described in Section 2.4.2. Measurements were made on a Micromeritics ASAP 2020 instrument (Micromeritics, Georgia, USA). The ASAP is a volumetric analyser. Fibres, of masses 1.5 to 2.0 g, were degassed at 573K for 10 hours before measurement. The vacuum system was provided by a turbo pump and degassing pressures reached ~60 Pa.

2.11 Immersion Calorimetry

2.11.1 Theory

When a solid held in a vacuum is immersed into a pure liquid at a constant temperature and pressure, a new interface is formed between the liquid and the solid at the expense of the solid and liquid surfaces, resulting in an energy change [2]. In the case of an isothermal calorimeter, a heat sink is employed to maintain the temperature of the system and the energy used to return the system to the initial temperature is a measure of the energy change involved [73]. The only variations in the energy measured will be due to differences in surface area or surface energy of the solid [74].

The enthalpy of a surface (H) is related to the internal energy (U) by Equation 2.23.

Equation 2.23
$$H = U + pV$$

where p is the pressure and V is the volume of the system. The pV term is negligible so enthalpy is approximately equal to internal energy [74]. The change in surface energy due to immersion in the liquid ($\Delta_{imm}G$) is given by Equation 2.24.

Equation 2.24
$$\Delta_{imm}G = \gamma_{SL} - \gamma_S$$

where γ_S is the surface energy of the solid in vacuum and γ_{SL} is the surface energy of the solid/liquid interface. Using a Gibbs-Helmholtz relationship, the enthalpy of immersion ($\Delta_{imm}H$) can be related to the free energy change by Equation 2.25.

Equation 2.25

$$\Delta_{imm}H = \Delta_{imm}G - T\left(\frac{\partial \Delta_{imm}G}{\partial T}\right)_{P}$$

And substituting in Equation 2.24 to Equation 2.25 gives Equation 2.26, the standard equation describing immersion enthalpy. The solid surface energy is the dominant term in this equation so the immersion enthalpy will be of the same order of magnitude as the surface energy [74].

Equation 2.26

$$\Delta_{imm}H = \left(\gamma_{SL} - \gamma_{S}\right) - T\left(\frac{\partial(\gamma_{SL} - \gamma_{S})}{\partial T}\right)_{P}$$

In 1962, Fowkes proposed that the energy at a surface consisted of contributions from different intermolecular forces which combined additively [75]. In the case of water, the surface energy could be written as in Equation 2.27.

Equation 2.27

$$\gamma_{LV} = \gamma_{LV}^{d} + \gamma_{LV}^{p}$$

where γ_{LV} is the surface energy of the liquid in equilibrium with it's vapour, and the d and p superscripts refer to the surface energy contribution from dispersion forces, and hydrogen bonding, or polar interactions, respectively. The dispersion forces are a combination of forces arising from molecules with permanent dipoles (Keeson forces), dipoles induced by molecules with permanent dipoles via polarisation (Debye forces), and forces from dipoles induced instantaneously by the motion of the molecule's electrons (London forces) [76]. It is possible to express the surface energy of the solid/ liquid interface in terms of additive

forces using an empirical geometric mean equation of state as shown in Equation 2.28 [77,78].

Equation 2.28

$$\gamma_{SL} = \gamma_S + \gamma_{LV} - 2\left(\gamma_S^d \gamma_{LV}^d\right)^{\frac{1}{2}} - 2\left(\gamma_S^p \gamma_{LV}^p\right)^{\frac{1}{2}}$$

Substituting Equation 2.28 into Equation 2.26 and applying the product rule gives Equation 2.29. The temperature, γ_{LV}, γ_{LV}^d, γ_{LV}^p, $\partial\gamma_{LV}\big/\partial T$ are all known and the immersion enthalpy can be measured calorimetrically. It is, however, more difficult to obtain the temperature coefficients of γ_{LV}^d, γ_{LV}^p, γ_S^d, γ_S^p [79].

Equation 2.29

$$\Delta_{imm}H = \gamma_{LV} - 2\left(\gamma_S^d \gamma_{LV}^d\right)^{\frac{1}{2}} - 2\left(\gamma_S^p \gamma_{LV}^p\right)^{\frac{1}{2}}$$

$$-T\left[\frac{\partial\gamma_{LV}}{\partial T} - 2\left(\gamma_S^d\right)^{\frac{1}{2}}\frac{\partial\left(\gamma_{LV}^d\right)^{\frac{1}{2}}}{\partial T} - 2\left(\gamma_{LV}^d\right)^{\frac{1}{2}}\frac{\partial\left(\gamma_S^d\right)^{\frac{1}{2}}}{\partial T} - 2\left(\gamma_S^p\right)^{\frac{1}{2}}\frac{\partial\left(\gamma_{LV}^p\right)^{\frac{1}{2}}}{\partial T} - 2\left(\gamma_{LV}^p\right)^{\frac{1}{2}}\frac{\partial\left(\gamma_S^p\right)^{\frac{1}{2}}}{\partial T}\right]$$

Equation 2.29 can be simplified to Equation 2.30 if a non-polar liquid is used.

Equation 2.30

$$\Delta_{imm}H = \gamma_{LV} - 2\left(\gamma_S^d \gamma_{LV}^d\right)^{\frac{1}{2}} - T\left[\frac{\partial\gamma_{LV}}{\partial T} - 2\left(\gamma_S^d\right)^{\frac{1}{2}}\frac{\partial\left(\gamma_{LV}^d\right)^{\frac{1}{2}}}{\partial T} - 2\left(\gamma_{LV}^d\right)^{\frac{1}{2}}\frac{\partial\left(\gamma_S^d\right)^{\frac{1}{2}}}{\partial T}\right]$$

We assume the polar nature of a liquid which is non-polar at room temperature does not change with temperature, i.e. remains non-polar.

The temperature coefficient of γ_S^d can be estimated from the fourth power of the density [80]. The surface energies of many solids do not change greatly with temperature [81] and the temperature coefficient of γ_S^d only contributes to 2% of the measured immersion enthalpy [82]. Zettlemoyer used a value of -0.07 mJ/m^2/K for $\frac{\partial \gamma_S^d}{\partial T}$ for hydrocarbons on low energy surfaces [80]. Using this value in Equation 2.30 and a non-polar probe liquid, it is possible to calculate the dispersive component of the solid surface energy.

In immersion calorimetry, the sample is degassed and sealed in an ampoule. The ampoule is placed in a probe liquid and allowed to equilibrate before being broken and the resulting heat measured. The degassing process is not intended to clean or alter the surface; it is in place to prevent adsorbed gases from blocking the probe liquid from reaching the surface [2].

When the ampoule breaks, several effects add to the heat measured including the heat of vaporisation in the ampoule (the rush in, or PV, effect), the heat of breaking the ampoule, the heat of vaporisation as the volume changes in the cell, and the heat of interaction between the sample and the liquid [2,83]. The heat of the ampoule breaking can be minimised by producing weak ampoules that are easy to break. Large interactions between the sample surface and the probe liquid will mask any small differences due to experimental variation in these quantities.

2.11.2 Probe Liquids

Using a series of alcohols with increasing alkyl chain length as probes, it is possible to track the transition from mixed specific-dispersion interactions to dispersion interactions only [3]. As the alkyl chain increases, there will be less specific interactions with surface groups resulting in a lower enthalpy being measured. Using a non-polar probe (e.g. toluene), it is possible to calculate a value for the dispersion component of the solid surface energy as described in Section 2.11.1. Table 2.5 lists the surface tension components and temperature

dependant components found in literature for the probe liquids used in this investigation.

Table 2.5 Surface tension values for probe liquids (mJ/m^2) [81,84-86]

Liquid	γ_{LV}	γ_{LV}^{p}	γ_{LV}^{d}	$\dfrac{\partial\gamma_{LV}}{\partial T}$	$\dfrac{\partial\gamma_{LV}^{d}}{\partial T}$
Water	72.8	51.0	21.8	0.148	0.09
Methanol	25.5	4.3	18.2	0.077	-
Ethanol	21.4	2.6	18.8	0.083	-
Propan-2-ol	23.0	3.5	19.5	0.079	-
Toluene	28.5	-	28.5	0.119	0.119

2.11.3 Carbon Black as a Model

Non-activated carbon fibres are difficult to perform experiments on because of their small surface areas and hence small surface concentrations of functional groups. In some cases it was necessary to use carbon black as a model for the fibre surface; the differences in structure have been described earlier in Chapter 1.7.3.

2.11.4 Equipment and Experimental Set-up

All calorimetry experiments were performed on a Setaram Isothermal C80 calorimeter (Setaram Instrumentation, Caluire, France). A glass ampoule was made of Schott Duran borosilicate glass with an external diameter of 11 mm and internal diameter of 10 mm (Schott UK Ltd, Stafford, UK). The ampoules were made such that the end was very narrow and weak and could be easily broken. Figure 2.16 shows an empty ampoule prior to filling and sealing. The empty ampoule was weighed three times before fibres were packed into it and weighed again three times after packing to record the average mass of fibres used. The ampoule was then degassed for 1 hour at room temperature before being sealed. The pressure in the sealed ampoule was approximately 5 Pa.
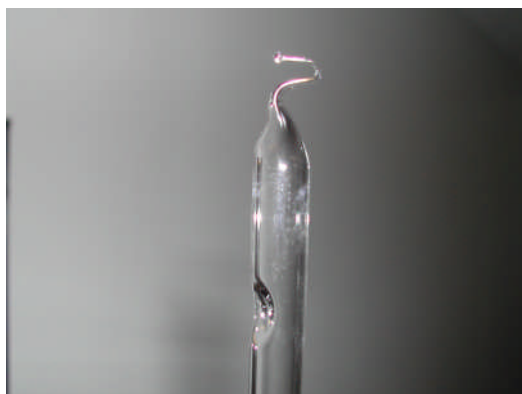
Figure 2.16 Glass ampoule before sealing.

The C80 calorimeter has two chambers; one for a reference and one for the sample. A cross section of the calorimeter is shown in Figure 2.17. Several different cells are available for use in the chambers. Figure 2.18 shows the cell used in this investigation, an identical cell was placed in the reference chamber.
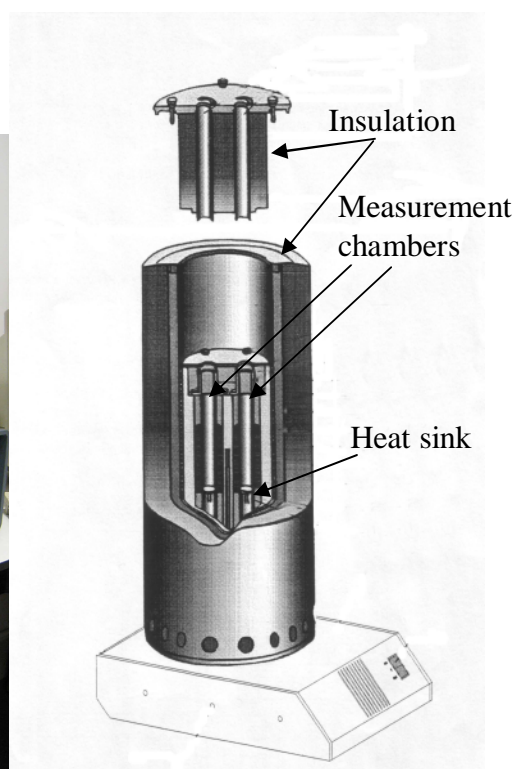

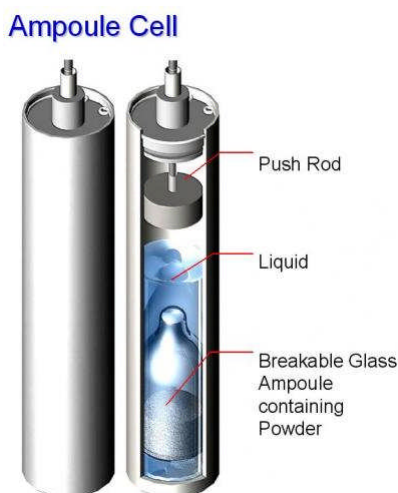
Figure 2.17 Isothermal calorimeter and cross section [87]**.**

Figure 2.18 Ampoule cell for a Setaram calorimeter [88]**.**

The ampoule was placed in the stainless steel cell along with 7 ml of the probe liquid and then left in the calorimeter for 2 hours to equilibrate. Once the cell came to thermal equilibrium with the calorimeter, the rod was pushed down to break the ampoule; allowing the probe liquid to be drawn into the ampoule. The rod is sealed into the cell via a series of tight fitting o-rings to prevent any variation being caused by vaporization of the probe liquid. The calorimeter recorded the heat flow between the sample and the heat sink. Integrating the heat flow against time, after applying a linear background subtraction, gave the total energy for the interactions (i.e. the enthalpy change).

The following pure liquids were used to investigate the carbon fibre surface: distilled water, methanol, ethanol, isopropanol and toluene (purity >99%). Dilute solutions of resin and the resin components were also used as probe liquids. The resin components were dissolved in acetone, dichloromethane (DCM) or dimethyl sulfoxide (DMSO) in varying concentrations. A series of dilute solutions of resin was also prepared by adding the individual components to DCM in the following order KM (20% by weight), PY (40 %), MY (20%) and DDS (20%). Initial tests with fibres showed no measurable interaction so carbon black was used as a model surface.

2.12 Temperature Programmed Desorption

2.12.1 Theory

As discussed earlier in Chapter 1.5, the type of functional group present on the surface of the carbon fibres is of interest, as well as the type and strength of bonds formed between the fibres and resin matrix when fibres are used in a composite. The kinetics and chemistry of adsorbed molecules present on the surface can be analysed using temperature programmed desorption (TPD). This method has been widely used since first described by Apker in 1948 [89]. In principle, when a gas is introduced to a clean surface free of adsorbed molecules, the surface will begin adsorption until equilibrium is reached [70]. In TPD, a sample is first cleaned by gentle degassing to remove any physisorbed species already attached to the surface. The surface (the adsorbent) is then dosed with a vapour of interest (the adsorptive) and allowed to equilibrate before any excess is pumped out. The temperature is then increased, ideally linearly, until there is enough energy to break surface bonds and the quantity of desorbed gas is recorded via a mass spectrometer. Plotting the mass fragments as a function of temperature produces a series of desorption spectrums [90].

The rate of desorption per unit area of adsorbent is calculated using Equation 2.31 [89,91].

Equation 2.31

$$\frac{d\theta}{dt} = \frac{V}{kTA_s}\left[\frac{d\Delta p}{dt} + \frac{S}{V}\Delta p\right]$$

where θ is the surface coverage (molecule/unit area), V is the volume of the chamber, k is Boltzmann's constant, T is the temperature, A_s is the adsorbent surface area, Δp is the change in pressure, and S is the pumping speed (volume/second). The equation can be rearranged and simplified to:

Equation 2.32

$$a\frac{d\theta}{dt} = \frac{d\Delta p}{dt} + \frac{\Delta p}{\tau}$$

where $a = kTA_s/V$ and $\tau = V/S$ and represents the characteristic pumping speed. When the pumping speed is very low ($\tau \rightarrow \infty$) the desorption rate is proportional to the first derivative of the change in pressure with time. When the pumping speed is very high ($\tau \rightarrow 0$) the desorption rate is conveniently proportional to the change in pressure [89]. Therefore, the area under a desorption peak in a desorption spectrum (A_i) is proportional to the quantity of species, i, desorbed from the surface.

In order to quantitatively analyse the different species desorbing from the surface, it is necessary to take into account the differences in ionisation efficiency (I_x) and mass fragment yield (F_m) for the desorbing particles. In addition, the effect of the mass spectrometer must be accounted for in terms of quadrupole transmission (T_m) and electron multiplier gain (G_m). Ko *et al.*, proposed the following method to determine a correction factor (CF_i) for the desorption spectrum of a mass fragment, i, relative to carbon monoxide (m/z = 28) [92].

The ionisation efficiency is mainly dependent on the number of electrons in the molecule (n_e) and can be calculated, relative to CO, using Equation 2.33. The electron multiplier gain and the quadrupole transmission are both dependent on the molecular weight of the ion (MW) and can be calculated relative to CO using Equation 2.34 and Equation 2.35 respectively. If the mass fragment pattern and percentage yield is known from either experimental methods or from literature values, the correction factor for a particular mass fragment can be calculated using Equation 2.36 [92]. The fragment patterns for the probe liquids used in this study were taken from the literature and are shown in Table 2.6.

Equation 2.33

$$I_x = 0.6\left(\frac{n_e}{14}\right) + 0.4$$

Equation 2.34

$$G_m = \left(\frac{28}{MW}\right)^{\frac{1}{2}}$$

Equation 2.35

$$T_m = 10^{(30-MW)/155} \qquad \text{if MW} > 30$$

$$\text{or}$$

$$T_m = 1 \qquad \text{if MW} \leq 30$$

Equation 2.36

$$CF_i = \frac{1}{F_{m,i}} \frac{1}{I_{x,i}} \sum_{mass\ fragments} \frac{F_m}{G_m T_m}$$

Table 2.6 Fragmentation patterns of probe liquids [93]

Probe	15	26	27	28	29	31	39	41	42	43	45	55	56	59	60	74
						m/z										
Methanol	12	-	-	5	45	100	-	-	-	-	-	-	-	-	-	-
Ethanol	7	10	22	3	30	100	-	1	5	11	51		-	-	-	-
1-propanol	2	6	16	6	18	100	7	9	14	4	2	1	-	11	7	-
1-butanol	10	14	57	20	38	98	25	88	43	68	8	28	100	-	-	1

The relative yield (*Y*) for a desorbed species, *i*, can then be calculated using the sum of all the mass fragments as shown in Equation 2.37 [94].

Equation 2.37

$$Y_i = \frac{A_i CF_i}{\sum_j^n A_j CF_j}$$

Since the system is constantly being evacuated, the temperature of the peak of maximum desorption (T_p) corresponds to the maximum desorption rate. By varying the heating rate of the TPD or the surface coverage of adsorptive, the activation energy of desorption (E_d) can be calculated using Equation 2.38 for a system with first order desorption ($n = 1$) or Equation 2.39 for a second order system ($n = 2$) [90,91].

Equation 2.38

$$E_d = RT_p \left[\log_e \left(\frac{\nu T_p}{\beta} \right) - 3.46 \right]$$

Equation 2.39

$$\frac{E_d}{RT_p^2} = 2\frac{vN}{\beta}\exp\left(\frac{-E_d}{RT_p}\right)$$

where R is the universal gas constant (J/mol), v is a pre-exponential factor, β is the heating rate (K/s), and N is the number of adsorbed molecules. This is known as the "Redhead method". This method has it's limitations as it requires a value, independent of coverage, to be assumed for the pre-exponential factor; usually 10^{13} s^{-1} is chosen for first order systems [90].

A simple approximation for the activation energy of desorption in kJ/mol is shown in Equation 2.40 and allows estimation of E_d to ± 20 % [90,95].

Equation 2.40

$$E_d = \frac{T_p}{4}$$

The order of a system can be inferred from the shape and the position of the peak desorption temperature using a series of desorption spectra with varying adsorptive coverage or heating rates. In the case of first order kinetics, the desorption peak is independent of coverage so will only increase in intensity with increasing coverage. In addition, the peaks are asymmetric, bias towards the lower temperature side. For second order kinetics the peak temperature decreases with increasing coverage and the curves are symmetric around the peak temperature [90,91,95]. Figure 2.19 shows an example of the two types of system. In the case of a multilayer system (not shown) the kinetics will be zero-order. The spectra will show a secondary peak at lower temperature corresponding to the multiple layers. With increasing coverage, this peak will not saturate. The peak temperature will also increase indefinitely [90].
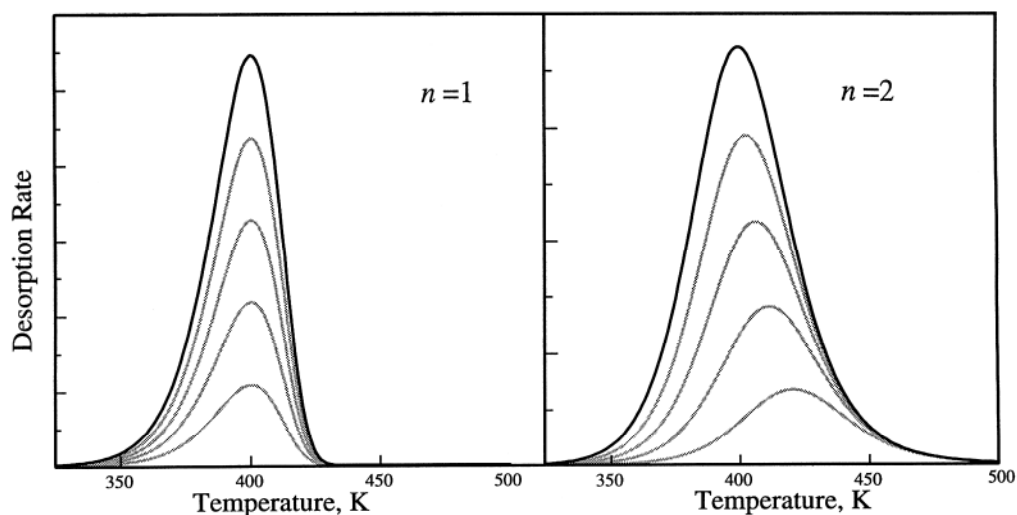
Figure 2.19 TPD curves showing first order (*n* = 1) and second order (n = 2) systems [95]**.**

Detailed analysis of the activation energy has not been performed in this work. Instead a series of alcohols were used to probe carbon fibres with increasing surface oxygen content in a manner similar to that used for the calorimetry experiments (Section 2.11.2). The amount of alcohol binding to the fibre surface as a function of surface oxygen was investigated as described in Section 2.12.2.

Introducing an adsorptive to a surface and recording the resultant desorption spectrum is a well known technique used in catalysis. In the case of carbon fibres, TPD has been used to quantify the functional groups on the fibre following surface treatments and the method is considered particularly useful as it provides average surface chemistry for the whole of the fibre [96]. No adsorptive is added and the fibres are heated to approximately 1200 $^{\circ}$C. The quantity of carbon monoxide and carbon dioxide released as the functional groups decompose can be measured and an estimate of the total amount of oxygen containing groups made [97]. The functional groups decompose at different temperatures, allowing some insight into the nature of the groups [97]. Unfortunately, the assignment of the different peaks is somewhat ambiguous in the literature due to the fact that the peak temperatures are known to be affected by the porous nature of the carbons, the heating rate, and the experimental set up, and it is useful to complement TPD data with other methods [98]. A good review of decomposition temperatures was included by Szymanski *et al.,* [98] in their

paper on activated carbons; a smaller review is shown in Table 2.7 which agrees with the temperature ranges collected in reference [98]. Although there is substantial variation of group assignment, the following general points can be made [43,97,98]:

- The CO_2 peaks generally occur at lower temperatures than the CO peaks.
- For the CO_2 spectra, carboxylic acid is evolved at low temperatures while anhydrides, lactones and lactols decompose at higher temperatures.
- Carboxylic anhydrides release both CO and CO_2 peaks simultaneously.
- Carbon monoxide is also generated by phenols, ethers, quinones, and carbonyls.

Table 2.7 Temperatures of desorption of surface groups on carbons

Gas	Surface group	Temperature (K)	Reference
CO_2	Carboxyl	400-623	[97]
		548	[96]
		550-650	[99]
		590	[100]
		473-523	[43]
	Carboxylic anhydride	623-673	[43]
		698	[96]
		710	[100]
	Peroxide	793	[96]
		823-873	[43]
	Lactones at different sites	600-950	[99]
		623-673	[43]
		960	[100]
		623-823	[97]
		893, 1013, 1153	[96]
CO	Adsorbed CO	523	[96]
	Aldehydes/ Ketones	530	[100]
	Carboxylic anhydride	673-723	[43]
		698	[96]
		800	[100]
	Hydroxyl	823	[96]
	Phenolic and hydroquinonic	873-973	[43]
	Ether or carbonyl	923	[96]
	Carbonyl (semiquinone)	980	[100]
		1053	[96]
		1073-1173	[43]
		1150	[99]
	Pyrone-type	1203	[96]

2.12.2 Equipment and Experimental Set-up

The TPD set up is shown in Figure 2.20. It consisted of a U shaped quartz glass reactor bed, a vacuum system, a furnace, a temperature controller and a mass spectrometer. The vacuum was provided by a Duoseal rotary vane pump, (WM Welch Manufacturing Company, Chicago USA), and a vapour diffusion pump (Edwards, West Sussex, UK, model number EO2) backed by an Edwards 5 vane rotary pump (model number E2M5). The base pressure in the system was typically 4×10^{-5} Pa. Pressures were measured using Dynavac model CG8 cold cathode gauge (Dynavac Engineering Pty. Ltd, Victoria, Australia). The temperature of the glass lined furnace was monitored using a K type thermocouple and was ramped by a Kaif digital temperature controller (Kaif Digital, Arizona, USA) at a linear rate of 20 K/min. The thermocouple was placed as close to the sample as possible in order to get accurate temperature readings of the sample. The mass spectrometer was a Spectra Vision quadrupole (LEDA Mass Ltd, Cheshire, UK) and was capable of measuring 12 masses simultaneously in the range 1 to 200 amu.
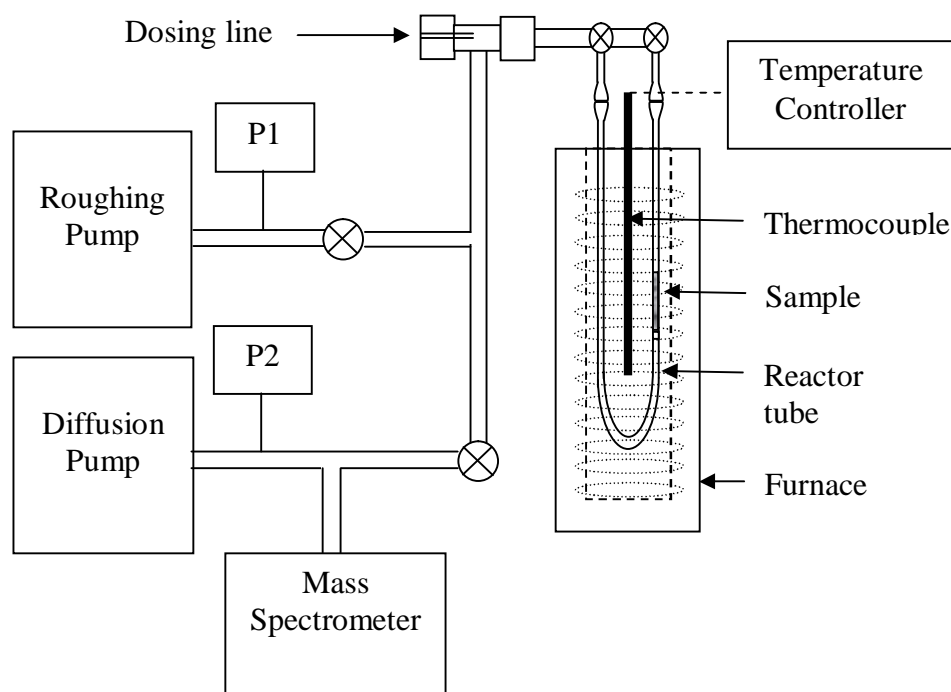

Figure 2.20 Temperature programmed desorption set up.

Long lengths of carbon fibres, weighing between 0.4 and 0.7 g were packed into the reactor. The fibres were degassed at 150 ^{o}C for 2 hours to remove any physisorbed gases. In the case of alcohol adsorption experiments, 1 μL of methanol, ethanol, 1-propanol or 1-butanol (purity > 99 %) was then injected into the system via the dosing line at room temperature with the sample isolated from the vacuum system. The sample and the injected alcohol were allowed 15 minutes to come to equilibrium before any excess was pumped out. The temperature of the system was raised from room temperature to 450 ^{o}C and the appropriate mass fragments for each alcohol, listed in Table 2.6, were monitored.

For the functional group TPD experiments, the dosing step was omitted and the temperature was raised from room temperature to 800 ^{o}C. The masses for carbon monoxide (m/z = 28), carbon dioxide (m/z = 44), water (m/z = 18), nitrogen (m/z = 14 & 28), oxygen (m/z = 32 & 16), and nitrogen oxides (m/z = 30) were recorded with temperature and the resulting desorption spectra were analysed using Table 2.7 as a guide.

The effect of heat treatment on probe uptake was also investigated using 3B fibres. The fibres were heated to 600 ^{o}C in the vacuum. Once cooled, a small sample was removed for XPS study and the fibres were degassed again for 1 hour at 150 ^{o}C. The fibres were then dosed with either methanol or 1-propanol at room temperature. Once the excess adsorptive was removed, the temperature was raised to 800 ^{o}C and the appropriate mass fragments were recorded. Fibres were again cooled and another sample removed for XPS before the dosing, degassing and TPD process was repeated.

The area under each peak was calculated by integration using the trapezoid rule after applying a linear background subtraction. The areas were corrected using the factors listed in Table 2.8 which were calculated using mass fragmentation yields from reference [93] and Equation 2.36.

Table 2.8 Adsorbent correction factors

Adsorbent	CF
Methanol	2.4
Ethanol	2.4
1-propanol	1.5
1-butanol	4.7

2.13 References

[1] Wang S, Chen Z-, Ma W-, Ma Q-. Influence of heat treatment on physical-chemical properties of PAN-based carbon fiber. *Ceramics International.* 2006; 32:291-295.

[2] Denoyel R, Rouquerol F, Rouquerol J. Porous texture and surface characterization from liquid-solid interactions: immersion calorimetry and adsorption from solution. In: Bottani EJ, Tascón JMD, editors. *Adsorption by carbons.* Amsterdam: Elsevier; 2008: 273-300.

[3] Andreu A, Stoeckli HF, Bradley RH. Specific and non-specific interactions on non-porous carbon black surfaces. *Carbon.* 2007; 45:1854-1864.

[4] Gulyas J, Foldes E, Lazar A, Pukanszky B. Electrochemical oxidation of carbon fibres: surface chemistry and adhesion. *Composites: Part A.* 2001; 32:353-360.

[5] Jones C. The chemistry of carbon fibre surfaces and its effect on interfacial phenomena in fibre/epoxy composites. *Composites Science and Technology.* 1991; 42(1-3):275-298.

[6] Alexander MR, Jones FR. Effect of electrolytic oxidation upon the surface chemistry of type A carbon fibres- Part II, analysis of derivatised surface functionalities by XPS ,and TOF SIMS. *Carbon.* 1995; 33(5):569-580.

[7] Alexander MR, Jones FR. Effect of electrolytic oxidation on the surface chemistry of type a carbon fibres—Part I, X-ray photoelectron spectroscopy. *Carbon.* 1994; 32(5):785-794.

[8] Strasser P, Ogasawara H. Surface electrochemistry. *Chemical bonding at surfaces and interfaces.* Amsterdam: Elsevier; 2008: 397-455.

[9] Losey MW, Kelly JJ. Electrodeposition. In: Yogesh Gianchandani, Osamu Tabata, Hans Zappe, editors. *Comprehensive microsystems.* Oxford: Elsevier; 2008: 271-292.

[10] Hughes JDH. The carbon fibre/epoxy interface—A review. *Composites Science and Technology.* 1991; 41(1):13-45.

[11] Chun B, Randall Davis C, He Q, Gustafson RR. Development of surface acidity during electrochemical treatment of pan-carbon fibers. *Carbon.* 1992; 30(2):177-187.

[12] Horie K, Hiromichi M, Mita I. Bonding of epoxy resin to graphite fibres. *Fibre Science and Technology.* 1976; 9(4):253-264.

[13] Mitchell S, inventor. Amoco Corporation, assignee. *Multielectrolyte shear treatment of carbon fibers.* United States patent 4,729,820. 1988.

[14] Bradley RH, Mathieson I. Chemical interactions of ultraviolet light with wool fiber surfaces. *Journal of Colloid and Interface Science.* 1997; 194(2):338-343.

[15] Lindsay B, Abel M, Watts JF. A study of electrochemically treated PAN based carbon fibres by IGC and XPS. *Carbon.* 2007; 45(12):2433-2444.

[16] Dusenbury JS, Cannon FS. Advanced oxidant reactivity pertaining to granular activated carbon beds for air pollution control. *Carbon.* 1996; 34(12):1577-1589.

[17] Bourrat X. Structure in carbons and carbon artefacts. In: Marsh H, Rodríguez-Reinoso F, editors. *Sciences of carbon materials.* Alicante: Universidad de Alicante; 2000: 1-97.

[18] Teare DOH, Emmison N, Ton-That C, Bradley RH. Cellular attachment to ultraviolet ozone modified polystyrene surfaces. *Langmuir.* 2000; 16(6):2818-2824.

[19] Voronov A. New generation of low pressure mercury lamps for producing ozone. *Ozone: Science & Engineering: The Journal of the International Ozone Association.* 2008; 30(6):395.

[20] Jüstel T, Krupa J, Wiechert DU. VUV spectroscopy of luminescent materials for plasma display panels and Xe discharge lamps. *Journal of Luminescence.* 2001; 93(3):179-189.

[21] Rakness K, Gordon G, Langlais B, Masschelein W, Matsumoto N, Richard Y, et al. Guideline for measurement of ozone concentration in the process gas

from an ozone generator. *Ozone: Science & Engineering: The Journal of the International Ozone Association.* 1996; 18(3):209-229.

[22] Lee HM, Chang MB, Wei TC. Kinetic modelling of ozone generation via dielectric barrier discharges. *Ozone: Science & Engineering: The Journal of the International Ozone Association.* 2004; 26(6):551.

[23] Chung DDL. *Carbon fiber composites.* 1st ed. Newton, USA: Butterworth-Heinemann; 1994.

[24] Abel M, Rattana A, Watts JF. Interaction of epoxy analogue molecules with organosilane-treated aluminium: A study by XPS and ToF-SIMS. *Langmuir.* 2000; 16(16):6510-6518.

[25] Blanco M, Lopez M, Fernandez R, Martin L, Riccardi C, Mondragon I. Thermoplastic-modified epoxy resins cured with different functionalities amine mixtures. Kinetics and miscibility study. *Journal of Thermal Analysis and Calorimetry.* 2009; 97(3):969-978.

[26] Awaja F, Gilbert M, Kelly G, Fox B, Pigram PJ. Adhesion of polymers. *Progress in Polymer Science.* 2009; 34(9):948-968.

[27] Carrott PJM. Molecular sieve behaviour of activated carbons. *Carbon.* 1995; 33(9):1307-1312.

[28] Barber A, Page S. *Axis HSi operator's manual.* 2.0th ed. Manchester, UK: Kratos Analytical Ltd.; 2000.

[29] Briggs D, Seah MP. *Practical surface analysis, Volume 1- Auger and x-ray photoelectron spectroscopy.* 2nd ed. Chichester, UK: John Wiley and Sons Ltd.; 1983.

[30] Watts JF, Wolstenholme J. *An introduction to surface analysis by XPS and AES.* Chichester, England: John Wiley & Sons Ltd.; 2003.

[31] Rivière JC. Instrumentation. In: Briggs D, Seah MP, editors. *Practical surface analysis, Volume 1- Auger and x-ray photoelectron spectroscopy.* 2nd ed. Chichester, UK: John Wiley and Sons Ltd.; 1983.

[32] Brundle CR. XPS. In: Brundle CR, Evans CA, Wilson S, editors. *Encyclopaedia of materials characterization - surfaces, interfaces, thin films.* Oxford: Elsevier; 1992: 282-299.

[33] Siegbahn K. Electron spectroscopy for chemical analysis (E.S.C.A.). *Philosophical Transactions of the Royal Society of London. Series A, Mathematical and Physical Sciences.* 1970; 268(1184):33-57.

[34] Xu B, Wang X, Lu Y. Surface modification of polyacrylonitrile-based carbon fiber and its interaction with imide. *Applied Surface Science.* 2006; 253:2695-2701.

[35] Dilsiz N, Wightman JP. Surface analysis of unsized and sized carbon fibers. *Carbon.* 1999; 37:1105-1114.

[36] Li J, Huang Y, Xu Z, Wang Z. High-energy radiation technique treat on the surface of carbon fiber. *Materials Chemistry and Physics.* 2005; 94:315-321.

[37] Morita K, Murata Y, Ishitani A, Murayama K, Ono T, Nakajima A. Characterization of commercially available PAN (Polyacrylonitrile)-based carbon fibers. *Pure and Applied Chemistry.* 1986; 58(3):455-468.

[38] Sherwood PMA. Surface analysis of carbon and carbon fibers for composites. *Journal of Electron Spectroscopy and Related Phenomena.* 1996; 81:319-342.

[39] Weitzsacker CL, Xie M, Drzal LT. Using XPS to investigate fiber/matrix chemical interactions in carbon-fiber-reinforced composites. *Surface and Interface Analysis.* 1997; 25:53-63.

[40] Gardner SD, Singamsetty CSK, Booth GL. Surface characterization of carbon fibers using angle-resolved XPS and ISS. *Carbon.* 1995; 33(5):587-595.

[41] Wang Y, Viswanathan H, Audi AA, Sherwood PMA. X-ray photoelectron spectroscopic studies of carbon fiber surfaces. 22. Comparison between surface treatment of untreated and previously surface treated fibers. *Chemistry of Materials.* 2000; 12:1100-1107.

[42] Park S-, Jang Y-. X-ray diffraction and X-ray photoelectron spectroscopy studies of Ni-P deposited onto carbon fiber surfaces: impact properties of a carbon-fiber-reinforced matrix. *Journal of Colloid and Interface Science.* 2003; 263:170-176.

[43] Zielke U, Huttinger KJ, Hoffman WP. Surface-oxidized carbon fibers: I. Surface structure and chemistry. *Carbon.* 1996; 34(8):983-998.

[44] Bradley RH, Ling X, Sutherland I. An investigation of carbon fibre surface chemistry and reactivity based on XPS and surface free energy. *Carbon.* 1993; 31(7):1115-1120.

[45] Yue ZR, Jiang W, Gardner SD, Pittman CU. Surface charcterization of electrochemically oxidized carbon fibers. *Carbon.* 1999; 37:1785-1796.

[46] Pittman CU, Jiang W, Yue ZR, Gardner S, Wang L, Toghiani H, et al. Surface properties of electrochemically oxidized carbon fibers. *Carbon.* 1999; 37:1797-1807.

[47] Xie Y, Sherwood PMA. X-ray photoelectron spectroscopic studies of carbon fiber surfaces. 10. Valence-band studies interpreted by X-α calculations and the differences between poly(acrylonitrile)- and pitch-based fibers. *Chemistry of Materials.* 1989; 1:427-432.

[48] Lawes G. *Scanning electron microscopy and x-ray microanalysis.* Chichester: John Wiley and Sons; 1987.

[49] Bindell JB. SEM, Scanning electron microscopy. In: Brundle CR, Evans CA, Wilson S, editors. *Encyclopaedia of materials characterization - surfaces, interfaces, thin films.* Oxford: Elsevier; 1992: 70-84.

[50] Sickafus KE. TEM, Transmission electron microscopy. In: Brundle CR, Evans CA, Wilson S, editors. *Encyclopaedia of materials characterization - surfaces, interfaces, thin films.* Oxford: Elsevier; 1992: 99-115.

[51] Macur JE, Marti J, Lui S. Microscopy. In: Sibilia JP, editor. *A guide to materials characterisation and chemical analysis.* 2nd ed. New York, USA: VCH Publishers, Inc.; 1996: 167-198.

[52] White WB. Raman spectroscopy. In: Brundle CR, Evans CA, Wilson S, editors. *Encyclopaedia of materials characterization - surfaces, interfaces, thin films.* Oxford: Elsevier; 1992: 428-441.

[53] Washer G, Blum FJ. Raman spectroscopy for the non-destructive testing of carbon fiber. *Research Letters in Materials Science.* 2008; 2008:3 pages.

[54] Pimenta MA, Dresselhaus G, Dresselhaus MS, Cançado LG, Jorio A, Saito R. Studying disorder in graphite-based systems by Raman spectroscopy. *Physical Chemistry Chemical Physics.* 2007; 9:1276-1290.

[55] Pelletier MJ, Pelletier CC. Raman Spectroscopy: Instrumentation. In: Worsfold P, Townshend A, Poole C, editors. *Encyclopaedia of analytical science.* Oxford: Elsevier; 2005: 94-104.

[56] Withnall R. Spectroscopy: Raman spectroscopy. In: Guenther BD, editor. *Encyclopaedia of modern optics.* Oxford: Elsevier; 2005: 119-134.

[57] Renishaw plc. *Renishaw's SynchroScan.* [homepage on the internet]. Gloucestershire, UK: Renishaw plc.; c. 2001-2007 [accessed 2010 Jun 21]. Available from:

http://resources.renishaw.com/details/Renishaw%27s+SynchroScan(24718)].

[58] Montes-Morán MA, Young RJ. Raman spectroscopy study of high-modulus carbon fibres: effect of plasma-treatment on the interfacial properties of single-fibre epoxy composites. Part II: Characterisation of the fibre-matrix interface. *Carbon.* 2002; 40:857-875.

[59] Alsmeyer YW, McCreery RL. Surface-enhanced Raman spectroscopy of carbon electrode surfaces following silver electrodeposition. *Analytical Chemistry.* 1991; 63(13):1289-1295.

[60] Melanitis N, Tetlow PL, Galiotis C. Characterization of PAN-based carbon fibres with laser Raman spectroscopy. *Journal of Materials Science.* 1996; 31:851-860.

[61] Chung DDL. Review graphite. *Journal of Materials Science.* 2002; 37:1475-1489.

[62] Reich S, Thomsen C. Raman spectroscopy of graphite. *Philosophical Transactions of the Royal Society of London. Series A: Mathematical, Physical and Engineering Sciences.* 2004; 362(1824):2271-2288.

[63] Thomsen C, Reich S. Double resonant Raman scattering in graphite. *Physical Review Letters.* 2000; 85(24):5214.

[64] Jin Z, Zhang Z, Meng L. Effects of ozone method treating carbon fibers on mechanical properties of carbon/carbon composites. *Materials Chemistry and Physics.* 2006; 97:167-172.

[65] Fukunaga A, Komami T, Ueda S, Nagumo M. Plasma treatment of pitch-based ultra high modulus carbon fibers. *Carbon.* 1999; 37(7):1087-1091.

[66] Fukunaga A, Ueda S. Anodic surface oxidation for pitch-based carbon fibers and the interfacial bond strengths in epoxy matrices. *Composites Science and Technology.* 2000; 60:249-254.

[67] Fukunaga A, Ueda S, Nagumo M. Air-oxidation and anodization of pitch-based carbon fibers. *Carbon.* 1999; 37:1081-1085.

[68] Cuesta A, Dhamelincourt P, Laureyns J, Martínez-Alonso A, Tascón JMD. Comparative performance of X-ray diffraction and Raman microprobe techniques for the study of carbon materials. *Journal of Materials Chemistry.* 1998; 8:2875-2879.

[69] Sing KSW. Overview of physical adsorption by carbons. In: Bottani EJ, Tascón JMD, editors. *Adsorption by carbons.* Amsterdam: Elsevier; 2008: 3-14.

[70] Gregg SJ, Sing KSW. *Adsorption, surface area and porosity.* 2nd ed. London, UK: Academic Press; 1982.

[71] Sing KSW. Reporting physisorption data for gas/solid systems with special reference to the determination of surface area and porosity (Recommendations 1984). *Pure and Applied Chemistry.* 1985; 57(4):603-619.

[72] Pittman CU, Jiang W, Yue ZR, Leon y Leon CA. Surface area and pore size distribution of microporous carbon fibers prepared by electrochemical oxidation. *Carbon.* 1999; 37:85-96.

[73] Wilson RJ. Calorimetry. In: Haines PJ, editor. *Principles of thermal analysis and calorimetry.* 1st ed. Cambridge, UK: Royal Society of Chemistry; 2002: 129-165.

[74] Douillard JM. What can really be deduced from enthalpy of immersional wetting experiments? *Journal of Colloid and Interface Science.* 1996; 182(1):308-311.

[75] Fowkes FM. Determination of interfacial tensions, contact angles, and dispersion forces in surfaces by assuming additivity of intermolecular interactions in surfaces. *The Journal of physical chemistry.* 1962; 66(2):382-382.

[76] Owens DK, Wendt RC. Estimation of the surface free energy of polymers. *Journal of Applied Polymer Science.* 1969; 13(8):1741-1747.

[77] Van Oss CJ, Ju L, Chaudhury MK, Good RJ. Estimation of the polar parameters of the surface tension of liquids by contact angle measurements on gels. *Journal of Colloid and Interface Science.* 1989; 128(2):313-319.

[78] Attension. *Application note #105: Surface free energy-background, calculation and examples by using contact angle measurements.* [homepage on the Internet]. Finland: Attension; c. 2009 [updated 2009 Jun 30; accessed 2010 June 27]. Available from:

http://www.attension.com/filearchive/1/1234/AttensionAN105_SFE_190710.pdf.

[79] Bradley RH, Sutherland I, Sheng E. Carbon surface: area, porosity, chemistry and energy. *Journal of Colloid and Interface Science.* 1996; 179:561-569.

[80] Zettlemoyer AC. Hydrophobic Surfaces. In: Fowkes FM, editor. *Hydrophobic surfaces, The Kendall Award Symposium; 1st-2nd April 1968;* London: Academic Press Inc. (London) Ltd; 1969: 1-27.

[81] Gonzalez-Martin ML, Janczuk B, Labajos-Broncano L, Bruque JM. Determination of the carbon black surface free energy components from the heat of immersion measurements. *Langmuir.* 1997; 13:5991-5994.

[82] Fowkes FM. Dispersion force contributions to surface and interfacial tensions, contact angles, and heats of immersion. In: *Contact angle, wettability, and adhesion.* Washington, USA: American Chemical Society; 1964: 99-111.

[83] Morimoto T, Kiriki M. Analysis of the heat of breaking glass ampoules. *Bulletin of the Chemical Society of Japan.* 1980; 53(12):3701-3702.

[84] Good RJ. Contact angle, wetting, and adhesion: a critical review. *Journal of Adhesion Science and Technology.* 1992; 6:1269-1302.

[85] van Oss CJ. *Interfacial forces in aqueous media.* 2nd ed. Florida, USA: CRC Press; 2006.

[86] Jasper JJ. The Surface tension of pure liquid compounds. *Journal of Physical and Chemical Reference Data.* 1972; 1(4):841-1010.

[87] Setaram Instrumentation. *C80 II User Manual.* Caluire, France: Setaram Instrumentation.

[88] Setaram Instrumentation. *Reaction, isotheramal and scanning calorimeter-C80- cells- Calorimetry and thermal analysis- Setaram.* [homepage on the Internet]. Setaram Instrumentation; c. 2011 [accessed 2009 June 30]. Available from: http://www.setaram.com/C80-Cells.htm.

[89] King DA. Thermal desorption from metal surfaces: A review. *Surface Science.* 1975; 47(1):384-402.

[90] Attard G, Barnes C. *Surfaces.* Oxford, UK: Oxford University Press; 1998.

[91] Redhead PA. Thermal desorption of gases. *Vacuum.* 1962; 12(4):203-211.

[92] Ko EI, Benziger JB, Madix RJ. Reactions of methanol on W(100) and W(100)-(5 × 1)C surfaces. *Journal of Catalysis.* 1980; 62(2):264-274.

[93] NIST Mass Spec Data Center, Stein SED. Mass spectra. In: Linstrom PJ, Mallard WG, editors. *NIST chemistry webbook, NIST standard reference database number 69.* National Institute of Standards and Technology [accessed 2010 Sept 23] Available from: http://webbook.nist.gov

[94] King R, Idriss H. Acetone reactions over the surfaces of polycrystalline UO_2: A kinetic and spectroscopic study. *Langmuir.* 2009; 25(8):4543-4555.

[95] Masel RI. Rate laws for reactions on surfaces I: kinetic models. *Principles of adsorption and reaction on solid surfaces.* Toronto, Canada: John Wiley & Sons, Inc.; 1996: 507-580.

[96] Zhou J, Sui Z, Zhu J, Li P, Chen D, Dai Y, et al. Characterization of surface oxygen complexes on carbon nanofibers by TPD, XPS and FT-IR. *Carbon.* 2007; 45(4):785-796.

[97] de la Puente G, Pis JJ, Menéndez JA, Grange P. Thermal stability of oxygenated functions in activated carbons. *Journal of Analytical and Applied Pyrolysis.* 1997; 43(2):125-138.

[98] Szymanski GS, Karpinski Z, Biniak S, Swiatkowski A. The effect of the gradual thermal decomposition of surface oxygen species on the chemical and catalytic properties of oxidized activated carbon. *Carbon.* 2002; 40(14):2627-2639.

[99] Boudou JP, Paredes JI, Cuesta A, Martínez-Alonso A, Tascón JMD. Oxygen plasma modification of pitch-based isotropic carbon fibres. *Carbon.* 2003; 41(1):41-56.

[100] Haydar S, Moreno-Castilla C, Ferro-García MA, Carrasco-Marín F, Rivera-Utrilla J, Perrard A, et al. Regularities in the temperature-programmed desorption spectra of CO_2 and CO from activated carbons. *Carbon.* 2000; 38(9):1297-1308.

3 Surface Modification

3.1 Overview

Intermediate modulus PAN-based carbon fibres have been treated by an industrial electrochemical treatment and by ultraviolet generated ozone as described in Chapters 2.3 and 2.4. Acidic and basic electrochemical treatments produced five batches each of the following treatment levels, 0.2B, 3B, 6B, and 3A. Three batches of untreated fibres are referred to as UST (1, 4 and 5). Untreated and treated fibres have been examined by XPS, SEM, TEM, nitrogen and krypton adsorption, and laser Raman as outlined in Chapter 2. The UV/O$_3$ treatment was found to increase the surface oxygen level of the fibres to that of the most treated electrochemical fibres within 5 minutes of treatment. XPS O1s/C1s ratios as high as 0.3 were produced, with saturation occurring at approximately 40 minutes exposure. The main functional groups introduced were, in addition to hydroxyl species, alkoxides (ca. 286.5 eV), carbonyl (288.0 eV), and carboxyl (289.5 eV). Examination of the full width half maximum of the graphite peak from XPS C1s showed some disorder was introduced to the first few layers of the fibre with treatment but the effect was not evident in the Raman, i.e. in the bulk of the fibre.

3.2 Surface Chemistry

3.2.1 Elemental Analysis

The main elements present in the XPS survey scans are carbon, oxygen and nitrogen. Figure 3.1 shows some example survey scans for the electrochemically treated fibres. Table 3.1 lists the average surface compositions, oxygen/carbon ratio (O/C) and the nitrogen/carbon ratio (N/C) for all batches of the untreated fibres and the electrochemically treated fibres found on initial XPS examination.

The untreated fibre contains about 1.6% of Si. The Si concentration decreases upon treatment indicating that it is most likely at the surface and near the surface,

and not in the bulk of the materials. While the untreated fibre did not contain Na, trace amounts were found on the surface of the base and acid treated fibres. Statistical analysis of the O/C ratio shows fibres 3B, 6B and 3A have significantly different surface compositions to the non-treated fibre (P< 0.05, t-test), whereas fibre 0.2B does not. Fibres 0.2B, 3B and 6B have been treated with increasing levels of charge using the same treatment solution and there is a trend of a slight increase in the O/C ratio. Treatments 6B and 3A are equivalent in terms of quantity of surface oxygen produced (both double the amount of surface oxygen) and, as discussed in the next section, are also equivalent in terms of chemical species and the effect they have on the structure of the fibre. Further XPS measurements, performed further along the tow and two years after the first set of measurements suggest a slight difference in O/C ratio between the 3A and 6B fibres depending on the batch. This is discussed in Section 3.2.3.
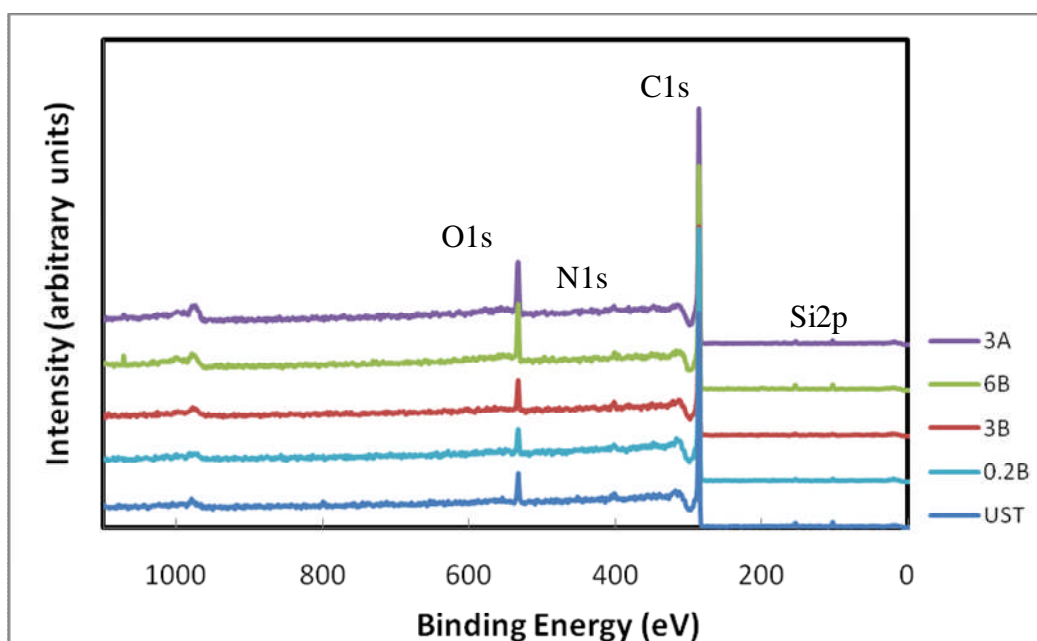
Figure 3.1 XPS survey spectra for untreated and electrochemically treated fibres.

Table 3.1 XPS surface compositions (atomic %) for electrochemically treated fibres; numbers in bold highlight the higher or lower value in the series and the base treated series is outlined in the table.

Treatment	%					Ratio		
	C	O	N	Si	Na	O/C	N/C	O/N
UST	92.1	5.1	1.2	**1.6**	0.00	0.06	0.01	4.24
0.2B	93.3	4.3	1.4	1.1	0.00	0.04	0.01	3.14
3B	90.6	7.3	1.7	0.4	0.00	0.08	0.02	4.36
6B	87.6	**10.0**	**1.8**	0.6	0.05	0.11	0.02	5.60
3A	**88.8**	9.2	1.7	0.3	**0.08**	0.10	0.02	5.54

The UV/O$_3$ altered fibres were treated for times between 1 minute and 120 minutes while held in an XPS stub. Figure 3.2 shows the O/C ratio for previously untreated fibres (UST) subjected to UV/O$_3$ treatment as a function of treatment time. The O/C ratio initially increases linearly with treatment time. A saturation point was reached after approximately 40 minutes of treatment. Error bars represent the average 90% confidence interval. Long tows of UST fibres were also treated for 4 hours in the UV/O$_3$ equipment with the tow being turned regularly to ensure all the surfaces of the fibres were treated. The O/C ratio for these fibres also varied between the saturation values of 0.25 to 0.3.
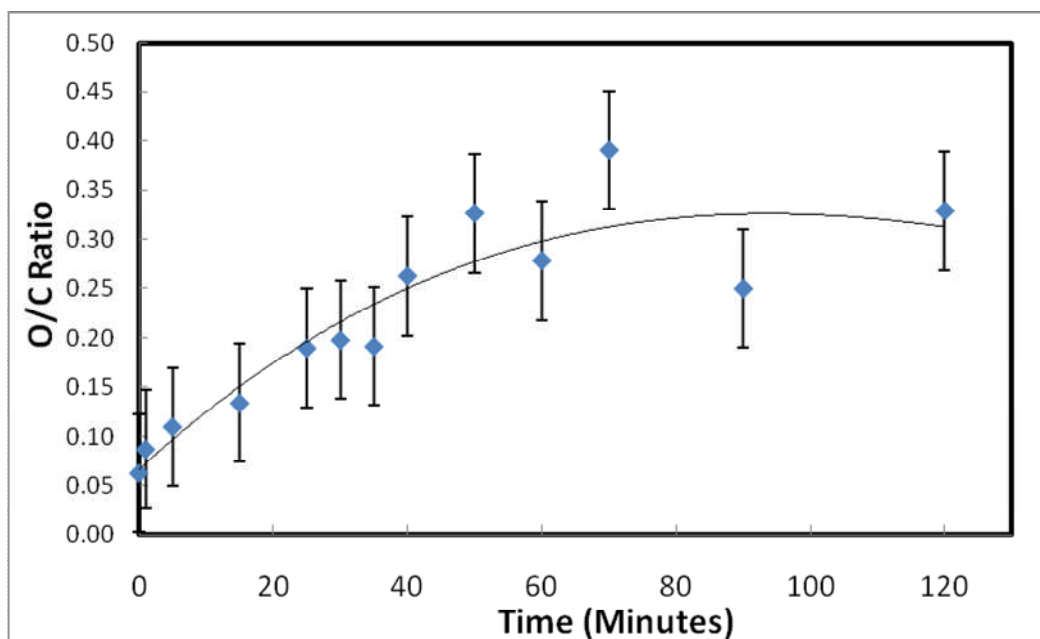
Figure 3.2 XPS O1s/C1s ratio as a function of UV/O$_3$ treatment time on previously untreated fibres (UST).

Previous work on UV/O$_3$ treatments by Rich *et al.* treated fibres with UV and additional ozone gas at a concentration of 700 ppm for times ranging from 5 seconds to several minutes. They reported that a near plateau of 0.22 in surface O/C ratio was reached after 90 seconds but extended treatments of 10 minutes produced a further increase to 0.27 [1]. In Figure 3.2, the treatment times required to achieve this level of oxidation are higher (~40 minutes) and the level of saturation is also higher; about 0.3. The difference in treatment efficiency could be due to differences in lamp output, distance of fibres to the lamp, the fibre composition and structure, air flow, and the fact that additional ozone was used in the other study. Without the additional ozone in the system, Rich *et al.* produced much lower O/C ratios (~0.04 for 90 seconds).

The molecular concentration of ozone in our equipment was estimated in Chapter 2.4.2 to be ~ 1.84×10^{15} molecules/cm^3 or 110 ppm. The amount of ozone in our set up is therefore substantially lower than in reference [1]. To further investigate this, additional ozone from a dielectric source was flowed into the UV/O$_3$ equipment at 5, 10, and 15 litres per minute (lpm) for a treatment time of 30 minutes. At 5 lpm of dry oxygen, this is equivalent to 18000 ppm of ozone. Increasing the ozone present did not alter the O/C ratio significantly.

Figure 3.3 shows the XPS O1s/C1s ratio for electrochemically treated fibres subjected to the additional treatment of UV/O_3. The 3B and 6B fibres show very similar trends to each other; there being very little difference between the O/C results for each treatment time. There is a small advantage to be gained by starting with a fibre that has more oxygen on the surface; however it is lost when higher treatment times are used and starting with an untreated fibre allows more control over the end level of oxygen desired.
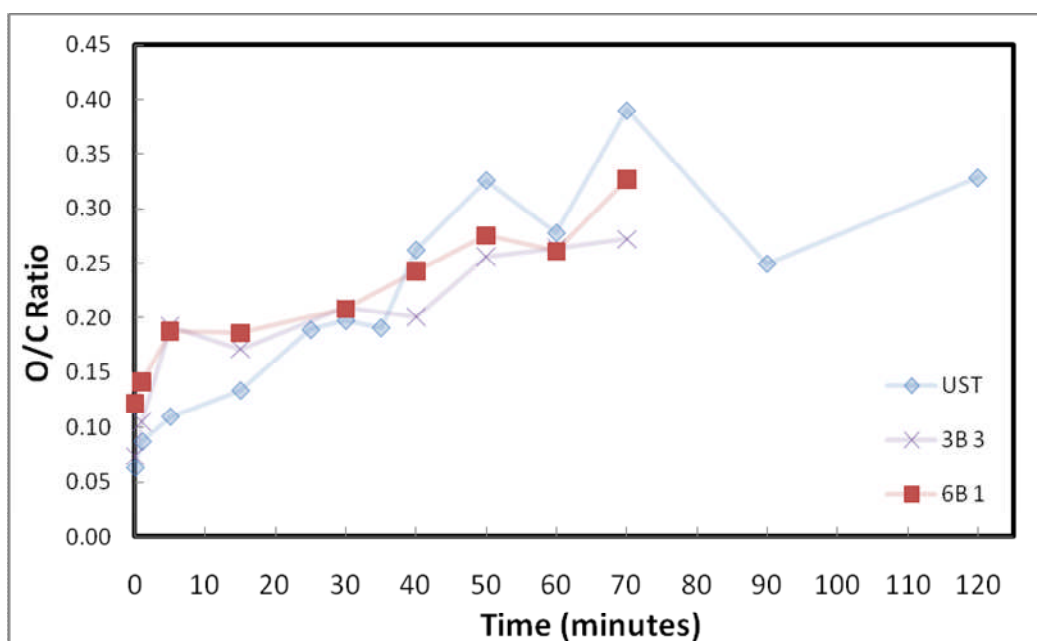
Figure 3.3 XPS O1s/C1s ratio as a function of UV/O_3 treatment time on untreated and electrochemically treated fibres.

Fibres were also altered using only the dielectric generated ozone. The ozone was flowed into a glass tube containing the fibres at a flow rate of 5 lpm for 20, 40, and 60 minutes. The untreated fibres were measured beforehand to have an O/C ratio of 0.03 while the ozone only treated fibres all produced O/C ratios of 0.06 no matter what the treatment time was. From this, we can see that the UV light provides a significant advantage over ozone alone.

3.2.2 Functional Groups

Peak fitting was performed on the Carbon 1s spectra as described in Chapter 2.6.3. Figure 3.4 presents the different components of the XPS C1s peak upon peak fitting while Figure 3.5 shows peak fitting for three different UV/O_3 treated fibres. The best fit was obtained when allowing for the most common functional groups ($\chi^2 \leq 5$). Five non-graphitic peaks, shifted from the graphite peak (~284.6eV) by 1.2, 2.6, 4.2, 6.0 and 6.6 eV and corresponding to alkoxide/ ethers/ C=N, carbonyl, carboxyl, carbonate/ adsorbed CO/CO_2, and Plasmon loss, respectively, were present. The area under each peak was used to calculate relative concentrations of each functional group. Attempts were made to analyse the oxygen 1s spectra with two and three peak models, however it was not possible to achieve a consistent result. Oxygen is more electronegative than carbon so the chemical shift is less sensitive to the bonding present [2]. Most functionalities are within 2 eV of the main oxygen peak [3], so it is more difficult to resolve overlapping peaks.
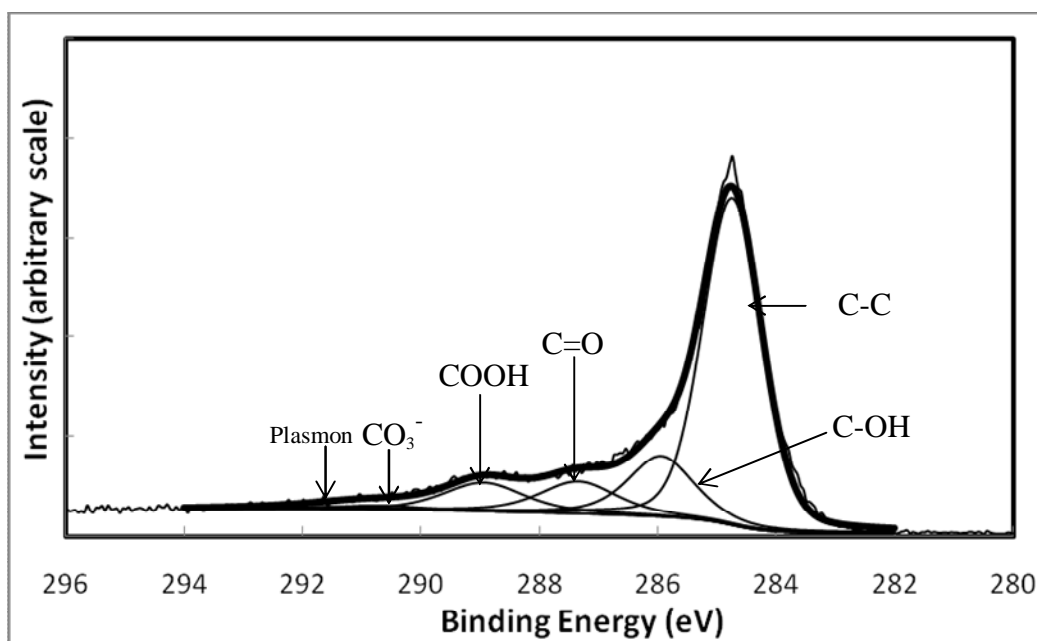

Figure 3.4 Example peak fit for carbon fibre showing 6 peaks fitted.
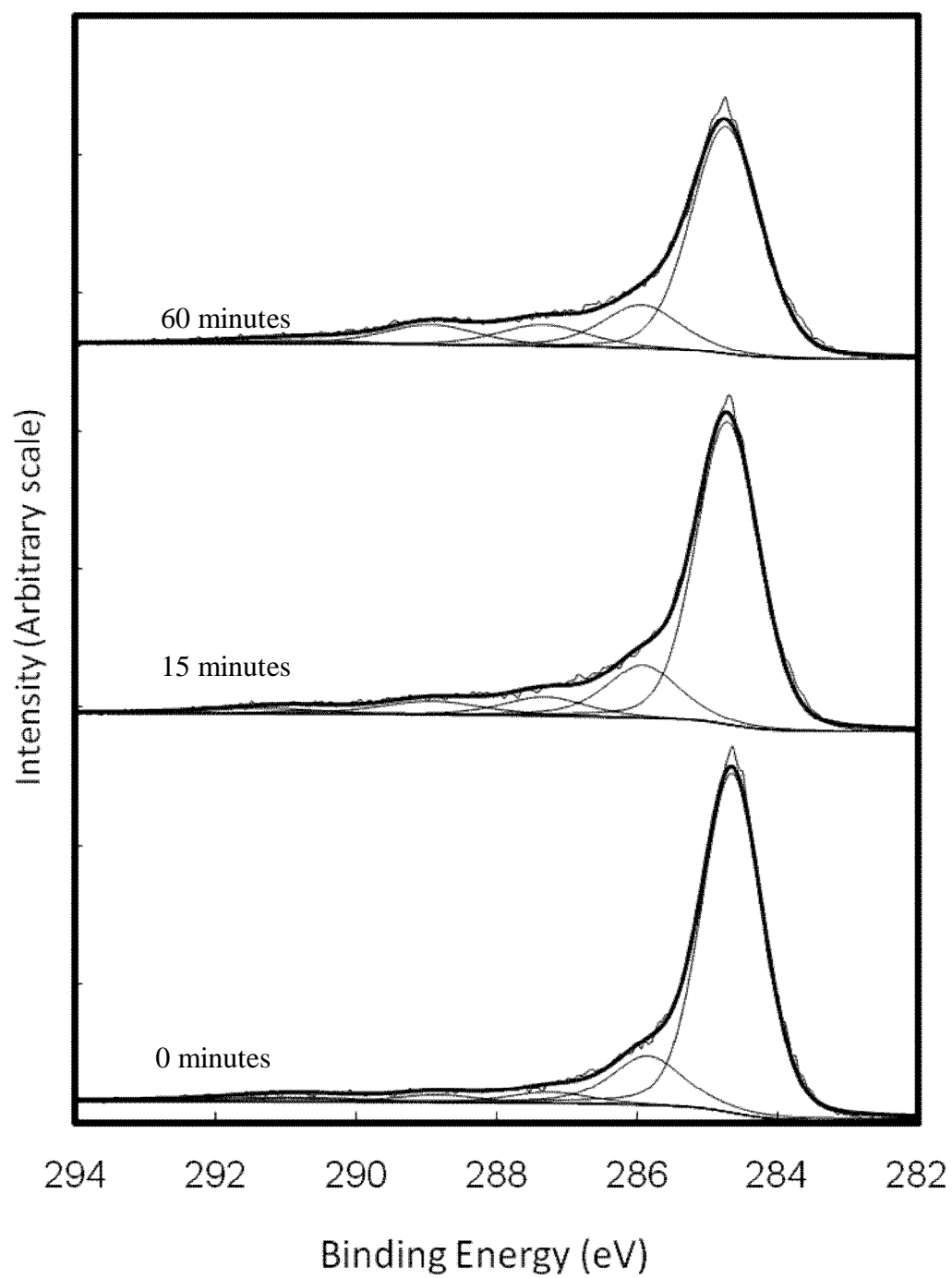
Figure 3.5 Peak fit of XPS C1s of UST fibre treated for 0, 15 and 60 minutes with UV/O₃.

Table 3.2 lists the curve fitting results for the electrochemically treated fibres while Table 3.3 lists those for the UV/O$_3$ treated UST fibres. The UV/O$_3$ treated 3B and 6B fibres did not show significantly different functional groups compared to the UST fibres at oxygen saturation levels, so the results have not been listed.

The most significant change produced by the electrochemical treatments was in the level of carboxyl groups (289.5 eV). Presence of the carboxyl group and hydroxyl groups allows strong bonding to occur between the fibre surface and the epoxy resin and is a desirable effect of treatment [4]. Increasing the charge of the base treatment increased the carboxyl, alkoxide and carbonyl groups but also reduced the level of carbonate and the level of Plasmon loss occurring. The trends were all linear. Kettle *et al.,* showed carboxylic acid and amine groups are more desirable than alkoxide groups as they have stronger bonding [5]. The 3A treatment produced similar levels of each functional group to the 6B treatment suggesting the acid is a more oxidising chemical since the voltage applied was half that applied to the base treatment. There is no difference between the 3B, 6B and 3A treatments in terms of effect on functional group make-up; i.e. the acid and base treatments are no more or less specific at adding carboxyl groups.

Table 3.2 % of the carbon functional groups as determined by XPS C1s on electrochemically treated fibres (highest observed reaction products are indicated in bold

Treatment	%				
	UST	0.2B	3B	6B	3A
Graphite (~284.6 eV)	75.1	74.5	71.7	72.1	71.7
Alkoxide/ phenolic/ ether (285.8 eV)	**14.1**	**14.5**	**15.4**	**15.8**	**15.3**
Carbonyl/ quinine (287.2 eV)	4.1	3.9	5.6	5.5	5.6
Carboxyl/ ester (288.8 eV)	2.7	2.8	3.7	4.1	4.1
Carbonate/ adsorbed CO/CO_2 (290.6 eV)	2.0	1.9	1.4	1.0	1.0
Plasmon (291.2 eV)	2.0	2.4	2.2	1.6	2.3
Ratio -COH to -COOH	5.2	5.2	4.2	3.9	3.7
Ratio total CO_x to graphite	0.30	0.31	**0.36**	**0.37**	**0.36**

The UV/O_3 treatment significantly altered the level of functional groups at even the lowest treatment time of one minute. As can be seen from comparing Table 3.2 and Table 3.3 one minute of UV treatment is equivalent to the strongest electrochemically treated samples. At 70 minutes treatment time, the carboxyl groups increased threefold. Overall, the treatment did not affect the level of carbonate and a small decrease in Plasmon loss occurred. A small decrease in the Plasmon peak suggests increase in surface disorder since the π orbitals will be disrupted and reduced. The increase in carboxyl groups shows a strong linear relationship with treatment time ($R^2 = 0.99$). It is also to be noted that the ratio of a single oxidation (-COH) to that of double oxidation (-COOH) has decreased considerably using the UV ozone treatment. The long tows of fibres treated for 4 hours were not significantly different to the fibres treated for 70 minutes.

Table 3.3 % of the carbon functional groups as determined by XPS C1s on UV/O$_3$ treated UST fibres

UV/O$_3$ time (minutes)	Relative Concentration (%)					
	0	5	15	30	60	70
Graphite (~284.6 eV)	75.7	70.8	68.4	67.5	64.9	64.7
Alkoxide/ phenolic/ ether (285.8 eV)	14.2	15.0	15.4	15.6	15.3	16.6
Carbonyl/ quinine (287.2 eV)	3.8	6.1	7.1	7.2	8.2	7.1
Carboxyl/ ester (288.8 eV)	2.8	4.1	5.1	6.3	8.5	9.3
Carbonate/ adsorbed CO/CO$_2$ (290.6 eV)	1.2	1.4	1.3	1.2	1.4	0.5
Plasmon (291.2 eV)	2.3	2.64	2.9	2.7	1.9	1.9
Ratio –COH/COOH	5.1	3.7	3.0	2.5	1.8	1.8
Ratio total CO$_x$ to graphite	0.29	0.38	0.42	0.45	0.51	**0.52**

3.2.3 Treatment Ageing and Homogeneity

A selection of electrochemically treated fibres was examined by XPS again, two years after the initial measurements. The new samples came from substantially further along the tow. Some slight differences in O/C ratio were observed between old and new fibres from the same batch, as shown in Table 3.4. Values in bold are significantly different from the old measurements for the same batch but are not significantly different from the treatment average values presented in Table 3.1. The functional groups present did not change with time. The small difference in O/C ratio may be due to either fibre aging or simply a difference in surface chemistry along the tow. With the untreated fibres, it is possible that the outer fibres were exposed to more air and moisture than the inner ones resulting in an exaggerated oxygen level.

UV/O$_3$ treated fibres were examined 1 month after a 40 minute treatment and showed no significant difference in elemental composition or function group make-up.

Table 3.4 O/C ratio after 2 years storage (figures in bold are significantly different to old values)

Treatment	O/C Ratio	
	Old	New
UST 1	0.05	**0.03**
0.2B 1	0.05	0.04
3B 3	0.07	0.09
6B 1	0.12	0.13
3A 1	0.08	**0.10**

3.3 Surface Morphology

3.3.1 SEM

Figure 3.6 shows a SEM image of an untreated carbon fibre. Fibres were a mix of kidney shape and circular cross sections with a diameter of ~5 μm. All fibres showed striations typical of the fibre manufacturing process and were relatively smooth. Examination of several images of each batch of fibres showed no visible alteration to the surface tomography with electrochemical treatment or UV/O$_3$ treatment. The striations seemed unaltered and no pitting occurred or debris generated.

Figure 3.7 shows a SEM image of a sheared 6B treated fibre. The internal structure of the fibre shows layers approximately aligned with the fibre axis as would be expected for a PAN fibre.
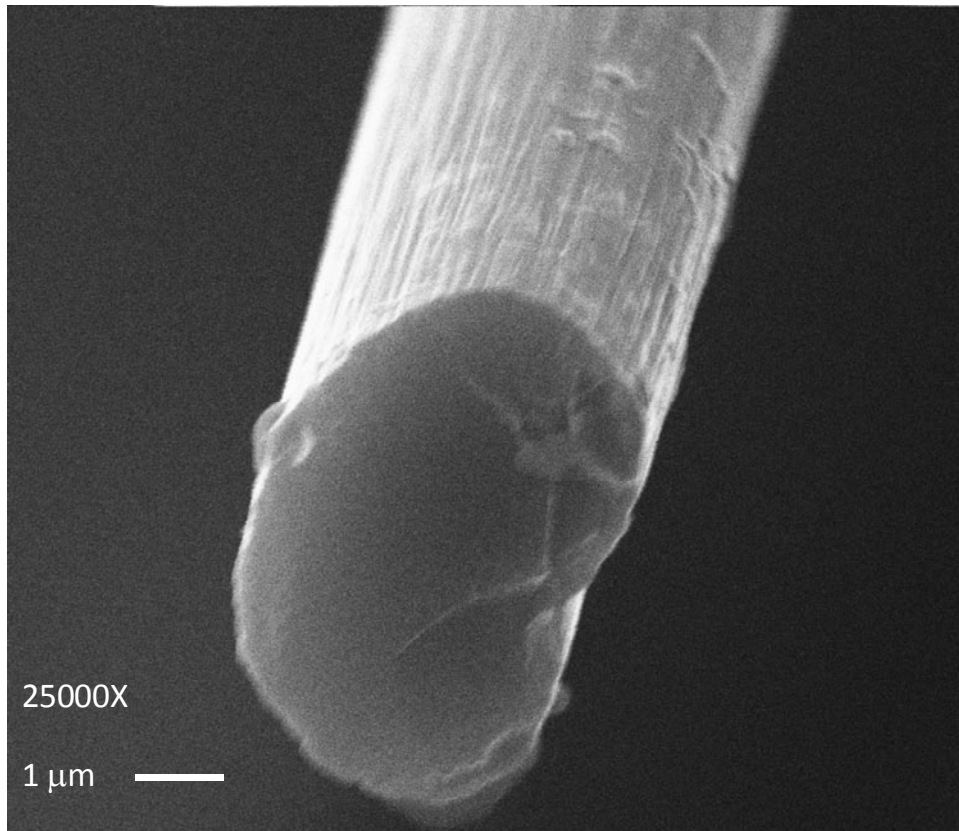
Figure 3.6 SEM image (25,000x magnification, 20kV) of untreated fibre.
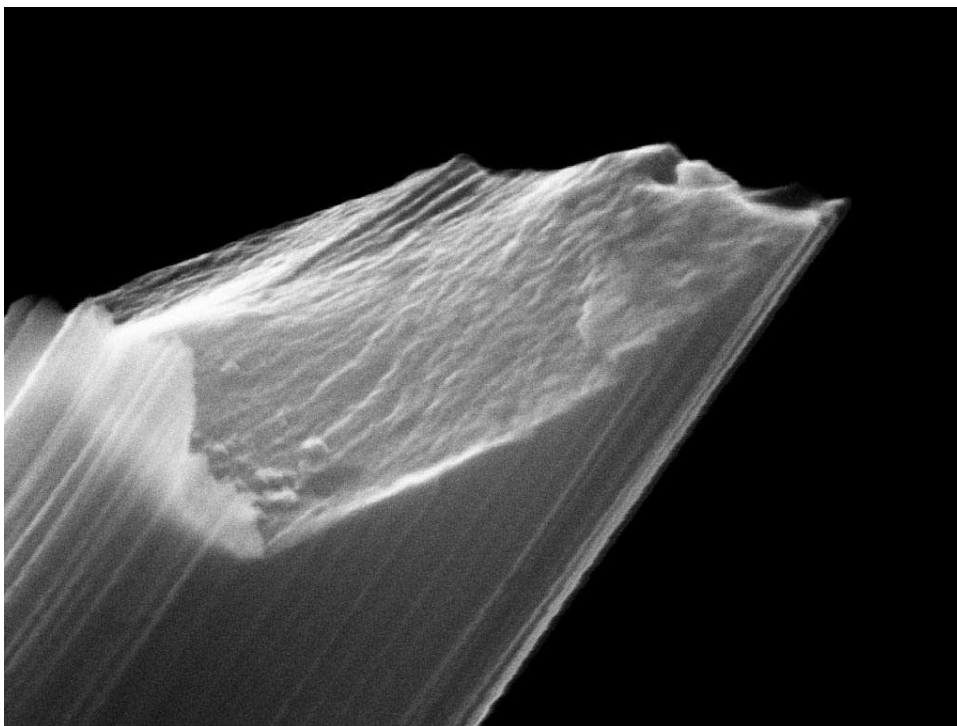
Figure 3.7 SEM image (15,000x magnification, 20kV) of 6B treated fibre.

3.3.2 BET Surface Areas

Nitrogen adsorption studies on the untreated and 6B treated fibres showed Type 2 isotherms, characteristic of non-porous or macroporous surfaces. Figure 3.8 shows the nitrogen isotherm for the 6B fibres. Surface area measurements from the nitrogen isotherms (molecular cross section 0.16 nm^2) gave areas of ~1 m^2/g for both the UST and 6B fibres. BET surface area measurements from the krypton isotherms (molecular cross-section 0.21 nm^2) also showed little difference between the untreated and 6B treated fibres; both gave areas of ~ 1 m^2/g. Figure 3.9 shows the BET plots. Taking the SEM images into account, the combined results suggest the electrochemical treatments cause little damage to the fibre surface. The fibres treated with UV/O_3 for 4 hours returned a surface area of 6.3 m^2/g using Krypton; a substantial and significant increase.
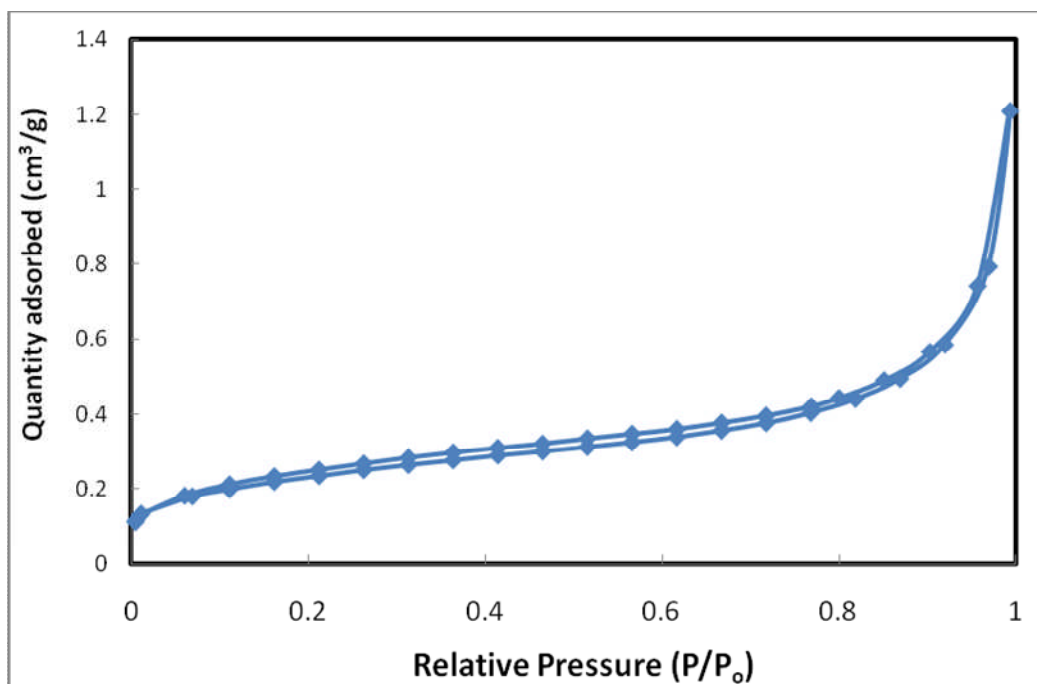
Figure 3.8 Nitrogen isotherm for 6B fibres.
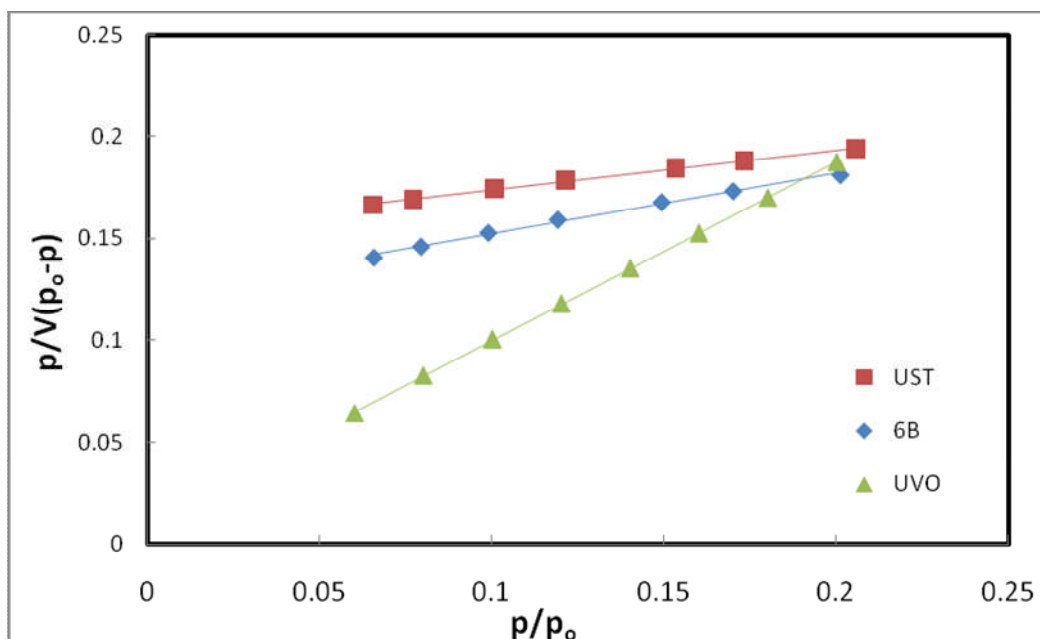
Figure 3.9 BET plot of UST, 6B and UV/O₃ treated fibres for Krypton.

3.3.3 XPS and Raman

The full width half maximum (FWHM) of the fitted graphite peak has been shown to correlate with the graphitic order of the surface [6,7]. The average FWHM for the electrochemically treated fibres obtained from the XPS peak fits was 1.00 ± 0.01 eV. No significant differences in FWHM were evident for any of the electrochemical treatments ($P > 0.05$, t-test). Figure 3.10 shows the effect of the UV/O₃ treatment on the FWHM for the untreated fibres. The FWHM increases with increasing treatment up to a plateau suggesting the surface is becoming less graphitic and more disordered. This was also the case for the 3B and 6B fibres treated with UV/O₃. To gain more insight on the effect of this treatment on the surface versus bulk, further investigation with Raman was conducted.
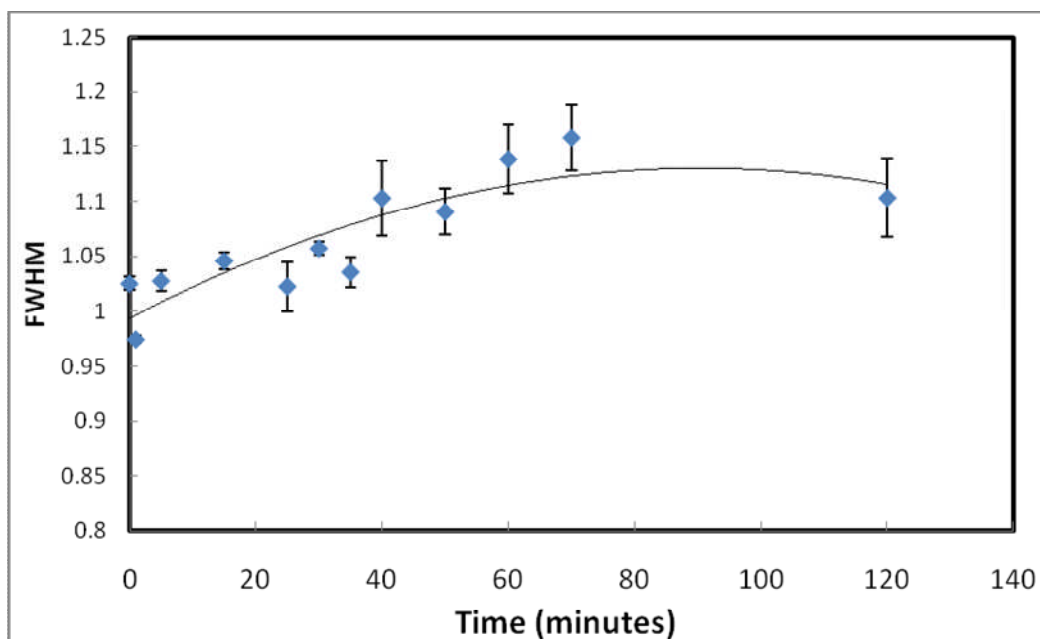
Figure 3.10 Effect of UV/O$_3$ treatment time on FWHM of XPS C1s (284.6 eV) attributed to graphite peak for UST fibres (untreated).

Four peaks were discernable in the Raman spectra for the carbon fibres at approximately 1360, 1600, 1200, and 1500 cm^{-1}. Figure 3.11 shows three peak fitted spectrums of fibres treated with different UV/O$_3$ times. The 1360 and 1600 cm^{-1} bands are attributed to the D and G band respectively as discussed earlier. The broad peaks at ~1200 and 1500 cm^{-1} are most likely due to aliphatic structures [8] and amorphous sp^2-bonded forms of carbon [9] respectively. The area under the curves was measured and used to calculate the ratio I_D/I_D+I_G. Table 3.5 lists the average values for the curve position (ν), FWHM and I_D/I_D+I_G ratio. The I_D/I_D+I_G ratio does not vary significantly with treatment and the position of the G band does not change; both are used as indicators of a change in the graphitic order [8]. However, the FWHM's of the D and G peaks decrease with all of the electrochemical treatments suggesting the graphitic order increases with treatment. Any increase in graphitic order is likely to be due to small debris being removed from the fibre surface with treatment.

Table 3.5 Average values from curve fit for Raman of electrochemically treated fibres

	ν_D (cm^{-1})	ν_G (cm^{-1})	FWHM$_D$ (cm^{-1})	FWHM$_G$ (cm^{-1})	I_D/I_D+I_G
UST	1369	1601	179	94	0.64
0.2B	1368	1600	169	94	0.63
3B	1365	1601	167	89	0.64
6B	1362	1601	162	83	0.65
3A	1366	1600	166	89	0.63
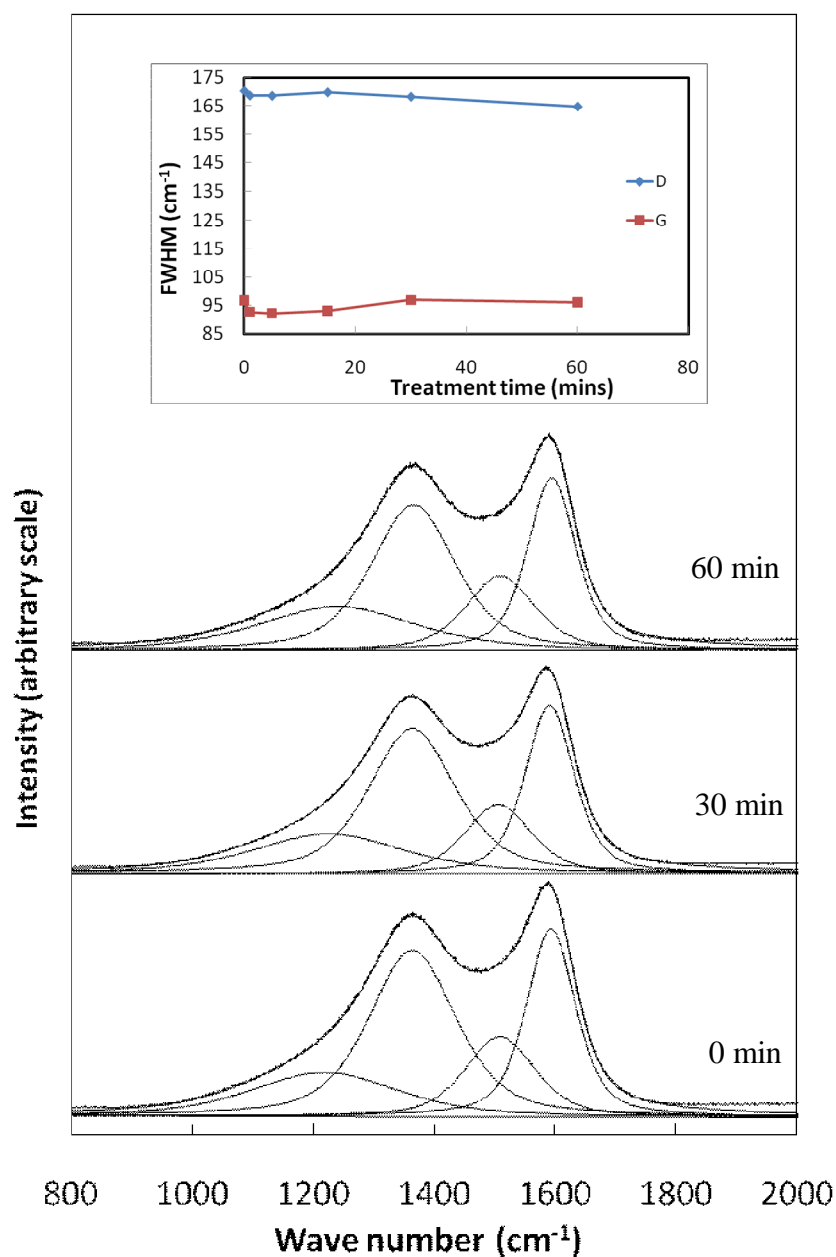
Figure 3.11 Raman spectra of UV/O₃ treated U fibres with four curves fitted as a function of time. Inset shows FWHM for D and G peaks.

Figure 3.11 shows the Raman results for the UV/O$_3$ treated UST fibres. There is no observed change in the peak profile or their FWHM (inset) with UV treatment with time. The results suggest the UV/O$_3$ treatment does not alter the graphitic order of the material. This does not correlate with the XPS data or the BET data but Raman probes deeper into the structure than XPS. For carbon, Raman is estimated to probe ~100 nm into the bulk [10] whereas information provided from the O1s lines is roughly from 2 nm deep in the carbon [11] or about 6 layers. An alteration in the surface disorder but not the bulk can be a desirable effect as more sites will be available for chemical bonding [12] but the mechanical properties of the fibre, will be unaffected [4].

The average I_D/I_D+I_G ratio for the fibres was ~0.64. To provide some kind of comparison, carbon black, and multiwall carbon nanotubes (MWNT) were also examined. Carbon black gave a similar ratio to the fibres of ~0.63 while the MWNT gave a ratio of ~0.16. MWNT are inherently more graphitic than fibres so it is possible to distinguish large differences in graphitic order using this method.

3.4 Structure (TEM)

Untreated and treated fibres were examined by TEM as described in Chapter 2.8.2. Fibres were prepared by grinding and dispersing in acetone or by embedding in resin and ultramicrotoming. Neither method produced images of sufficient quality for in-depth study. Figure 3.12 shows a longitudinal image from the core of a UV/O$_3$ treated fibre prepared by ultramicrotomy. It is possible to distinguish ribbons of carbon which are generally aligned to the fibre axis. Figure 3.13 shows a transverse image of the fibre. The ribbons of graphene have a twisted, random, structure in the radial direction. These images are typical of PAN fibres [13,14].
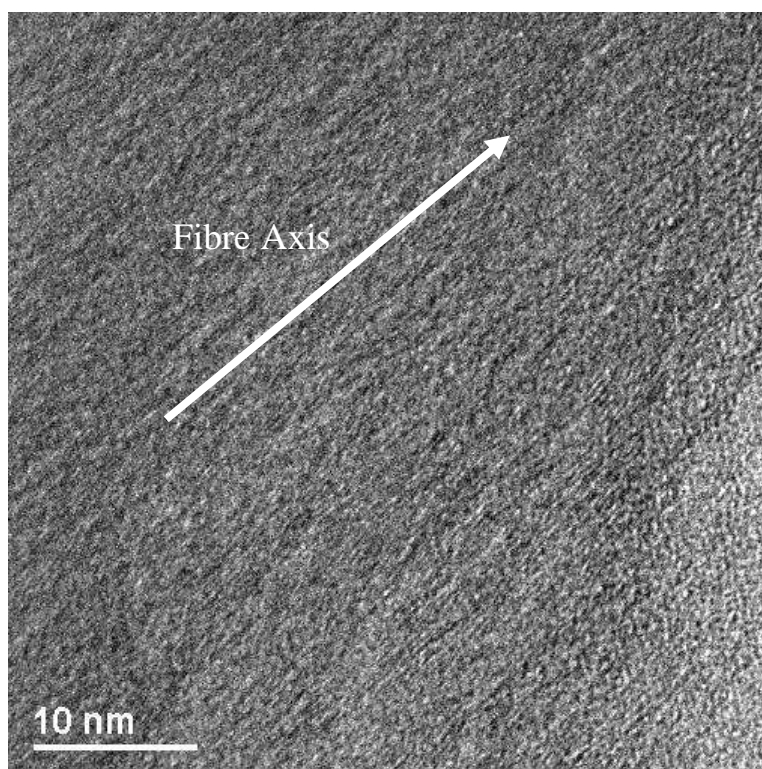
Figure 3.12 TEM image of UV/O₃ treated fibre prepared by an ultramicrotome showing the alignment of carbon ribbons to the fibre axis.
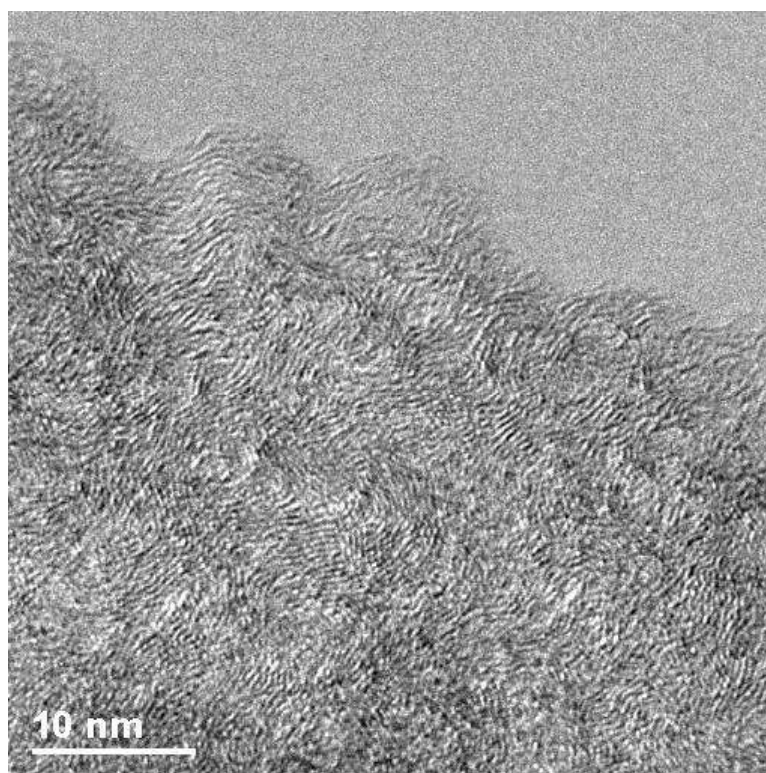

Figure 3.13 TEM image of UV/O₃ treated fibre prepared by an ultramicrotome showing the twisted layer structure typical to PAN fibres.

Theoretical diffraction patterns were generated from the TEM images and the interlayer spacing (d_{002}) was calculated from the diffraction patterns. Figure 3.14 and Figure 3.15 show examples of UST and 6B fibres respectively and their associated diffraction patterns. Table 3.6 lists the average interlayer spacing taken from several images for the three types of fibres examined. The error quoted represents the 90% confidence interval.

Table 3.6 Interlayer spacing from TEM

	d_{002} (nm)
UST	0.386 ± 0.015
6B 1	0.370 ± 0.017
UV/O_3	0.373 ± 0.019

An ideal graphitic material would have an interlayer spacing of 0.335 nm [6]. The fibres therefore display a high level of turbostratic structure. From the error involved in these measurements, it is not possible to tell if there is a difference between fibres. It is unlikely that the treatments would change the internal structure of the fibre, although the BET and XPS suggest the surface layers may be altered. Ideally the surface layers of the fibres would be visible in the images and it would be possible to qualitatively and quantitatively examine the fibre surface layers.
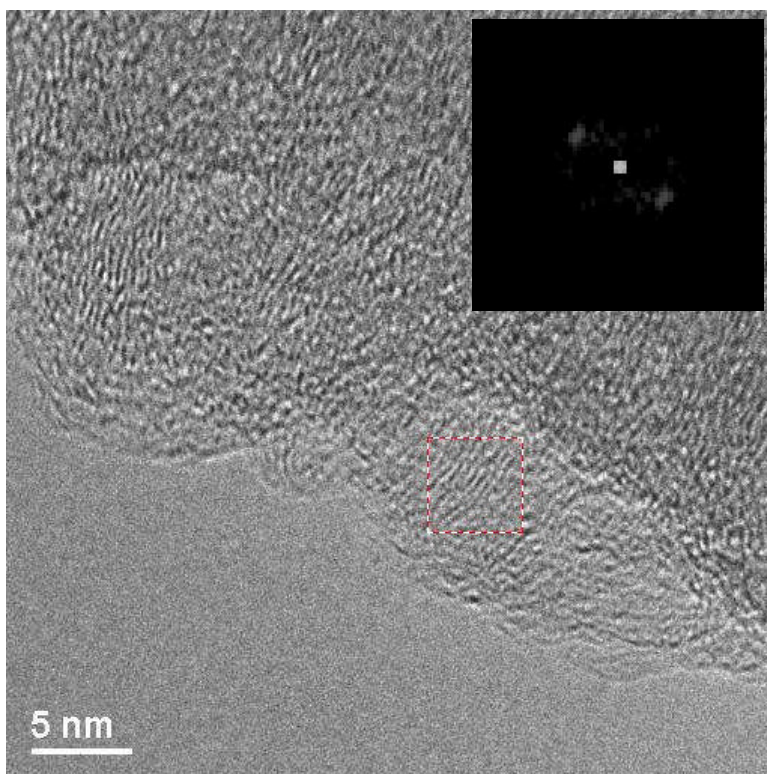
Figure 3.14 TEM image of UST fibre prepared by dispersion and (inset) associated diffraction pattern.
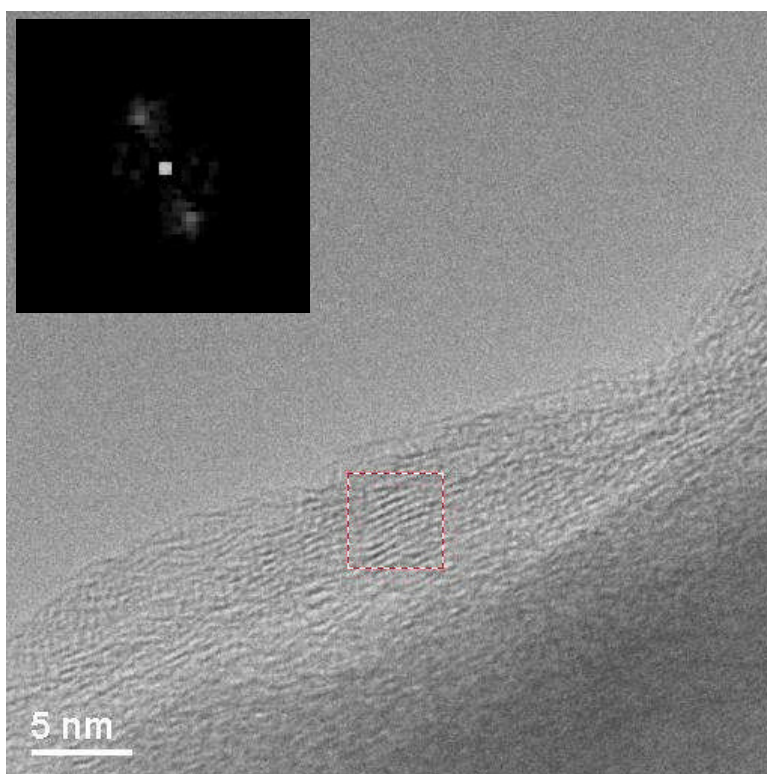

Figure 3.15 TEM image of 6B fibre prepared by dispersion and (inset) associated diffraction pattern.

3.5 Discussion

Various proprietary treatments have been examined by other researchers using several techniques including XPS and SEM. For example, Dilsiz and Wightman examined proprietary treatments on unsized PAN based fibres using XPS [15]. The Hercules AS-4 fibres had an O/C ratio of 0.12; similar to the highest level of base treatment presented here or to 15 minutes UV/O_3 treatment [15]. While there are variations in the assignment of fitted peaks to XPS data throughout the literature, in general similar groups have been found on treated fibres to those presented here, namely Alkoxides/amines , carbonyl, carboxyl, and the $\pi \rightarrow \pi^*$ shake up.

Bismarck *et al.,* examined a variety of salts and bases to treat PAN based fibres using SEM among other methods [16]. They found no changes in the surface morphology in the SEM images until treatment times reached 10 minutes and no differences in surface morphology were observed between the types of electrolytes [16]. Jin *et al.,* used ozone to treat a set of carbon fibres in a heated environment [17]. XPS showed an increase in O/C ratio from 0.1 to 0.3. Functional group analysis suggested the main increase was in carbonyl group followed by the carboxyl group [17]. The same authors also used micro-Raman to investigate the graphitization. Four peaks were fitted to the D and G peaks. A decrease in the I_G/I_D ratio (0.5473 to 0.4983) was reported with ozone treatment suggesting there was a slight increase of the surface disorder; AFM images supported this [17].

The SEM images presented in this work did not show any obvious differences in surface roughness for the anodic treatments or the UV/O_3 treatments. The BET data and the XPS FWHM of the graphitic peak do suggest the surface is altered when treated with UV/O_3. Further investigation with AFM and STM would be of interest.

To the author's knowledge, Rich *et al.,* is the only group to have published data on UV/O_3 treatments on carbon fibres [1] although there is a Japanese Patent [18]. In the Rich et *al.* study, untreated PAN fibres were treated with ultraviolet

light and ozone [1]. The UV light was generated by a 300W pulsed Xenon flash lamp and the emitted light had a wavelength of less than 200 nm. Approximately 700 ppm of ozone was passed over the sample in addition to the UV light. XPS showed the fibres had an initial O/C ratio of 0.02 which increased to 0.12 following just 5 seconds of UV/O_3. A 10 minute treatment produced an O/C ratio of 0.27 [1]. As presented in Section 3.2.1, our UV/O_3 took longer to produce these levels of oxygen, most likely due to the difference in lamp intensity as adding more ozone during the treatment did not alter the oxidation level significantly. Types of functional groups generated were not investigated by Rich *et al.* though [1]. The surface roughness was measured using STM and compared to a commercially treated Hexcel fibre (AS4). UV/O_3 treatment increased the surface roughness marginally (~10%). It was suggested that the UV/O_3 treatment removed a weakly bound, incoherent layer on the fibre surface and this was backed up by measurements of fibre diameter [1]. In this work, the BET data and XPS results suggested a small amount of disorder was created at the surface of the fibres due to the UV/O_3 treatment but it did not affect the bulk. In addition, the electrochemical treatments examined, did not affect the surface structure.

It is not simple without in situ spectroscopic studies to understand the formation of carboxylates, carbonyls and alkoxides upon acid or base treatments on the surface of the fibre carbon. It is however clear that the process involves reaction with protons (acid) and hydroxyl ions (base) as has been indicated previously by other researchers [19]. Mechanisms for the progressive oxidation of carbon by acids and bases were outlined in Chapter 2.3.1. Generally, the progression involves a single oxidation (-COH) being eventually further oxidised to a double oxidation (-COOH). As can be seen from Table 3.2 the main reaction product for anodic treatment is that of alkoxides and/ or alcohols and this indicates that further oxidation of alkoxides is not efficient with this type of treatment.

The UV treatment under O_3 involves radical reactions [20]. As discussed in Chapter 2.4.1, O atoms are also formed. Excitation of the surface with UV also results in the formation of hydroxyl radicals since the work was conducted on fibre carbons that were not out-gassed and that contained hydroxyl species. This, in addition to the inevitable presence of water, would result in OH radicals under

UV excitation. Therefore both the O atoms directly and O atoms from O_3 decomposition on the surface, and hydroxyl radicals contribute in the sequential oxidation of the surface to alkoxides, carbonyls and carboxylates. While the reaction mechanism is beyond the scope of this work it is highly likely that water will affect the photoreaction rates and this would be needed to optimise the process.

The main difference in the functional groups present on the surface of the fibre upon UV/O_3 treatments is the relative distribution of the alkoxide to carboxyl groups. Figure 3.16 compares this ratio of partial oxidation (the alcohol/alkoxide) and total oxidation (the the carboxyl group). The data of the UV/O_3 treatment is taken after 60 minutes to emphasize the activity; as seen from Table 3.2 and Table 3.3, the total oxidation is already pronounced after 5 minutes of treatment. This result suggests the UV/O_3 treatment could be used as an efficient alternative to electrochemical treatments.
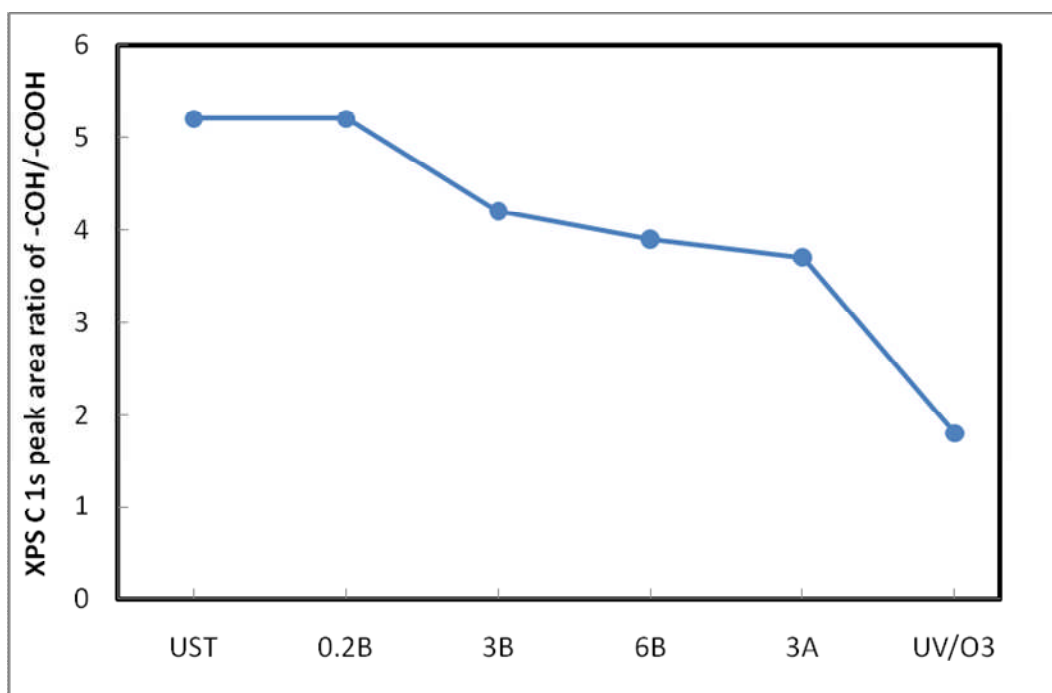

Figure 3.16 Partial versus total oxidation of the surface of fibre carbon as a function of different prior treatment. UST= untreated, xB=base treatment, 3A=acid treatment. The ratio –COH/-COOH represents the partial/total oxidation ratio as determined from XPS C1 peak areas ratios. The UV/O_3 value is taken after 60 minutes of exposure.

3.6   Conclusions

The oxidation of carbon fibres using ultraviolet radiation generated ozone was studied and compared against a series of electrochemical shear treatments. Treatment times of a few minutes of UV/O_3 produced a marked increase in the surface oxygen containing organic compounds.   Five minutes of UV/O_3 treatment can produce similar O/C ratios to a high level electrochemical shear treatment. There was no evidence of fibre aging one month after treatment. The UV/O_3 treatment does not alter the bulk structure of the fibre at the µm level as studied by Raman. It does, however, alter the graphitization of the first few atomic layers of the surface (as studied by XPS C1s and BET), creating a more disordered surface at the atomic/molecular level. Significant increases in hydroxyl, carbonyl and carboxyl groups occurred with UV/O_3 treatment; however the relative proportions of the different groups matched that of the electrochemical treatment. Electrochemically treated fibres subjected to additional UV/O_3 treatment showed increases in O/C ratio with treatment time. UV/O_3 fibres showed a six fold increase in BET surface area, as measured by krypton. TEM images showed both anodic and UV/O_3 fibres to have a structure typical to PAN based fibres with an interlayer spacing of ~0.38 nm. Overall the UV/O_3 treatment method was shown to produce high levels of oxygen containing functional groups (up to a third of the surface carbon was oxidised). The high level of O containing species on the surface is poised to enhance the adhesion to the resin matrix. Further surface characterisation using techniques such as AFM and STM would be of use in the future to determine the exact effect of the UV/O_3 treatment on the surface roughness.

3.7 References

[1] Rich MJ, Askeland P, Liang X and Drzal L. Photo-oxidative treatment of carbonaceous fibers to promote adhesion in polymer matrix composites. *Carbon 2004; 11-16th July 2004.*

[2] Boehm H. Surface Chemical characterization of carbons from adsorption studies. In: Eduardo J. Bottani, Juan M.D. Tascón, editors. *Adsorption by carbons.* Amsterdam: Elsevier; 2008: 301-327.

[3] Briggs D. Applications of XPS in polymer technology. In: Briggs D, Seah MP, editors. *Practical surface analysis, Volume 1- Auger and x-ray photoelectron spectroscopy.* 2nd ed. Chichester, UK: John Wiley and Sons Ltd.; 1983: 437-483.

[4] Jones C. The chemistry of carbon fibre surfaces and its effect on interfacial phenomena in fibre/epoxy composites. *Composites Science and Technology.* 1991; 42(1-3):275-298.

[5] Kettle AP, Beck AJ, O'Toole L, Jones FR, Short RD. Plasma polymerisation for molecular engineering of carbon-fibre surfaces for optimised composites. *Composites Science and Technology.* 1997; 57(8):1023-1032.

[6] Xie Y, Sherwood PMA. X-ray photoelectron-spectroscopic studies of carbon fiber surfaces. 11. Differences in the surface chemistry and bulk structure of different carbon fibers based on poly(acrylonitrile) and pitch and comparison with various graphite samples. *Chemistry of Materials.* 1990; 2(3):293-299.

[7] Smiley RJ, Delgass WN. AFM, SEM and XPS characterization of PAN-based carbon fibres etched in oxygen plasmas. *Journal of Materials Science.* 1993; 28:3601-3611.

[8] Darmstadt H, Sümmchen L, Ting J-, Roland U, Kaliaguine S, Roy C. Effects of surface treatment on the bulk chemistry and structure of vapor grown carbon fibers. *Carbon.* 1997; 35(10-11):1581-1585.

[9] Jawhari T, Roid A, Casado J. Raman spectroscopic characterization of some commercially available carbon black materials. *Carbon.* 1995; 33(11):1561-1565.

[10] Montes-Morán MA, Young RJ. Raman spectroscopy study of high-modulus carbon fibres: effect of plasma-treatment on the interfacial properties of single-fibre epoxy composites. Part II: Characterisation of the fibre-matrix interface. *Carbon.* 2002; 40:857-875.

[11] Briggs D, Seah MP. *Practical surface analysis, Volume 1- Auger and x-ray photoelectron spectroscopy.* 2nd Edition ed. Chichester, UK: John Wiley and Sons Ltd.; 1983.

[12] Hughes JDH. The carbon fibre/epoxy interface—A review. *Composites Science and Technology.* 1991; 41(1):13-45.

[13] Diefendorf RJ, Tokarsky E. High performance carbon fibers. *Polymer Engineering and Science.* 1975; 15(3):150-159.

[14] Dobb MG, Guo H, Johnson DJ. Image analysis of lattice imperfections in carbon fibres. *Carbon.* 1995; 33(8):1115-1120.

[15] Dilsiz N, Wightman JP. Suraface analysis of unsized and sized carbon fibers. *Carbon.* 1999; 37:1105-1114.

[16] Bismarck A, Kumru ME, Song B, Springer J, Moos E, Karger-Kocsis J. Study on surface and mechanical fiber characteristics and their effect on the adhesion properties to a polycarbonate matrix tuned by anodic carbon fiber oxidation. *Composites: Part A.* 1999; 30:1351-1366.

[17] Jin Z, Zhang Z, Meng L. Effects of ozone method treating carbon fibers on mechanical properties of carbon/carbon composites. *Materials Chemistry and Physics.* 2006; 97:167-172.

[18] Enomoto H, Yoshikawa T, inventors. *Method and apparatus for surface treatment of carbon fiber.* Japanese patent 3547824. 1996 28/07/2004.

[19] Chun B, Randall Davis C, He Q, Gustafson RR. Development of surface acidity during electrochemical treatment of pan-carbon fibers. *Carbon.* 1992; 30(2):177-187.

[20] Dusenbury JS, Cannon FS. Advanced oxidant reactivity pertaining to granular activated carbon beds for air pollution control. *Carbon.* 1996; 34(12):1577-1589.

4 Calorimetry

4.1 Overview

Immersion calorimetry was performed on carbon fibres of differing surface oxygen level using probes of decreasing polarity as described in Chapter 2. The fibres were characterized extensively in Chapter 3. Interactions between dilute resin components and carbon surfaces were also examined. Carbon black was used in the resin experiments as fibres, due to their very low surface areas (about 1 m^2/g), produced exotherms which were too small to allow statistically meaningful interpretation of the calorimetry data. Carbon black is characterized in this chapter using XPS, SEM, TEM and Raman, and the results of the immersion calorimetry experiments are presented. Immersion calorimetry of fibres in water showed a relationship between heat of immersion and fibre surface oxygen level. The rush-in effect was found to substantially affect the results. Differences in surface oxygen level, functional group make-up, and surface texture were found between the carbon black and fibres. Immersion of carbon black into dilute resin solutions was not successful, most likely due to concentration gradients in the solution.

4.2 Fibre Interactions with Polar Liquids

Fibre interactions with water, methanol, ethanol, isopropanol, and toluene were investigated using immersion calorimetry. Figure 4.1 shows an example exotherm recorded for untreated fibres immersed in water. A small endothermic region signifies the work put into breaking the glass ampoule. Ideally this energy would be small compared to the signal and would be of the same size in each experiment. This was not the case due to the small surface areas, and hence signal, involved and due to the manufacture of the ampoules. Figure 4.2 shows exotherms for carbon black and UV/O_3 treated fibres, plotted separately to the UST fibres for clarity. The UV/O_3 treated fibres were part of a long tow exposed to 4 hours of UV/O_3 as described in Chapter 3. The enthalpy of immersion was calculated by applying a linear background subtraction and integrating the heat flow.

Initial measurements were performed on two different weights of fibres, ~0.3 g and ~0.4 g, for three fibres with different surface oxygen levels. It was found that the measured enthalpy varied with the weight of the fibre used. The difference was found to be significant ($P < 0.05$, t-test). This is probably due to differences in the heat of vaporisation; more fibres means less liquid will vaporise. Thus the enthalpies cannot be considered absolute but instead must be considered relative to each other. Figure 4.3 shows the spread of enthalpies against weight calculated for 6B fibres immersed in water. Comparison of the two weights showed that the lighter sample produced more consistent enthalpies with lower 90% confidence intervals. Further experiments were performed using the lower mass.

The undulations of approximately ±0.01 mW in heat flow that appear at equilibrium in Figure 4.1 represent the limits of the temperature control of the instrument in the particular lab environment. The calorimeter needs a stable room temperature at least 5 K below its running temperature. The room temperature was controlled by an air-conditioning unit normally resulting in less than a 0.002 K variation in calorimeter temperature. For larger signals, e.g. the carbon black signal, the variance appears less pronounced purely due to scale. The undulations were present in immersion studies on empty ampoules so they are unlikely to be caused by the type of sample.
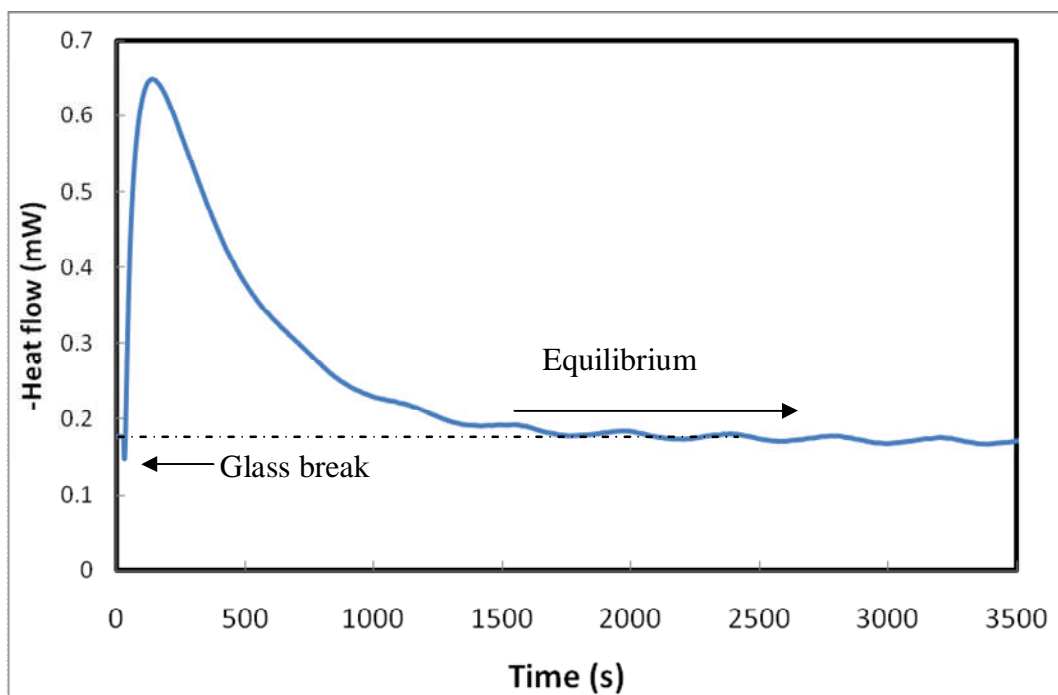
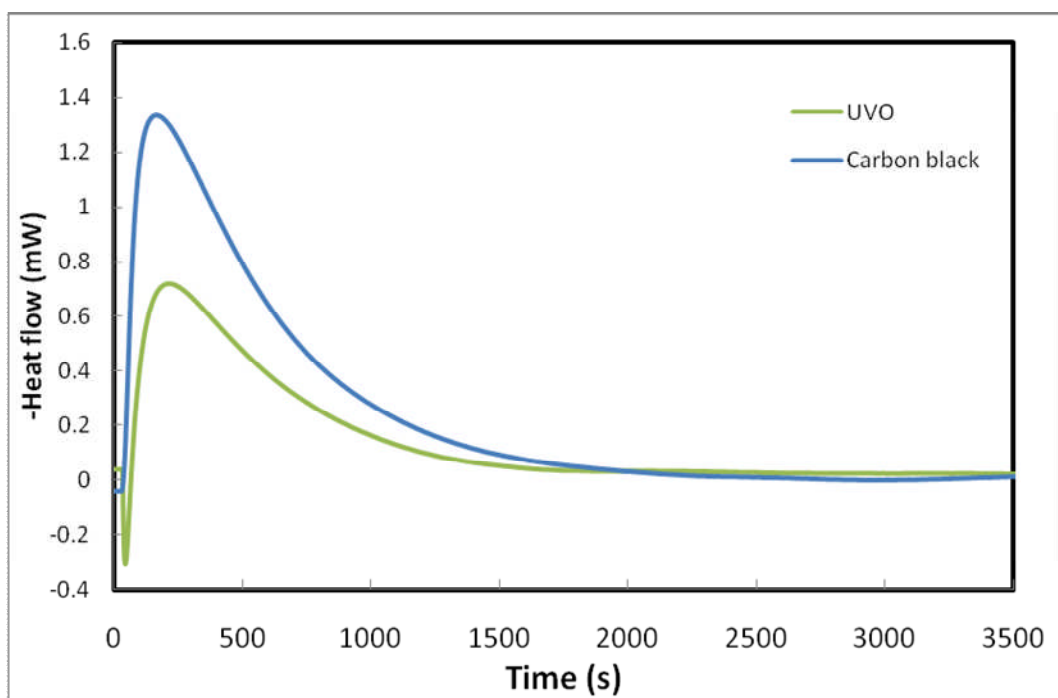**Figure 4.1 Example exotherm for UST fibres immersed in water.**

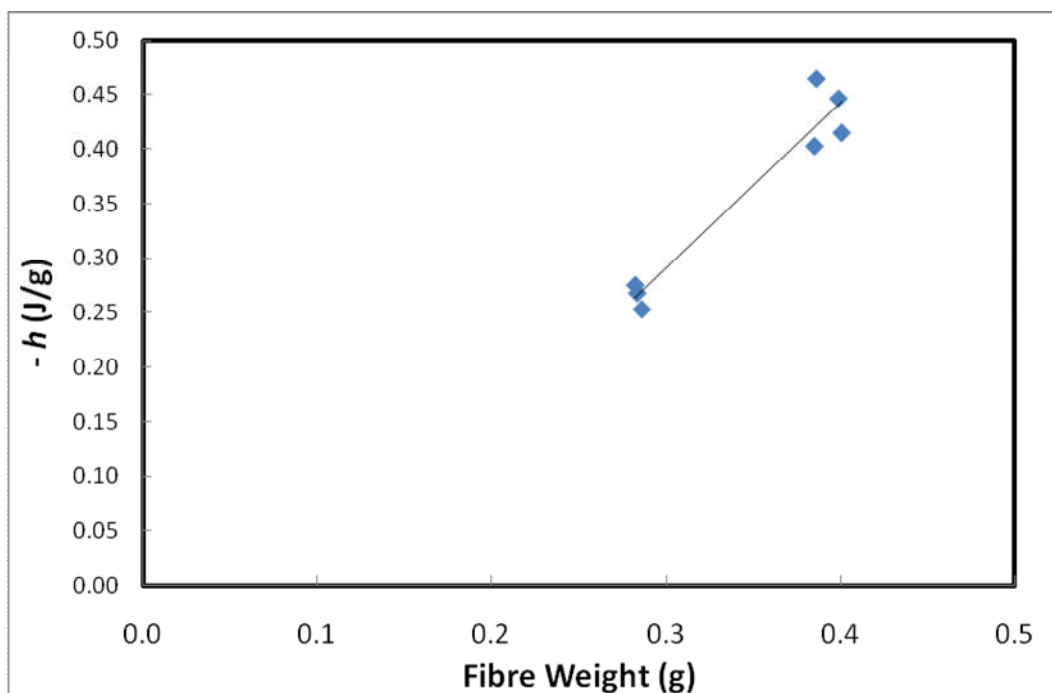**Figure 4.2 Example exotherms for UV/O$_3$ treated fibres and carbon black immersed in water.**

Figure 4.3 Enthalpy vs. weight of 6B fibres immersed in water.

During this investigation, the ampoules used were obtained from different sources. The first set of ampoules (type 1) had two turns in the end piece meaning they were very easy to break and when broken would leave a small tube for the liquid to be drawn through. The second set (type 2) were more simplistic and only had one turn meaning they were more difficult to break and a large opening was created on breaking for the liquid to enter. In order to get reproducible results when working with small signals, it is necessary to have consistent ampoules. Measurements were made for both sets of ampoule and are compared here.

The reproducibility of the measurements with methanol and ethanol was judged to be inadequate as considerable deviations occurred from one experiment to the other. On the contrary it was possible to obtain reproducible measurements for water, toluene and isopropanol. Figure 4.4 shows the heats of immersion per gram of fibre in water as a function of surface oxygen for the first set of ampoules. The series shown is that of a base treated one (i.e. UST, 3B, and 6B) as it gave the most consistent results.

Figure 4.5 shows the heats of immersion per gram of fibre in water, isopropanol, and toluene as a function of the surface oxygen for the second set of ampoules. The fibres used for that series were UST, 3B, 6B and the 4 hour UV/O$_3$ treated fibres. As can be seen, the values for the heats of immersion in water between the two sets of ampoules were significantly different for all the fibres. The first set of ampoules produced more consistent results with substantially lower confidence intervals, most likely due to the consistent manufacture of ampoules. The treated fibres show significantly different values to the untreated fibres. The second set of ampoules was less reliable with only the most treated UV/O$_3$ fibres being significantly different to the untreated fibres. While the absolute energy involved is different between the ampoules, the gradients of the trend lines are practically the same suggesting the trends are real.
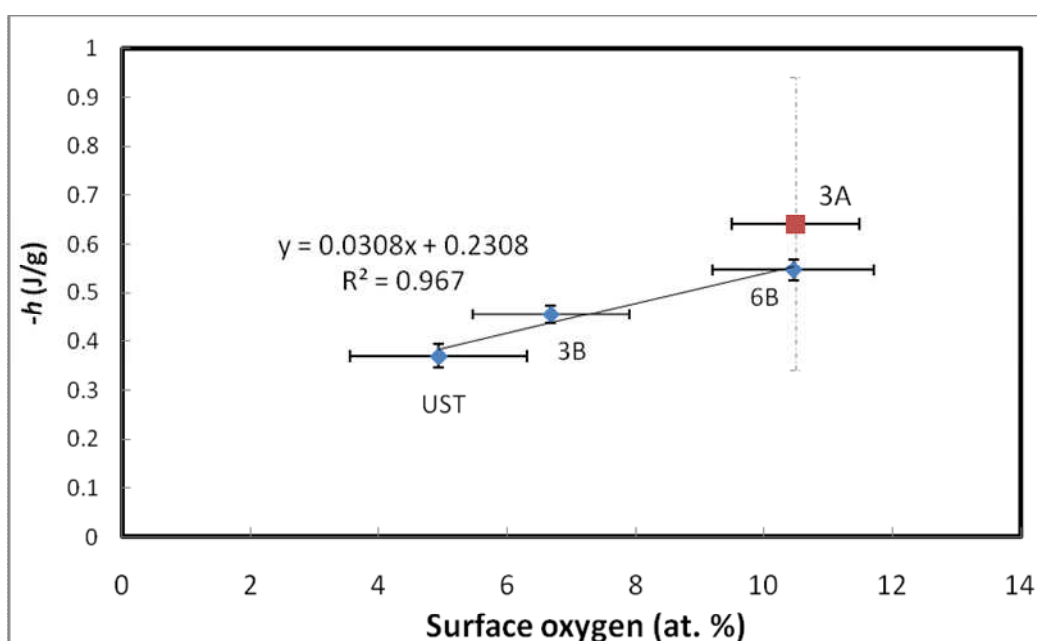

Figure 4.4 Heat of immersion for untreated, 3B, 6B, and 3A treated fibres in distilled water using type 1 ampoules.
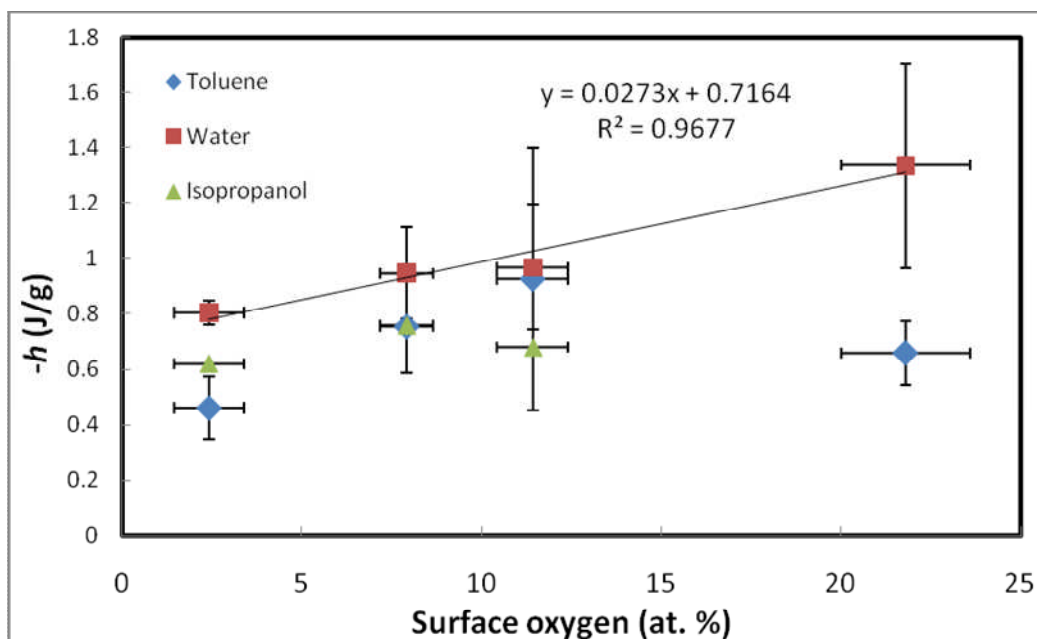
Figure 4.5 Heat of immersion for untreated, 3B, 6B, and UV/O₃ treated fibres in distilled water, toluene and isopropanol using type 2 ampoules. The purpose of this figure is to indicate the inadequacy of this set up to obtain a reliable trend.

Extrapolating from the trend lines, the non-specific interaction between an oxygen-free carbon surface and water gives a value of 230 mJ/g or 716 mJ/g for the first and the second set of ampoules respectively. Using the exact BET surface area of 0.85 m²/g, this would be equivalent to 270 mJ/m² and 842 mJ/m² respectively. Other workers have performed similar experiments on carbon blacks and found the non-dispersion interactions to be approximately 35 mJ/m² [1-3]. As already discussed, the measured enthalpy cannot be considered to be absolute. The signal for carbon fibres is small enough to be affected by noise, the heat of the ampoule breaking, the rush-in effect, and the heat of evaporation of the liquid in the cell and ampoule as the volume of liquid changes. In addition, the liquid will be interacting with the glass. Since the overall volume was not altered between sets of ampoules, the difference is likely to be caused by a change in the rush-in effect, and/ or the heat of the glass break.

The acid treated fibres show a slight difference in immersion enthalpy for water compared to the base treated fibres with the same level of oxygen. The overlap is within the error margins; however we can also take into account the functional

groups on the fibres. The function groups for these fibres have been outlined in Chapter 3.2.2. Plotting the immersion enthalpy against the percentage of each functional group present showed one clear linear relationship for carboxyl groups. Figure 4.6 shows this relationship. The higher enthalpy for the 3A treated fibres may well be real.
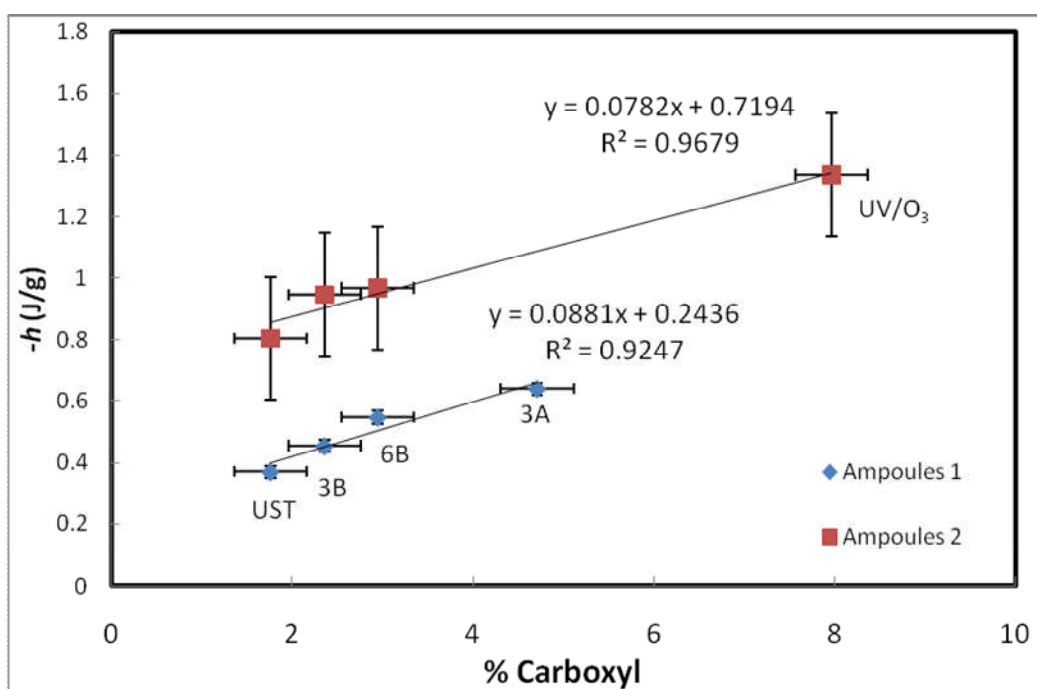

Figure 4.6 Heat of immersion for untreated, 3B, 6B, 3A and UV/O$_3$ treated fibres in distilled water as a function of the amount of carboxyl on the surface.

In an attempt to reconcile the current data with that in the literature, further investigations into the signal contributions were carried out. A set of empty type 2 ampoules of different sizes were degassed and sealed before being used for calorimetry in water. Due to the different sizes, different masses of water were drawn into the ampoules upon breaking. Figure 4.7 shows the energy released on immersion as a function of the mass of water.
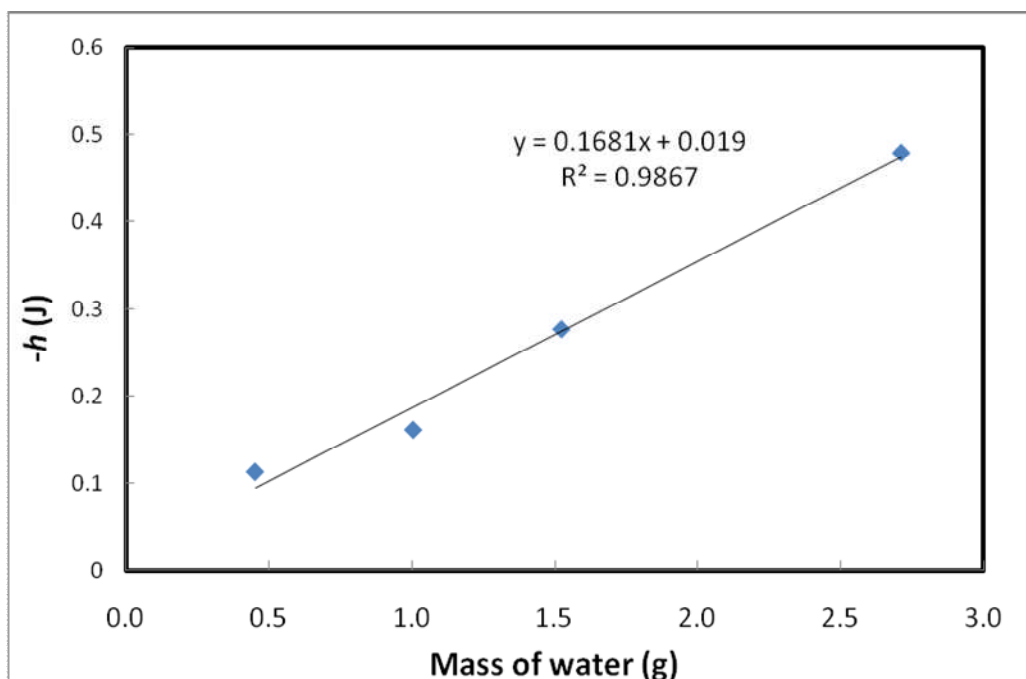
Figure 4.7 Energy of immersion for empty ampoules of different volumes in water.

The relationship between the heat released and the mass of water drawn in is clearly linear and the magnitude of the energy is high enough to interfere with the signal from the fibre interaction. If the volume of the ampoules varied during manufacture, the mass of water being draw in, and hence the energy involved would also vary thus adding to the experimental error. Ideally each ampoule could be measured following immersion and the mass of liquid calculated and accounted for. This was not always possible due to the nature of the break in the ampoule and due to evaporation effects. The few that could be measured showed masses of liquid between 1.1 and 1.4 g were involved. Figure 4.7 only looks at the mass of water involved; due to the set up of the experiment, it does not fully take into account the evaporation effects or the surface area of glass involved. Since the volume of the ampoules was altered to change the mass of water involved, the surface area of glass present and the volume available for evaporation will also have changed. Additionally, when fibres are involved the energy measured caused by the liquid rushing in will be affected. The fibres reduce the volume of space available to the water to evaporate into and provide frictional surfaces for the water to pass over. The overall system is complicated and would benefit from further investigation.

4.3 Carbon Black as a Model Surface

Initial experiments using dilute solutions of resin were performed with carbon fibres. Due to their low surface areas, the fibres produced exotherms which were too small to provide meaningful data. Carbon black was used as a model surface instead. Several characterisation techniques including XPS, SEM, and TEM were performed on the carbon black sample and the results are detailed below.

4.3.1 Elemental Composition and Functional Groups

Only carbon (98.1 %) and oxygen (1.9 %) were found on the carbon black sample using XPS. The oxygen level is lower than that of the untreated carbon fibres. Functional group analysis was performed on the carbon 1s peak using the same fitting techniques performed on the fibres. Table 4.1 shows the functional groups present on the carbon black and the untreated fibres for comparison.

Table 4.1 % of the carbon functional groups as determined by XPS C1s on carbon black (CB) compared to untreated fibres (UST)

Temperature (oC)	%	
	CB	UST
Graphite (~284.6 eV)	73.5	75.1
Alkoxide/ phenolic/ ether (285.8 eV)	11.6	14.1
Carbonyl/ quinine (287.2 eV)	4.5	4.1
Carboxyl/ ester (288.8 eV)	4.0	2.7
Carbonate/ adsorbed CO/CO2 (290.6 eV)	3.1	2.0
Plasmon (291.2 eV)	3.4	2.0
Ratio -COH to -COOH	2.9	5.2
Ratio total COx/graphite	0.32	0.30

The carbon black has a different functional group make up to the fibre. While having similar levels of carbonyl, it has substantially more double oxidations to single oxidations than the untreated fibre. The ratio of total oxidizations to graphite is similar however. From Figure 4.6, it was found that the level of carboxyl on the surface of the fibre played a significant role in the measured immersion enthalpies. The increased level of carboxyl on the carbon black compared to that of the fibres may result in a difference in the liquid-surface interaction. Ideally the carbon black would have a similar proportion of functional groups to the fibre, however since the carbon was not altered for this set of experiments but the probe liquids were, a difference in functional groups was considered acceptable.

4.3.2 Surface Structure

Carbon black N330, like the fibres used here, is non-porous. The manufacturers quote a surface area of 77 m^2/g and other BET studies using nitrogen have returned surface areas of 80 ($\pm$ 8) m^2/g [1]. The relatively large surface area means it is more suited for calorimetric measurements than the fibres.

The carbon black was examined by SEM. Figure 4.8 shows an extended view (magnification 140x) of the carbon black along with a carbon fibre for comparison. The fibres are obviously much smaller in size than the carbon black. Further magnification to 1000x in Figure 4.9 shows the carbon black has a rough and pitted surface with high levels of small debris across it unlike the fibre surface.

The FWHM of the carbon 1s peak in the XPS was 0.94 eV. The untreated fibres had a FWHM of 1.01 eV. Carbon black is probably more graphitic on the surface than the fibres. The plasmon level is also higher for the carbon black again suggesting a more structured surface.
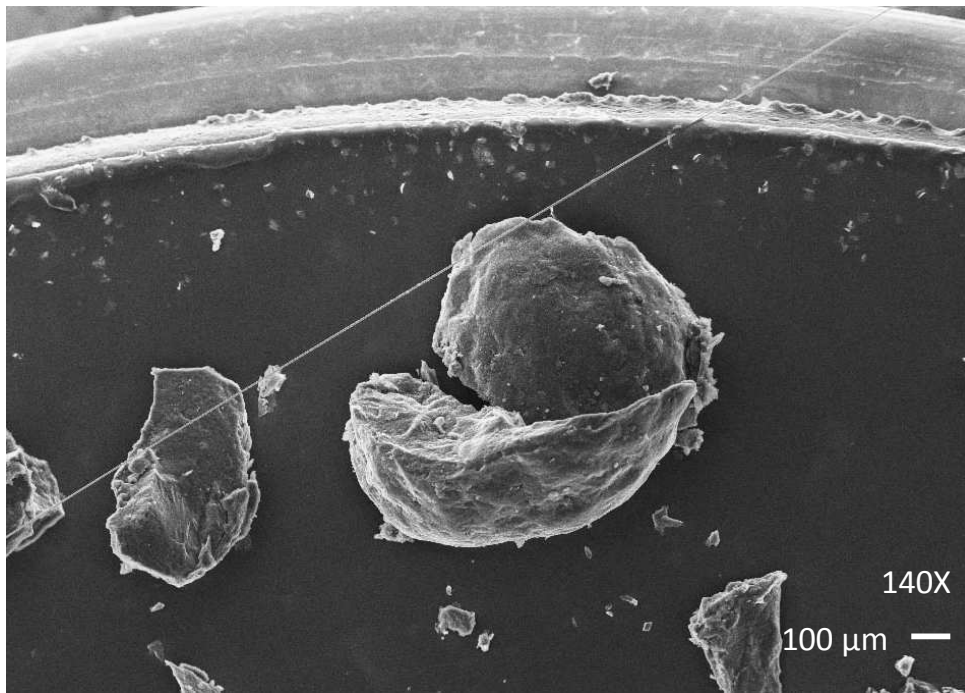
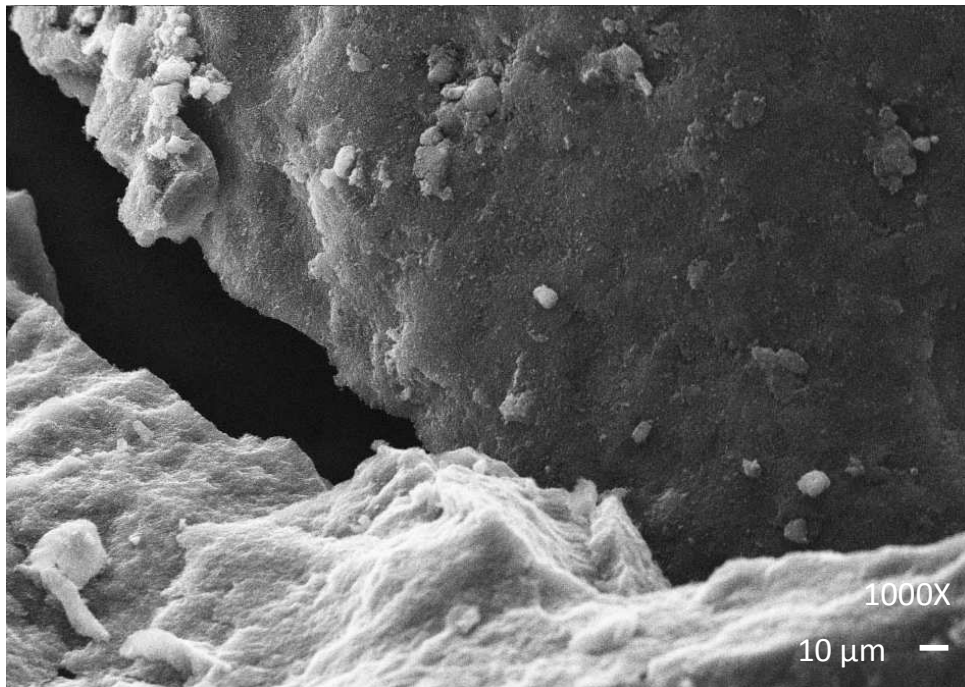**Figure 4.8 SEM image (140x magnification, 20kV) of carbon black and a single carbon fibre.**

Figure 4.9 SEM image (1000x magnification, 20kV) of carbon black.

The average I_D/I_D+I_G ratio for the fibres from laser Raman measurements was ~0.64. Carbon black gave a similar ratio of ~0.63. The XPS FWHM and the Raman suggest that while the first few layers of the carbon black surface may be more graphitic than the fibres, deeper into the sample they are alike.

4.3.3 Internal Structure

The carbon black was examined using TEM after grinding by pestle and mortar and dispersion in acetone. Figure 4.10 shows an example image and the associated diffraction pattern. Examining the layer patterns of the carbon black, the structure can be described best as a turbostratic columnar pile [4]. The average interlayer spacing (d_{002}) calculated from the diffraction patterns was 0.36 $\pm$ 0.04 nm. Practically the same as the fibres (~0.38 $\pm$ 0.02 nm).
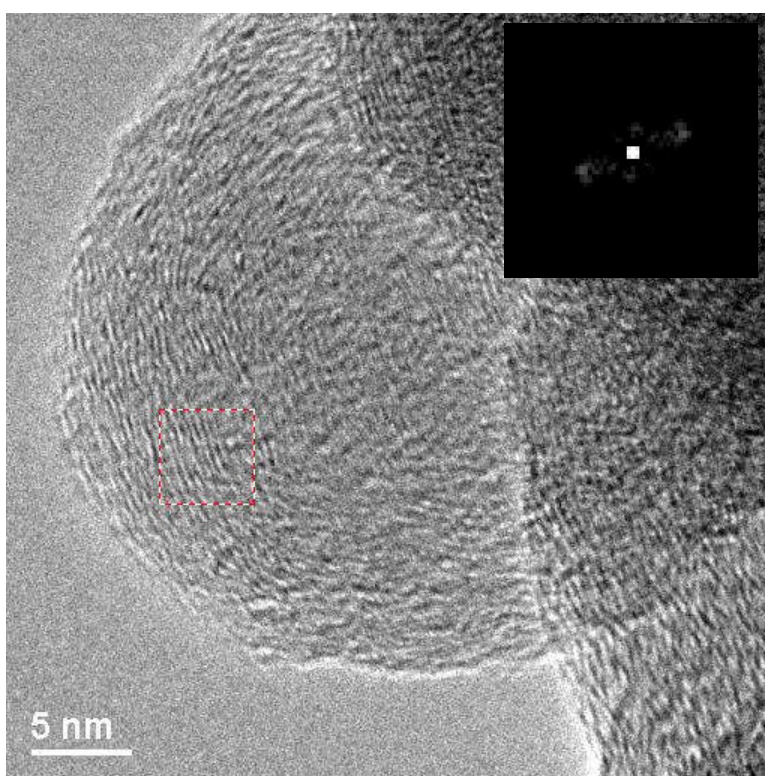

Figure 4.10 TEM image of carbon black prepared by dispersion, and (inset) associated diffraction pattern.

4.3.4 Discussion

Carbon black provides a substantial improvement in surface area compared to carbon fibres while still being non-porous. The level of surface oxygen is not as high as on the carbon fibres but there are more carboxyl groups present on the carbon black. Slight differences in functionality were not deemed important for the initial experiment. XPS suggests the carbon black is more graphitic than the carbon fibres while TEM and Raman revealed the internal structures have similar levels of order. The internal structure should not play a part in the calorimetry measurements as the interactions should be limited to the surface. Overall, there are differences between the carbon black and fibre surfaces but these can be ignored for the initial experiments. Ideally if further research is performed on this technique the model surface should be more similar.

4.4 Carbon Black Interactions with Resin Molecules

4.4.1 Solution Concentrations

The cross-sectional areas of the component molecules (a_m) for the resin were estimated using Equation 2.14 as described in Chapter 2.5.2. The number of molecules, and hence the weights of components, required to cover 0.2 g of carbon black in one monolayer were calculated using the BET area. Table 4.2 lists the results of the calculations for each resin component.

Table 4.2 Estimated cross-sectional areas for resin components and amount required for one monolayer coverage on 0.2g of carbon black

	a_m (10^{-19} m^2)	Number of molecules (10^{19})
MY	5.75	2.78
KM	54.2	0.30
PY	6.61	2.42
DDS	5.07	3.15

Initially, each resin component was dissolved in DCM, with the exception of the MY epoxy which was dissolved in acetone. A dilute form of the resin was produced by dissolving all the components in the same solution of DCM. The choice of solvent that can successfully dissolve all the components is limited. Problems arose with acetone and DCM in that they readily evaporate at room temperature so solution concentrations may change with time. Further experiments were performed with DMSO as the solvent since it has a higher boiling point. The experiments with DMSO were performed with the type 2 ampoules while the rest were performed with type 1.

4.4.2 Heats of Immersion

Table 4.3 lists the immersion enthalpies of carbon black in water and the pure solvents. The enthalpy of immersion in water (equivalent to -53 ± 2 mJ/m^2) is a magnitude of order larger than for the fibres. Acetone, DCM and DMSO all show higher levels of interaction with the carbon black than water. The liquids show similar levels of confidence intervals except for the DMSO which was substantially higher. This could be partly due to a difference in the ampoule used as discussed earlier.

Table 4.3 Immersion enthalpy for carbon black (error represents 90 % confidence intervals)

	$- h$ (J/g)
Water	4.3 ± 0.2
Acetone	7.3 ± 0.2
DCM	6.3 ± 0.2
DMSO	9.0 ± 1.4

Figure 4.11 shows the heats of immersion for different concentrations of the resin components in DCM and acetone solutions. Due to evaporation effects, most of these measurements were only performed once. Where measurements were repeated with the same concentration of solution, 90 % confidence intervals

were as high as ± 1.2 J/g. The increase in error associated with the measurements could be due to uncertainty in the solution concentration or concentration gradients near the carbon black surface. Since the errors involved are so large, it is not possible to determine any trends from this data other than a general decrease in the enthalpy as the concentration increases.
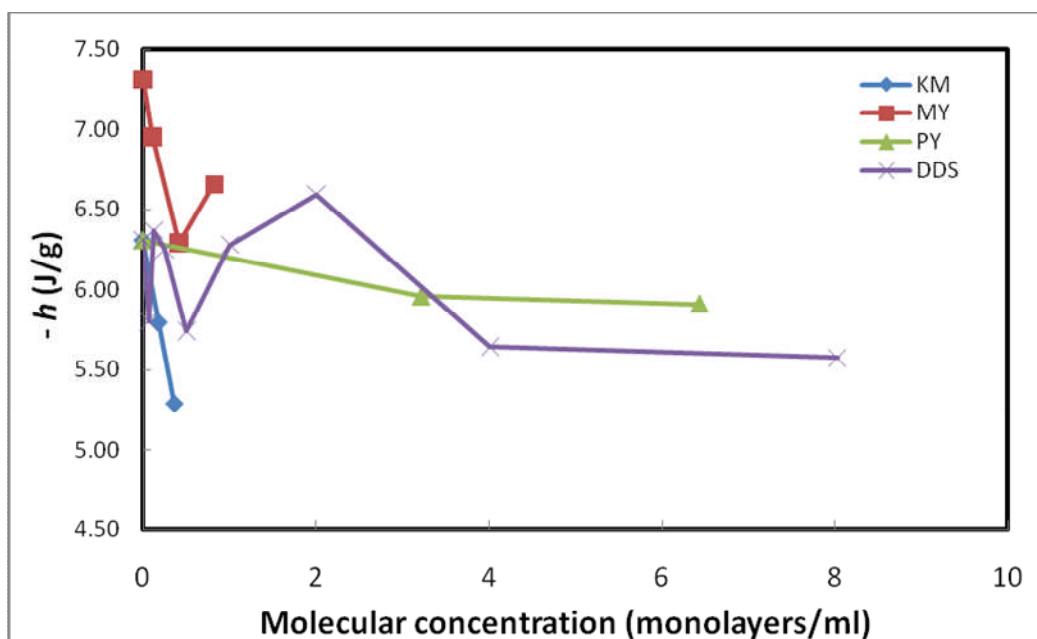

Figure 4.11 Heats of immersion for carbon black in DCM solutions of the resin components.

Figure 4.12 shows the heats of immersion for different concentrations (referenced to the MY molecule) of the dilute resin in DCM. Again errors were higher than measurements with the pure liquid (± 0.8 J/g) and it is difficult to determine a trend. Measurements with DMSO as the solvent did not improve the results. Figure 4.13 shows the heats of immersion for different concentrations of the MY epoxy and the DDS curing agent in DMSO. The errors involved for the DDS averaged ± 1 J/g while for the MY they averaged ± 2.5 J/g. Further work was not carried out using this method as it is likely that concentration gradients are too influential and the technique itself may not be sensitive enough.
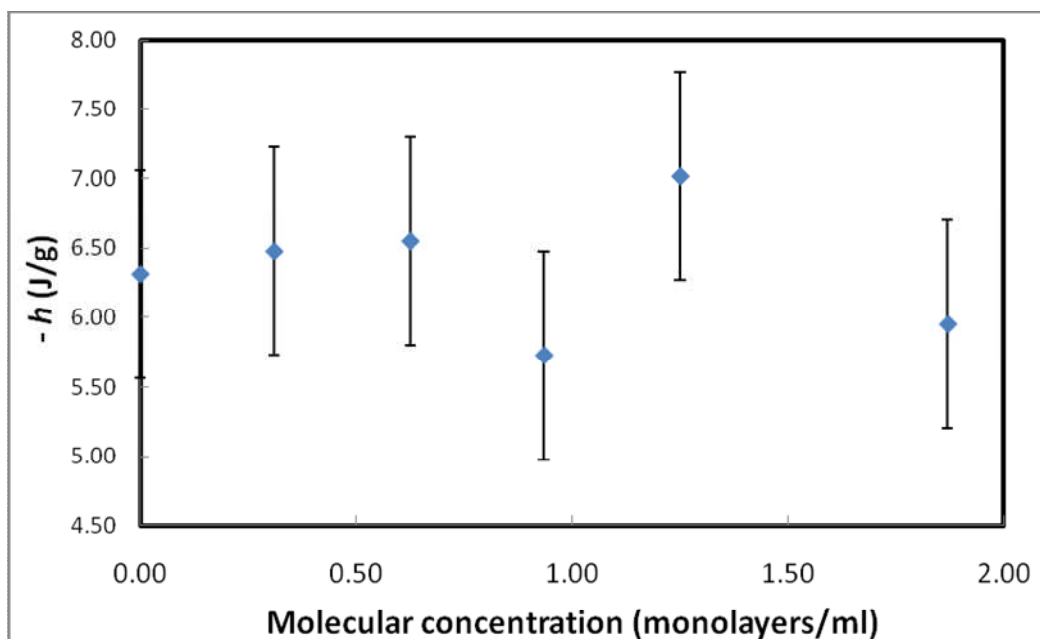
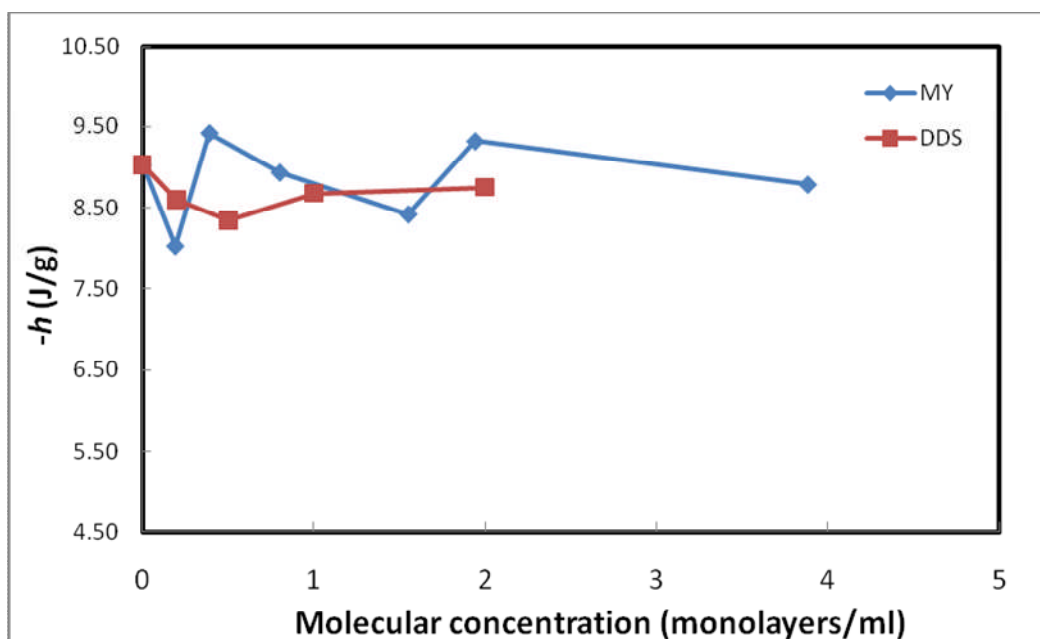**Figure 4.12 Heats of immersion for carbon black in DCM solutions of the resin.**

Figure 4.13 Heats of immersion for carbon black in DMSO solutions of the resin components.

4.5 Discussion

As discussed in Chapter 1, immersion calorimetry has been applied to many different carbon surfaces including activated carbon fibres [5] but never to fibres with surface areas as small as these. Previous research by several different authors using immersion calorimetry found the non-dispersion interactions on oxygen free carbon surfaces to be approximately 35 mJ/m^2 [1-3,6,7]. The surfaces investigated included various carbon blacks, and graphite. While difficult to perform, measurements of the surface energy of carbon fibres using contact angle analysis have been undertaken in the literature. For example Ho *et al.,* measured the contact angles of water on PAN fibres using the modified Wilhelmy technique [8]. The fibres had a N_2 BET surface area of 0.22 m^2/g and 18% surface oxygen. They found the dispersion contribution to the surface energy was 38.6 ± 1.7 mJ/m^2; the overall surface energy being 49.8 ± 2.8 mJ/m^2 [8]. Bradley *et al.,* also used the Wilhelmy technique on PAN fibres with oxygen levels between 3 and 9 % [9]. The dispersion contribution ranged between 48.2 and 50.8 mJ/m^2 [9]. The contact angle determined values of the dispersion contribution are close to the calorimetric determined values; reinforcing the argument that the immersion enthalpies measured in this investigation on fibres cannot be absolute.

Due to the surface areas involved with fibres, the calorimetry signal is heavily influenced by experimental factors. The calorimeter has a resolution of 10 µW. For the water interaction on an untreated fibre, approximately 0.14 Joules were measured in 1500 seconds giving an average heat flow of 93 µW which is very close to the limits of detection. As discussed earlier in addition to the heat of interaction between the sample and the liquid, the calorimeter signal also includes the rush-in effect, the heat of breaking the ampoule, and the heat of vaporisation of the immersion liquid [10,11].

Previous researchers have investigated the effect of the ampoule break. Morimoto and Kiriki filled ampoules with different pressures of nitrogen, and nitrogen saturated with water [10]. They also filled ampoules with different

masses of water. The heats of immersion for breaking the ampoules in water were then recorded. It was found that the ampoules that were filled with only nitrogen produced lower heats than the ampoules with water saturated nitrogen. The difference of 0.21 J was attributed to the endothermic heat of vaporisation of the water. Extrapolating from the graph of water mass vs. heat of immersion, the heat of breaking was found to be – 0.28 J. By subtracting these values from the total heat for an empty ampoule, - 0.53 J, the rush-in effect was calculated to be - 0.46 J which was higher than theoretically expected. They concluded that the rush-in effect must also include dynamic interactions such as collisions between molecules in the immersion liquid as well as collisions with the walls of the ampoule and friction effects [10].

In Figure 4.7, the mass of water was plotted against the heat of immersion and a straight-line relationship was found. The slope of the line is proportional to the vaporisation energy and the rush-in effect, and the intercept represents the average heat of breaking [10,11]. From Figure 4.7, the average heat of breaking for the type 2 ampoules was -0.019 J, substantially lower than in reference [10]. However, it is recommended that the heat of the ampoule breaking is less than -5 mJ [11]. The large heat of breaking will add significantly to the final signal. From Morimoto and Kiriki's work, it is evident that the rush-in effect is the largest factor affecting the heat measured [10]. The rush in effect and the endothermic vaporisation energy increase with increasing ampoule size. Since the trends of immersion enthalpy with oxygen in Figure 4.4 and Figure 4.5 overestimate the level of non-specific interaction on an oxygen free carbon surface, it is likely the rush-in effect plays the most significant role in these measurements as well.

In the calorimetric work by Bradley $et\ al.,$ Equation 4.1 was found to describe the heat of carbon black immersion in water ($-\Delta H(H_2O)$, in mJ/m^2), where $[O]_T$ is the XPS measured surface oxygen concentration (at. %) [3].

Equation 4.1

$$-\Delta H(H_2O) = 14[O]_T + 35$$

In the case of untreated carbon fibres (O = 2.42%), the enthalpy of immersion would be 68.9 mJ/m^2 or 0.08 J/g, a magnitude smaller than what was measured. For a fibre sample weighing ~0.3 g, this would result in a measured heat of – 0.02 J, the same magnitude as the average heat released on the glass break. The first set of ampoules showed significant differences between fibres with different oxygen levels in water and the trend was reproduced using the second type of ampoules. It is likely that the trends are real.

Calorimetry work by Rodríguez-Reinoso *et al.*, showed a linear relationship existed between the amount of CO desorbed from the surface of activated carbons (measured by TPD) and the heat of immersion in water [12]. Detailed functional group analysis was not performed but the CO groups were attributed to anhydrides, phenol groups and quinones. Surfaces that desorbed more CO, i.e. had more anhydrides etc. present, showed greater heats of immersion. The relationship between the heat of immersion and the desorbed CO_2, attributed to carboxyl groups, showed a steep increase followed by levelling off; i.e. surfaces with high levels of carboxyl groups showed similar immersion enthalpies [12]. The work in reference [12] also showed that the enthalpy of immersion in water was not affected by porosity. Further investigation into the porosity and surface area of the UV/O$_3$ treated fibres would be useful in the future.

Calorimetry using solutions of resin and resin components was not successful. Denoyel *et al.*, noted that pure liquids must be used for calorimetry in order to avoid concentration gradients unless stirring can be achieved [11]. The success of an adsorption process from solution can also be determined by measuring the net concentration of the solute left after interaction [11]. The resin components could not be used in calorimetry in their pure form due to either their natural state being unsuitable (e.g. powder) or the viscosity being too high. Another investigation on PAN fibres reported in the literature used inverse gas

chromatography to investigate interactions between fibres, and polar and non-polar liquids [13]. The dispersive surface energy component for fibres examined with long chain hydrocarbons, such as hexane and heptane, varied between 74 and 80 mJ/m^2 [13] which is similar to calorimeter determined values for toluene on carbon black [1]. Water was not used as a polar probe but acetone, ethyl acetate, methyl glycidyl ether and butyl oxirane were used as resin analogues [13]. Methyl glycidyl ether has low viscosity [14] and could be used in calorimetry measurements on fibres if reproducibility can be improved.

4.6   Conclusions

Immersion calorimetry using water, toluene, and isopropanol has been used to characterise electrochemically treated and UV/O$_3$ treated fibres. Measurements with water showed increasing heats of immersion with increasing surface oxygen content while the non-polar toluene probe was unaffected. The signals were found to be largely influenced by the rush-in effect and heat of ampoule breaking. Due to the small heats involved, it was not possible to get absolute values for the dispersion and polar components. Carbon black was examined as a model surface for the fibres using XPS, TEM, SEM and Raman. Differences in elemental composition and level of graphitization were found. The carbon black was still used as a model surface to examine whether calorimetry could be used to investigate carbon surfaces with dilute solutions of resin, as only proof of concept was required. Large variations in signal were found when dilute solutions of resin and resin components were used as probe liquids. This was attributed to concentration gradients in the solution.

Calorimetry using pure probe liquids of differing polarity or resin analogues could be useful for carbon fibres if issues of reproducibility can be resolved. This could involve a combination of improvements such as: increasing the sensitivity of the calorimeter, increasing the mass of fibres used, decreasing the mechanical energy released during ampoule break, and increasing the reproducibility of ampoule manufacture.

165

4.7 References

[1] Andreu A, Stoeckli HF, Bradley RH. Specific and non-specific interactions on non-porous carbon black surfaces. *Carbon.* 2007; 45:1854-1864.

[2] Sheng E, Sutherland I, Bradley RH, Freakley PK. Heat of immersion calorimetry studies of carbon blacks. *Materials Chemistry and Physics.* 1997; 50(1):25-30.

[3] Bradley RH, Daley R, Le Goff F. Polar and dispersion interactions at carbon surfaces: further development of the XPS-based model. *Carbon.* 2002; 40(8):1173-1179.

[4] Bourrat X. Structure in Carbons and Carbon Artefacts. In: Marsh H, Rodríguez-Reinoso F, editors. *Sciences of carbon materials.* Alicante: Universidad de Alicante; 2000: 1-97.

[5] Stoeckli F, Centeno TA, Fuertes AB, Muniz J. Porous structure of polyarylamide-based activated carbon fibres. *Carbon.* 1996; 34(10):1201-1206.

[6] Stoeckli F, Lavanchy A. The adsorption of water by active carbons, in relation to their chemical and structural properties. *Carbon.* 2000; 38:475-494.

[7] López-Ramón MV, Stoeckli F, Moreno-Castilla C, Carrasco-Marín F. Specific and non-specific interactions of water molecules with carbon surfaces from immersion calorimetry. *Carbon.* 2000; 38(6):825-829.

[8] Ho KKC, Lamoriniere S, Kalinka G, Schulz E, Bismarck A. Interfacial behavior between atmospheric-plasma-fluorinated carbon fibers and poly(vinylidene fluoride). *Journal of Colloid and Interface Science.* 2007; 313(2):476-484.

[9] Bradley RH, Ling X, Sutherland I. An investigation of carbon fibre surface chemistry and reactivity based on XPS and surface free energy. *Carbon.* 1993; 31(7):1115-1120.

[10] Morimoto T, Kiriki M. Analysis of the heat of breaking glass ampoules. *Bulletin of the Chemical Society of Japan.* 1980; 53(12):3701-3702.

[11] Denoyel R, Rouquerol F, Rouquerol J. Porous texture and surface characterization from liquid-solid interactions: immersion calorimetry and

adsorption from solution. In: Bottani EJ, Tascón JMD, editors. *Adsorption by Carbons.* Amsterdam: Elsevier; 2008: 273-300.

[12] Rodrí-guez-Reinoso F, Molina-Sabio M, González MT. Effect of oxygen surface groups on the immersion enthalpy of activated carbons in liquids of different polarity. *Langmuir.* 1997; 13(8):2354-2358.

[13] Lindsay B, Abel M, Watts JF. A study of electrochemically treated PAN based carbon fibres by IGC and XPS. *Carbon.* 2007; 45(12):2433-2444.

[14] Kushida H. Methyl glycidyl ether as an auxiliary to infiltration for embedding with epoxy resins. *Journal of Electron Microscopy.* 1976; 25(2):115.

5 Temperature Programmed Desorption

5.1 Overview

The adsorption properties of untreated and treated carbon fibres were investigated using TPD as described in Chapter 2. Probes of decreasing polarity were used with electrochemically treated fibres of differing surface oxygen level. Fibres treated with UV/O_3 for 4 hours were also examined. TPD spectra were acquired of several mass fragments after fibres were dosed with an alcohol. Qualitative analysis on the spectra shape as well as quantitative analysis of peak area was performed and the amount of alcohol desorbed was correlated to surface oxygen level. Alcohol desorption from the fibre surface appears to be second order in nature indicating a re-combinative desorption type. The surface uptake as determined from alcohol-desorption was found to increase with the level of oxygen on the surface of the fibres giving further evidence for a dissociative adsorption. Electrochemically treated fibres (3B) were heat treated up to 1073 K (800 ^{o}C) and further adsorption studies using methanol and propan-1-ol were performed. XPS was used to examine the effect of the heat treatment on the surface groups. Heating to 1073 K reduced the overall level of surface oxygen as evidenced by the change in the carbon functional groups. The level of alcohol adsorption was also shown to decrease with increasing heat treatment; i.e. with decreasing surface oxygen.

5.2 Interactions with Alcohols

All fibres were heated to 423 K (150 ^{o}C) under vacuum to remove reversibly adsorbed water and other weakly adsorbed contaminants, unless otherwise indicated. Upon cooling to room temperature the base pressure in the system was typically 4 x10^{-5} Pa. Fibres were dosed with 1 μL of the alcohol and allowed 15 minutes for equilibrium before any excess and weakly bound alcohol was pumped out. The fibres were degassed until the pressure reached approximately the pre-dosing level. The time for degassing varied between 30 minutes and 2 hours depending on the alcohol. Butan-1-ol took the longest time to degas

following dosing. Table 5.1 presents the number of moles in 1 μl of liquid for the series of alcohols used. Because the surface area of the carbon fibre is about 1 m^2/g and a densely packed carbon hexagonal structure with 0.25 nm carbon to carbon distance contains about 5×10^{18} sites/g (one site is taken as half the total number of surface carbon sites because the van der Waals radius of the adsorbed alcohol is larger than the 0.25 nm distance), the number of alcohol molecules used is enough for surface saturation. In other words the analysis of the results will assume that surface coverage is not affected by the amount of molecules exposed prior to TPD.

Table 5.1 Molecules of probe in 1 μl of liquid and computed radius

Liquid	kg/m^3	g/mL	MW	g (x 10^{-4})	moles	molecules	Radius (nm)*
Methanol	786.5	0.787	32	7.87	2.46×10^{-5}	1.5×10^{19}	0.22
Ethanol	785.1	0.785	46	7.85	1.71×10^{-5}	1.0×10^{19}	0.26
n-Propanol	800.0	0.800	60	8.00	1.33×10^{-5}	8.0×10^{18}	0.29
n-Butanol	809.7	0.810	74	8.10	1.09×10^{-5}	6.6×10^{18}	0.31

* Computed radius of alcohol molecules using B3LYP Density Functional Theoy (DFT) with 631+G* basis set as implemented by the Spartan 08 code.

All fibres dosed with an alcohol, showed desorption spectra similar to that shown in Figure 5.1. The spectra show two desorption domains. The first domain found at about 450 K consists of masses related to the alcohol (with the parent ion mass of m/z 31 $-CH_2OH^+$) as well as its reaction products. The second desorption above 600 K consists mainly of decomposition products of the functional groups present on the fibre (water (m/z 18), carbon monoxide (m/z 28), and carbon dioxide (m/z 44)). Blank desorption spectra of fibres (i.e. where there was no alcohol dosing) did not show the first desorption domain. We will focus on the first peak for m/z 31 as it is the most representative of the alcohol-fibre interaction since it is composed exclusively of products resulting from the alcohol desorption/reaction and not from the decomposition of the function groups on the fibre surface. When peak areas are discussed they will refer to peaks in the 450 K region.
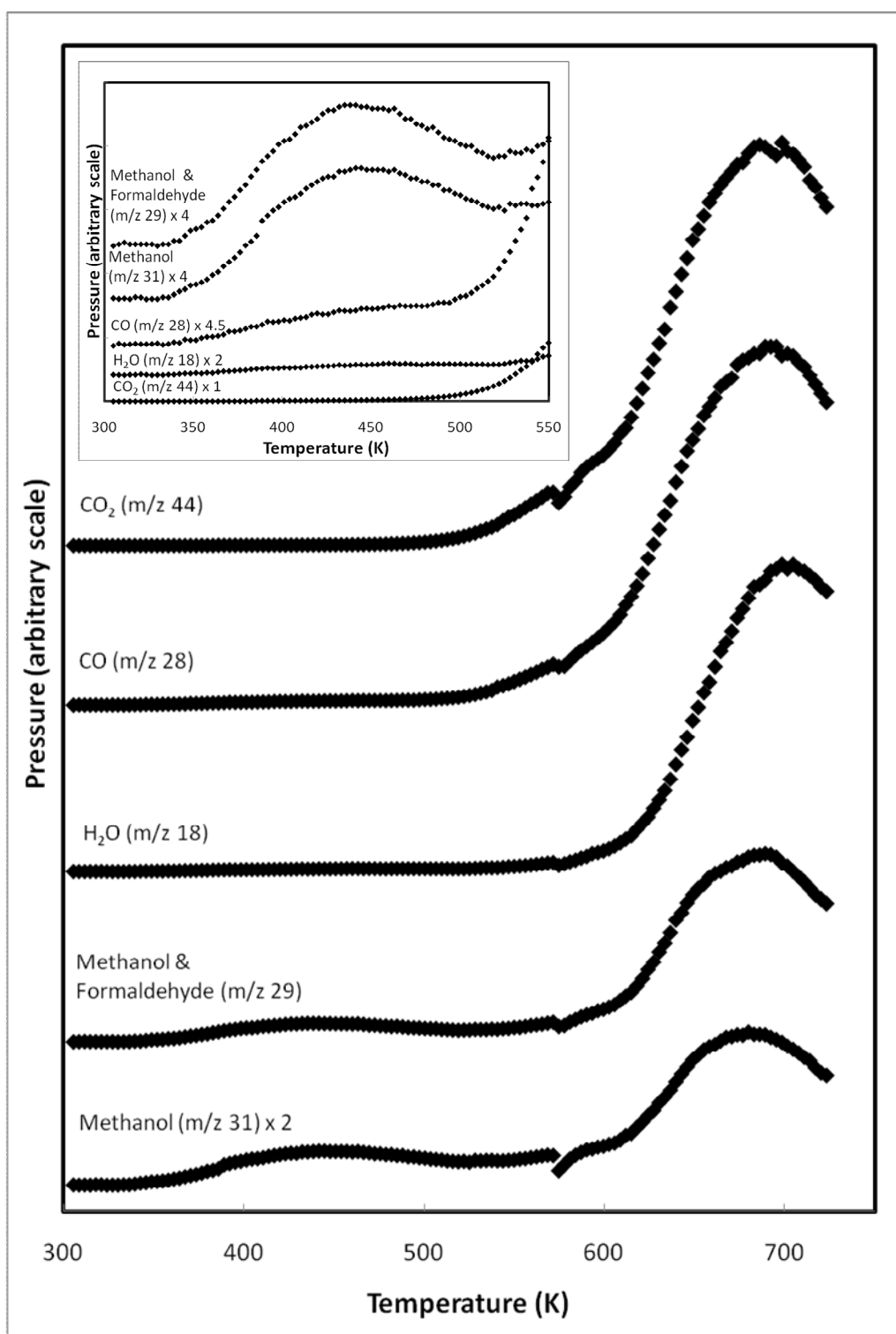
Figure 5.1 TPD for methanol on 6B fibres showing selected m/z. Inset: expanded lower temperature region.

Figure 5.1 presents the main desorption products of methanol on the 6B fibre. It can be seen that methanol desorbs in the two domains as described earlier. The first is composed of methanol and formaldehyde (see below for more details)

while the second one contains, in addition, the decomposition products. In order to understand the reaction, quantitative analysis of masses was conducted. Peak areas were calculated for several mass fragments and the percentage desorbed with respect to m/z 31 was calculated and compared against those of pure molecular desorption. It should be noted that errors due to changes in base pressures between experiments and peak integrations are typically 10 to 15%. Table 5.2 shows the results of this calculation for m/z 29 for a selection of the fibres. M/z 29 is the main fragment of aldehydes (-CHO) that can be formed by dehydrogenation of the linear alcohol. It can be noted that for methanol, ethanol and propan-1-ol a greater level of desorption of m/z 29 than that provided from the alcohol occurs. Methanol shows the greatest deviation at over twice the percentage expected. Butan-1-ol shows the least deviation, with levels being approximately equal to those of the parent alcohol.

Table 5.2 Mass fragment yield (%) of m/z 29 with respect to m/z 31

	Methanol	Ethanol	Propan-1-ol	Butan-1-ol
UST	96	40	23	31
3B	121	49	28	33
6B	110	56	31	38
UV/O_3	109	46	23	21
Theoretical	**45**	**30**	**18**	**39**
Deviation for 6B	**65**	**26**	**13**	**-1**
Ratio*	**2.4**	**1.5**	**1.8**	**0.5**

*Ratio of % measured to % expected m/z 29 for UV/O_3 treated fibres.

In the case of methanol, formaldehyde is the corresponding aldehyde the structure of which is shown in Figure 5.2. A likely formation mechanism of formaldehyde from methanol (CH_3OH) on an oxidized carbon surface is presented in Equation 5.1, where V_O is an oxygen vacancy, the subscript s represents surface molecules or atoms and the subscript a represents adsorbed

molecules or atoms. Such a mechanism is described as oxidative dehydrogenation [1]. Equation 5.2 shows the mechanism of oxidative dehydrogenation for ethanol; similar reactions would occur for the higher alcohols to a lesser extent.
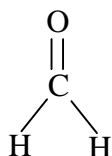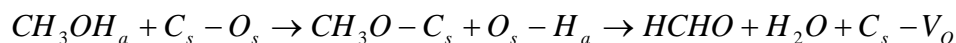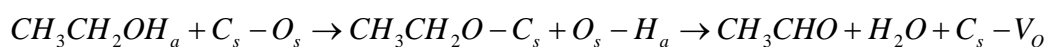
$$\begin{array}{c} O \\ \| \\ C \\ \diagup \quad \diagdown \\ H \qquad H \end{array}$$

Figure 5.2 Formaldehyde.

Equation 5.1

$$CH_3OH_a + C_s - O_s \rightarrow CH_3O - C_s + O_s - H_a \rightarrow HCHO + H_2O + C_s - V_O$$

Equation 5.2

$$CH_3CH_2OH_a + C_s - O_s \rightarrow CH_3CH_2O - C_s + O_s - H_a \rightarrow CH_3CHO + H_2O + C_s - V_O$$
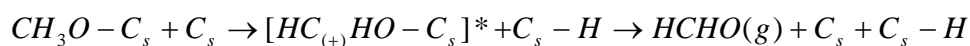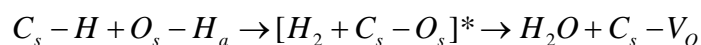
Methanol showed the greatest degree of aldehyde production. The ratio of measured to expected aldehydes (acetaldehyde from ethanol, propionaldehyde from propanol and butyraldehyde from butanol) decreased with increasing number of carbons in the chain. The driving force for this reaction is the removal of one hydrogen atom and two electrons in the alpha position from the functional group. This hydrogen atom, removed as hydride, will react with the hydroxyl making H_2 that may, in a transition state, react with surface oxygen to give H_2O and leave the two electrons in the lattice to complete the reduction process as described by Equation 5.3 and Equation 5.4, where the [ ]* indicates a reaction intermediate.

Equation 5.3

$$CH_3O - C_s + C_s \rightarrow [HC_{(+)}HO - C_s]^* + C_s - H \rightarrow HCHO(g) + C_s + C_s - H$$

Equation 5.4

$$C_s - H + O_s - H_a \rightarrow [H_2 + C_s - O_s]^* \rightarrow H_2O + C_s - V_O$$

In the case of methanol all the three hydrogen atoms are equivalent, while in the case of ethanol one of them is replaced by -CH$_3$ that in addition to its steric effect will have an inductive effect. As the number of carbons in the molecule increases, i.e. as the structure and charge changes, the probability of dehydrogenation occurring will also change. Figure 5.3 shows this trend for the UV/O$_3$ treated fibres. It is clear that increasing the chain, decreases the dehydrogenation reaction. The other reaction that may also occur is a dehydration reaction to make an olefin, except in the case of methanol where the dehydration reaction may only occur via a bi-molecular interaction to make dimethyl ether. Equation 5.5 shows the dehydration reaction for ethanol. To monitor this reaction m/z 27 is the main pattern (CH=CH$_2$), see Equation 5.5. Table 5.3 lists the expected quantity of m/z 27 compared to m/z 31 (%) and the percentage actually measured.
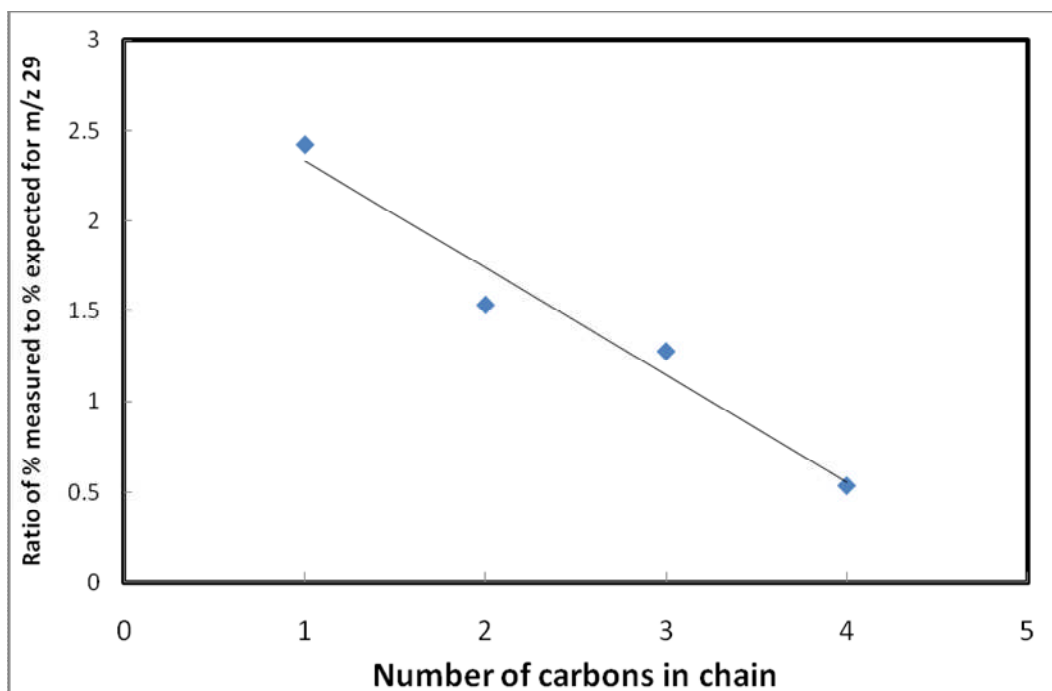

Figure 5.3 Ratio of % measured to % expected m/z 29 with carbon chain length for UV/O$_3$ treated fibres.

Equation 5.5

$$\left[C_2H_5OH\right]_a + C_s - O_s \rightarrow \left[C_2H_5O\right]_a C_s + O_s - H_a \rightarrow C_2H_4 + H_2O + C_s$$

Table 5.3 Mass fragment yield (%) of m/z 27 with respect to m/z 31

	Ethanol	Propan-1-ol	Butan-1-ol
UST	21	24	44
3B	21	29	47
6B	-*	30	49
UV/O$_3$	19	13	21
Theoretical	**22**	**16**	**57**

*Due to errors during data acquisition the peak area of m/z 27 could not be computed with accuracy.

The percentages listed in Table 5.3 do not deviate, within experimental errors, from those for the parent molecule suggesting that the dehydration reaction is unfavoured compared to the dehydrogenation reaction.

Figure 5.4, Figure 5.5, and Figure 5.6 show the TPD spectra of m/z 31 for the alcohol series on untreated fibres, 6B fibres, and fibres treated to 4 hours of UV/O$_3$. The order of desorption can be inferred from the TPD curves. All the TPD curves acquired generally showed similar shapes; broadly symmetric curves with a bias towards higher temperatures. The desorption is likely to be second order; i.e. recombinative desorption. In other words, dissociative adsorption occurs at room temperature as generalised in Equation 5.6.

Equation 5.6

$$ROH(g) + \mathbf{O_s\text{-}C_s} \rightarrow RO\text{-}C_s + \mathbf{O_s\text{-}H} \text{ at 300K}$$

Upon heating, energy is given to the adsorbate providing the activation energy needed for the association of H, from **O$_s$-H**, to the alkoxide. Because the

molecular adsorption would be largely unstable it desorbs upon formation. The tail at high temperature is due to stronger interactions occurring with the surface at lower coverages. This is because at high coverage, lateral interactions between adjacent molecules may result in slight destabilisation due to repulsive interactions taking place.

5.3 Quantitative Analysis of the Series of Linear Alcohols on the Series of Carbon Fibres

Figure 5.4 shows the m/z 31 TPD spectra for the series of alcohols desorbing from the untreated carbon fibre surface. Figure 5.5 and Figure 5.6 show the same results for the 6B and UV/O$_3$ treated fibres. The UST fibres show very low levels of m/z 31 desorption for methanol and ethanol compared to the 6B and UV/O$_3$ treated fibres. As can be seen for the UST and 6B fibres, the intensity of the m/z 31 peak for butan-1-ol is greater than the intensity of the other alcohols. For the UV/O$_3$ treated fibres, propan-1-ol shows the largest peak in the raw data. The general trend is for larger peaks to occur as the carbon chain in the alcohol increases.

In the case of the 6B fibres in Figure 5.5, the second desorption domain is very noticeable. The desorption of m/z 31 is concomitant with other masses resulting from further reactions and decomposition of surface functional groups. While it is beyond the scope of this study to understand these high temperature reactions some additional information will be provided in Section 5.6
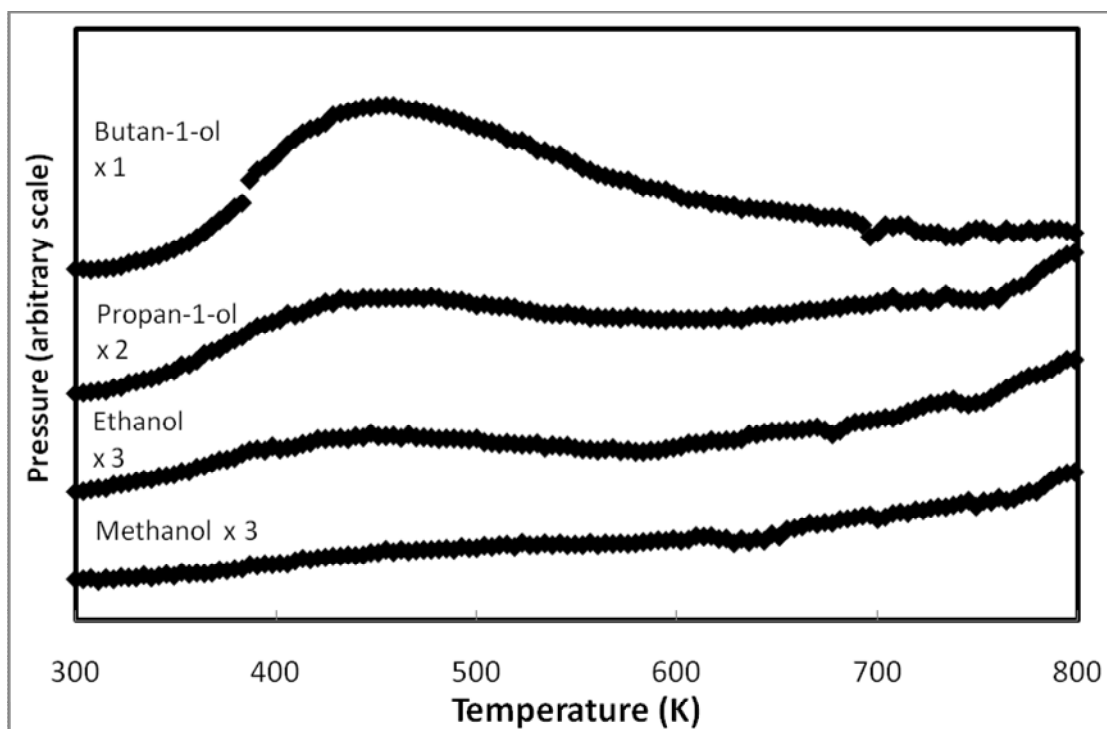
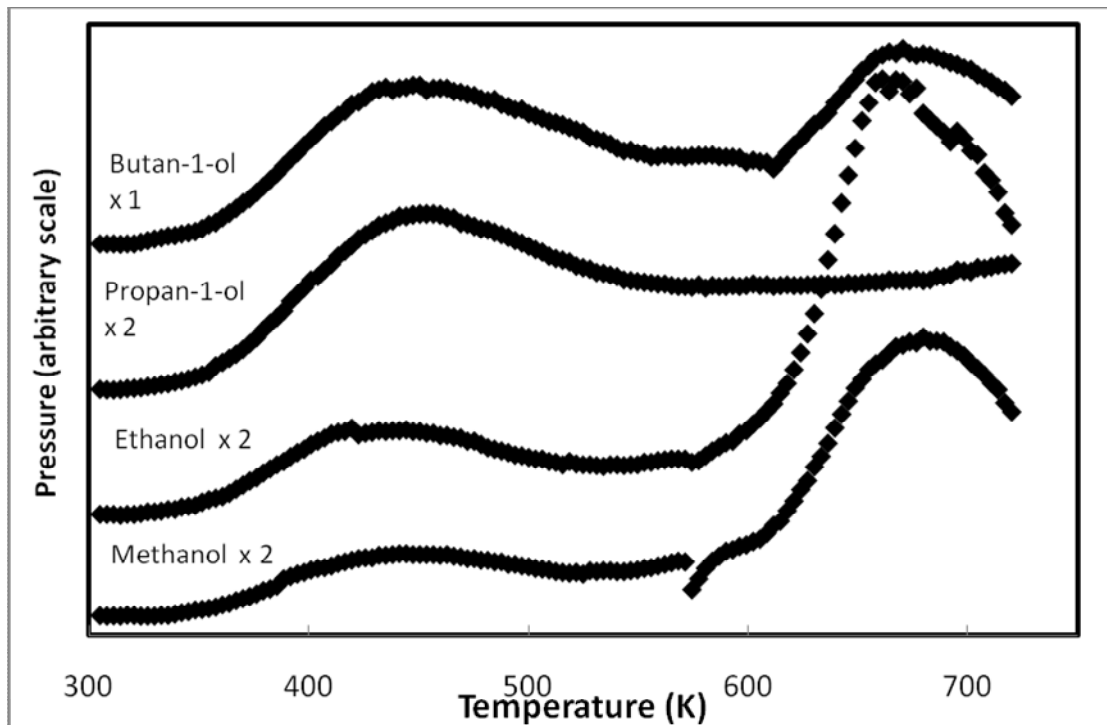**Figure 5.4 TPD alcohol series for UST fibres, m/z 31.**

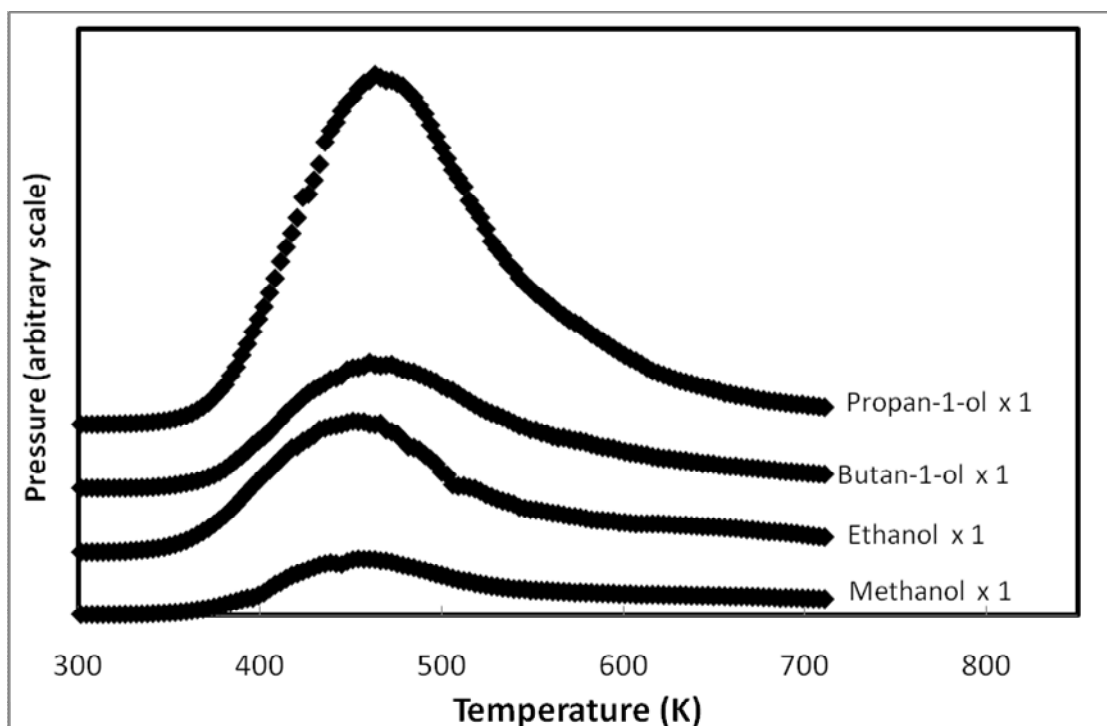**Figure 5.5 TPD alcohol series for 6B fibres, m/z 31.**

Figure 5.6 TPD alcohol series for UV/O$_3$ treated fibres, m/z 31.

Peak areas for the m/z 31 spectra were calculated by integrating the curve and then applying a correction factor, as described in Chapter 2.12.1. Table 5.4 lists the results for all the fibre and probe combinations.

Table 5.4 Integrated peak areas for m/z 31 for alcohol series per gram of carbon fibre or approximately per m^2 (BET surface area = ca. 1m^2/g)

	% O	Methanol	Ethanol	Propan-1-ol	Butan-1-ol
UST	2.4	8.0×10^{-9}	2.8×10^{-8}	4.8×10^{-8}	7.1×10^{-7}
0.2B	4.0	2.4×10^{-9}	2.0×10^{-8}	7.0×10^{-8}	1.8×10^{-7}
3B	7.9	3.5×10^{-8}	1.3×10^{-7}	3.9×10^{-7}	1.2×10^{-6}
3A	8.5	8.9×10^{-9}	4.4×10^{-8}	4.0×10^{-7}	1.5×10^{-6}
6B	11.4	1.7×10^{-7}	1.3×10^{-7}	4.2×10^{-7}	2.3×10^{-6}
UV/O$_3$	21.9	7.5×10^{-6}	2.1×10^{-5}	4.3×10^{-5}	4.4×10^{-5}

As seen in Table 5.4, the surface uptake, as monitored by the main desorption fragment of each alcohol, increases with increasing alkyl chain length of the probe, which is opposite to what occurs in immersion calorimetry (liquid phase). As the alkyl chain increases for an organic molecule, the dipole moment decreases, i.e. the molecule becomes less polar [2]. For liquids, this would result in less polar interactions occurring at the surface and dispersion interactions becoming the dominant force, as seen in the calorimetry results in Chapter 4 [2]. In the case of gases however, the polarizability of the molecule becomes the most important factor [3].

The chemisorption of a molecule on a surface can be treated as a series of bond breaking and bond making processes. The adsorbate must have free electronic density to make a bond with the surface [4] or empty electronic states to accept electrons from the surface or both. Dissociative adsorption will therefore be affected by how easily the bonds in the adsorbate break, how strongly it bonds to the surface, and whether interactions occur between the adsorbed species [3].

How easily the bonds in a molecule break is related to the acidity which for gases is determined by the polarizability of the molecule [3]. As the polarizability increases, the acidity also increases, i.e. it becomes easier to dissociate the hydrogen atoms from the molecule. Table 5.5 lists the polarizabilities of the alcohols used in this study. The polarizability increases linearly with the number of carbons in the molecule. Therefore as the chain length increases, the likelihood of dissociation occurring increases. From Table 5.4 and Table 5.5, it seems probable that the molecules with longer alkyl chains are being polarized more than those with shorter chains. The alcohol molecules on the surface of the fibre in the TPD experiments are most likely at monolayer coverage. Multilayer formation can be described as resembling condensation of the adsorptive into a liquid on the surface [5]. Therefore at the point of multilayer formation in adsorption experiments, the adsorbate will act as a liquid and the dipole moment will again be the determining factor in the level of interaction between the surface and the adsorbate such as in calorimetry. Since the alcohol molecules on

the fibre are only at monolayer coverage, the interactions between the molecules and surface will be dominated by the polarizability and not the dipole moment.

Table 5.5 Polarizability of probes [6]

	#C	Polarizability (10^{-24} cm^3)
Methanol	1	3.29
Ethanol	2	5.41
Propan-1-ol	3	6.74
Butan-1-ol	4	8.88

Figure 5.7, Figure 5.8, Figure 5.9, Figure 5.10, Figure 5.11, and Figure 5.12 show the trend in the peak area of m/z 31 per gram of fibre for the alcohol series on the UST, 0.2B, 3B, 6B, 3A and UV/O_3 treated fibres respectively . The untreated and electrochemically treated fibres all showed exponential trends with increasing alkyl chain while the UV/O_3 treated fibres showed a linear trend with chain length. The exponent of the trend lines for the electrochemically-base treated fibres decreases with increasing treatment level suggesting the trend becomes more linear as the oxygen on the fibre increases. While the polarizability of the adsorbate will play a significant part in the amount adsorbed on the fibre, from these figures it seems likely that other factors are influencing the adsorption or desorption. For example, delocalised π-electron rich areas on the carbon basal layers have been found to act as Lewis base sites on carbon catalysts [7,8]. On an oxygen free fibre surface, a background level of adsorption would still occur at the basal sites. As the oxygen level increases on the fibre surface, the number of delocalised π-electrons will decrease and therefore the number of these weak base sites will also decrease. Indeed for the base treated fibres the Plasmon level in XPS measurements decreases, as shown in Table 5.6 presented below, suggesting less delocalised electrons exist. The decrease in weak, background base sites with the increase in strong localised base sites could account for the gradual change from the exponential to linear trend in peak area of m/z 31 with increasing alkyl chain length although further investigation would be of interest.
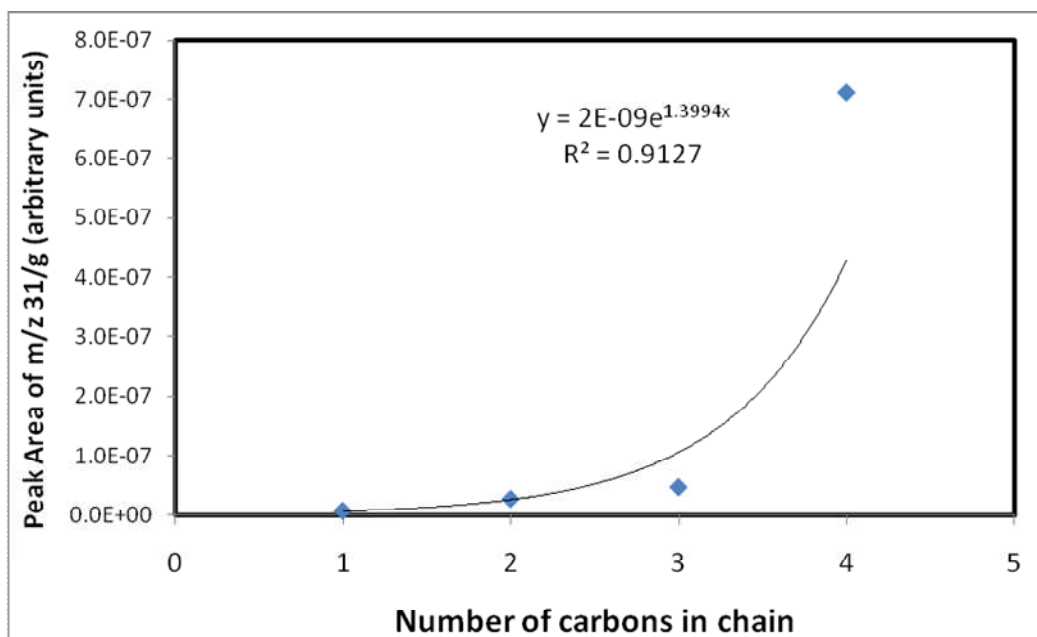
Figure 5.7 Peak area of desorbing alcohol (measured by m/z 31) per gram of UST fibres as a function of the number of carbons in the alcohol.
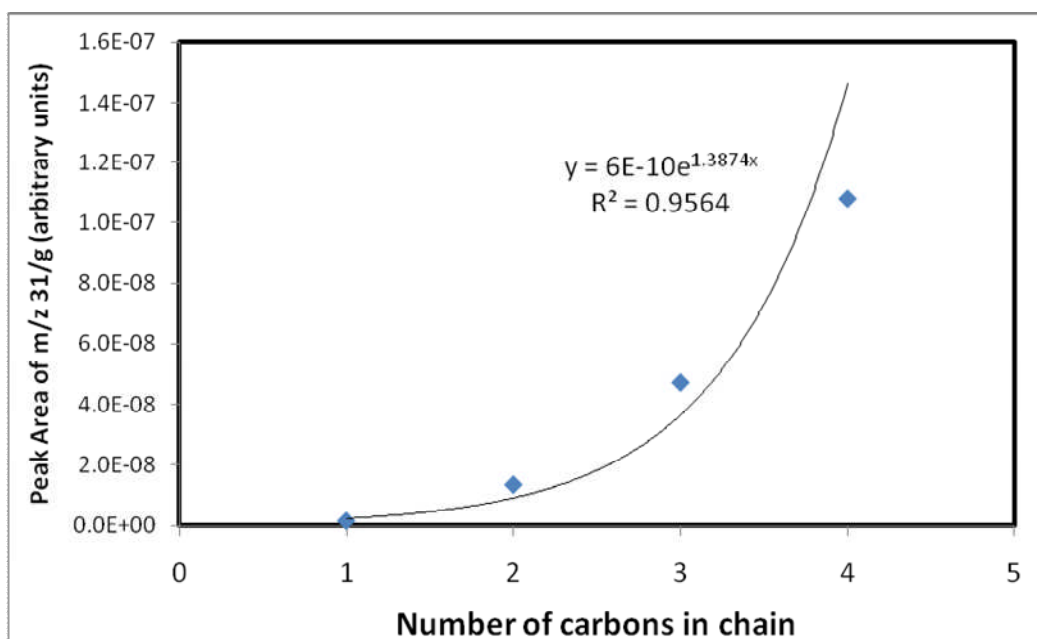

Figure 5.8 Peak area of desorbing alcohol (measured by m/z 31) per gram of 0.2B fibres as a function of the number of carbons in the alcohol.
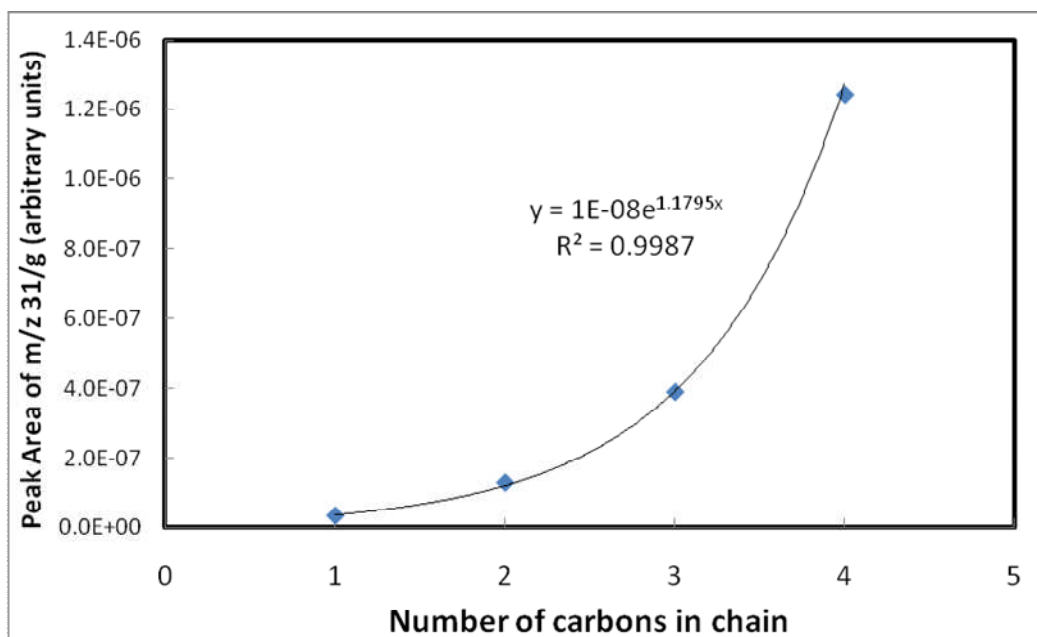
Figure 5.9 Peak area of desorbing alcohol (measured by m/z 31) per gram of 3B fibres as a function of the number of carbons in the alcohol.
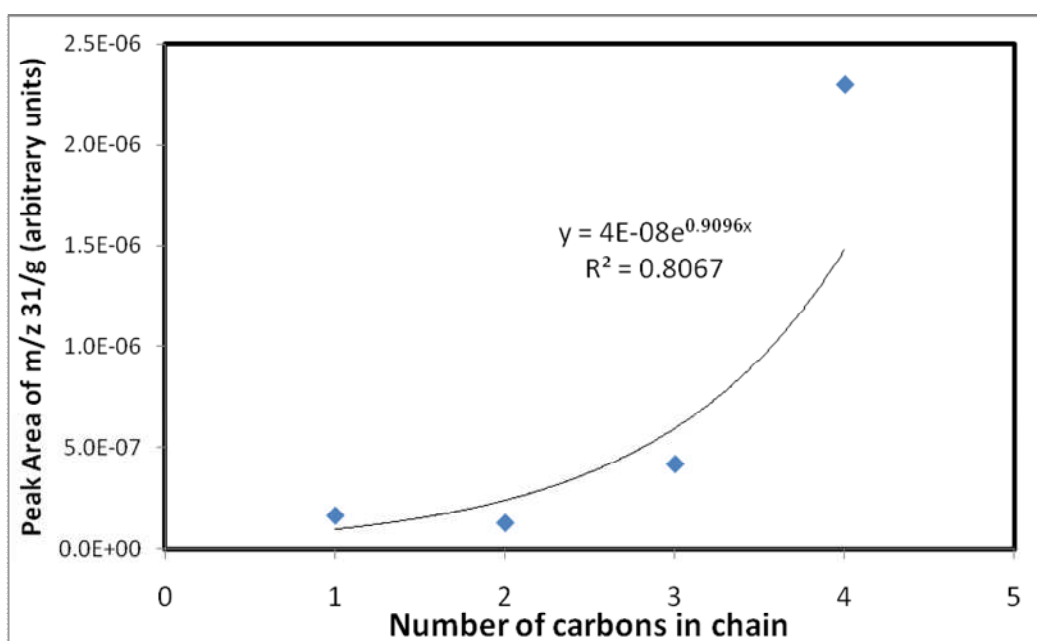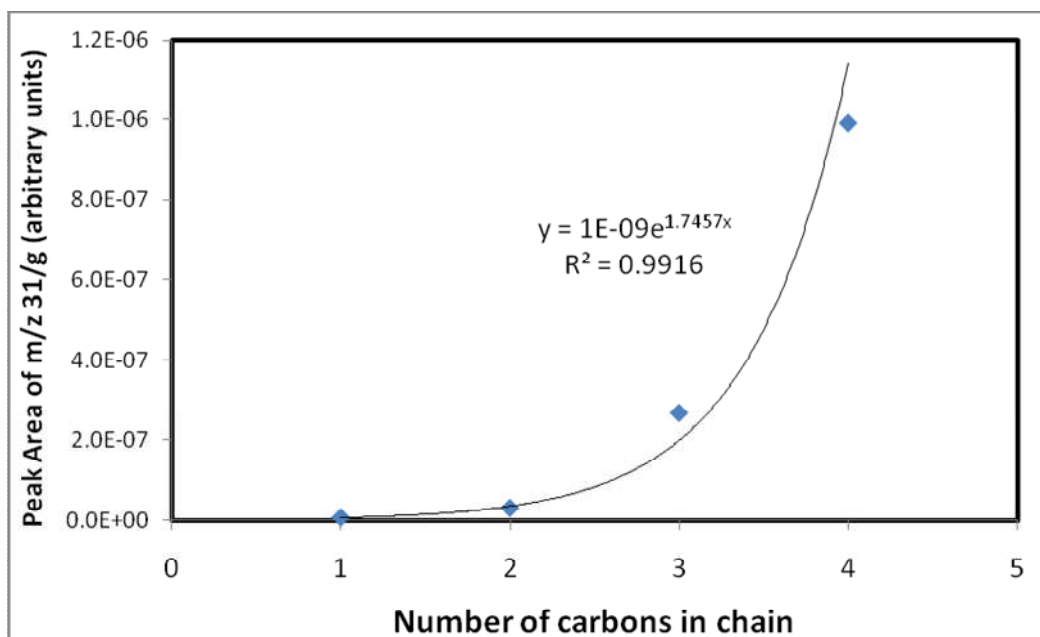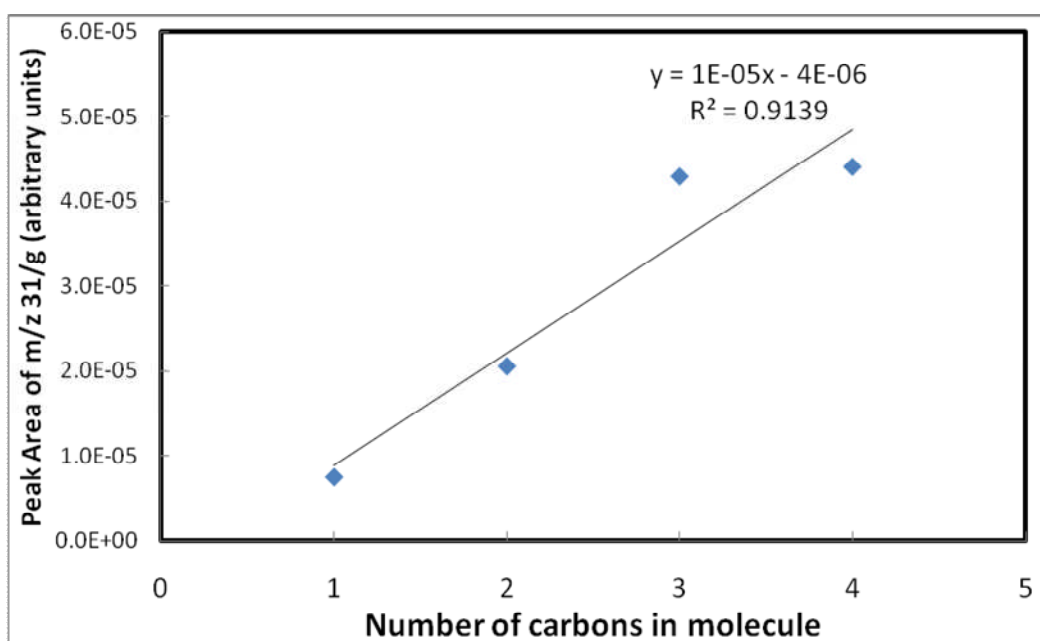

Figure 5.10 Peak area of desorbing alcohol (measured by m/z 31) per gram of 6B fibres as a function of the number of carbons in the alcohol.

Figure 5.11 Peak area of desorbing alcohol (measured by m/z 31) per gram of 3A fibres as a function of the number of carbons in the alcohol.

Figure 5.12 Peak area of desorbing alcohol (measured by m/z 31) per gram of UV/O₃ treated fibres as a function of the number of carbons in the alcohol.

In addition to alkyl chain length, the peak area of m/z 31 recorded also increased with increasing surface oxygen on the fibre as can be seen in Table 5.4 . Figure 5.13 shows the TPD spectra of m/z 31 for the untreated fibres and the 3B, 6B,

and UV/O$_3$ treated fibres after dosing with ethanol. Figure 5.14 and Figure 5.15 show the TPD spectra for mass fragments 27 and 29 respectively. The peaks of m/z 27, 29, and 31 are small for the untreated fibres compared with the 6B fibres; suggesting less adsorption occurs on the untreated fibres. These peaks are much bigger for the UV/O$_3$ than any other fibre, suggesting even greater uptake of ethanol compared to the electrochemical treatments. This trend was seen for all the alcohol molecules.
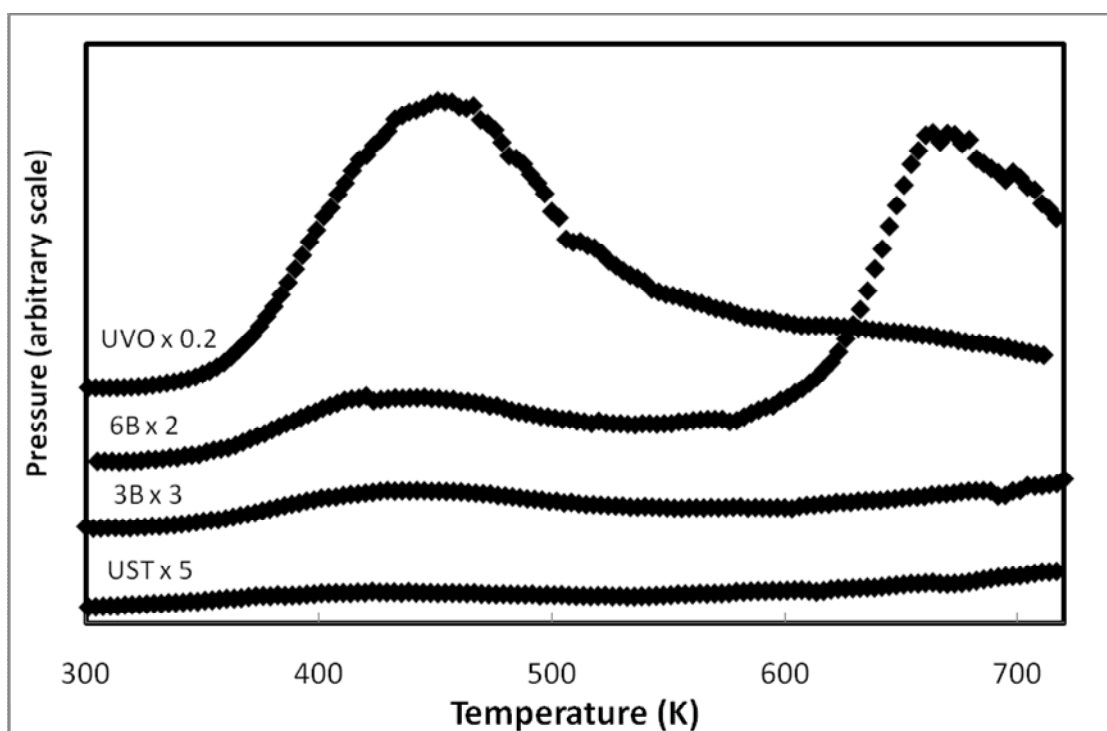

Figure 5.13 TPD of m/z 31 from ethanol desorption on UST, 3B, 6B and UV/O$_3$ treated fibres.
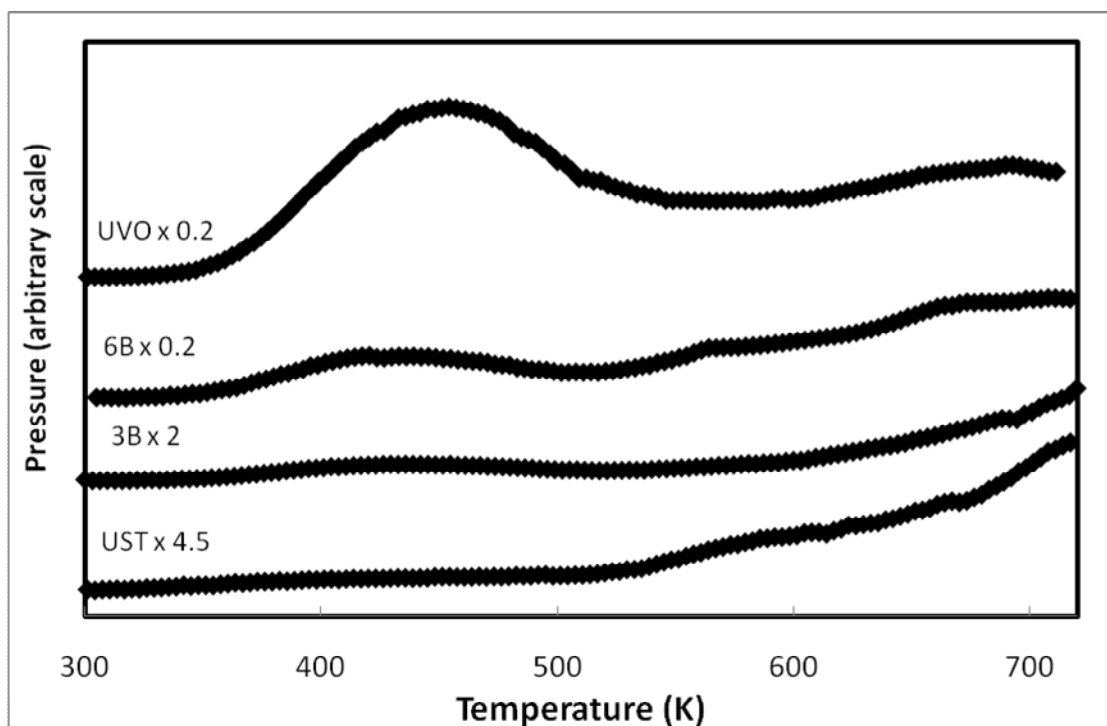
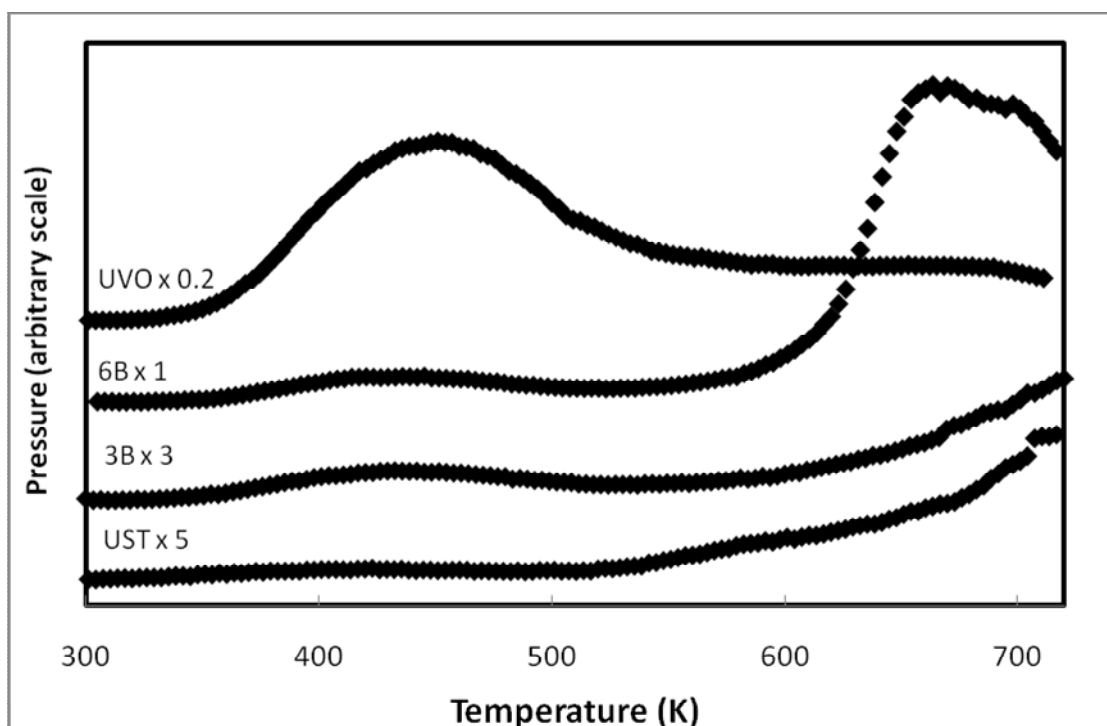**Figure 5.14 TPD of m/z 27 from ethanol desorption on UST, 3B, 6B and UV/O$_3$ treated fibres.**

Figure 5.15 TPD of m/z 29 from ethanol desorption on UST, 3B, 6B and UV/O$_3$ treated fibres.

184

5.4 Correlation with Surface Oxygen

Figure 5.16, Figure 5.17, Figure 5.18, and Figure 5.19 show the quantity of methanol, ethanol, propan-1-ol and butan-1-ol desorbed per gram of fibre as a function of surface oxygen respectively. The trends are best described by exponential curves so the plots are provided on a logarithmic scale.
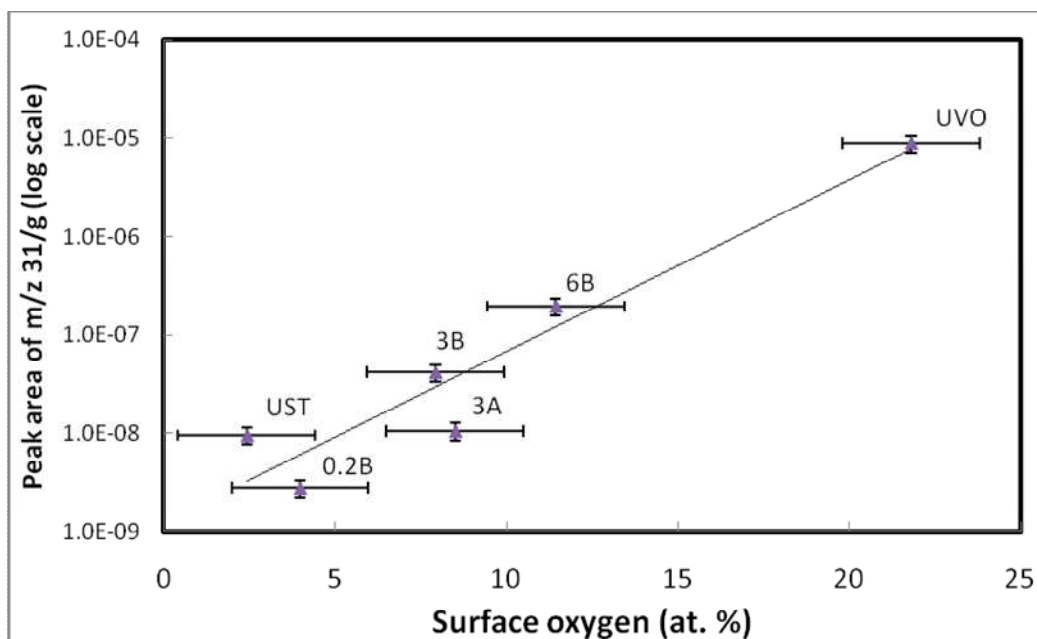

Figure 5.16 Logarithmic plot of the peak area of m/z 31 for methanol desorption (arbitrary units) as a function of surface oxygen. Error bars represent estimated 20% error in peak area measurements and maximum 95 % confidence interval for oxygen level.
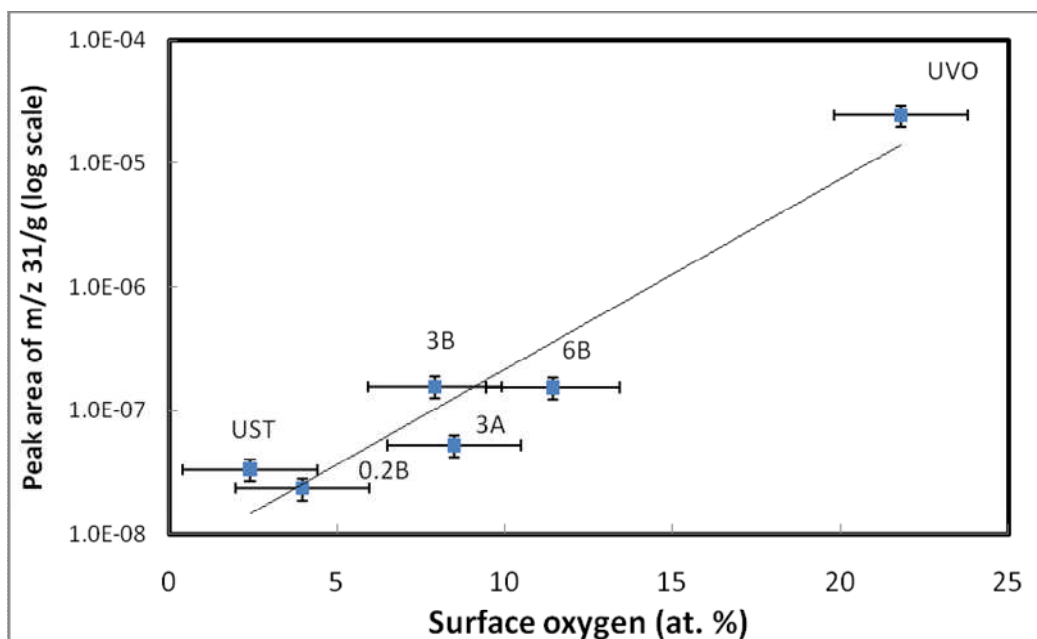
Figure 5.17 Logarithmic plot of the peak area of m/z 31 for ethanol desorption (arbitrary units) as a function of surface oxygen. Error bars represent estimated 20% error in peak area measurements and maximum 95 % confidence interval for oxygen level.

Figure 5.18 Logarithmic plot of the peak area of m/z 31 for propan-1-ol desorption (arbitrary units) as a function of surface oxygen. Error bars represent estimated 20% error in peak area measurements and maximum 95 % confidence interval for oxygen level.

Figure 5.19 Logarithmic plot of the peak area of m/z 31 for butan-1-ol desorption (arbitrary units) as a function of surface oxygen. Error bars represent estimated 20% error in peak area measurements and maximum 95 % confidence interval for oxygen level.
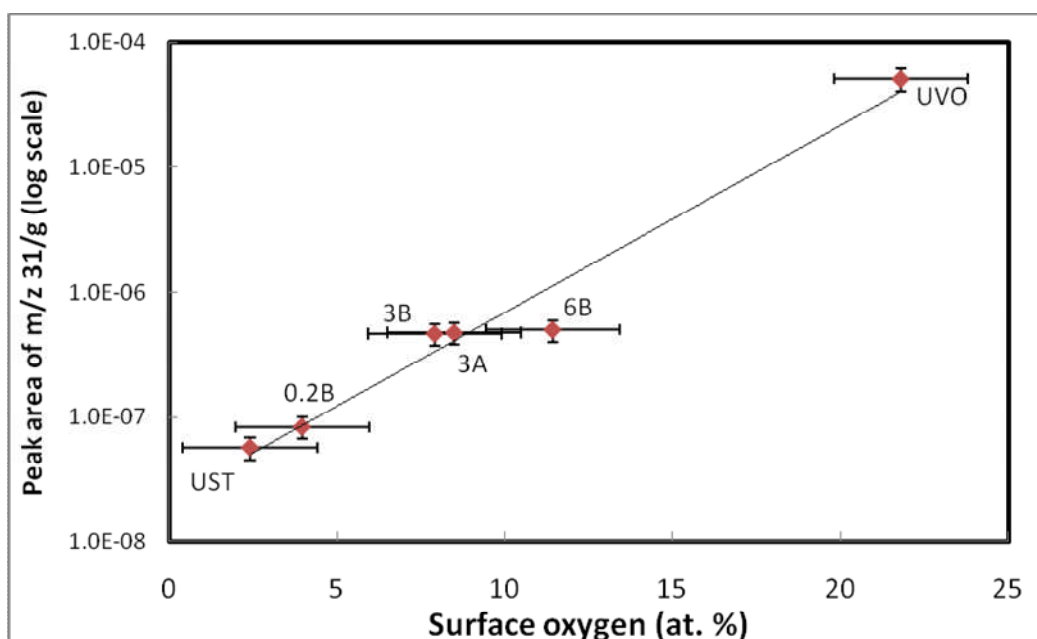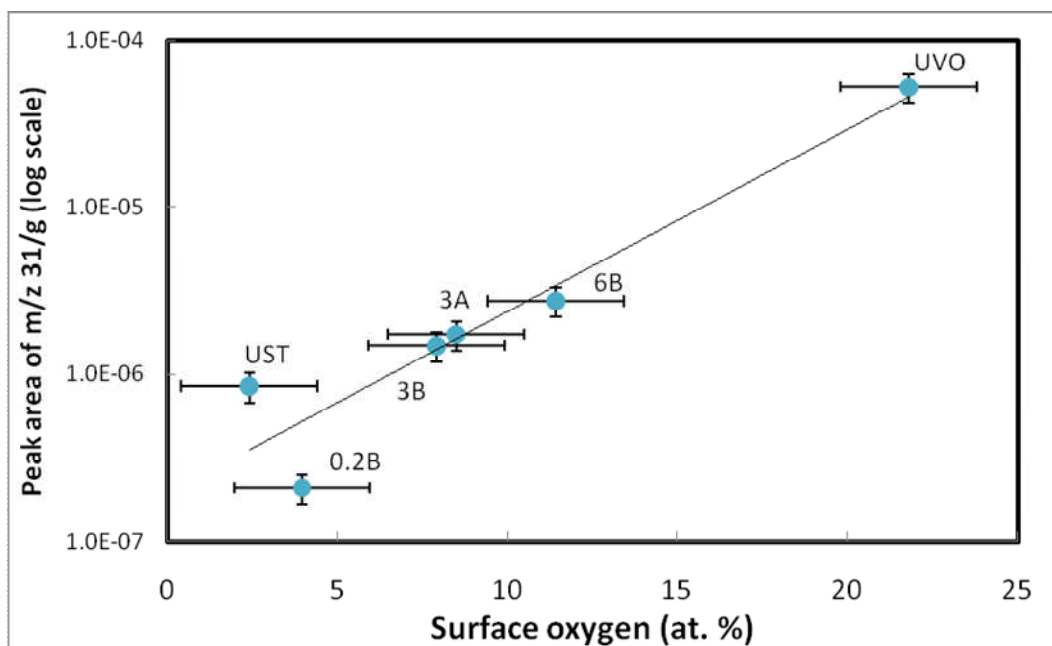
It is very clear that more alcohol adsorbs on fibres with greater levels of oxygen. The average functional groups for each treatment type were reported earlier in Chapter 3.2.2. Table 5.6 lists the functional groups on the surfaces of the fibres used in the TPD experiments as found from the peak fitting performed on the XPS C1s spectra. Plotting the change in the percentage of functional groups against the quantity of m/z 31 desorbed, produces exponential trends for all of the oxygen containing groups with the exception of carbonate which did not show a relationship. One possible reason is that unlike the alkoxides ($R-O_s$) and carboxylate ($RCOO_a$) groups, the carbonate groups ($OCOO_a$) may not allow for adsorption as they are the most stable.

Table 5.6 Functional groups on fibres used in TPD as determined by XPS C1s

Treatment	%					
	UST 1	0.2B 1	3B 3	6B 1	3A 2	UVO 2
Graphite (~284.6 eV)	74.8	73.5	73.3	73.4	75.6	64.9
Alkoxide/ phenolic/ ether (285.8 eV)	14.2	14.5	14.9	16.0	13.8	17.7
Carbonyl/ quinine (287.2 eV)	4.1	4.5	5.1	5.2	4.0	6.6
Carboxyl/ ester (288.8 eV)	2.9	3.0	3.3	3.6	3.0	8.0
Carbonate (290.6 eV)	1.4	2.3	0.9	1.2	1.1	1.0
Plasmon (291.2 eV)	2.6	2.3	2.4	0.7	2.6	1.9
Carbon	94.8	93.1	89.6	86.7	89.2	73.9
Oxygen	2.4	4.0	7.9	11.4	8.5	21.9

How strongly the adsorbed species is held on the fibre can be estimated from the temperature of peak desorption. If the strength of the bond increases, the temperature of desorption should also increase. Figure 5.20 and Figure 5.21 show the variation in temperature with level of oxygen present on the fibre surface for propan-1-ol and butan-1-ol respectively. The trends for methanol and ethanol were less clear and reliable so are not presented. There is a trend however for propan-1-ol and butan-1-ol. This suggests the surface species from propan-1-ol and butan-1-ol adsorption are more tightly bound when there is more surface oxygen present.
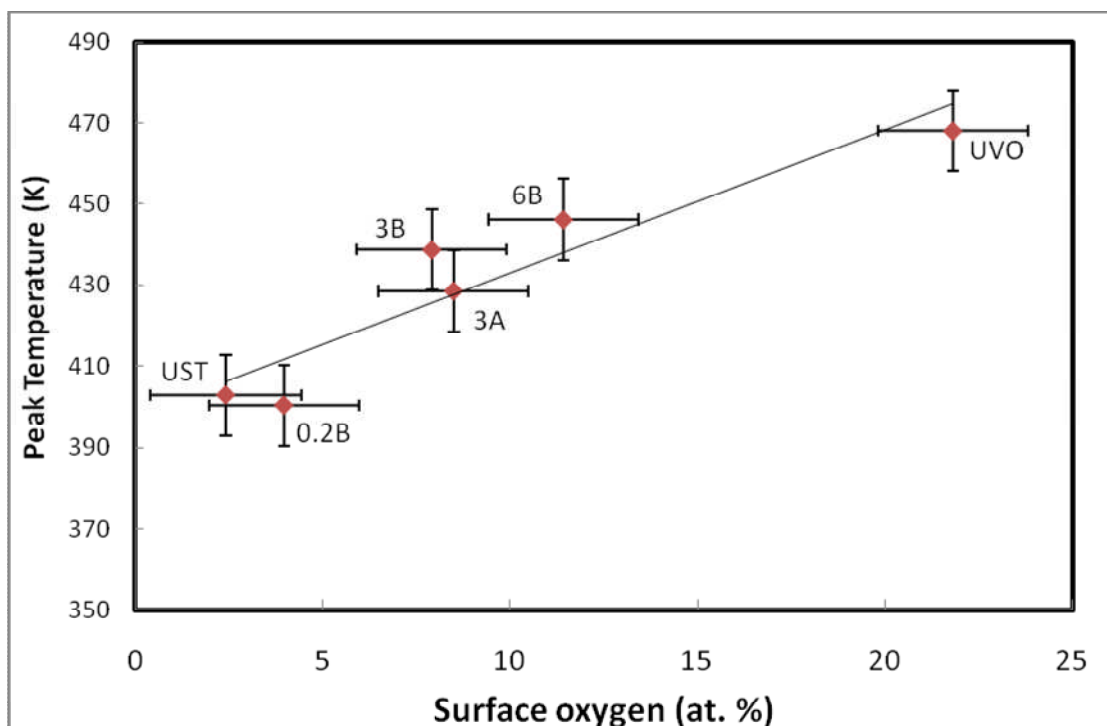
Figure 5.20 Temperature of peak desorption of propan-1-ol as a function of surface oxygen. Error bars represent estimated ± 10 K error in temperature and maximum 95 % confidence interval for oxygen level.
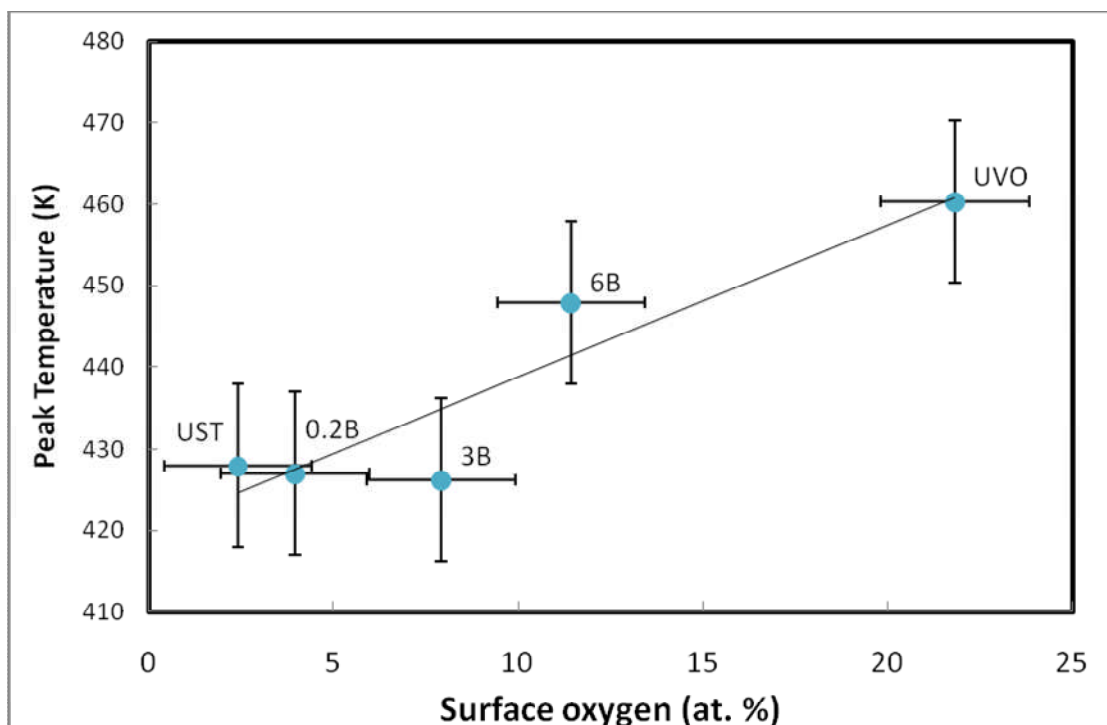

Figure 5.21 Temperature of peak desorption of butan-1-ol as a function of surface oxygen. Error bars represent estimated ± 10 K error in temperature and maximum 95 % confidence interval for oxygen level.

5.5 Effect of Heating on Functional Groups

Untreated, 3B treated, and 6B treated fibres were heated without dosing and TPD spectra were recorded. Figure 5.22 shows the TPD spectra for several mass fragments of interest released from heated 3B fibres. The untreated and 6B fibres showed similar spectra. Products desorb at about 800 K in one large peak preceded by a shoulder at about 700 K.

Clear desorption of CO and CO_2 is seen but in addition, desorption of m/z 31, 29, 42, and 14 is also seen. M/z 31 is the fingerprint of CH_2OH^+ species while m/z 29 could be from formyl radicals (CHO) and/ or ethyl radicals (CH_3-CH_2-). It is possible that ketene (CH_2=CO) is also being formed as shown by m/z 42 and 14; although 42 can also be due to propene (CH_3-CH=CH_2) and 14 can be due to nitrogen. Ketene is the main desorption product following the decomposition of acetates ($CH_3CO_2^-$) on many surfaces [9]. The peak fitting of the XPS C 1s spectra in Chapter 3 showed carboxyl groups were on the fibre surfaces which could take the form of acetates.
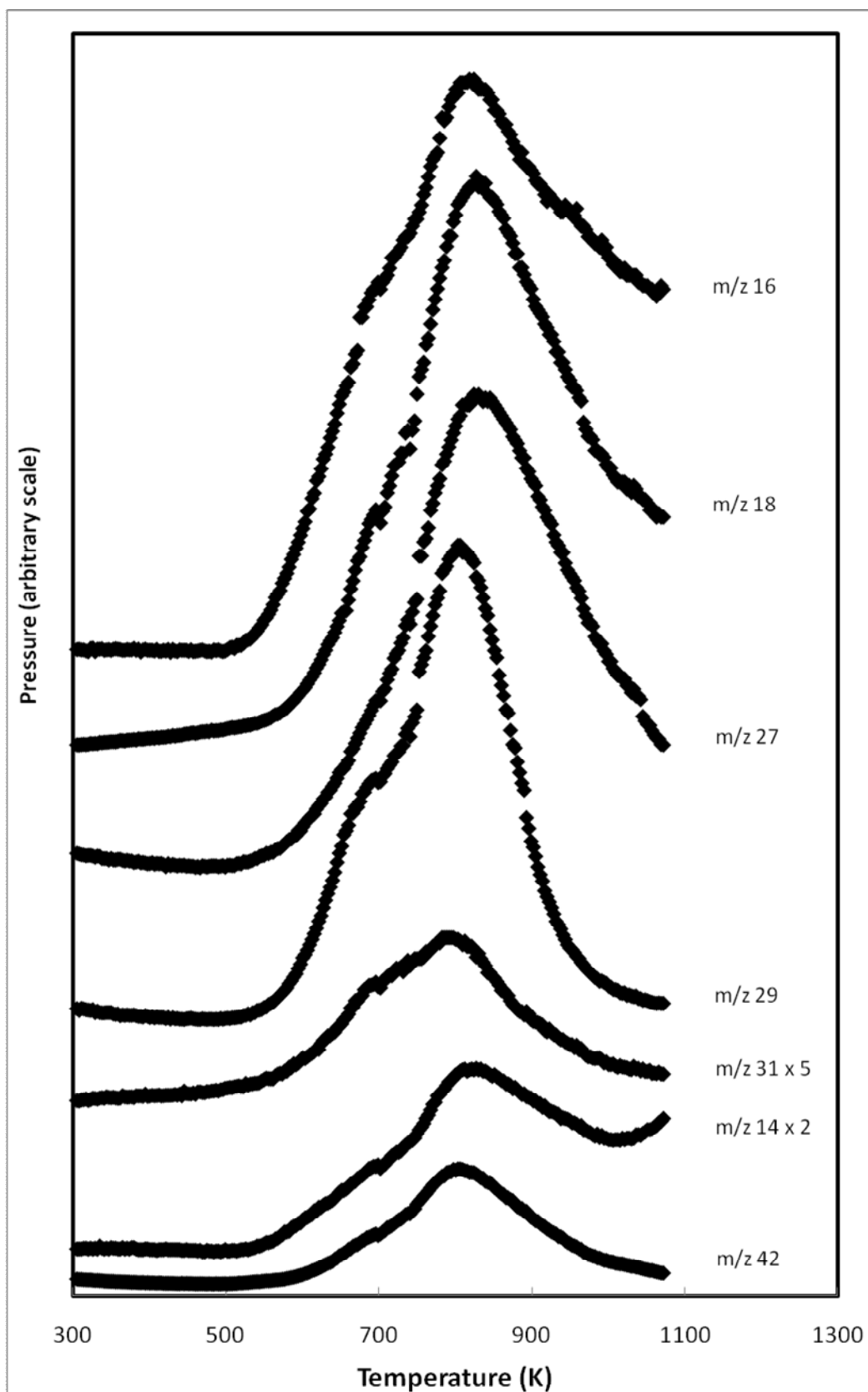
Figure 5.22 TPD spectra for blank 3B fibres heated to 1073 K (800 $^{\circ}$C).

Figure 5.23 and Figure 5.24 respectively show the amount of carbon monoxide (m/z 28) and carbon dioxide (m/z 44) released from the fibre surfaces. The untreated fibres were only heated up to 923 K (650 °C) while the 3B and 6B fibres were heated up to 1073 K (800 °C). Heating beyond 1073 K was not possible with the furnace available. As can be seen, the amount of CO and CO_2 released increases with fibre treatment level, i.e. with the level of oxygen present on the surface.

Comparing the data to the discussion in Chapter 2.12.1, it is possible to make some general statements about the desorption. The peak temperature of CO desorption is higher than that of CO_2 as is seen previously by others [10-12]. Desorption of functional groups is not complete at 1073 K as evidenced by the intensity of the spectra. The peak temperature of both CO and CO_2 is lower for the 6B fibres than for the UST fibres (marked by a dashed line on the graphs) suggesting a different chemical composition on the fibres. This was visible in the XPS data in Chapter 3. The wide desorption with multiple peaks indicates the complexity of the desorption profile that originates from the removal of functional groups. The objective of the heat treatment is to see into the effect of removal of these functional groups on the adsorption of alcohols.

In order to monitor the decomposition products, *ex-situ* XPS measurements were made on 3B fibres heat treated to 873 K (600 °C) and 1073 K. Peak fitting was performed on the C 1s peak. Table 4.1 shows the percentage of functional groups identified; it has been assumed that the 473 K heated fibres used in the TPD are unchanged from the unheated fibres used in XPS. This assumption is based on the fact that heating to this low temperature mainly affects reversibly adsorbed water. XPS results indicate that the 1073 K treatment has resulted in a slight but noticeable decrease in some of the functional groups, although the alkoxide group remains unchanged. Table 5.8 shows the XPS elemental analysis. The heat treatment has removed some oxygen and nitrogen from the surface of the fibres; the surface oxygen has decreased over two fold upon heating to 1073 K.
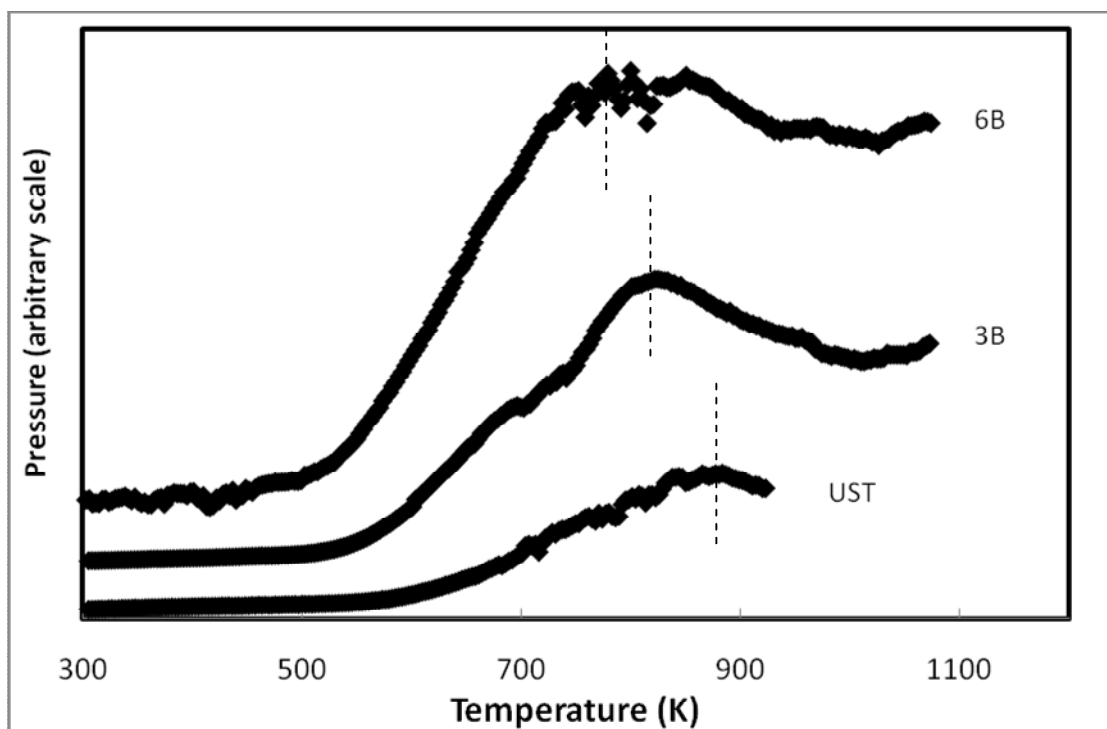
Figure 5.23 Carbon monoxide (m/z 28) released on heating selection of fibres.
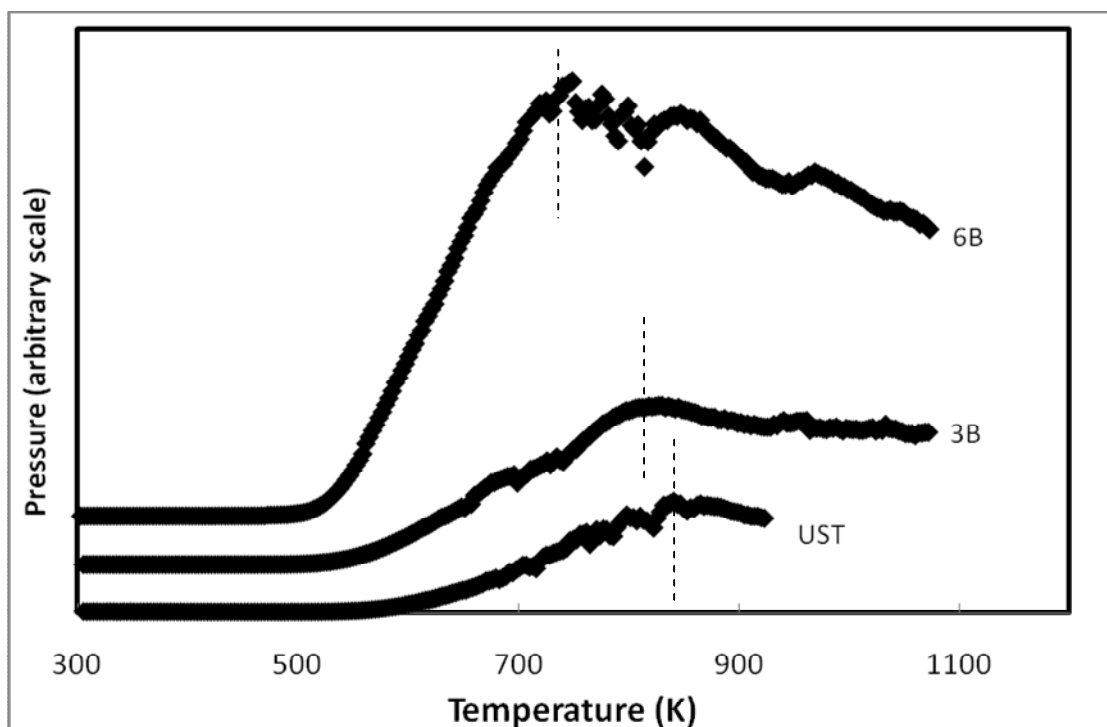

Figure 5.24 Carbon dioxide (m/z 44) released on heating selection of fibres.

193

Table 5.7 % of the carbon functional groups as determined by XPS C1s on heat treated 3B fibres

	%		
Temperature (K)	473	873	1073
Graphite (~284.6 eV)	73.3	74.0	74.1
Alkoxide/ phenolic/ ether (285.8 eV)	14.9	14.8	14.9
Carbonyl/ quinine (287.2 eV)	5.1	5.3	4.3
Carboxyl/ ester (288.8 eV)	3.3	2.1	2.6
Carbonate (290.6 eV)	0.9	1.0	0.9

Table 5.8 XPS surface compositions (atomic % from computed areas of C1s, O1s, N1s and Si2p peaks) for heat treated 3B fibres (estimated error ~10%)

Temperature	%				Ratio		
(K)	C	O	N	Si	O/C	N/C	O/N
473	89.6	**7.9**	1.8	0.7	0.09	0.02	4.39
873	92.6	**5.0**	1.7	0.8	0.05	0.02	2.94
1073	95.2	**3.3**	1.3	0.3	0.03	0.01	2.54

5.6 Effect of Heating on Alcohol Uptake

Following heat treatment up to 873 K, and subsequent removal of a sample for XPS, the 3B fibres were dosed with methanol or propan-1-ol. The fibres were then heated again up to 1073 K. The amounts of m/z 31 and several other mass fragments desorbed were recorded. The dosing and measurement steps were then repeated for methanol. For propan-1-ol, the fibres were heated directly up to 1073 K, avoiding the 873 K step.

XPS shows the oxygen level on the fibres decreases with increasing heat treatment. Figure 5.25 shows the TPD spectra of m/z 31 for the desorption of methanol from the heat treated 3B fibres. The fibres heated to 473 K, i.e. those only cleaned of physisorbed gases, showed greater levels of m/z 31 desorption than the heat treated fibres. A second peak due to fibre decomposition starts at ~ 600 K and is absent from the spectra of the heated fibres. This is probably because the heated fibres have already had some functional groups removed that would have otherwise contributed to further stabilization of the methanol. Table 5.9 shows the integrated areas for several mass fragments, uncorrected for mass spectrometer sensitivity. The levels of m/z 31 desorption and hence methanol adsorption corresponds to the levels of oxygen on the fibres as seen in section 5.4. The fibres with the highest level of oxygen, the 473 K fibres, desorbed substantially more m/z 31 than the 873 and 1073 K heated fibres. Mass fragment 15 shows a similar trend and m/z 29 shows it to a lesser extent.
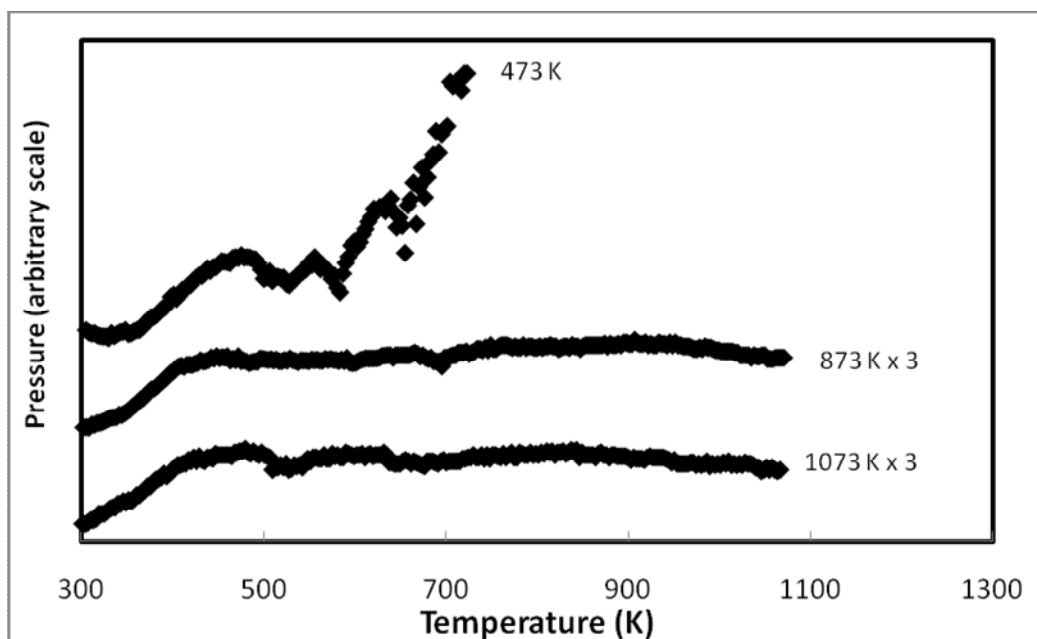

Figure 5.25 TPD of m/z 31 from methanol desorption on 473, 873, and 1073 K treated fibres.

Table 5.9 Integrated peak areas per gram of carbon fibre for methanol desorption from heat treated fibres

Temperature (K)	15	18	29	31
473	4.2×10^{-9}	--	1.9×10^{-8}	3.4×10^{-8}
873	3.6×10^{-9}	1.1×10^{-10}	4.7×10^{-9}	5.4×10^{-9}
1073	2.6×10^{-9}	1.9×10^{-9}	6.9×10^{-9}	4.8×10^{-9}

Figure 5.26 shows the m/z 31 TPD spectra for the fibres dosed with propan-1-ol. In this case, the 473 K heated fibres also show greater intensity in the m/z 31 peak than the 873 K and 1073 K heated fibres. Due to the shape of the peaks, it is difficult to integrate the areas. An attempt was made however and Table 5.10 lists the results for several mass fragments, uncorrected for the mass spectrometer sensitivity.

The heat treated fibres show less m/z 31 desorption than the 473 K fibres suggesting that adsorption of propan-1-ol increases with increasing surface oxygen. Similarly mass fragments 27 and 29 also decrease with increasing heat treatment. Figure 5.27 and Figure 5.28 show the desorption spectra of several mass fragments for the 873 K and 1073 K heated fibres respectively.
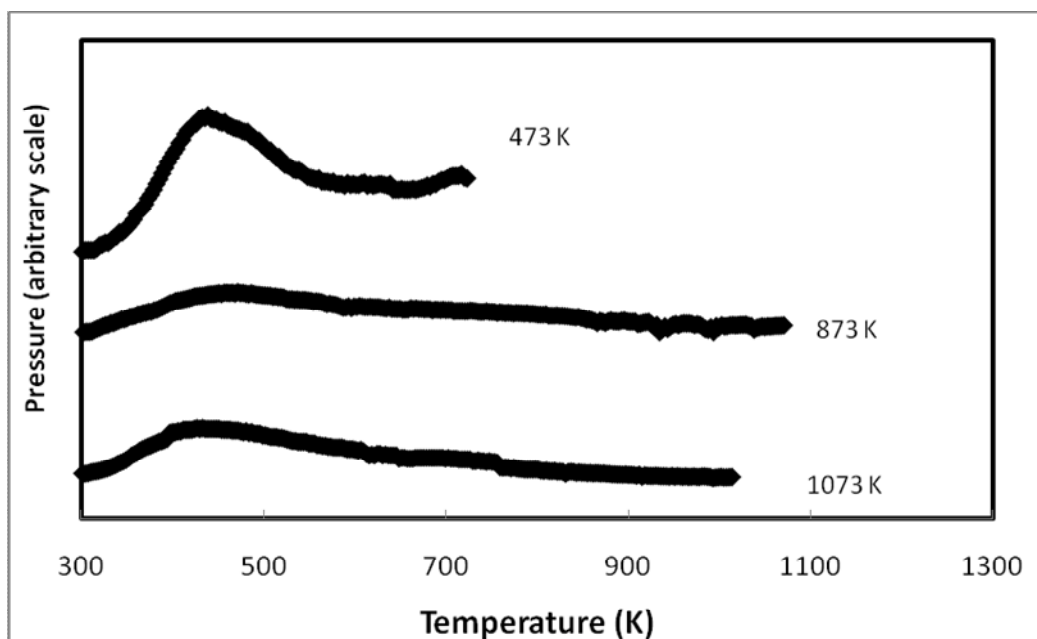
Figure 5.26 TPD of m/z 31 from propan-1-ol desorption on 200, 600, and 800 °C treated fibres.

Table 5.10 Integrated peak areas per gram of carbon fibre for propan-1-ol desorption from heat treated fibres

Temperature (^{o}C)	14	16	18	27
473	--	9.3×10^{-10}	--	7.9×10^{-8}
873	7.1×10^{-9}	3.7×10^{-9}	2.5×10^{-9}	3.3×10^{-8}
1073	2.6×10^{-9}	1.2×10^{-10}	6.5×10^{-10}	2.8×10^{-8}

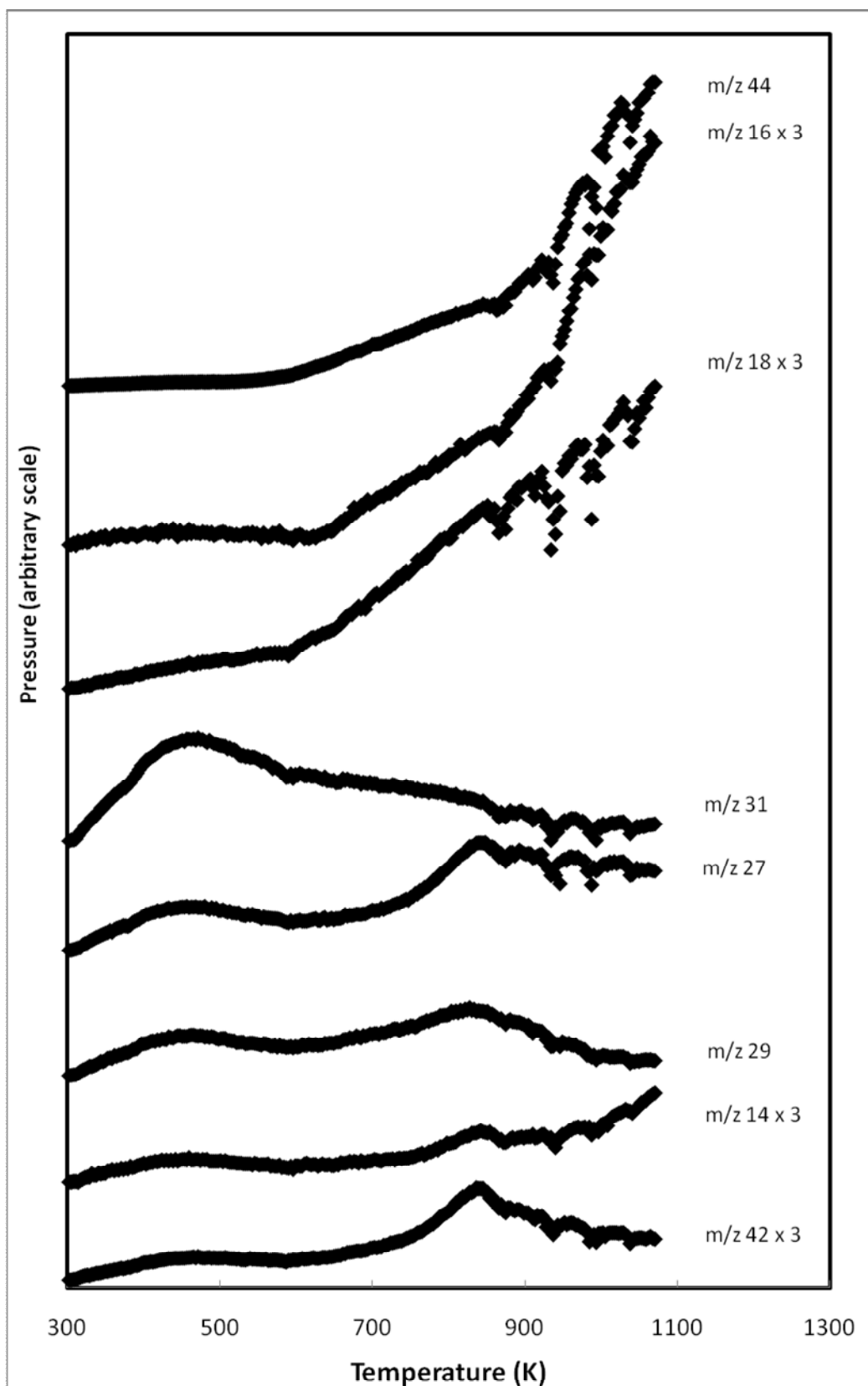|	28	29	31	44
473	--	7.3×10^{-8}	2.5×10^{-7}	--
873	1.1×10^{-8}	2.7×10^{-8}	6.7×10^{-8}	-6.6×10^{-10}
1703	5.4×10^{-9}	2.7×10^{-8}	1.1×10^{-7}	6.1×10^{-10}

Figure 5.27 TPD spectra for 3B fibres heat treated to 873 K and dosed with propan-1-ol.
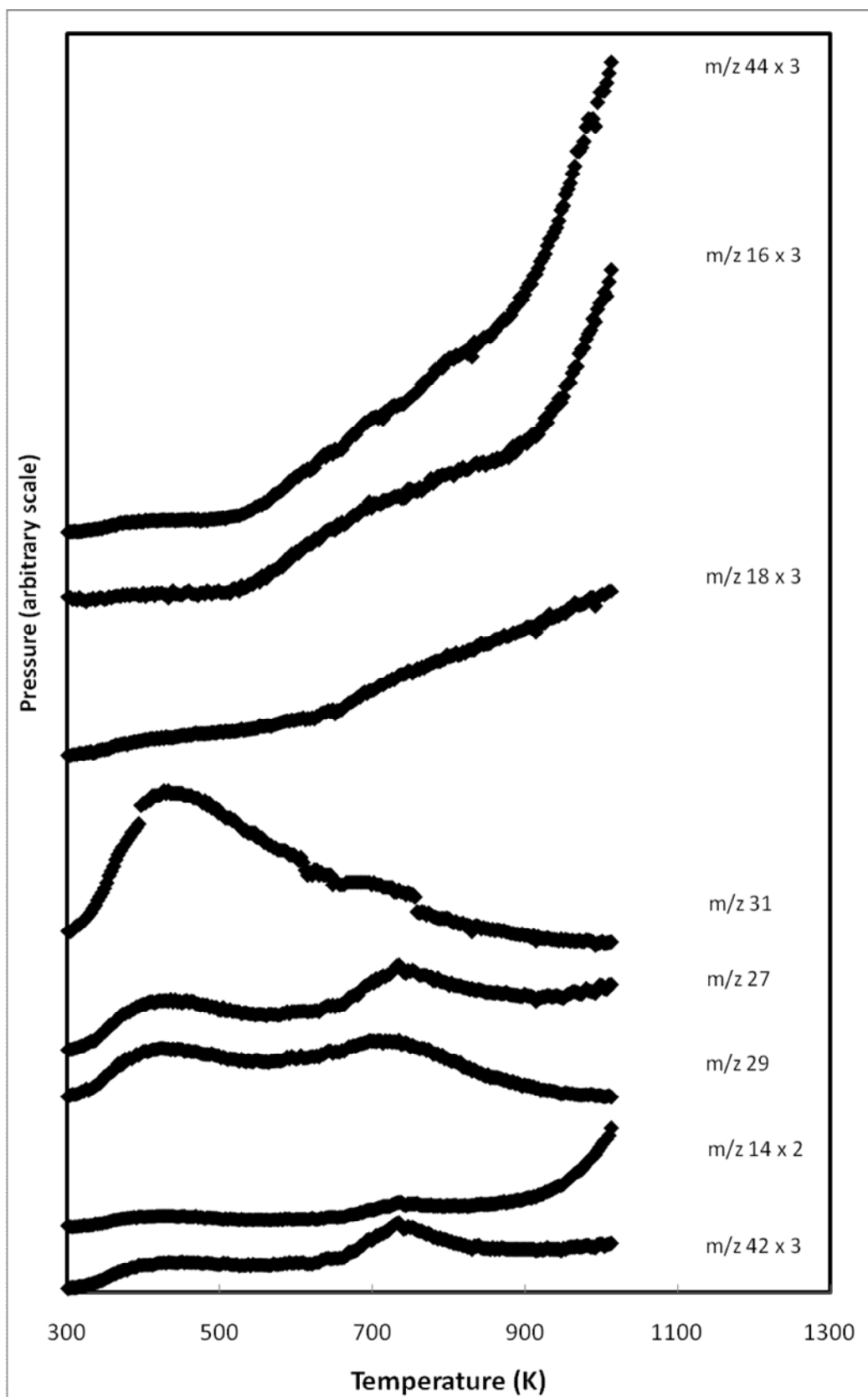
Figure 5.28 TPD spectra for 3B fibres heat treated to 1073 K and dosed with propan-1-ol.

5.7 Discussion

The TPD study of the series of C1 to C4 linear alcohols on carbon fibres modified by electrochemical and UV/O$_3$ methods has shown the following:

1. All products desorbed in two temperature domains. The first temperature domain at 450-500K mainly consisted of the reactant desorption while the second temperature domain (> 600K) mostly consisted of decomposition products (e.g. CO, CO$_2$, and ketene among others).

2. At the low temperature domain, a small fraction of the adsorbed alcohols was dehydrogenated to the corresponding aldehydes. The extent of dehydrogenation was inversely proportional to the number of carbon atoms in the alcohol. The dehydration reaction to olefins was not observed.

3. The surface uptake showed dependence on the nature of the alcohols; it increased with increasing number of carbon atoms. This increase was co-related to the increase in the acidity of the molecule in the gas phase where the polarizability is the main factor.

4. The surface uptake also increased with increasing surface oxygen atoms. This was understood as being due to the dissociative adsorption nature whereby two sites are needed: one to accommodate the O atom of the alcohols (surface carbon atom site) and the other to accommodate the hydrogen ion of the alcohol (a surface oxygen site).

5. Heating the carbon fibre to 873K and 1073K resulted in a noticeable decrease of surface oxygen as evidenced by the decrease of the XPS O1s peak when compared to the XPS C1s peak. This decrease resulted in reducing the surface uptake farther validating point 4 above.

A literature search reveals that TPD desorption of alcohol probes on carbon fibre surfaces has not been reported on so there is limited work to compare these results against. The blank TPD spectra, i.e. heated fibres that were not dosed with alcohols, are similar to those in the literature, an example of which was presented in Chapter 1.7.2, Figure 1.15. Adsorption of volatile organic compounds (VOC)

on carbon materials has been investigated in the literature [13,14]. VOCs are known to cause health problems such as respiratory irritation and cancer, and their removal from the environment is desirable [13]. Porous carbons are generally used due to their large surface areas. For example, TPD investigations of the adsorption of n-butanol, toluene, and butylacetate on activated carbons (surface area ~1200 m^2/g) were performed by Popescu *et al*., [14]. Figure 5.29 shows the desorption profile for butan-1-ol leaving the carbon surface. Only one temperature domain is visible but it coincides with the first temperature domain seen in this thesis. No information is given regarding the functional groups present on the activated carbon which precludes a discussion on the absence of a second, higher temperature, peak [14].
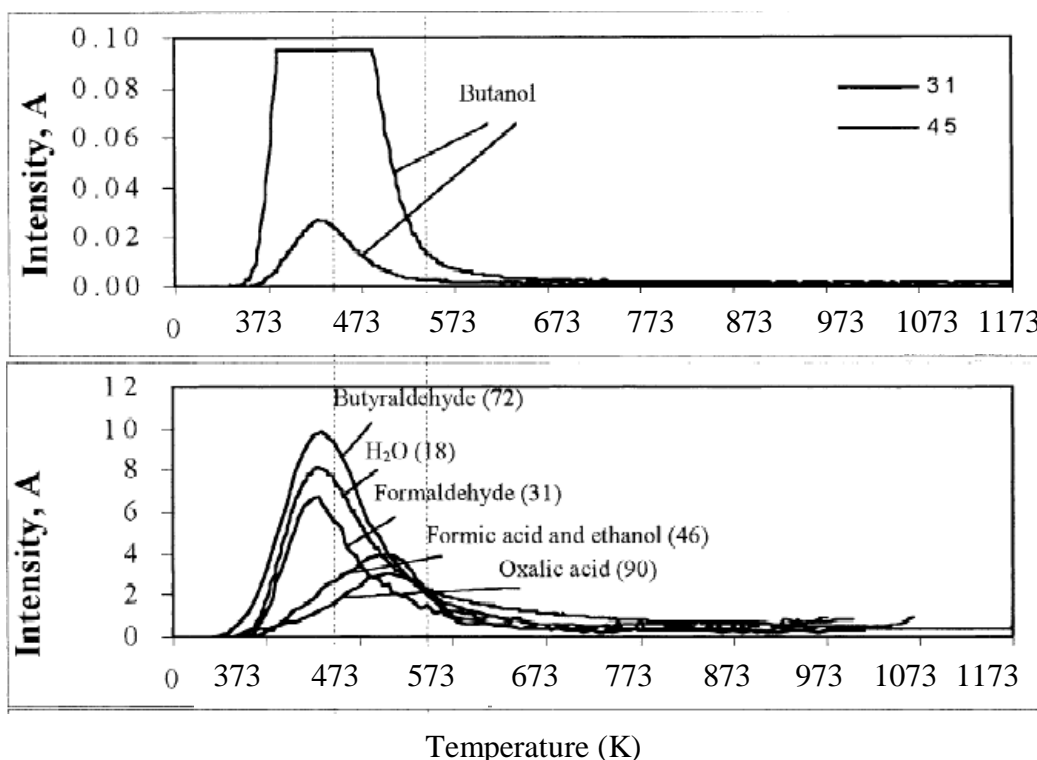
Figure 5.29 TPD spectra of butan-1-ol desorption and oxidation products from a study on activated carbon surfaces [14].

In the study by Popescu *et al*., [14] the heats of desorption for the toluene and the butylacetate were only slightly greater than the heat of vaporisation for the pure liquids and therefore the molecules were considered to be physisorbed. The heat of desorption for n-butanol was found to be greater that the heat of vaporisation.

In one case the enthalpy of desorption was found to be 98.8 kJ/mol; more than twice the enthalpy of vaporisation (43.7 kJ/mol). This suggests a reaction occurred between the adsorbed butan-1-ol and the surface oxygen groups. The authors found aldehydes, particularly formaldehyde (assigned to m/z 31) and butyraldehyde (m/z 72), were produced as well as oxalic acid (m/z 90), formic acid and ethanol (m/z 46) but they concluded further work was required to fully understand the mechanisms involved [14]. This agrees with the findings summarised in point 2 above.

Yi *et al.*, also investigated VOC adsorption, looking at the adsorption of benzene, toluene, methanol, and ethanol on activated carbon fibres by examining the increase in weight of degassed fibres exposed to the VOC vapour [13]. Methanol was seen to adsorb more than ethanol, unlike the results presented here (point 3), however the vapour pressures were high and coverage was likely to be greater than monolayer. The trend was attributed to differences in vapour pressure, molecular polarity and molecule size. Mixtures of benzene and toluene showed greater levels of adsorption than when each liquid was used pure suggesting different adsorption sites were on the fibre. The authors proposed that as the surface oxygen level increased, the fibre polarity increased thus more polar molecules adsorbed on the surface. The activated fibres had surface areas of ~1700 m^2/g and also a network of pores [13]. The gravimetric method applied by Yi and co-workers is straight forward and does not rely on measuring the desorption products, thus avoiding any ambiguity caused by dissociative desorption, however characteristics are for a multilayer system.

In work undertaken by Andreu *et al.,* gravimetric adsorption studies on untreated, non-porous, carbon black showed similar trends to those summarised in point 3 in the adsorption isotherms for methanol, ethanol and isopropanol at low pressures [2]. The isopropanol adsorbed the most on the carbon black while methanol adsorbed the least. At increased pressures, the level of adsorption changed; the methanol showing greater levels of adsorption than the isopropanol. The point of change was approximately at the knee of the isotherm, i.e. the point

of monolayer completion. After the monolayer was completed, multilayer formation took place [2]. This furthers the argument that adsorption on the fibres in this study is at monolayer coverage.

Carrott *et al*., also examined methanol adsorption on non-porous carbon blacks gravimetrically [15]. BET areas were calculated from the adsorption isotherms. The mean area associated with an adsorbed methanol molecule was found to be much larger than the molecular area calculated from liquid density measurements. Their results showed between one-in-eight to one-in-four of the surface oxygen atoms were covered depending on the carbon type. This suggests certain types of surface oxygen interact more strongly with the methanol, but specific groups were not investigated [15]. In the results presented here, a direct relationship between the peak desorption temperature and surface oxygen was not found for methanol. This could be due to the peak temperature varying with specific functional groups on the surface rather than total oxygen level. Further investigation would be of interest.

Oxidative dehydrogenation and dehydration has been studied on carbon materials of high surface areas for use as catalysts. Carrasco-Marín *et al*., examined the catalysis of ethanol on activated carbons using gas chromatography (GC) in an attempt to account for contradictions in catalysis mechanisms proposed in the literature [7]. The activated fibres were oxidised to various levels and a He/ethanol gas flowed over them. The resulting products were recorded by the GC. On the unoxidised carbons, only dehydrogenation occurred; the sole product being acetaldehyde. The oxidized carbons showed dehydrogenation and dehydration with ethene, ether, 1,3-butadiene, and ethyl acetate being recorded in addition to acetaldehyde. The level of dehydrogenation taking place increased with increasing oxygen level on the fibre. The unoxidised carbons were mainly basic in nature whereas the oxidised carbons were acidic as measured by Boehm titrations [7]. Carrasco-Marín *et al*., concluded that dehydrogenation reactions could occur on acid and basic sites but dehydration could only occur on acid sites and the occurrence would increase with the total acidity of the surface. The

catalysis was ascribed to carboxyl acids on the carbon surface [7]. As stated in point 2 above, dehydrogenation was observed in this study but dehydration was not. The complexity of the spectra could have masked any dehydration event that took place or, as Carrasco-Marín *et al.* suggested, water produced from the dehydrogenation reaction could have inhibited the dehydration process [7].

Work by Pittman *et al.*, on electrochemically oxidised fibres showed adsorption of toluene, ethanol and ammonia increased with increasing surface oxygen on the fibres [16] as seen in this work (point 4 and 5). They used a gravimetric technique to weigh the fibres while dosing them with a vapour [16]. This gives further confidence in the quantitative analysis of alcohol uptake.

In addition to alcohol adsorption/desorption, other investigations using TPD could be performed on carbon fibres. Damjanovíc and Auroux reviewed TPD as a method to investigate the acid/ base properties of zeolites using ammonium and other basic molecules [17]. The peak temperature of desorption is related to the energy of acid sites on the zeolite while the area under the peak is related to the total number of acid sites. Figure 5.30 shows example TPD spectra for ammonia on two different zeolites. M/z 16 is normally used for quantification rather than the parent peak (m/z 17) since it is heavily influenced by water [17]. The zeolites have very different spectra suggesting different strengths of acid sites. It is, however, not possible to determine the nature of the acid sites (e.g. Brönsted or Lewis) without addition investigation such as inline infra-red characterisation [17]. For example, Niwa *et al.*, measured the amount of ammonia desorbing from $NH_4\beta$ zeolite and an H-type zeolite as 1 mol/kg and 0.8 mol/kg respectively [18]. Two types of acid sites were assumed to exist based on the IR results; strong Brönsted, and weak Brönsted and TPD data was fitted on this assumption. Brönsted acid sites in zeolites are at hydroxyl groups that bridge Si and Al atoms in the structure and their strength will vary with the layout of the zeolite. The $NH_4\beta$ zeolite had a ratio of 0.14 weak to strong sites while the H-type zeolite had a ratio of 0.46 [18]. Applying this method to carbon fibres could investigate the exact nature of the strengths of function group-adsorbate interactions.
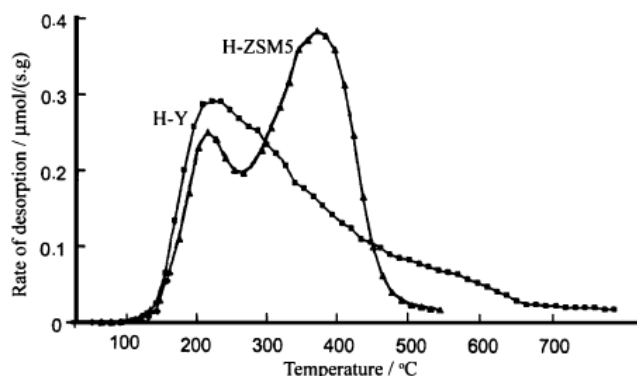
Figure 5.30 Ammonia (m/z 16) TPD spectra for two different zeolites [17]**.**

Physisorption could also be investigated by reducing the temperature of the system to below room temperature. Zacharia examined the adsorption of ethylbenzene (C_8H_{10}) onto graphite and carbon nanotubes using a liquid cryogen to reduce the TPD system to 30 K and found benzene interactions on graphite were mainly caused by van der Waal forces [19].

5.8   Conclusions

Temperature desorption spectroscopy has been used to investigate the chemical nature of the surfaces of carbon fibres. Alcohol desorption from the fibre surface appears to be second order in nature which means that the adsorption was dissociative. Two main factors affected the linear alcohols adsorption on the carbon fibre surface: (i) the number of carbon atoms present in the alcohol and (ii) the amount of oxygen present on the surface. (i) The interactions between the alcohols and the fibre surface are heavily influenced by the polarizability of the alcohol molecules with longer chain alcohols behaving more acidic than shorter chains. (ii) Increasing the level of oxygen on the surface of the fibres was shown to increase the level of adsorption of alcohol groups as expected from an acid (the alcohol molecules) -base (the surface oxygen atoms) type of interaction. However the relationship between these two points was found to be more complex. The extent of the increase in alcohol uptake with increasing chain length was found to reduce with increasing oxygen level. This might be due to

repulsive interactions which can be linked to preferential oxidation sites of the carbon fibre at step edges and defects. The temperature of peak desorption increased linearly with surface oxygen for propan-1-ol and butan-1-ol implying the alcohols were more tightly bound with increasing oxygen. Overall the TPD study showed the method to be promising for further examinations using alcohol probe molecules to understand the surface properties of carbon fibres.

5.9   References

[1] Idriss H, Seebauer EG. Reactions of ethanol over metal oxides. *Journal of Molecular Catalysis A: Chemical.* 2000; 152(1-2):201-212.

[2] Andreu A, Stoeckli HF, Bradley RH. Specific and non-specific interactions on non-porous carbon black surfaces. *Carbon.* 2007; 45:1854-1864.

[3] Chong SV, Idriss H. The reactions of carboxylic acids on UO2(1 1 1) single crystal surfaces. Effect of gas-phase acidity and surface defects. *Surface Science.* 2002; 504:145-158.

[4] Brown WA, Kose R, King DA. Calorimetric measurements of the adsorption heat for ethene on Pt{211} and Pt{311}. *Surface Science.* 1999; 440(1-2):271-278.

[5] Attard G, Barnes C. *Surfaces.* Oxford, UK: Oxford University Press; 1998.

[6] Lide DR. *CRC Handbook of chemistry and physics.* 73rd Edition ed. Florida, USA: CRC Press Inc.; 1992.

[7] Carrasco-Marin F, Mueden A, Moreno-Castilla C. Surface-treated activated carbons as catalysts for the dehydration and dehydrogenation reactions of ethanol. *The Journal of Physical Chemistry B.* 1998; 102(46):9239-9244.

[8] Leon y Leon CA, Solar JM, Calemma V, Radovic LR. Evidence for the protonation of basal plane sites on carbon. *Carbon.* 1992; 30(5):797-811.

[9] Quah EL, Wilson JN, Idriss H. Photoreaction of the rutile TiO2(011) single-crystal surface: reaction with acetic acid. *Langmuir.* 2010; 26(9):6411-6417.

[10] Szymanski GS, Karpinski Z, Biniak S, Swiatkowski A. The effect of the gradual thermal decomposition of surface oxygen species on the chemical and catalytic properties of oxidized activated carbon. *Carbon.* 2002; 40(14):2627-2639.

[11] Zielke U, Huttinger KJ, Hoffman WP. Surface-oxidized carbon fibers: I. Surface structure and chemistry. *Carbon.* 1996; 34(8):983-998.

[12] de la Puente G, Pis JJ, Menéndez JA, Grange P. Thermal stability of oxygenated functions in activated carbons. *Journal of Analytical and Applied Pyrolysis.* 1997; 43(2):125-138.

[13] Yi F-, Lin X-, Chen S-, Wei X-. Adsorption of VOC on modified activated carbon fiber. *Journal of Porous Materials.* 2009; 16:521-526.

[14] Popescu M, Joly JP, Carré J, Danatoiu C. Dynamical adsorption and temperature-programmed desorption of VOCs (toluene, butyl acetate and butanol) on activated carbons. *Carbon.* 2003; 41(4):739-748.

[15] Carrott PJM, Carrott MMLR, Cansado IPP. Reference data for the adsorption of methanol on carbon materials. *Carbon.* 2001; 39(2):193-200.

[16] Pittman CU, Jiang W, Yue ZR, Gardner S, Wang L, Toghiani H, et al. Surface properties of electrochemically oxidized carbon fibers. *Carbon.* 1999; 37:1797-1807.

[17] Damjanovíc L, Auroux A. Determination of acid/base properties by temperature programmed desorption (TPD) and adsorption calorimetry. In: Derouane EG, editor. *Zeolite characterization and catalysis.* Netherlands: Springer; 2009: 107-167.

[18] Niwa M, Nishikawa S, Katada N. IRMS–TPD of ammonia for characterization of acid site in β-zeolite. *Microporous and Mesoporous Materials.* 2005; 82(1-2):105-112.

[19] Zacharia R. *Desorption of gases from graphitic and porous carbon surfaces.* [Unpublished PhD thesis]. Berlin: Freien Universität Berlin; 2004.

6 Conclusions and Future Work

6.1 Conclusions

This thesis has examined the effects of different industrial electrochemical treatments and UV/O$_3$ treatment on the surface chemical composition and surface structure of PAN-based HT carbon fibres using XPS, SEM, TEM, Raman and BET surface areas. It also examined immersion calorimetry as a technique to measure the surface energies of the fibres and fibre-resin interactions. Carbon black was used as a model surface for examining the resin interactions where dilute solutions of resin were used as the probe liquids. TPD was used to investigate the adsorption of polar molecules on the surface of carbon fibres. The results of this work are summarised below.

- Increasing the charge applied in the electrochemical treatments was shown to increase the level of oxygen present on the fibre surface.

- UV/O$_3$ treatments increased the O/C ratio with time from ~ 0.06 to a saturation of ~ 0.30 after approximately 40 minutes treatment.

- Five minutes of UV/O$_3$ treatment was shown to produce levels of oxygen equivalent to the highest electrochemical treatment and fibre ageing did not occur one month after treatment.

- UV/O$_3$ treatments were found to increase the disorder of the surface but not the bulk structure.

- The heat of immersion of treated fibres in water showed similar trends to those reported in the literature; it increased with increasing surface oxygen level while it remained unchanged for immersion in the non-polar probe of toluene.

- Due to the small surface areas involved, the calorimetry signals were found to be overshadowed by the rush-in effect and heat of ampoule breaking and it was therefore not possible to measure surface energies.

- Immersion calorimetry measurements with dilute solutions of resin and resin components for carbon blacks showed too much variation due to concentration gradients in the probe liquid.

- TPD spectra for the main mass fragment for each alcohol probe showed two desorption peaks, one at ~450 K which was taken to be desorption of the pure probe and the other in the 600- 700 K region which was taken to be a mixture of desorbing alcohol, reaction products and decomposition of surface functional groups.

- The desorption kinetics inferred from the shape of the first desorption domain were best described as being second order.

- Dehydrogenation of the adsorbed alcohols to the corresponding aldehydes occurred on the fibre surface but dehydration to olefins was not observed.

- Adsorption of the alcohols increased with increasing length of the carbon chain in the alcohol. This was attributed to the polarizability of the alcohol, and hence the alcohol acidity and probability of dissociation occurring, increasing with increasing chain length.

- The relationship between alcohol adsorption and chain length changed from exponential to linear with increasing surface oxygen suggesting a complicated system that needs further investigation.

- The level of adsorption of any one alcohol increased exponentially with increasing level of surface oxygen.

- The peak temperature of desorption, i.e. the bond strength between the probe liquid and the fibre surface, increased linearly with increasing surface oxygen for propan-1-ol and butan-1-ol.

Overall, this thesis has shown UV/O_3 to be a promising treatment method for altering the surface of carbon fibres. Immersion calorimetry and TPD have also been shown to be promising techniques for the characterisation of carbon fibres and further study into each method would be of considerable interest. TPD is of particular interest as it uses relatively small quantities of fibres and has not been used on carbon fibres in this way before.

6.2 Future Work

UV/O_3 treatment offers several advantages over the standard electrochemical treatment including environmental benefits and improved processing times. Further investigations into the exact nature of the treatment would be of interest. Ideally a purpose built UV/O_3 treatment unit could be created to treat fibres to different levels of surface oxygen and BET surface area data, including pore sizes, acquired. This would allow tracking of the development of the surface area with treatment time. Mechanical tests on individually treated fibres and fibres embedded in resins would show whether the UV/O_3 treatments alter the fibre strength and adhesion capacity.

Immersion calorimetry in pure liquids could prove useful for measuring surface energies if either more fibres could be examined at once, or if the sensitivity of the method could be improved. In order to perform immersion calorimetry measurements using resin solutions, a stirring mechanism would be required to remove uncertainties in the concentration gradient of the solution and measurements of the solution concentration before and after immersion would also be needed. In preference to this, liquids analogous to the epoxy resins could be used although this would only be useful if the sensitivity issue was overcome.

The method of TPD investigation presented in this thesis has not been applied to non-porous carbon fibres before. Here, it has been shown to be a very promising technique to examine bond strength on fibres as samples of less than 1g in weight produced measurable results. Further work using varying levels of surface coverage, non-polar probes, and resin analogues would be of interest.

Varying levels of surface coverage could be used to calculate the activation energy of desorption and would allow bond strengths to be estimated. Resin analogues, such as methyl glycidyl ether, could be used to examine in-depth the interactions of epoxy groups with surface functional groups. Using such analogues and fibres with different surface chemistries, the exact nature and

strength of the bond between the resin and the functional groups could be identified from the peak temperature of desorption and XPS data.

Acidic or basic probes could be used to identify the exact number and nature of acid/ basic sites on the fibre surface. Examining the effect of the delocalised π-electrons on the basic nature of the fibre surface would be of particular interest to help explain the change in the relationship between alcohol chain length and level of alcohol adsorption. Non-polar probes could be used to examine the dispersive interactions on the fibres.

Careful calibration of a system would allow quantitative measures of the adsorption/ desorption system. Ideally *insitu* measurements by XPS or by a calibrated mass spectrometer would allow the exact surface composition of the fibres to be examined after heat treatment and the relationship between strength of bond and exact surface functional groups examined.

Overall, this thesis has shown several promising avenues of research that will hopefully help further the understanding of the bonding regime between carbon fibres and resin matrices.